Dynamic Interactions Between Voltage and Frequency Events in Future Power Systems

PhD Thesis

September 2024

Samuel Gordon

Future Power Networks and Smart Grids Centre for Doctoral Training

Department of Electronic and Electrical Engineering

University of Strathclyde, Glasgow

Declaration

This thesis is the result of the author's original research. It has been composed by the author and has not been previously submitted for examination which has led to the award of a degree.

Signed: Sam Gordon

Date: 30th September 2024

Acknowledgements

I wish to express sincere gratitude to Professor Keith Bell for his primary supervision of this work. Keith has provided high-quality technical advice, constructive feedback, and personal support throughout this PhD. I will miss our interesting and productive discussions. Sincere thanks are also due to Dr Qiteng Hong, who has co-supervised this work. Qiteng's valuable insights and support have been greatly appreciated. Keith and Qiteng have enabled me to seek advice from various experts within the industry and participate in interesting research projects, which helped maintain industrial relevance for this work. I would also like to thank Cornel Brozio of Scottish Power Energy Networks for offering his time and extensive knowledge of the behaviour and performance of the GB power system.

Personal thanks are also due to my family. I dedicate this Thesis to my parents, who have encouraged and supported me in this endeavour. To my father, as an accomplished forensic psychiatrist and a trained medical doctor, you will always be more of a doctor than I will ever be, but I know you still aspire to complete your own doctorate. It is my pleasure to serve as your conduit in this regard. To my mother, who helped me through many challenging times by offering guidance and invaluable lessons from her own PhD experience and long academic career. Last but far from least, thanks to my partner Anna, who has stood by me day-in and day-out throughout this lengthy process. Thank you for your patience. Without you, life would be much less fun!

Finally, I would like to acknowledge the funding sources that have allowed this work to be completed. The development of this research is supported by UK Engineering and Physical Sciences Research Council (EPSRC) through Centre for Doctoral Training in Future Power Networks and Smart Grids [EP/L015471/1] and the Pathways to Collapse project through the Supergen Energy Networks Hub flexible fund.

Abstract

The dynamic behaviour of power systems changes as the share of non-synchronous Inverter Based resources (IBRs) increases. These changes are typically characterised by a reduction in the inertia and fault levels on the system, which, in turn, alter the sensitivity of the system's frequency and voltages to changes in operating conditions. This Thesis investigates the changing dynamic behaviour of the power system in response to network faults, focussing on the interaction between voltage dips and the system frequency. Traditionally, these phenomena are studied separately, but their coupling has the potential to increase in IBR dominated power systems.

A new dynamic power system model is introduced, called the 'North-GB Test System' (NGBTS), which incorporates the long-term electricity system infrastructure plans in GB required to operate a zero-carbon system by 2035. It is demonstrated that disturbances in the IBR-dense locations of the network can lead to transients of the system's centre of inertia frequency nearing the statutory limits of 49.5 Hz, with high initial rates of change exceeding 2 Hz/s. Regional frequency deviations in the fault region are found to be more severe than at the centre of inertia, posing risks of generation tripping and load shedding. The work assess several solutions to mitigate these risks and proposes grid code modifications aimed at improving the performance of IBRs during faults. It is shown that increased active power injection from IBRs can mitigate frequency transients, improve rotor angle stability of synchronous machines (SMs), and maintain voltage stability.

This Thesis also presents a quantitative assessment of fault level changes in the Scottish network from 2022 to 2032. Contrary to common assumptions of declining fault levels, the analysis reveals a significant increase in fault levels across the region by 2032, largely driven by IBRs, that can be leveraged for dynamic voltage support in future grids. It is recommended that issues related to elevated fault levels, such as exceeding equipment ratings or misconfigured protection systems, be identified and addressed to avoid unnecessary costs and delays in connecting new renewable generation and transmission infrastructure. This work highlights the growing need to accurately define the system's needs relating to fault level requirements, converter stability and quasi-steady-state voltage sensitivity as it transitions to low-carbon operation.

Table of Contents

Chapter 1: Introduction and Research Overview

Power systems in many countries around the world are undergoing revolutionary change. A critical goal of the energy transition is achieving a very high penetration of renewable energy technologies while maintaining an equivalent level of reliability, security, and resilience. However, numerous policy and technical challenges must still be resolved before achieving secure and efficient operation of the future zero-carbon electricity grid.

This chapter provides the motivations for, and contributions of the research presented in this Thesis. While much of the work focuses on the Great Britain (GB) system, many of the findings can also give insights into the behaviour of other systems. This Chapter first describes the motivations for the research and is set in the context of the electricity network transformation in GB. Then, the contributions of this Thesis are presented, along with an outline of the document's structure.

1.1 Motivation for the research

The greenhouse gasses emitted by human industrial activity lead to accelerated global warming. There is a scientific consensus on this fact [1]–[3]. The severity and dangers of climate change are becoming more evident, and its impacts are affecting nature, people's lives and infrastructure everywhere [4]. The UK and 185 other countries have become parties to the Paris Agreement [5], which agreed to pursue efforts to limit the average global temperature increase to 1.5 °C above pre-industrial levels[1]. In fact, in 2019, the UK became the first major economy to pass net zero emissions into law [6]. A big part of the response to climate change is providing electricity from renewable energy sources.

As power systems around the world increase renewable energy penetration and transition towards low carbon operation, they must accommodate a high penetration of non-synchronous

---

[1] Unfortunately, recent scientific evidence suggests that there is a high likelihood that the global target of 1.5 °C will be exceeded during this century [3]. What's more, efforts to limit climate change remain highly dependent on political will, public opinion, corporate interests and other complex and global societal influences. However, that is another story.

Inverter Based Resources (IBRs). Among these new technologies are wind turbine generators (WTs), photovoltaic (PV) generators, Battery Energy Storage Systems (BESS), Flexible AC Transmission Systems (FACTS), High Voltage Direct Current (HVDC) transmission systems and power electronic interfaced loads. As the penetrations of IBRs increase, the differences between traditional fossil-fuelled thermal power plants, mainly based on Synchronous Generators (SGs), and IBRs become more apparent. These differences influence the system's dynamic behaviour, driving a need to study its performance as it transitions.

A properly designed and operated power system should meet the following fundamental criteria [7]:

1. Supply electrical energy at the least cost and with minimum ecological impact.
2. Continually meet a changing load demand for active and reactive power, which involves maintaining adequate generation or energy storage assets.
3. Meet minimum security standards in terms of the 'quality of supply', which involves:
    a) maintaining the voltage and frequency of electrical power to within acceptable limits and
    b) delivering it within an acceptable level of reliability.

For the system to be reliable and respect the fundamental criteria mentioned above, it must be capable of withstanding a wide variety of disturbances. As such, power systems are typically designed with enough redundancy and are operated in such a way as to survive the most likely contingencies. This Thesis focuses on part 3a) of the criteria above, which implies that the system must remain stable following disturbances, and the network voltages and frequencies should only deviate within acceptable bounds. In GB, the Security and Quality of Supply Standards (SQSS) [8] and the Grid Code [9] define the requirements for securing the system and maintaining a stable frequency and voltage, and are referenced throughout this thesis.

1.1.1 Effects of increasing IBR penetration on system dynamic properties

Increasing IBRs has had, and continues to have, several wide-ranging impacts on the planning and operation of a power system. The power system is a complex and highly nonlinear system whose dynamic performance strongly depends on the characteristics of its component parts. The nature of the interface between generators and the network strongly influences the dynamic performance of the power system and, traditionally, many of the principles of power system operation and control have been designed around the fundamental characteristics of SGs.

The inertia and fault levels in the network are two fundamental indicators of the system's ability to maintain a balanced and synchronised state following disturbances, such as faults. They mainly relate to the sensitivity of the system's frequency and voltages and its ability to resist sudden changes. Higher inertia generally means that frequency deviations are less during an active power imbalance, and higher fault levels generally mean that the severity of the voltage depression is less during a network fault.

In an SG, a rotor with field windings is rotated by a mechanical source, such as a turbine, which induces an AC current in the stator windings. An important characteristic of the SG is that the rotor rotates at a near constant speed that is synchronised with the grid frequency and maintains a near constant frequency and phase relationship. By being mechanically coupled to the grid, the SG will provide an inherent response to changes in voltage or frequency at its interface. During a disturbance, the energy stored in the rotor is naturally exchanged with the grid. Hence, it provides an inherent inertial response.

IBRs utilise several different energy sources, e.g. mechanical, chemical or photovoltaic. WTs have mechanical turbine generator systems but typically produce power at variable frequencies, and their rotors are coupled to the grid through power electronic converters. Hence, they do not provide a natural inertial response. A IBR's behaviour during disturbances is driven by the control strategies in place to interface with the grid. In addition, the internal IBR currents must remain within the limited short-term rated capability of the power electronic switches [10]. Therefore, the power provided during short circuits is reduced compared to an equivalently rated SG.

It is now common to see wind and solar based IBRs displacing SGs in system operation due to their low short-run marginal cost and a priority to utilise low-carbon generation. HVDC interconnection between different synchronous systems is also increasing. Energy markets connected through HVDC are non-synchronously coupled and can offset the use of SGs in the energy market on the import side. As such, deploying IBRs can reduce inertia and fault levels by pushing the SGs out-of-merit or displacing SG capacity. The new challenges that must be overcome can, in some cases, only become apparent at high levels of IBR penetration.

1.1.2 Electricity network transformation in the UK

The decarbonisation of the electricity system in the UK has been relatively fast in recent years. Emissions from power generation have fallen by 69% from 2010 to 2023, attributed mainly to phasing out coal and fostering offshore wind development [11]. Decarbonising the whole economy requires that a substantial amount of the heating and transportation sectors become electrified. Low-carbon generation capacity is set to significantly increase over the coming decades to meet this additional demand. The UK government has an ambition of up to 50 GW of offshore wind by 2030 [12], an increase from 13 GW in 2022. There is also a target to decarbonise electricity supply by 2035 [11]. Figure 1 shows the installed generation capacity, peak demand and percentage of Distributed Generation (DG) in 2022, 2030 and 2050 from NGESO's[2] Future Energy Scenarios (FES) [13]. A large increase in IBR technologies is expected in both future years, with most of this capacity coming from additional onshore wind, offshore wind, and PV.

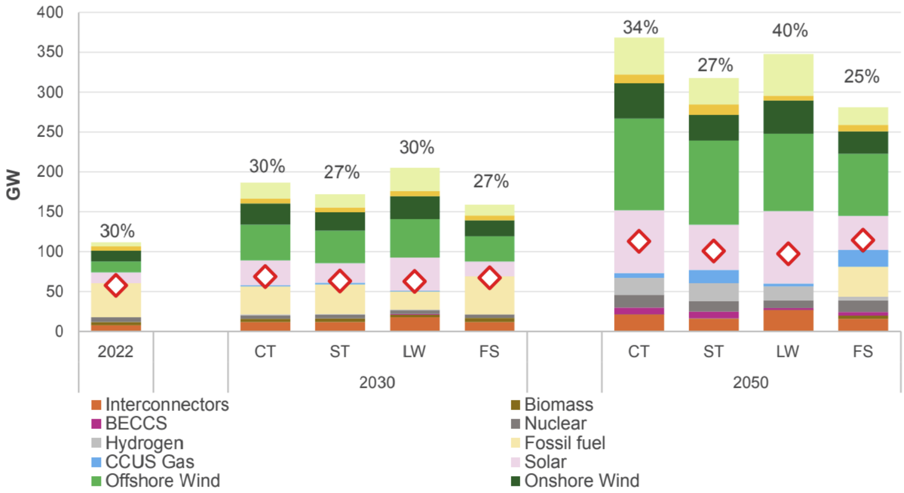

Figure 1: Installed generation capacity, peak demand (diamond) and percentage of distributed generation [13]

Figure 1 shows that the proportion of DG to the total generation capacity remains similar in future years, highlighting that the continued growth of DG is expected. High penetration of variable DG presents several challenges to centralised power system planning, operation and control. These challenges include a growing need for management of constraints in distribution networks, an increasing need for transmission and distribution network coordination, increasingly localised supply resulting in a less schedulable generation portfolio for the Transmission System Operator (TSO) and increased IBRs reducing the system's inertia, changing fault levels and changing the system's dynamics [14].

Across all FES scenarios, there is a significant increase in wind generation. Figure 2 shows the GB system's generation outputs and demand locations [13]. Much of the new generation capacity will be in Scotland to exploit high average wind speeds and a relatively favourable

[2] National Grid Energy System Operator (NGESO) operates the electricity system in GB.

planning regime. Scotland is already a net exporter of power to England and has a high share of the nation's wind power (primarily onshore). According to the FES 'Leading the Way' scenario (shown in Figure 2), the net generation supply in Scotland is expected to increase by a factor of 5.7 in energy terms. This increase in net supply implies average hourly power flows between Scotland and England of 3.9 MW in 2022 and 21.9 MW in 2035. As such, The rapid growth in wind generation capacity must be accompanied by an equally fast growth in North to South network transfer capacity, which is already constrained during high wind conditions. The new network capacity is planned to be delivered through new infrastructure, including enhancing the onshore AC system capacity and building new offshore HVDC capacity, introducing a growing need for strategic and centralised network investment to be made.

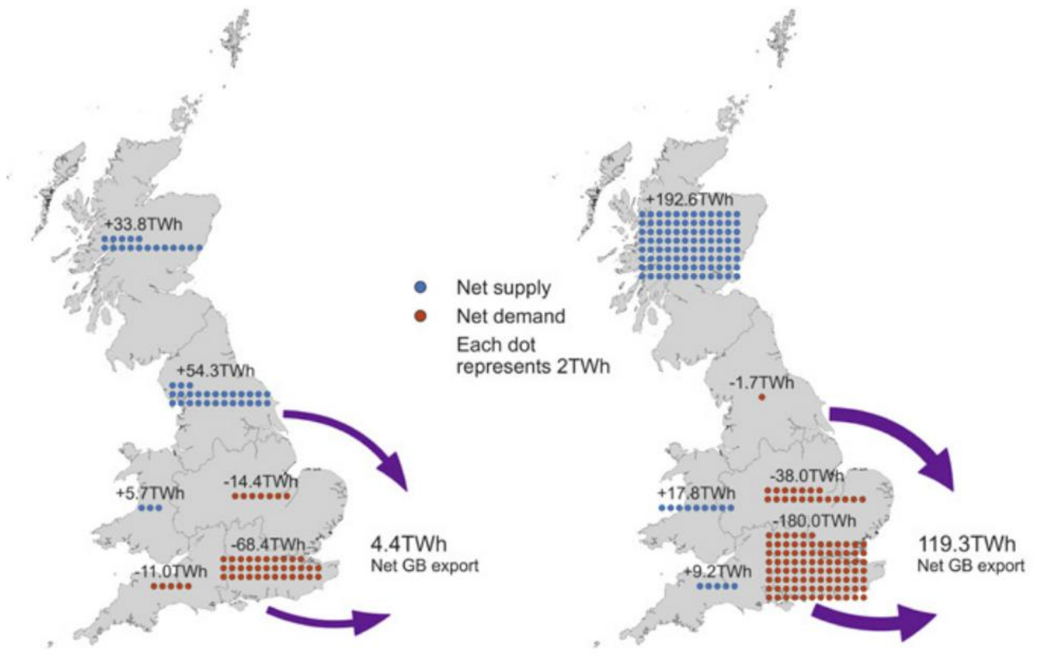

Figure 2: Locations of electricity generation output and demand for FES 'Leading the Way' scenario in 2022 and 2035 [13].

As a result of the changing generation mix in GB, the national inertia and regional fault levels are expected to continue to decline in the coming decade [15]–[17]. These properties are often used to measure how 'strong' a system is in dealing with disturbances. As the system's dynamic response is altered, new challenges emerge that threaten system security at both a regional and system-wide level [16], [18]–[20]. To address some of these challenges, NGESO has gone some way towards defining minimum inertia and fault level requirements [16], [21]. Via the Stability Pathfinder (SPf) tender exercises, NGESO seeks to procure inertia and fault level in the GB transmission network. NGESO is also reforming GB's frequency response and reserve services.

1.2 Overview and contributions of the research

The research presented in this Thesis investigates the changing dynamic behaviour of the power system in response to severe disturbances. The work focuses on the effects of network faults (sometimes called 'voltage events') and the interactions between these faults and the system frequency. Traditionally, the study of network voltages and frequency has been performed separately. However, they are intrinsically linked, and the coupling between them has the potential to increase. This coupling is hypothesised to increase due to several inter-related factors, including:

(1) increasing IBR penetration is generally considered to reduce inertia and fault levels;
(2) the reduction of fault levels leads to more severe disturbances that have a wider reach in the power system;
(3) the reduction in system inertia will make frequency more sensitive to changes in active power;
(4) the increase in IBR capacity in some areas means that a large amount of power might be interrupted by faults; and
(5) the power interruption and possible impact on frequency will depend on how IBRs are programmed to respond to faults.

The overarching research question being addressed is: "With the significant increase of IBRs and associated changes in the system's dynamic properties, to what extent do the transient effects of network faults – and the responses of network elements to the fault – present a risk to the frequency stability of the system?" In this Thesis, this phenomenon has been termed fault-induced frequency excursions (FIFE).

The literature review in Sections 2.4 and 2.5 reveals several additional related open questions regarding the interactions between fault events and frequency stability, which are outlined as follows:

- How do grid code requirements for IBRs influence a possible FIFE?
- What are the relative benefits and trade-offs of different IBR requirements? In particular, if changing IBR requirements benefits short-term frequency stability, how might the system's performance be degraded in other areas, such as voltage or transient stability?
- To what extent could faults lead to frequency excursions in the GB system?
- Taking account of the generation, storage, and network expansion plans in GB, to what extent could FIFEs become an issue in a future version of the power system?

- What measures can be taken to mitigate the detrimental effects of fault-induced active power deficits and improve FIFEs through existing IBR control measures, and how do these compare to alternative solutions?

It is important to understand these mechanisms as the power system evolves so that they do not lead to unexpected adverse system conditions. Suppose a fault could lead to extreme frequency deviations, either on regional or system-wide levels. In that case, they can, for example, lead to the unintentional triggering of protection systems such as Rate of Change of Frequency (RoCoF) or the operation of system defence measures such as the Low Frequency Demand Disconnection (LFDD) scheme, threatening the system's security. Operational security requirements should take into account the probability and severity of such events. If these types of events could become a stability challenge in GB, this could introduce a need to (1) rethink the principles regarding how frequency stability security criteria in GB are defined or (2) change operational security practices to account for short-term active power deficits that can result from network faults, or (3) make updates to existing technical performance requirements mandated by the relevant codes.

These questions are answered in Chapters 3, 5 and 6 of this Thesis.

1.2.1 Contributions of the research

The main contributions of this Thesis are categorised into three main areas and are summarised below:

1. ***On the development of a new power system model representing the GB system***

This work introduces the North-GB Test System (NGBTS), a model providing a spatial representation of the northern GB power system, with a focus on Scotland and an aggregated view of England and Wales (E&W). The NGBTS represents both the current system (2022) and a credible future system (based on data available to 2032), offering a more up-to-date and detailed representation compared to existing reduced models, particularly in the Scottish region, which faces significant development. The long-term electricity system infrastructure plans that are incorporated into the NGBTS model represents the foundation of the network required to operate a zero-carbon system by 2035 and beyond.

The NGBTS enables independent studies of real system development and operational challenges, especially those impacting Scotland and its capacity to integrate increasing wind power. Unlike generic test systems, the NGBTS is based on a real network with known parameters that constrain its operation in credible ways, allowing for the exploration of critical questions about resource interoperability without overwhelming complexity [22].

2. ***On the review and analysis of the system's dynamic properties***

This research examines the expected changes in fault levels in the Scottish area of the GB transmission network, over the next decade. It reassesses the use of fault level as a metric for system strength, finding that while it remains relevant, it does not fully capture the challenges often associated with system strength.

Using the NGBTS, it has been found that the fault levels in 2032 significantly increased throughout the Scottish transmission system, going against the familiar narrative of reducing fault levels. However, much of this increase in fault level is supplied by IBRs. These findings improve the understanding of the nature of the fault level challenge in Scotland and, more broadly, highlight the requirement to define the system's needs better when related to a fault level deficiency.

Simulations demonstrate that higher fault levels in 2032 improve voltage dips across various generation dispatch scenarios, showing that the expansion of IBRs alongside network reinforcements increases the system's resilience to faults. This analysis also reveals the nature of dynamic reactive power support from IBRs and how it differs from SGs. IBRs can, if specified to do so, provide consistent reactive power support over a wide area that is less dependent on the energy market.

3. ***On the occurrence of Fault-Induced Frequency Excursions***

Dynamic power system simulations in this work have described the fundamental mechanisms that lead to FIFEs. These mechanisms are first explained using a simple 'two-area' power system model and further demonstrated on the NGBTS model. It is shown that network faults can lead to significant short-term active power deficits, which can lead to sizeable and rapid frequency excursions.

A comprehensive analysis of the influence of various WT current controls on the FIFEs during the fault and post-fault recovery period has been provided. Studies using the two-area system model demonstrate that sacrificing some of the reactive current for some additional active current can give notable gains in the frequency dip with only a minimal reduction in the voltage dip. These findings challenge the current approach of prioritising reactive current during faults, especially in the future when there is a high penetration of IBRs.

A novel screening methodology has been proposed and applied to the NGBTS to scan for the worst-case generation dispatch conditions and fault locations from the perspective of FIFEs. The method uses steady-state studies and saves on computational burden compared with performing numerous time domain simulations. In addition, it captures the effects of voltage dip severity and grid code fault ride-through (FRT) requirements, which goes beyond existing screening metrics used for power system stability issues.

This work provides the first evaluation of fault-induced frequency stability risks in the IBR-dense northern GB power system, examining both the current (2022) and future (2032) systems. By assessing system-wide and regional frequency stability, a heightened risk of reaching critical protection thresholds in faulted regions is identified, which could escalate into cascading failures and jeopardise system security. This analysis makes a significant contribution by addressing a phenomenon yet to be thoroughly studied in GB.

An appraisal of various available methods to improve the system-wide and regional frequency sensitivity has been performed on the NGBTS system. This appraisal contributes to understanding the most technically beneficial ways to reduce frequency excursions during faults. The findings demonstrate that adjustments to FRT controls, current limiting strategies and grid-following converter current ratings are more effective than established solutions such as fast frequency response or adding system inertia.

This work also evaluates the technical trade-offs of the control system adjustments, investigating the impact on the system's voltage performance and the transient stability of Synchronous Machines (SMs). This analysis contributes the first published assessment of these trade-offs on a spatially disaggregated model of a future GB system and finds that, contrary to other published works, increasing active power delivery during fault-ride-through improves the rotor angle stability of the local synchronous machines.

1.3 Project outputs

The outputs listed in this section have been produced during the research. They include academic journal publications, conference proceedings and research project reports.

The following published papers do not form individual chapters in this Thesis, but elements of these published works are utilised throughout, and they are frequently referenced as they remain relevant to the research presented.

1. S. Gordon, C. McGarry, J. Tait and K. Bell, "Impact of Low Inertia and High Distributed Generation on the Effectiveness of Under Frequency Load Shedding Schemes," in IEEE Transactions on Power Delivery., vol. 37, no. 5, pp. 3752–3761, 2022.

2. S. Gordon, Q. Hong and K. Bell, “Implications of Reduced Fault Level and its Relationship to System Strength: A Scotland Case Study,” in CIGRE Paris Session – Study Committee C4. 2022.
3. S. Gordon, C. McGarry and K. Bell, “The growth of distributed generation and associated challenges: A Great Britain case study,” in IET Renewable Power Generation, pp. 1–14, 2022.
4. S. Gordon, K. Bell and Q. Hong, “Fault-induced frequency excursions in a future GB power system,” in preparation for submission to reputable journal.

In addition, the following reports have been produced for industrial research projects:

1. S. Gordon, D. Liu, Q. Hong, A. Dysko, and A. Alvarez, “Reduced System Fault Level,” Supported by SSE Renewables and ScottishPower Renewables, project report to Funders, 2021.
2. S. Gordon and K. Bell, “Development of a new power system model: the North GB Test System,” report for an EPSRC-funded project on “Pathways to Collapse”, supported through the Supergen Energy Networks Hub Flexible Fund, in preparation for publication, 2023.
3. S. Gordon and K. Bell, “A decade of electricity system transition in GB: effects on system dynamic properties,” report for an EPSRC-funded project on “Pathways to Collapse”, supported through the Supergen Energy Networks Hub Flexible Fund, 2023.

1.4 Structure of the Thesis

Chapter 1 has introduced the motivations for performing the research, outlined its primary contributions and listed the authors' publications and project outputs. The remaining chapters of this Thesis are as follows.

Chapter 2 provides the technical background for the work. The Chapter discusses the fundamentals governing the system’s dynamic performance during disturbances. It outlines what happens during large system events and the measures taken to protect against them. In this context, the stability of the system and the performance of generators are covered, as well as their different physical behaviours. Chapter 2 also introducing the main mechanisms where network faults can lead to deviations in frequency, and reviews system stability studies relevant to GB.

Chapter 3 studies the potential for fault-induced frequency excursions on a simplified two-area power system model. The analysis investigates the effects of increasing wind power penetration on fault severity, system inertia and the possibility of frequency deviations during faults. Possible system responses to the unintended operation of an example LFDD scheme are presented. In addition, the sensitivity of FIFE to several WT control parameters is simulated. The results gained in this chapter confirm the need for further investigations performed in Chapters 4, 5 and 6.

Chapter 4 describes the development of the NGBTS power system model (introduced in Section 1.2.1). The aspects discussed in the development of the model include the modelling approach, the assumptions and data sources utilised, the steady-state and dynamic construction, model validation and the methodology for dispatching generation.

Chapter 5 quantitatively reviews the critical system dynamic properties that influence system stability in GB: the inertia and fault levels. A series of scenarios are used to represent a wide range of system conditions. Simulations are performed on the NGBTS using these scenarios to assess the changes in inertia and fault levels in the system. More focus is given to the fault level change, as this is a highly locational metric which has been increasingly used to measure system stability in the context of IBRs.

Chapter 6 provides fault analysis through dynamic time domain simulations using the NGBTS to assess the risks of fault-induced frequency excursions in the future Scottish power system. It presents a method to screen for worst-case conditions and follows with in-depth assessments of the worst-case fault. Several sensitivities are tested to assess FIFE risks, and simulations that cover the maloperation of protection systems and large loss of infeed events are presented. The section concludes with an appraisal of various solutions to improve FIFEs.

Chapter 7 discusses findings, draws conclusions, makes recommendations and presents ideas for further work.

Chapter 2: Technical Background

Chapter 1 discussed the changing mix of generation and demand technologies as the power system transitions to operate with a lower carbon intensity. This shift in technology type, i.e. from a system dominated by SMs to one dominated by IBRs, changes the system's dynamic behaviour and can lead to voltages and frequencies being more sensitive to change.

The security of a power system refers to the degree of risk in its ability to survive disturbances (i.e. contingencies), such as short circuits or non-anticipated loss of system components without customer service interruption [23]. The power system is designed and operated to withstand a defined set of contingencies, referred to as “secured events”, selected on the basis that they have a significant likelihood of occurrence. In GB, the Security and Quality of Supply Standards (SQSS) [8] requires that, in summary, the system is secure against a double circuit fault on an overhead line and system instability or unacceptable frequency and voltage conditions are not allowed as a result.

TSOs and Transmission Owners (TOs) employ various methods to maintain the system's security, ensuring it remains stable for secured events. These methods generally include monitoring the system, implementing automatic and manual control of the network and user assets and holding reserves of active and reactive power to be dispatched over various timescales. Moreover, the system’s response to different types of contingencies over a wide range of operating conditions must be known as accurately as reasonably practicable, which depends on the system’s dynamic characteristics and the ability of engineers and modelling tools to replicate its behaviour.

This section provides the technical background in the context of maintaining the voltage and frequency limits of the system. The focus lies on the fundamental concepts, system dynamic properties and operational requirements. Disturbances are described in the context of the two main types of contingency events: network fault events (sometimes referred to as ‘voltage events’) and loss of infeed events concerning frequency stability.

2.1 Faults in AC power systems

Faults in AC transmission systems disrupt the normal flow of current. They can pose safety hazards and seriously impact the reliability of the power supply. In three-phase AC power systems, short-circuits can occur between phases, between phases to earth, or both. They can also occur in various power system components, e.g. overhead lines, cables, substation equipment and busbars. In GB, approximately 300 short-circuit faults occur each year; 80 - 90 % occur on overhead lines, and 5 % are three-phase faults [24]. This work considers balanced three-phase-to-ground faults. While these occur less frequently than other single-phase-to-ground or phase-phase faults, they can result in a more severe disturbance.

During the pre-disturbance steady-state environment, changes, e.g. in voltages or current flows, occur only gradually. The occurrence of a fault is described by a transient environment, where the network conditions are forced to change suddenly from their steady state. The following steps summarise what happens if a fault occurs on a transmission line:

1. **Short Circuit inception:** the three-phases are shorted to the ground during the fault, creating a very low impedance path.
2. **Voltage depression:** due to the low impedance, the voltage drops close to zero, causing a near collapse of the voltage at the fault location. The depressed voltage propagates through the system. The severity of this voltage depression, i.e. its depth and how far it is observed in the network, depends on the equivalent impedance to the fault location and the amount of short circuit current infeed, as the current acts to 'prop-up' the voltage.
3. **Short circuit currents:** The nearby connected sources will contribute fault current towards the fault location, causing a rapid increase in current magnitude typically much higher than the load currents. The amount of fault current depends on the network impedances and the type of connected sources. Fault currents must be within equipment short-term ratings.
4. **Phase angle disturbances:** the relative phase difference of the voltages between locations around the fault is forced to change. Rapid phase angle shifts can occur at locations throughout the system due to the imbalance caused by the fault. If the difference in phase angles exceeds a critical value, these two areas can lose synchronism, oscillate against one another, and lead to area separation.
5. **Loss of active power transfer:** the depressed voltage at the fault location prevents the pre-fault active power from being transferred across the transmission line. The voltage depression observed at nearby generator terminals also reduces their active power output proportional to the local voltage drop.
6. **Generator systems ride through fault:** most transmission-connected generation must remain connected to the network during the fault period to continue to supply the load when the fault has been cleared.

7. **Protection system operation:** protective relays detect the fault and signal circuit breakers to actuate, isolating the faulted transmission line and clearing the fault. Some types of protective relays rely on sufficient fault current to detect the fault.
8. **Transient recovery**: after the fault has been cleared, the voltage recovers, and generators, loads and other ancillary equipment must recover to normal "pre-fault" operation. The transient effects of the fault can lead to oscillations as the system stabilises.

The concepts in the steps listed above and how they are changing in the context of increasing IBR penetration are discussed further in the subsections below.

2.1.1 Fault current infeed

Short circuits typically cause a rapid increase in current magnitude, followed by decaying current transient. The current waveform changes dynamically during the period of a short circuit fault, which comprises an AC component with a relatively slow decay rate and a DC component with a faster decay rate. Depending on the application of the results, different magnitudes measured during the fault period could be of interest. For example, the peak break current (at a given break time (i_b)) and peak current (i_p) are used to determine the circuit breaker duties when opening and closing onto faulted circuits, respectively.

Figure 3 represents the short circuit current over time for a near-to-generator fault, which has been taken from BS EN 60909-0 [25]. For a far-from-generator fault, the decaying AC component is typically lower, and the sub-transient current ($I_k^{''}$) is close to the steady-state current (I_k).

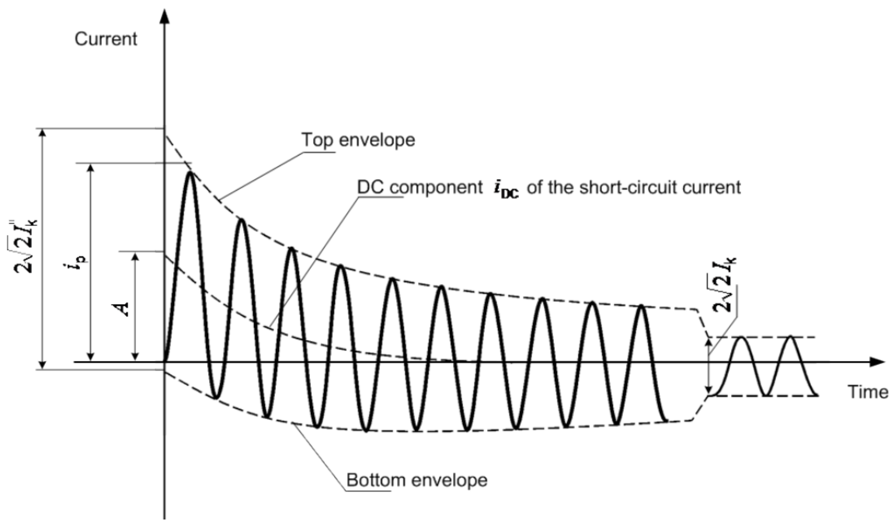

Figure 3: Short-circuit current of a near-to-generator short circuit with decaying AC component (image from BS EN 60909-0: 2016)

Considering fault infeed calculations, the various elements that make up the power system can be considered either passive or active. Passive elements, such as lines, busbars, and transformers, contribute to the impedance of the network and influence the currents that flow into a fault. Active components, such as rotating generators, motors and IBRs, also form part of the network impedance. However, they act as a source of fault current where the characteristics of different elements vary in their fault current contributions.

2.1.1.1 Fault infeed from synchronous machines

When modelling synchronous and induction machines, these sources can be represented by a voltage source behind an equivalent impedance based on the 50 Hz Thevenin equivalent. This approach is generally suitable for synchronous generators, motors, and induction machines. The positive sequence reactances of synchronous machines are time-dependent [24] (see Figure 3). During the sub-transient period, typically considered the first 2 or 3 cycles following fault inception, the sub-transient reactance is usually lower than transient and steady-state periods, and therefore, the generator provides a higher AC fault current.

Large SGs are the primary sources of fault currents in the transmission network. Being a voltage source behind an impedance that is mechanically coupled to the grid, the SG will provide an inherent response to changes in voltage or phase at its terminals, e.g. due to a network fault. This inherent response means the SG will change the phase of its current injection during a fault. The short circuit response of an SG is instantaneous and proportionate and can typically provide a short circuit current in the region of 6-7 times their nominal rating [10].

2.1.1.2 Fault infeed from Converter interfaced resources

IBRs use measurement and control systems to measure the voltage and phase at its interface to the grid, and a IBR with a grid-following control strategy will attempt to synthesise a power output that matches the frequency and phase of the grid. A IBR's behaviour during faults is typically like a controlled current source, and their response to a network fault, including the delivery of fault current, is driven by their control strategy. IBRs can quickly control the active and reactive current that is exchanged with the grid. However, these currents must remain within the limited short-term rated capability of the power electronic switches, including during fault conditions. Therefore, the magnitude of the fault current delivered by IBRs is significantly lower than an SG and is often assumed to be close to its nominal current rating [26].

Depending on the grid connection requirements, most IBRs must activate fault ride through (FRT) behaviour during a fault-induced voltage dip (see Section 2.1.4). During FRT, IBR controls are often required to deliver reactive current as a function of the post-fault retained voltage to support the network [9] while respecting the thermal limits of the device. Therefore, during a fault, the short-circuit contribution of IBRs should be modelled by a current vs. voltage relationship. However, this current vs. voltage relationship is non-linear due to the current limitation. Therefore, they cannot be represented by the classical model of a voltage source behind an impedance at the fundamental frequency.

2.1.2 The concept of fault level

Fault level is a measure of the amount of current that would flow at a given location if there was a short-circuit fault at that location. It is dependent on the equivalent source impedance at the fault location and the response characteristics of nearby sources of fault currents. It can be used to characterise the contribution of short circuit current from a group of sources or the entire system.

Typically, it is quoted as the product of the RMS short circuit current and pre-fault voltage at the point of fault. For an apparent power (MVA) fault level at a given point in the system, the equivalent system impedance in per unit form ($Z_{s\ (p.u.)}$), which is also equal to the Thevenin impedance of the system [24], is given by

$$Z_{s\ (p.u.)} = \frac{MVA_{base}}{MVA_{fault\ level}} \times \frac{V^2_{phase-phase(kV)}}{V^2_{base(kV)}} \tag{1}$$

Or, where the pre-fault phase-to-phase voltage and the base voltage are equal, the p.u. equivalent system impedance is given by

$$Z_{s\ (p.u.)} = \frac{MVA_{base}}{MVA_{fault\ level}} \tag{2}$$

Therefore, a high fault level at a given point in the network also means a low equivalent system impedance, which is often characterised as a ‘strong system’, and vice versa. Over the past few decades, a low fault level has increasingly been used, directly or indirectly, as a measure of likely power system stability, particularly in the context of IBR operation, often termed ‘system strength’. The meanings of system strength, its metrics, challenges and limitations are reviewed in Section 2.2.

2.1.3 Protection systems

Protection systems are designed to detect and remove faults and their hazardous transient conditions from the system. The action of the protection system typically intends to take the faulted element out of service before it – or its interconnecting elements – suffers catastrophic damage. Isolating the faulted components before damage occurs, i.e. isolating them fast enough that any excessive over-voltages or currents are within their short-term ratings, usually means that the affected components can be brought back into service once the fault has been removed.

Figure 4 describes the functional elements of a protection system [27]. The protection system must continually monitor the network conditions via measurement systems. The measured quantities must then be filtered and processed, calculations must be made, and decisions must be made based on their comparison with a pre-defined threshold. Where thresholds have been exceeded for sufficient time, indicating a decision to take action, the protective relay signals to circuit breakers to actuate, typically opening the circuit.

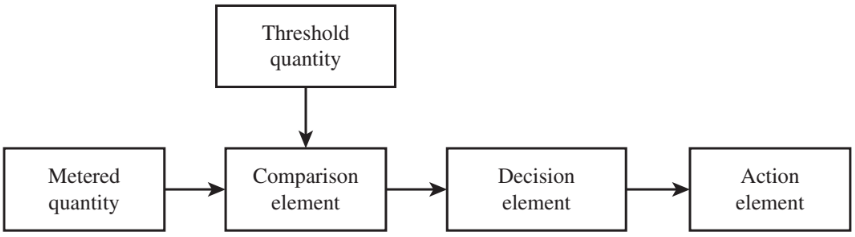

Figure 4: functional description of protection system elements [27]

The clearing time, i.e. the total time taken to detect and remove a fault from the system, is a critical feature of the protection system. The total clearing time comprises the time taken for all the subsystems to perform their tasks, including providing accurate measurement, processing and making calculations, communicating signals between devices and opening the circuit breaker. Depending on the objective, clearance times might need to be as fast as possible, or sometimes, intentional delay is needed to measure a reliable signal or confirm the trajectory of a system quantity. For example, referring to the transient stability of SGs or IBRs (see Sections 2.1.5 and 2.1.6, respectively), the less time the fault remains on the system, the lower the risk of instability. In fact, for SGs, there is a 'Critical Clearing Time' to limit the accelerating area and maintain stability, see Section 2.1.5. For transmission line protection in GB, clearing times are typically in the region of 50 – 100 ms [28]. However, for reliable frequency measurements, a few cycles of the AC waveform are required just for the measurement time (e.g., 60-100 ms), leading to longer total clearance times. When measuring the Rate of Change of Frequency (RoCoF), measurements are usually taken over a longer measurement window (e.g. 500 ms) before action is taken to reduce the unintended operation of the protection. Various assumptions applicable to the GB system for fault clearance times of transmission lines, frequency relays and RoCoF relays are used throughout the studies performed in this Thesis, see Chapter 6.

The potential impact of protection system failure is very high. Therefore, to ensure that protection systems can be relied upon, they are designed and built with a very high level of redundancy. According to the SQSS, the protection system shall tolerate any single failure, i.e. it operates with N-1 redundancy (as a minimum) [8]. In GB, transmission line protection systems are redundant with '1st main' and '2nd main' systems, each implementing a different protection philosophy. These can be, for example, a distance protection and a differential protection scheme operating in parallel to detect and isolate faults. These arrangements give protection systems a very high degree of reliability. The discussion in Section 2.2 outlines some of the novel challenges to protection systems with a high penetration of IBRs.

2.1.4 Fault ride-through requirements in GB

Fault ride-through (FRT) refers to the ability of generators to withstand and remain connected to the grid during faults. Generators must remain connected to quickly restore the pre-disturbance system state following the disturbance. Most modern grid codes mandate FRT requirements for IBRs and SGs, including in GB. Until recently, FRT requirements only applied to transmission-connected generation. However, more stringent FRT requirements have been imposed for MW-scale generators connected to distribution systems [29].

The FRT requirement is assessed by a voltage against time (V-t) profile. The V-t profile describes the transient conditions for the voltage at the generator's connection point, within which the generator must stay connected to the network. In other words, if the connection point voltage is below the V-t profile, the generator is permitted to trip. The FRT requirements for SGs and IBRs in GB are shown in Figure 5, showing that IBRs are required to remain connected over more extreme voltage conditions than SGs.

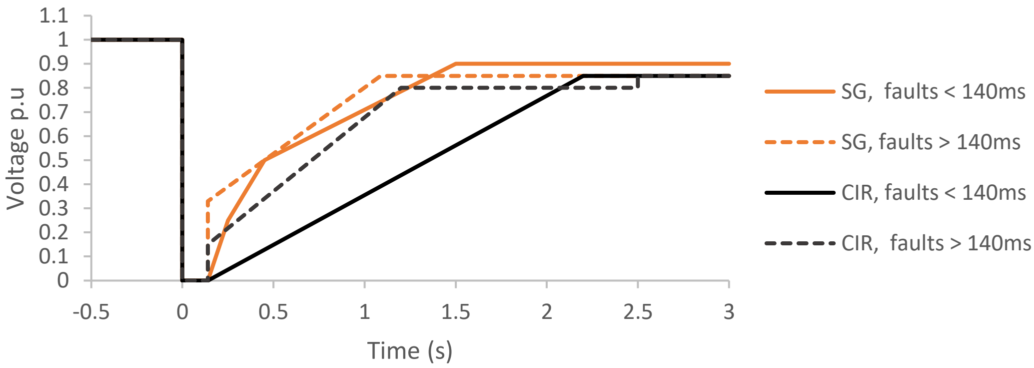

Figure 5: low voltage ride through V-t requirements for SGs and IBRs for connection point voltages above 110 kV, requirements from [29], [30]

2.1.5 Transient rotor angle stability of SGs

According to [31], "*Rotor angle stability is concerned with the ability of the interconnected synchronous machines in a power system to remain in synchronism under normal operating conditions and to regain synchronism after being subjected to a small or large disturbance*."

Consider a synchronous generator delivering power to a large power system through parallel transmission circuits. Figure 6 is the equivalent reduced circuit diagram representing two sources separated by an impedance.

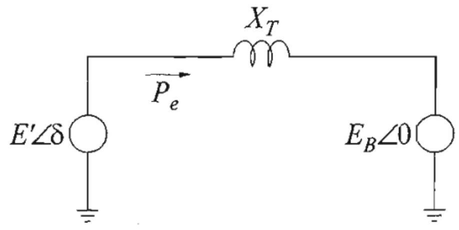

Figure 6: - Reduced equivalent circuit of a synchronous generator feeding an ideal voltage source through a transmission line [7]

The reduced equivalent circuit can be viewed similarly when applied to any two sources at different locations, i.e. conceptually, as a single generator and the rest of a system (as considered here), or groups of equivalent generators with active power transfer over an impedance. The power transfer across the line, in its simplified form, can be expressed as

$$P_e = \frac{E' \cdot E_B}{X_T} sin\,\delta \tag{3}$$

where P_e is the electrical power, δ is the voltage angle at the source, E' is the voltage magnitude of the sending end voltage source, E_B is the voltage magnitude at the receiving end voltage source and X_T is the equivalent reactance of the system. During a disturbance, the magnitude of E' remains the same and the angle δ changes. It can be inferred from (3) that as power transfer or the impedance between the two sources changes, so does the angular difference δ.

The rotor speed of the SG, also known as the angular velocity, is the derivative of the rotor angle with respect to time ($\omega_r = d\delta/dt$). The rotor speed refers to how fast the machine's rotor is rotating and sets the electrical output frequency of the voltage source. The acceleration of the rotor is the second derivative of the rotor angle, i.e. the rate of change of angular deviation ($d^2\delta/dt^2$) and can be described by the common form of the swing equation for an SG [7], as

$$\frac{d^2\delta}{dt} = \frac{\omega_0}{2H}(P_m - P_e) \tag{4}$$

where ω_0 is the synchronous speed, H is the inertia constant of the machine in seconds and P_m is the mechanical input power of the SG.

Equation (4) shows that angular acceleration occurs as a function of the power balance between the mechanical input power, e.g. from the turbine, and the electrical output power $(P_m - P_e)$. Equation (4) also shows that the rate of angular acceleration or deceleration is inversely proportional to the machine inertia. Figure 7 shows an example power - load angle curve (P - δ) for an SG during pre-fault, fault and post-fault conditions, derived from the equivalent circuit shown in Figure 6.

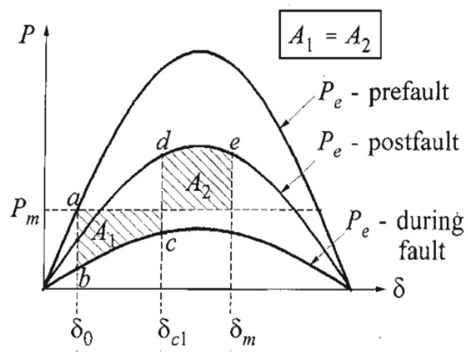

Figure 7: Power - angle curve for transient stability of a synchronous generator [7]

During steady-state conditions, there is an equilibrium between the input mechanical power (P_m) and the output electric power (P_e) of a machine. In terms of the machine torques, $\omega \cdot P_m$ and $\omega \cdot P_e$ are equal and opposite, resulting in no accelerating motion of the shaft. Therefore, for as long as the load demand on the system remains constant and there are no disturbances no the system, the rotor of a synchronous machine runs at a constant speed, and the speed of all interconnected machines is maintained at this constant value [23], [32].

Following a severe disturbance close to the SG, the voltage depression reduces the SG's electrical power output P_e (formula (3)), and P_e drops from point a to point b in Figure 7. However, the machine's mechanical input power is maintained, thus $P_e < P_m$. The net surplus of torque goes into accelerating the rotor of a synchronous generator, and the angle difference begins to increase from δ_0. The fault is then cleared by protective relays at the time δ_{c1} is reached and the voltage recovers. P_e increases according to the post-fault system conditions moving from point c to point d. Now, with $P_e > P_m$, the rotor should decelerate. However, due to the inertia of the machine, the angle δ continues to increase until all the energy gained during acceleration is expended, i.e. area 2 equals area 1. This energy must be expended before

P_e falls back below P_m on the curve to allow the rotor angle to decrease again and the system to remain stable. Otherwise, if area 2 is smaller than area 1 and $P_e < P_m$ in the 1st swing, the angle δ will continue to increase, and the system will become unstable. This method for assessing stability is known as the equal area criterion (EAC).

The angle stability of SGs is dependent on several factors, including the equivalent impedance between the generator and the grid, the generator pre-disturbance loading, generator excitation control, and the system's regional characteristics, such as regional inertia [7], [33]. If the generator becomes unstable (when the angle passes 180 degrees), the generator is said to be out-of-step with the system, a loss of synchronism occurs, and generator side protection systems will typically trip the generator to protect it from damage. Some SOs will be required to limit power transfers to address the risk of transient instability of SGs. The EAC is a simplistic analysis. In large multi-machine power systems, rotor angle stability is usually assessed through time domain simulations in RMS simulation tools that take account of the detailed system and generator design and control systems.

2.1.6 Transient stability of IBRs

As shown in Section 2.1.4, IBRs are expected to stay connected to the grid (and remain stable) during network faults. However, fault events and their transient effects can induce instability in converters and their control systems, especially for very deep voltage dips [31], [34], [35]. There have been several reported events where faults led to the erroneous disconnections of IBRs in response to network faults; some of these have been reviewed in more detail in Section 2.4.1.

One of the most well recognised issues for IBRs is synchronisation to the grid frequency and phase. As mentioned in Section 2.1.1.2, grid-following converters (the most prominent type of converter control philosophy) rely on measurement and control systems to measure and 'follow' the grid. Controllers utilise phase-locked loop (PLL) control techniques to synchronise the converter's output current with the grid voltage phase. The PLL operates as a closed-loop control system, measuring the grid's voltage phase angle and continuously adjusting its output while minimising the error between them. During a large disturbance causing a rapid phase angle shift, the converter can struggle to accurately track the grid's phase angle, causing the current injection at the output to be out of phase. The incorrect phase of the current injection can lead to further degradation of the voltage and angle at the connection point, resulting in a feedback loop which leads to instability of the PLL and loss of synchronism [34], [36]. PLL synchronisation can be more challenging when the grid is more sensitive to change. Hence, it can often be termed as 'weak-grid' stability of IBRs and related to the fault level at the connection point as a measure of the equivalent system impedance. The use of the fault level and the meaning of ‘system strength’ is discussed further in the next section 2.2.

2.1.7 Section summary and relevance to the research

This section (2.1) has outlined the fundamentals of power system transient responses during three-phase faults, a central theme of this thesis. It highlights how the lower fault currents from IBRs compared to SGs reduce system fault levels as IBRs displace SGs. However, the next section (2.2) challenges the relevance of fault level as a metric for stable system operation. Chapter 5 further quantifies future changes of fault levels in Scotland, finding that they significant increase, contrary to popular discourse.

The provision of active and reactive power during faults is also assessed in detail in Chapters 3 and 6 with time-domain simulations, considering FRT requirements and the current-saturated behaviour of IBRs. These chapters show that the proportion of active to reactive current delivered by IBRs during faults is an important consideration for the system’s frequency and rotor angle stability.

2.2 The concept of system strength and its relationship to fault level

The concept of system strength has been increasingly discussed concerning the challenges associated with a high penetration of IBRs. As these are often new and emerging issues, they have led to varied definitions of system strength, which can differ in scope. The over-arching theme of the definition of system strength relates to the power system's ability to maintain its core characteristics when the system becomes altered from its normal state, which strongly correlates with the concept of power system stability [18]. A strong system is more tolerant to perturbations and recovers more easily from major disturbances. reviews the definitions and descriptions of system strength from various international SOs and industry organisations.

Table 1: various descriptions of system strength

Organisation	Description of the term 'System Strength'
CIGRE [37]	"a metric used to describe the ability of a power system to maintain the core characteristics through which it interacts with a connection, namely voltage and frequency, as steadily as possible, under all operating conditions."
NERC [38]	"Grid strength is a commonly used term to describe how stiff the grid is in response to small perturbations such as changes in load or switching of equipment." And, in the context of IBR: "electrical system strength refers to the sensitivity of the resource's terminal voltage to variations of current injections."
NG ESO [10], [39]	"a regional characteristic which can be expressed as short circuit level (SCL), measured in kA. It provides an indication of the local dynamic performance of the system and behaviours in response to a disturbance."
AEMO [40]	"The ability of the power system to maintain and control the voltage waveform at any given location in the power system, both during steady state operation and following a disturbance. The system strength at a given location is proportional to the fault level at that location, inversely proportional to effective grid-following IBR penetration seen at that location. System strength is also a function of the severity of system events on the stability of IBR."
ENTSOE [41]	(1) "its impedance which is made up of generators, transformers, transmission lines and loads. This can be expressed as either Fault Level (in MVA at connection) [or] SCR (SCR in pu of the size of installation)". And (2), "its mechanical rotating inertia. This can be expressed as TSI." Where TSI is: "The inertia is expressed for a total Synchronous Area (SA) or a contribution from a distinct part of the SA."

For the most part, the definition of system strength relates to the ability of the power system to maintain an appropriate voltage magnitude and phase at a given location [10], [38], [40]. However, some definitions above, such as the one by ENTSOE and CIGRE, also link system strength to system inertia [37], [41]. Including the system inertia and, therefore, implying that frequency sensitivity is included in the definition of system strength might unnecessarily broaden the topic. In general, the practical application of a metric requires quantification, and it is only useful if it can be used to distinguish between acceptable and unacceptable conditions.

2.2.1 Fault level-based metrics for stable system operation

The Short Circuit Ratio (SCR) is the ratio of the fault level (S_K) to the nominal active power of an infeed (P_n) and has been a widely used index for assessing the strength of the connection point for IBRs. The SCR aims to describe the kinds of system conditions that IBRs may be required to operate under [42] and is defined as

$$SCR = \frac{S_K}{P_n} \tag{5}$$

The lower the SCR, the weaker the system is said to be. The classic SCR is only appropriate when considering a single IBR at a single point of connection and does not account for the presence of other converters [38].

The Weighted SCR (WSCR) metric accounts for the effects of multiple IBRs and has been used by ERCOT (the SO in Texas) to set wind dispatch limits from the Panhandle region [14]. The WSCR determines an aggregate SCR at a common "virtual" point of connection [37], [38] and is defined as

$$WSCR = \frac{\sum_i^N S_{K\,i} * P_{n_i}}{(\sum_i^N P_{n_i})^2} \tag{6}$$

where *N* is the number of IBRs with full interaction and *i* is the IBR index.

A single WSCR value may represent multiple IBRs with varying amounts of interaction but does not consider the impedances between them. System strength assessments in the ERCOT system highlight that, as wind penetration increases and the connections are spread across broader areas, the definition of the boundaries for using the WSCR metric becomes blurred, and it becomes less reliable when setting real-time operating limits [43].

SCR with Interaction Factors methods (SCRIF) [37], [44], [45], aim to directly account for impedances between multiple IBRs and assess their interaction within an area of the power system. The approach is based on assessing the observed voltage change at one bus for a small voltage change at another bus, i.e. the voltage sensitivity between IBRs, to more accurately estimate the grid strength. In general, SCRIF can be defined as

$$SCRIF_i = \frac{S_{K\,i}}{P_{n_i} + \sum_j \left(IF_{ji} * P_j\right)} \tag{7}$$

where IF is the change in bus voltage at bus i (ΔVi) for a change in bus voltage at bus j (ΔVj), as follows: $IF_{ji} = \Delta\text{Vi}/\Delta\text{Vj}$. However, there is a lack of experience and published studies applying this metric in real-world planning or operational practices.

Another alternative is the 'available fault level' method (AFL) introduced in the CIGRE brochure [37]. The AFL assesses the impact of new IBR connections on existing IBR locations connected to the AC network. Based on the premise that IBRs require a minimum fault level to operate in a stable manner, this method assumes that synchronous machines provide a positive fault level and IBRs provide a negative fault level. Therefore, connecting a new grid-following IBR is a 'sink' of fault level and is equivalent to reducing the fault level at surrounding network locations. The bigger the capacity of the new connection, the more fault level is needed in the system to maintain the minimum SCR at both connections.

AEMO (the SO in Australia) has applied the AFL method as a screening metric to determine the need for detailed studies using Electromagnetic Transient (EMT) simulations. However, in some areas with a high IBR penetration, the AFL can be considered too approximate and complete EMT analysis is always required in Australia [46].

2.2.1.1 Further limitations of SCR metrics

Another limitation of the SCR metrics is one of consistency. Each SCR metric will suggest different system limits and sets of requirements to be imposed on network users. What appear to be the critical limits will be different for each converter manufacturer based on the variation in control strategies and parameters used [38]. In addition, inconsistency can be experienced when interpreting the fault level to be used in the calculation. Short-circuit currents change dynamically during the fault period with symmetrical and asymmetrical components (see Section 2.1.1). Therefore, a different fault apparent power can be chosen during the sub-transient or transient periods, including only the AC symmetrical RMS and sometimes the DC components [24].

The SCR metrics described in this section are all based on the fault level and the equivalent Thevenin impedance at the fundamental frequency. The impedances of converters vary across a wide frequency range, which is influenced by their output filter, control strategy, control mode and the network operating conditions [18], [19]. Therefore, stability in IBR dominated systems exhibits multi-frequency dynamics and SCR metrics based on the fault level do not capture the true behaviour of IBRs [49]. Fault level metrics may remain useful for early indicative screening of system strength challenges. However, there is a necessity to move towards a multi-frequency response characteristic model and, in some cases, detailed EMT analysis to determine stability in IBR dominated networks.

2.2.2 Relationship between Fault Level and System Strength – Classification of Issues

Many emerging challenges related to operating the system with an increasing penetration of IBRs are often attributed to a 'low system strength' [40], [41]. The challenges typically quoted span the topics of power system stability, power quality and protection systems [18], [50]. Furthermore, as discussed in Section 2.2.1, the established metrics for system strength that are based on the fault level may not correctly represent the system's behaviour in the context of high IBR penetration. The need to mitigate against this broad set of potential operational challenges is often quantified via expressing a need for fault level. However, while it remains important and necessary to plan for potentially very low fault levels, not all actions to mitigate 'low system strength' challenges require an increase in fault level, suggesting that the single term 'system strength' can lead to ambiguity. Therefore, there is a need to make a clearer distinction between low system strength and low fault level issues. These are discussed in the subsections below.

2.2.2.1 System strength and quasi-steady state voltage sensitivity

When electrically distant from a strong voltage source, changes in system conditions such as network switching and load changes will lead to wider voltage variations, i.e. high voltage sensitivity. Assuming the converter controls are appropriately tuned for the prevailing system conditions, IBRs are as able as similarly rated SGs to maintain voltages at near-nominal levels during non-faulted conditions. However, they are less able to supply fault currents during a short circuit fault. Therefore, a distinction can be made between the issues associated with voltage sensitivity during non-fault conditions and the issues during fault conditions and a low fault level [51].

One of the most prominent emerging challenges concerning system operation is converter control interactions. IBR converter control loops typically have fast response times and can act over multiple timescales when regulating the current and power exchanged with the grid, which may lead to voltage and power oscillations across a wide frequency range [18], [50], [52]. Control interactions can be more prominent where the voltage sensitivity is high between IBRs.

The most cost-effective mitigation of high voltage sensitivity may or may not require an increase in the fault level. For example, mitigating actions for converter control interactions can include using damping control methods implemented in the existing or new IBR devices on the network [53], [54]. In addition, implementing grid forming (GFM) converters over traditional grid following (GFL) converters can reduce voltage sensitivity and make the grid appear ‘stiffer’ due to their voltage-source behaviour [41] and can be investigated as a mitigating action [55], even though these solutions might not contribute additional fault level above their nominal current ratings.

2.2.2.2 Fault conditions and fault level

During faulted conditions that lead to a voltage depression outside of statutory limits, the system’s state is dependent on the ability of sources within the network to supply fault current, and therefore, the fault level metric remains highly applicable. The system’s state is also dependent on the behaviour of IBRs during fault conditions, during which the IBRs implement different control modes to fulfil their FRT requirements, as described in Section 2.1.4.

A major impact of increasing penetration of IBRs and lower fault levels is on the performance of protection systems, i.e. the ability to detect, locate and clear faults in a timely manner. High penetration of IBRs can lead to an increased risk of delayed or failed tripping of protection relays, resulting in faults remaining on the system for a longer duration [56]. The impact depends on the type of protection scheme. For example, conventional over-current protection schemes will sense the magnitude of fault current, which is jeopardised by the lower fault current contribution from IBRs. In addition, protection schemes such as directional overcurrent and distance protection often rely on sequence components to detect the fault direction and select the faulted phase. Standard IBR control implementations do not produce zero sequence and negative sequence components, i.e. they supply balanced fault current for unbalanced faults, which can jeopardise the correct operation of these schemes [57]. Therefore, the protection system performance challenges are not only related to fault level magnitude, but also the different characteristics of the supplied fault current from IBR and can sometimes be addressed by improving IBR controls [58], [59].

As highlighted in Section 2.1.6, a consequence of a lower voltage magnitude and fast voltage angle change during faults can degrade the FRT performance of grid-following IBR due to its PLL controls losing synchronism [39], [60]. GFM converters are a potential solution as they can be less reliant on the PLL during fault conditions [61]. However, during a fault, a GFM converter is likely to still provide limited and balanced fault currents only in the positive sequence unless grid codes are modified to specify otherwise. Therefore, the GFM might not mitigate all low fault level issues [62].

2.2.3 Section summary and relevance to the research

This section (2.2) has qualitatively reviewed the concept of system strength and its relationship to fault level. It finds that established metrics for system strength may not accurately represent system behaviour in the context of high IBR penetration. A key distinction is made between fault level contribution and voltage sensitivity, which is later shown in Chapter 5 to be important. Chapter 5 demonstrates that fault levels in Scotland are expected to significantly increase, going against the common narrative of reducing fault levels, and leading to improved voltage magnitudes during faults.

2.3 Frequency stability and control

Maintaining the system frequency is an essential part of system operation. In GB, NGESO has a license obligation to maintain the frequency within defined limits, achieved by procuring a range of services from generators, storage systems and demand users. The main factors determining the size and speed of system frequency deviations and its ability to return to a stable state following an imbalance are the system inertia, the amount and speed of frequency responsive reserves and the inherent damping of the system loads. In recent years, the increase of non-synchronous technologies has presented challenges to frequency management due to reducing system inertia. This section covers the basic principles of frequency stability, the requirements in GB, the ancillary services, and the automatic defence measures in place.

2.3.1 Frequency stability

According to [23], frequency stability is "*the ability of a power system to maintain steady frequency following a severe system upset resulting in a significant imbalance between generation and load.*"

In large, interconnected power systems, such as in the continental European grid, frequency stability concerns are often related to system splitting, where areas become detached from one another, and each area must reach a new equilibrium. In island systems, such as in GB, frequency stability concerns are usually related to the loss of a significant proportion of the system's generation or load. Considering single contingencies (i.e. N-1), the most onerous situation is typically losing the largest generator (in MW output terms), referred to as a 'loss of infeed' (LoI) event.

The system frequency is a measure of the active power balance of the system. i.e. it is balanced if the power generated is equal to the power demand, including losses. A simplified form of the swing equation is shown in (8) and describes the relationship between the system power balance and the rate of change in system frequency (df/dt or RoCoF).

$$\frac{df}{dt} = \frac{f_0}{2 \cdot H_{system}} \cdot \Delta P \quad (8)$$

where f_0 is the nominal frequency, H_{system} is the total system inertia and ΔP is the balance between power generation and system demand: $\Delta P = P_{load} - P_{gen}$.

The RoCoF is directly proportional to the size of the power imbalance and indirectly proportional to the total inertia of the system. Conventionally, the system inertia is defined by the total stored energy in the rotors of all synchronous machines. During a generation deficit, a decelerating force is applied to the rotors, causing the system frequency to decline at a rate defined by the system inertia. As the rotors are mechanically coupled to the grid, their kinetic energy is released, providing a natural balancing effect. The inertial response of the system is delivered almost instantaneously and lasts for a few seconds. Therefore, it influences the initial period of frequency decline. Figure 8 shows the typical transient response of the system frequency to a loss of infeed event.

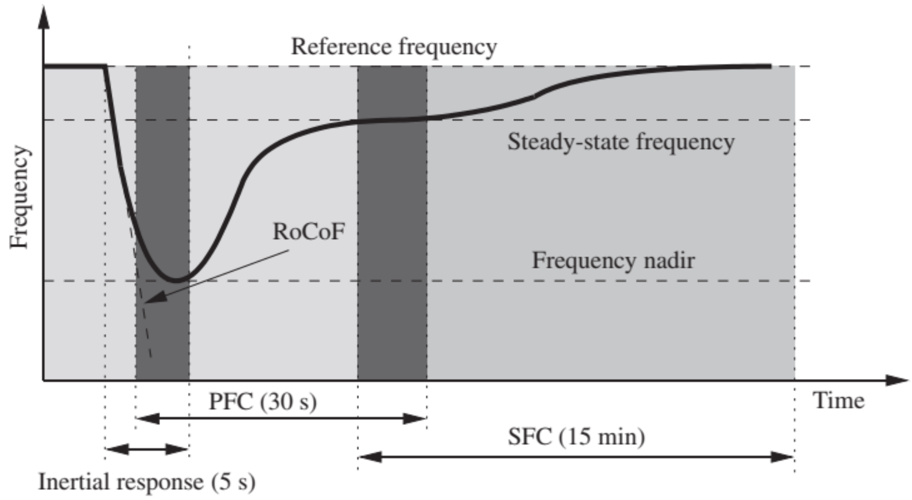

Figure 8: transient response of the system frequency during a loss of infeed event, showing the timescales of inertial response and frequency regulation [35]

Traditionally, there are three main timescales in which power reserves are delivered to the system to address the power imbalance. The inertial response is the first, which affects the initial rate of change and gives time for other power reserves to be delivered. The second is Primary Frequency Control (PFC), e.g. automatic action from governor systems or power electronic control systems, which act to contain the initial decline in frequency. The third stage is Secondary Frequency Control (SFC), which consists of slower-acting but longer-duration reserves to return the frequency to its reference value. SFC is not discussed further in this Thesis as the timescales these services operate are outside the timescales considered.

2.3.2 Frequency response services in GB

According to the SQSS and the Grid Code, NGESO must operate the GB system within a tight range of frequency limits for pre-defined contingencies [8], [30]. The normal operating frequency range adopted by NGESO is ± 0.2 Hz. However, during transient conditions, 'infrequent' frequency deviations are allowed to a minimum of – 0.8 Hz but must be recovered within 60 seconds. Therefore, in practice, NGESO operates the system such that the loss of the largest infeed does not breach 49.2 Hz. Power reserves are procured to fulfil the operational frequency criteria, which either increase or decrease the power setpoint of generators and demand users through various frequency response and reserve services.

Traditionally, the main service for containing post-fault frequency excursions in GB is Primary Frequency Response (PFR). PFR is delivered by de-loaded SGs with turbine governor control systems. However, SG governor controls have some inherent delay, which is incorporated into the service requirements. It is clear from the swing equation in (8) that the RoCoF increases as inertia decreases, meaning that, in a low inertia system, the frequency is more sensitive to change for the same power imbalance. This effect is more prominent in isolated systems such as GB. As the penetration of IBRs displaces SGs (along with their inherent inertia properties), faster frequency response products are required [63].

More recently, some types of IBRs, e.g. BESS with lithium-ion battery cell chemistry, have been participating in PFR markets. The power converters used in IBRs can be controlled to respond much faster than SGs, allowing faster response services to be designed [17], [64]. NGESO has launched a new suite of frequency response services in GB, categorised into pre-fault and post-fault services. Two new pre-fault services exist: Dynamic Moderation and Dynamic Regulation (DM and DR). These services provide a continuous response within the normal operating range of ± 0.2 Hz. DM and DR will make minor adjustments to keep frequency more constant and within operational limits. The new post-fault service, Dynamic Containment (DC), delivers a fast-acting response designed to arrest the system frequency following a large loss of infeed and during low inertia scenarios. The post-fault services, i.e. PFR and DC, are of most concern for the work in this Thesis and their main technical requirements are summarised in Table 2.

Table 2: Comparison of traditional primary frequency response and new dynamic containment frequency response services [65]

Requirement	Primary response	Dynamic containment
Frequency deadband (Hz)	0.015	0.2
Maximum delay to first response (seconds)	2	0.5
Time to full delivery (seconds)	10	1
Minimum duration of sustained delivery (minutes)	0.5	15

2.3.3 Unintended operation of RoCoF protection

Distributed Generation (DG) has not traditionally contributed towards maintaining the system's stability in the same way that larger transmission system connected generating units do. This is mainly attributed to DGs not being required to remain connected to the system during disturbances. In GB, DG must install Loss of Mains (LoM) protection, designed to disconnect the generator and prevent unintentional islanded operation on the distribution network.

Early versions of the DG connection code in GB required DG to disconnect from the network if the locally measured RoCoF exceeded the maximum threshold of 0.125 Hz/s. In a low inertia system, protection devices with these settings proved overly sensitive and can undesirably trip in response to system-wide power imbalances, worsening the effects of the original disturbance [14], [66]. Through the 2010s, a considerable amount of DG was added to the distribution networks in GB [14], and the risk of losing infeed from DG became a dominant constraint on the system when managing frequency.

To manage this risk, NGESO has been required to intervene in the energy market to secure the system and ensure the RoCoF limits of DG protection are not breached during a LoI event. Operational actions include limiting the size of the largest infeed loss to the system, ‘constraining-on’ generation that was otherwise out-of-merit to add inertia and procuring more frequency response volumes. Constraining-on SGs for system inertia often requires curtailment of output from renewable generators, usually wind [67], ultimately increasing the system balancing costs.

Since April 2017, the updates to the connection standard have required DG to have RoCoF protection settings of 1 Hz/s with a time delay of 0.5 s [29]. Regardless of these technical code mandates, DG owners were slow to change protection settings, and changes proved challenging to enforce [68]. At the time of writing, the 'accelerated LoM change programme', which pays DG owners to update DG protection settings retroactively, has reduced the RoCoF risk on the system. However, the risk remains present, and the current operational procedure involves determining the expected consequential loss of DG, based on system inertia and forecast DG outputs, and including the DG loss within the largest loss of infeed to the system, increasing the volumes of frequency response required [69].

2.3.4 System frequency limits during severe contingencies

So far, the operational frequency limits, which apply to a pre-defined set of contingencies [3], have been discussed. However, during more severe events, i.e. those not normally secured against, the scheduled frequency response holding may be insufficient to cover demand, causing frequency to fall outside operational limits. Synchronous generators and motors, among other apparatus, have frequency limits which, if reached, will trigger their protection systems to disconnect them from the system to avoid damage. High frequencies (or high rotor speeds) can result in rotating machines losing synchronism (pole slipping), while a low frequency can cause machines to stall and generators to lose their auxiliary power supplies [32]. The Grid Code defines the frequency range over which the system's users must remain connected [30]. These limits and the main operational frequency limits from the SQSS [8] are shown in Figure 9.

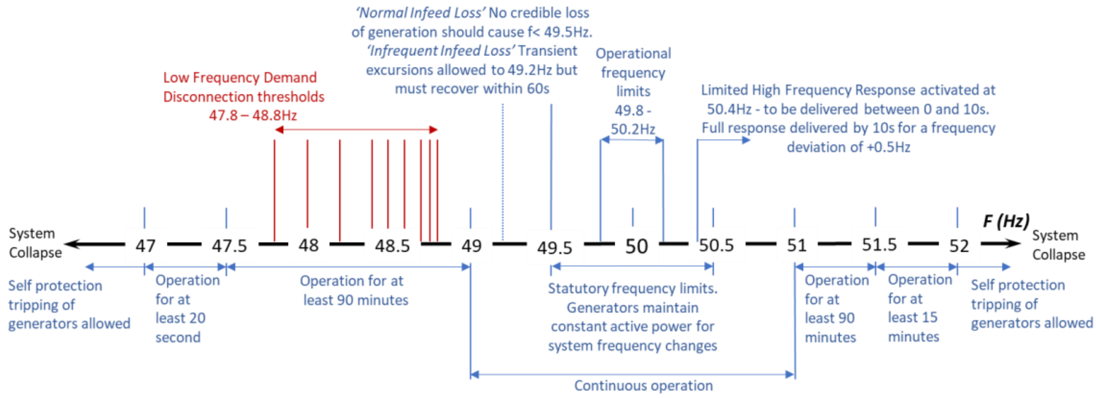

Figure 9 - Frequency range and connection requirements for users, extracted from the GB Grid Code and SQSS [8], [30]

Reaching under-frequency protection limits of generating equipment risks suffering a complete frequency collapse. To avoid such a situation, Low Frequency Demand Disconnection (LFDD)[3] schemes are implemented to automatically shed demand to restore

[3] In some countries the LFDD scheme is called the Under Frequency Load Shedding (UFLS) scheme.

system frequency and allow a new equilibrium to be reached [70], [71]. Traditional LFDD schemes are generally implemented in stages to prevent excessive load shedding and to allow the frequency to recover before the next step. The total load shed, the frequency range in which the scheme operates, the number of stages and the block size of each stage vary in different systems depending on the system characteristics. The conventional type of static LFDD scheme has offered reliability but is relatively inflexible and settings are hard programmed into relays. The proportion of load being shed at each stage and the time-delays between them are intended to be the same for every event. However, successful operation of the LFDD scheme is challenged by the increase in IBR penetration due to (1) the reduction in inertia and (2) the increase in DG capacity. As system frequency changes faster in a low inertia system, there is an increased risk that multiple stages of LFDD will be triggered before the previous stage has had enough time to operate. This can increase the risk of over-shedding demand, leading to an over-frequency situation, the loss of further generation and potential collapse of the system frequency [72]. In addition, as DG penetration increases and demand is increasingly met locally, the effectiveness of the LFDD scheme is challenged, and its success depends on the demand and generation mix downstream of each relay at the time of operation. Without visibility of DG, uncertainty is introduced into the amount of true demand on the system at any given time and, therefore, the net effect of automatic load shedding on system frequency when activated is uncertain [72], [73].

Several updated LFDD schemes have been proposed in the literature. Instead of local frequency measurements and fixed load shedding stages, adaptive schemes typically use additional information, e.g. measuring RoCoF and/or utilising wide-area frequency measurements made by Phasor Measurement Units (PMUs), to compute the amount of load to be shed and better suit the specific contingency [74], [75]. Many of the proposed techniques face practical challenges in real-world systems, as they rely on online monitoring and communications, which might not be available in distribution networks. Additionally, making centralised control decisions based on wide-area measurements introduces additional signalling risks and time delays, potentially compromising the reliability of the load-shedding schemes [72], [76].

LFDD schemes demand a very high level of reliability, and currently, very few adaptive schemes are in use worldwide [76]. While LFDD scheme settings and configurations require periodic review and updating [72], [77], [78], most TSOs, such as in GB and in Continental Europe, rely on a traditional staged approach [30], [79].

In GB, the relays are distributed throughout medium and high voltage distribution networks and isolate selected supply points to shed load [72], [80]. The LFDD scheme settings for the GB system are shown in Table 3. The table shows the cumulative percentages of demand that must be disconnected for Distribution Network Operators (DNO) connected to each TO area[4].

Table 3: LFDD scheme settings in GB [30]

Frequency (Hz)	**% demand disconnection for each distribution network operator in each transmission area**		
	NGET	SPEN	SSEN
48.8	5		
48.75	5		
48.7	10		
48.6	7.5		10
48.5	7.5	10	
48.4	7.5	10	10
48.2	7.5	10	10
48.0	5	10	10
47.8	5		
Total % demand	60	40	40

2.3.5 Section summary and relevance to the research

This section (2.3) has outlined the fundamentals of maintaining a stable system frequency, with emphasis on the GB power system. The background principles described in this section are utilised and referred in the analysis presented in Chapters 3, 4, 5 and 6.

In the next section (2.4), the concept of fault induced frequency excursions (FIFE) is introduced and reviewed. Then, in section 2.5, a review of existing literature identifies a need to study these frequency stability risks using spatially disaggregated models, which is not common practice. Chapters 3 and 6 contribute fault-induced frequency stability studies using multi-area power system models. It is found that in a future network with high IBR penetration,

[4] The three TOs in GB are National Grid Electricity Transmission (NGET) for England and Wales, Scottish Power Energy Networks (SPEN) for central Scotland, and Scottish and Southern Energy Networks (SSEN) for northern Scotland.

network faults can cause significant and rapid frequency variations, and these can be dealt with through updates to grid code requirements for IBRs.

2.4 Fault Induced Frequency Excursions: Underlying Mechanisms

This section reviews the key mechanisms that couple large voltage events (i.e. network faults) and frequency excursions. The two main mechanisms considered are the risk of unintended disconnection of power sources and the way IBRs respond when producing active and reactive power during and immediately after a fault, and are elaborated below:

(1) **Faults leading to the disconnection of generation.** A loss-of-infeed event can occur for several reasons, for example, an electrical or mechanical fault on the generation equipment or interconnection circuits, leading to the operation of the generator protection. However, generator disconnections can also occur due to instabilities induced by changing grid conditions, e.g. during a network fault.

(2) **The programmed vs inherent response of IBRs compared to SGs during faults**. The way that IBRs are programmed to respond influences the system's dynamic performance during the event. Often, reactive power provision is prioritised during fault. However, this must be provided at the sacrifice of its available active power to respect the strict thermal limits of the device, introducing the possibility of short-term active power deficits, which can lead to frequency excursions.

Increased IBR capacity and the changes to system dynamic behaviour often attributed to high IBR penetration can exacerbate points (1) and (2) above. For example, reductions in fault levels and inertia might imply the following:

- Reducing the fault levels increases the severity of a voltage depression, potentially driving more IBRs into FRT control modes.
- IBRs can introduce new unstable modes, e.g. controller interactions, potentially failing to ride through faults and causing them to trip (see Section 2.1.6 and 2.2).
- Reduced inertia and fault levels resulting in an increased sensitivity of frequency and voltages might also expose existing IBRs and SGs to more extreme system conditions than before, increasing the risks of transient instability of IBRs (Section 2.1.6) and SGs (Section 2.1.5).

2.4.1 Unintended disconnection of generation due to network faults

Modern grid codes typically require generators to ride through network faults, so they do not lead to generator disconnection and a subsequent power deficit. IBRs use active control systems that implement complex software to ride through disturbances. There have been several recent examples where network fault events led to undesirable control and protection system responses of both SGs and IBRs and caused either a permanent or temporary loss of generation.

This section reviews some of these international events where the spurious disconnection or de-loading of generators occurred because of network faults, causing an impact on system frequency.

2.4.1.1 GB system disturbance - 2019

On August 9th 2019, during an electrical storm, a lightning strike to an overhead transmission line caused a single-phase-to-earth fault that was subsequently cleared by local network protection systems. The disturbance led to the combined loss of two large generators, Hornsea offshore wind farm and Little Barford gas plant, and a significant loss of DG due to the operation of Vector Shift (VS), RoCoF or internal protection against under frequency. The total loss of power infeed from Hornsea and Little Barford was 1,378 MW, and there was an estimated additional loss of between 1,300 MW and 1,500 MW of DG. During the event, frequency response and reserve holdings became exhausted, and the system frequency dropped to 48.8 Hz, triggering the first stage of LFDD and cutting supplies to 1.15 million customers [68].

An unexpected wind farm control system response caused the de-loading of the Hornsea wind farm. The fault event triggered an un-damped electrical resonance, and most of the wind turbines were disconnected by automatic protection systems. For the little Barford gas plant, the steam turbine tripped due to a discrepancy in the speed signals after the network fault was cleared, which subsequently led to disconnections of the gas turbines. NGET, the TO, reported that the response of the electricity network and its protection systems to the lightning strike was as expected [81].

The electricity regulator in GB, Ofgem, made many recommendations following their investigation of the event. One of these recommendations was to improve the robustness of the processes for testing compliance of generators with the industry codes as well as improving the modelling of the performance of generators [68].

2.4.1.2 Northeast Scotland circuit faults - 2021

A circuit in the northeast of Scotland faulted twice in the nighttime and early morning hours of the 4th and 5th of April 2021. Both faults were cleared within expected primary protection timescales, and the circuits were restored by auto-reclose schemes. The first fault resulted in the loss of 915 MW and a frequency drop to 49.66 Hz, while the second fault led to the loss of 716 MW with a frequency dip to 49.74 Hz. At the time of writing, no detailed event report is available, and the number or type of generators that tripped is unclear. However, it is understood that the generators tripped due to non-compliant behaviour, as they should have ridden through the fault events according to the GB grid code [82].

2.4.1.3 Texas and California disturbances – multiple events 2020 - 2022

In the U.S., several disturbances resulting in undesirable responses by generator control and protection systems have been reported by the North American Electric Reliability Council (NERC). The selection of fault events reviewed here occurred in recent years in the Texas and California power systems. All events involved a normally-cleared transmission system fault that triggered generator de-loading, slow recovery or disconnection.

The San Fernando disturbance event in Southern California occurred on July 7th 2020, where two faults, the first a single-phase fault and the second a low-impedance three-phase fault, caused numerous solar PV resources to reduce power output. Network protection systems cleared both faults within three cycles. The reduction in PV power was found to be for three reasons: (1) some inverters ceased current injection during the fault, with varying recovery times, some being very slow, (2) some plants experienced partial tripping of inverters on inverter-level protections, and (3) active power reductions due to anomalous behaviour of the plant-level controller restricting power output and ramping it back over a period of minutes. Their behaviour did not meet the recommended performance guidelines [83].

The Odessa Disturbance in Texas took place on May 9th 2021, and led to the reduction of over 1,100 MW of solar PV resources in the Texas Interconnection. The fault occurred on a step-up transformer at a CCGT plant. The CCGT unit supplying 192 MW was subsequently tripped, and the fault was cleared. However, in response to the fault, power reductions occurred across several PV plants due to either inverter-level or feeder-level tripping or undesirable control system behaviour [84].

Another disturbance in Odessa, Texas, occurred on June 4th 2022. Again, the initiating fault event, a normally-cleared single-phase fault, occurred at an SG plant and tripped 535 MW of local generation. In addition, a separate SG facility tripped 309 MW of generation and, across a large geographical area, a total of 1,711 MW of infeed from PV generation was lost due to protection and control responses across multiple sites. In this case, the size of the disturbance nearly exceeded the security criteria, but the responsive reserve was able to arrest and recover the frequency [85].

The Panhandle wind disturbance occurred on March 22nd 2022, which resulted in a reduction of wind power across the Texas Panhandle area. Two transmission network faults occurred during severe weather conditions, such as freezing rain, snowfall, and high winds. The two faults occurred within a half-hour period, and both were normally-cleared phase-to-phase faults. The first tripped 273 MW of wind generation, leading multiple other WTs in the area to reduce power output by 492 MW. Similarly, the second fault led to multiple WTs reducing their power output by 457 MW. The most common reason for the power reductions was reported to involve controller interactions that hindered the ability of the plant controllers to return the power to its pre-fault level [86].

2.4.1.4 Victoria, Australia power system fault - 2023

On July 9th 2023, a flash-over fault in a current transformer resulted in tripping a 500 kV line and 500/220 kV transformer in the state of Victoria, Australia. The fault was cleared in 117 ms by the circuit-breaker-fail protection scheme, slower than primary protection but within expected timescales for backup protection. The incident led to the islanding and disconnection of 254 MW of wind generation, as expected. However, addition incidents occurred on four other wind farms; one tripped entirely, two partially tripped (with several individual turbines disconnected reducing the plant’s output), and the fourth temporarily reduced its output and ramped back over 46 seconds [87].

There was no further impact on the broader power system or loss of loads. Nonetheless, the event highlights the potential for faults to trigger unexpected responses from generating facilities, which can affect the overall contingency size.

2.4.1.5 Common threads and conclusions of reviewed events

All these events involved abnormal responses of generation to network faults. The events involved SGs and IBRs. In some cases where IBRs lost power, they remained online but showed undesirable control system behaviour that led to temporary reductions in power that were sometimes recovered too slowly.

The abnormal responses of control and protection systems were generally non-conformant to the local technical requirements for interconnection. Concurrent and unexpected losses of generation can pose a serious threat to the system's reliability. Where the sources of the reduction in the power supply are widespread and many different factors can contribute towards the issue, the impact can be high, and the issues are difficult to detect in advance.

Wind and solar PV farms are modular by design. The generation plant consists of many smaller units with individual protection and control systems that are typically interconnected via plant-level controls to deliver the required aggregated performance at the Point of Connection (PoC). A particular inverter design and inverter controller will usually be common across the plant level, and the same inverter might also be used in many other plants connected to the network with different owners. Therefore, an incorrect response, which might only be revealed by a particular type of disturbance, could affect many different generation facilities. Hence, these types of problems can be systemic in nature.

The events in GB and the US all highlighted gaps in the suitability of the connection studies. The type of issues highlighted are rarely captured before or during the commissioning phase of the plant. Particularly for the events in the U.S., where repeated issues are shown, the IBRs are not configured to perform in the same way as was apparently studied in the connection process [85]. Furthermore, a key factor to consider in the connection study process is the accuracy of the model provided to the TO or SO (or whichever party is responsible for the studies). Another aspect is whether the models provided include sufficient detail for Electromagnetic Transient (EMT) analysis tools and whether the surrounding network is modelled in the EMT domain to capture all the possible control system interactions.

One thing is clear: countries worldwide are installing IBRs at pace, and the amount of mass-produced modular generation units in the system is set to increase rapidly. Robust assessments should be able to study how new technologies will respond to a wide variety of system events as accurately as possible. Furthermore, the development of methods to classify, assess and manage new types of risks may be required by system operators. These events show that there may be an increased risk of infeed loss resulting from network faults, increasing the interaction between fault events and system frequency excursions.

2.4.2 Effects of fault-ride-through requirements on system frequency

During a fault, IBRs enter FRT mode as mandated by most grid codes. FRT requires the IBR to remain connected to the grid and dictates the kind of responses the asset should provide during voltage dips. It is common for grid codes, such as in GB [30], to prioritise reactive current over active current during the fault to provide dynamic voltage support. Hence, current-limited IBRs might have to reduce their active current to deliver the requirement for voltage-dependent reactive current.

Another important factor affecting frequency dynamics during transient fault conditions is the active power recovery profile following fault clearance. During the fault recovery period, SGs typically recover their active power very quickly (in milliseconds), whereas the speed of active power recovery can be limited in IBRs due to the mechanical constraints of the turbines [88].

The curtailment of active power during faults and the sustained reduction in active power post-fault can lead to short-term active power deficits that might impact the system's frequency. On the other hand, several works that are discussed in this section suggest that a slowing down of active power recovery rates of IBRs can benefit the angular stability of SGs. Therefore, the FRT requirements of IBRs significantly influence the system's dynamic performance during transients, including voltages, SG transient stability and frequency stability. The literature on FIFE and active power recovery of IBRs is reviewed further in this section.

2.4.2.1 Fault-induced frequency excursions

Most publicly available system stability studies regarding FIFE have been performed on the all-island power system on the island of Ireland (the combined Ireland and Northern Ireland networks). The island of Ireland system is a relatively small synchronous island network with a high penetration of non-synchronous generation. The island of Ireland Grid Code requires that, during transmission system voltage dips, IBRs shall provide voltage-dependent active power, which is given priority over reactive power [89] (i.e. the opposite of GB and many other grid codes).

The studies performed in [88] highlight the potential for increased coupling between voltage and frequency dynamics in systems with high wind penetration. This work uses the IEEE 39-bus New England test system to study the impact of post-fault delayed active power recovery from wind farms. In this study, the WT controls are aligned with the island of Ireland grid code requirements (active current priority). The study identifies that the delayed active power recovery of WTs can lead to a frequency excursion, which is more severe during high wind penetration (penetration levels of up to 60% were assessed). This study discusses potential mitigating solutions, including dynamic reactive power compensation to improve the voltage profile, introducing fast frequency response and changes to grid code requirements. However, these aspects are not quantitatively assessed.

The study in [90] evaluated the frequency stability challenges for the island of Ireland system considering high wind power penetration. This study introduced the widely used 'system non-synchronous penetration' (SNSP) ratio as a measure of the instantaneous IBR power penetration in the system. The SNSP is used as an operational limit in Ireland to ensure system stability and is defined as

$$SNSP = \frac{P_{wind} + P_{HVDC(import)}}{P_{load} + P_{HVDC(export)}} \tag{9}$$

The frequency stability studies in [90] considered both conventional contingencies, i.e. the loss of the largest infeed and the temporary loss of power due to faults. It was found that a voltage disturbance in the island of Ireland system during operational periods with a high SNSP can represent a more severe contingency than a loss of infeed and result in a lower frequency nadir.

Reference [91] is an updated study focusing on the impacts of wind farms' FRT behaviour on system stability in the island of Ireland grid. This study is by the TSOs on the island of Ireland and uses recorded PMU measurements and a complete dynamic model of the network and control models provided by plant owners. The study considers several sensitivities around the delayed delivery of active and reactive power responses from WTs during and after faults. It notes that responses from some IBRs in the system can be outside those required by the grid code. The authors propose that technical challenges arising from the non-ideal FRT behaviour of wind farms can be mitigated through TSO led measures.

The TSOs on the island of Ireland developed a suite of new ancillary services products as part of the 'DS3' programme [92]. The proposed services include adding synchronous inertial response, increasing the speed of frequency response services, implementing 'Fast Post-fault Active Power Recovery' (FPFAPR) and increasing the available dynamic reactive power. The FPFAPR service incentivises generators to provide fast post-fault active power recovery to mitigate the impact of voltage events on the system frequency. FPFAPR requires that active power export be recovered to at least 90 % of its pre-fault value within 250 ms after the voltage recovers to at least 90%. The DS3 program also introduces faster frequency response services [91], [93]. However, the study in [91] does not assess the relative benefits of each of these services or their impact on other aspects of the system's dynamic performance, e.g. voltage or angular stability.

2.4.2.2 Influence of active power control

The studies from Section 2.4.2.1 show that, for the island of Ireland system, controlling the active power profile of IBRs can improve possible FIFE issues. The studies focus on faster active power recovery rates. However, several other studies have investigated active power control of IBRs during the fault and the fault recovery period, as a means of improving the transient stability of SGs. In general, the approach found to improve transient stability is to reduce active power from IBRs during the fault and slow down its recovery, i.e. the opposite approach to the island of Ireland grid code and DS3 services.

Referring to Section 2.1.5 and the swing equation in formula (4), the rate of change of angular deviation of an SG is higher for a greater imbalance between P_m and P_e. During the fault and a reduced P_e, any means of increasing the exported power of an SG could reduce the rotor acceleration. As such, it has been found that, in some circumstances, when a IBR is electrically close to the SG, its reactive current support can improve voltages, reduce the reactive power burden on the SG, and improve its stability margin [94]. A braking resistor is another method to increase the exported power and transient stability. The braking resistor is switched in between the SG and the fault so that the SG can dump energy through this resistance and increase its P_e, resulting in a lower accelerating power [95].

An SG's angular stability can also be improved by reducing the IBR active power output as far as possible during the fault [96]. However, this benefit depends on the location of the IBR to the SG and many other influencing mechanisms, such as generator control modes, making it a complex problem [94], [96]. The active power recovery ramp rates of IBR might also influence the transient stability of SGs. Some studies have shown that, depending on their relative location, slower ramp rates applied in the WT control can improve the transient stability of the SGs in the studied systems.

The work in [97] provided an extensive review of grid code requirements for wind power and early practical experience of the dynamic behaviour of wind in power systems. Studies for the German power system (from 2012) identified that rotor angle stability can be improved by slowing down the active power recovery rate of WTs. The examples given in [97] suggest that the recovery rate should be 10 % to 20 % of the WT rating per second. However, more recent grid code requirements are often much faster and can mandate full recovery of active power within 1 second or less [30].

The study in [98] investigates the effect of the FRT behaviour of voltage source converter (VSC) HVDC-connected offshore wind farms on the dynamics of AC/DC power systems. Time-domain simulations were performed on a sample test system and a Northwestern Continental European system with a 2025 time horizon. The study analysed the active power recovery rates of the onshore VSC system, and it was found that slower recovery rates influence the AC system dynamics, slowing down the acceleration of SGs in the post-fault period. These impacts were also shown to be less prominent for stronger systems, i.e. those that are relatively large with higher inertia and fault levels. The study also notes that future systems with fewer conventional power plants and reduced total rotating inertia will have increased effects on system stability. However, this work does not consider faults that lead to large active power deficits.

[99]–[102] also investigate active power recovery from the WTs. The general findings are that a longer active power recovery in exporting areas can assist the local SGs in supplying more

of their kinetic energy to the load (like the braking resistor concept). However, these studies are performed on highly simplified or standardised test systems. Studies in [100], [101] consider a single-machine infinite bus system and [102] considers a three-bus representation of the GB system, where a WT is connected adjacent to a highly loaded SG located behind the fault on a single constrained transmission route. The work in [99] assesses adding a WT connection to the IEEE 16-machine 68-bus system. However, this is the only WT in a system dominated by SGs. The setup used in these studies does not allow for the effects of a fault propagating in a meshed network and causing a fault-induced active power deficit from multiple IBRs.

2.4.3 Section summary and relevance to the research

This section (2.4) reviewed real-world international examples of fault events leading to generator disconnections and examined the impact of FRT requirements on system frequency and angular stability. The events reveal that generators may exhibit undesirable, non-conformant behaviour during network faults, potentially causing temporary power loss or tripping, thereby increasing the risk of infeed loss and system frequency excursions. Additionally, due to the current-limited nature of IBRs, FRT requirements can result in short-term active power deficits during transients.

Later in this work Chapter 3 explores fault-induced frequency stability in a two-area fictitious power system, demonstrating that the severity of voltage dips and WT current control significantly affect the post-fault frequency dip. The findings suggest reconsidering the approach of maximising reactive current during faults in high-IBR systems.

In response to these challenges, TSOs in Ireland have introduced new services prioritising active power delivery through ancillary services. However, other studies indicate that prioritising reactive power during faults and allowing slower active power recovery may better support voltage and angular stability. Later, Chapter 6 assesses FRT requirements in relation to the GB system and finds that faster active power recovery can enhance SG angular stability and frequency stability in the cases studied. Furthermore, Chapter 6 concludes that adjusting FRT requirements can yield greater benefits than procuring fast frequency response or increased system inertia through ancillary services.

2.5 GB system stability studies: literature review

This section reviews the prominent literature concerning system stability studies in the GB transmission system. The section is separated into two parts; works focusing on frequency stability, where it is common to use lumped equivalent models for both the network and its power sources, and those focusing on voltage or transient stability, where spatially disaggregated models are required. Traditionally, frequency and voltage events have been studied separately. However, as shown in section 2.4, frequency and voltage phenomena are intrinsically linked.

2.5.1 Frequency stability studies

The work in [63] discusses maintaining frequency stability in GB. The studies are performed on a 'single bus' model to represent different operational conditions and response providers. The work highlights that, as inertia declines in the system, the current frequency response services (in particular PFR, see Section 2.3.2) are insufficient to keep frequency deviations within practical limits, which calls for additional measures to ensure system security. The study finds that the activation delay and time to full delivery of frequency containment services becomes more critical to manage system frequency within RoCoF and frequency limits in low-inertia scenarios. At the time of publication of [63] (2020), which remains relevant at the time of writing, the SO had implemented a temporary solution by limiting the largest loss risk, but the study highlights that this is not a sustainable long-term solution and faster frequency responses are required.

Some other studies also utilise generic frequency control models (equivalent to 'single bus') to demonstrate the effects of declining inertia in GB and the influence of increasing the speed of frequency response. For example, the authors in [103] demonstrate that the amount of reserve power can be reduced by deploying a faster frequency response when containing a loss-of-infeed event. In [104], a single bus representative model of GB built-in PowerFactory is proposed and validated against a real disturbance event. This work focuses on understanding the relationship between the penetration of IBR and frequency management. It highlights that the amount of IBR penetration is not an inherent limitation to frequency containment and does not account for other factors, such as critical inertia. Further, a method is presented to develop expressions that help quantify the factors contributing to these limits.

Frequency stability assessments on moderately sized island systems such as GB are often performed on a single bus model, and this is typical industry practice in GB and the EU [78], [105]. Single bus models usually suffice in respect of the main effects and assessing the need for volumes of frequency response and reserve. In practice, and especially during transient system conditions, the frequency varies throughout the system, and there is no such thing as a single system frequency. These studies and Section 2.3.1 demonstrate how the reduction of system inertia impacts frequency stability at the system level. However, inertia distribution affects the dynamics within and between different areas of a synchronous system.

In [106], the authors investigate conditions for regional frequency stability in a mathematical representative model of a two-area GB power system split across the Scotland-England boundary. The case studies highlighted that inertia and frequency response cannot be considered system-wide magnitudes in power systems with inter-area oscillations in frequency. The findings suggest that there may be a higher need for ancillary services than in the uniform frequency model. The study proposes a methodology to represent these conditions as linear constraints and presents a generation-scheduling model that optimizes energy production and ancillary services.

A wide-area measurement-based frequency control solution was investigated in the Enhanced Frequency Control Capability (ENCC) project [107], a nationally-funded innovation research project with NGESO. Figure 10 illustrates the variation in frequency at different locations in the GB network following a loss of infeed event [107]. Variations in local frequency (and corresponding local RoCoF) are largest immediately after the event and converge soon after the event: in this case, within approximately 1 second. At the time of writing, GB has no defined regional frequency response requirements [16].

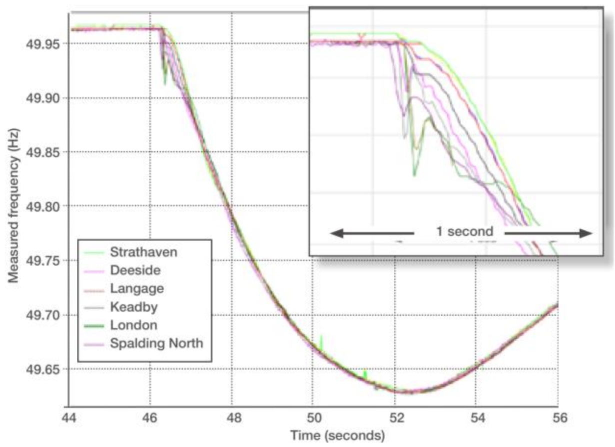

Figure 10: variation in frequency at different locations in the GB network following a loss of infeed event, image from [107]

2.5.2 Transient stability and fault analysis studies

The studies reviewed in the previous section were focused on frequency stability and consider a loss-of-infeed event as the disturbance event. The assessment of many other system stability mechanisms, e.g. transient or voltage stability, requires modelling the network impedances and the connecting elements, and network faults are often the concerning disturbance event (e.g. short circuits to transmission lines).

At least some spatial representation of the network is usually required to represent the propagation of voltage magnitude dips and voltage angle movement during a disturbance. Many factors, such as network power flows, fault levels, system-wide and regional inertia, and network topology, affect the system's stability in response to severe network faults [7], [35]. This section concerns GB system stability assessments. Most published studies reviewed utilise the National Grid ESO 36-bus GB transmission system model (here referred to as the 'NG 36-bus' model), which has recently been made publicly available [108]. This model was originally developed by National Grid in PowerFactory software intended for RMS simulations and is based on network data from 2013. Therefore, most authors of the following studies are expected to have made some updates or amendments to the model depending on the type of study and when it was performed.

The study in [109] cites the challenges with low system inertia and fault levels in GB that can lead to instability. The NG 36-bus model is used to investigate the improvements that can be made from adding a SC and a STATCOM considering a fault on the Scotland-England boundary (one of the two double circuits, typically considered the worst-case secured fault). The study shows that the SC and STATCOM units can increase the short circuit level and provide reactive power support during and after the three-phase line fault. The focus is on the potential improvements to the voltage profile.

[110] also uses the NG 36-bus model to investigate the effects of the spatial distribution of inertia in the system. Similar to [103], the study demonstrates that the speed deviation of synchronous machines can be greater when located far from the bulk of the inertia, i.e. high local RoCoFs can occur. In addition to higher local frequency deviations, [110] finds that the magnitude and frequency of inter-area oscillations and the Critical Clearing Time (CCT) of embedded transmission lines can increase between low and high inertia areas.

The NG 36-bus model is used in [111], which performed stability studies to investigate the maximum system non-synchronous penetration limits in GB. Like in [109], a 3-phase double circuit fault across the Scotland-England boundary is considered in various dispatch scenarios, including consideration for a future version of the grid in 2030. It was found that exceeding 65 % IBR penetration would result in instability. This analysis focuses on the transient stability of an equivalent SG in Scotland. The study highlights that IBR penetrations of greater than 65 % will be required in the future and that adding 9 GVA of SCs in the system can increase the penetration ratio to 80 %. However, it is highlighted that the SCs are unlikely to be either the only or the most economical solution. This work acknowledges that the stability analysis conducted is narrow in scope, and that other aspects of system stability during high IBR penetration must be studied. The work also concludes that options for solutions should be defined and that these are likely to be a mix of options, from adding synchronous assets to making IBR control system adjustments.

In [112], a 'swing equation based inertial response' (SEBIR) control strategy is investigated in the NG 36-bus model. The SEBIR control is a form of 'synthetic inertia' like several other documented approaches, such as [113]. Although most WTs are decoupled from the grid, kinetic energy is still available in the rotor. Synthetic inertia control extracts the stored energy from the rotor, which causes the rotor to decelerate as it provides extra power to the grid. However, after the initial frequency transient, the rotor must re-accelerate to its optimal speed, requiring energy to be drawn from the grid, which, if not appropriately controlled, can lead to another frequency transient [114]. The study in [112] finds that, in some cases, the IBR penetration limits can be marginally improved when implementing SEBIR control with higher values of the synthetic inertia constant. However, the improvements depend on system conditions and, in some cases, the system's stability can be degraded by SEBIR control. Furthermore, the work does not study the possible negative impacts of the recovery period.

The IBR penetration limits observed in [111] were improved by adding SCs to the system. In addition, the technical limitations of synthetic inertia control show that it may not provide a promising solution. In this context, the work in [115] revisits the stability challenges found in GB from [111] and investigates the use of the Virtual Synchronous Machine (VSM) converter control strategy to increase IBR penetration limits. The VSM is modelled as a voltage source behind an impedance but has current limiting during faults. The studies suggest that, using the VSM converter model and the NG 36-bus model, VSM can potentially increase the penetration level of IBRs while maintaining transient and steady-state stability. Assuming a minimum level of VSM is present, the study finds that 100 % penetration of IBR can be achieved.

Another study in [116] assesses the IBR penetration limits in the GB system and the use of grid-forming converter control to improve them. This work uses the same NG 36-bus GB model but with EMT modelling assumptions to overcome some of the limitations of RMS modelling tools. As such, this study assesses short-term voltage stability, i.e. during faults, and long-term voltage stability, i.e. post-fault quasi-steady-state period. The study finds that sub-synchronous oscillations in the system voltages can be observed due to control interactions in the IBRs for IBR penetration above 68 %. Like in [115], [116] finds that maintaining a share of IBRs with the grid-forming strategy can increase the overall IBR penetration from this perspective. The percentage of grid-forming IBR that achieves a given IBR penetration is a system-dependent variable that depends on, for example, their location in the grid, grid impedance, and power flows.

2.5.3 Section summary and relevance to the research

This section (2.5) reviewed published works on GB transmission system stability. Frequency stability studies typically focus on the speed and volume of response, using single-bus equivalent models and considering the largest loss of infeed event. However, the dynamics of 'network-side' short circuits are often overlooked. Chapters 3 and 6 of this Thesis extensively assess fault-induced frequency excursions.

Many transient stability studies focus on the maximum IBR penetration before instability occurs, typically analysing the worst-case fault, such as a double circuit fault across the Scotland-England boundary. However, existing studies have not addressed faults that lead to significant active power deficits or their interactions with frequency stability. In Chapter 6, a novel screening process and metric is developed to identify worst-case conditions from a fault-induced frequency stability perspective.

Some existing studies highlight the regional effects of inertia and localised frequency sensitivity. However, little attention has been given to the risks of increased regional frequency deviations during faults in GB. Chapter 6 addresses this gap by examining the growing risk of localised generation or load tripping due to faults. Chapter 6 also provides several recommendations for potential grid code changes to address the challenges posed by fault-induced short-term active power deficits in IBR-dense areas of the GB power system.

2.6 Functional specification of required power system models

The remaining parts of this Thesis will develop and use power system models to generate results for analysis seeking answers to the research questions. This Section outlines the functional specification required for these power system models to simulate fault events and their impact on system frequency stability. Specific network topologies and descriptions of models used are found in Chapters 3 and 4.

Modelling Objectives:

- To simulate the system's transient response to balanced three-phase network faults.
- To assess the impact of network faults on critical system variables including frequency, voltage, phase angles and SG rotor angles.

- To have flexibility in adjusting key control parameters of model components to assess their impact on the system variables.
- To assess varied system operating conditions and scenarios to enable the identification of critical states that may lead to instability.
- Specific network topologies should provide sufficient resolution to address the specific study topic.
- Steady-state and dynamic models of power system elements should provide a representative response to what is seen in real-world power systems while considering the study requirements.

Modelling technique:

Modelling power system stability involves using various techniques to simulate and analyse the system's dynamic response to disturbances. Time-domain simulation (TDS) is commonly employed to capture the system's transient behaviour over time, enabling simulation of faults. Frequency-domain analysis, on the other hand, focuses on the system's response to disturbances across a range of frequencies. It is particularly useful for assessing small-signal stability and understanding how the system reacts to oscillations or resonance conditions.

This work performs fault analysis using TDS such that the dynamic and time-varying effects of large disturbances are captured. TDS captures transient behaviours, events and controls, such as system inertial responses, frequency responsive assets and operation of protection systems.

Model Bandwidth:

In TDS, time is divided into discrete time steps, and the simulation progresses by iteratively solving mathematical equations that describe the system's behaviour at each time step. Figure 11 shows the timescales of different classes of power system phenomena [31].

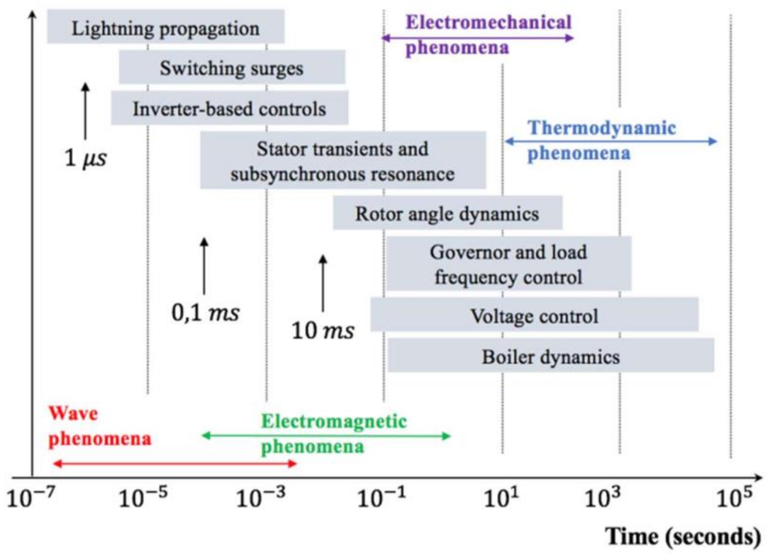

Figure 11: Timescales of power system phenomenon [31]

The equations being solved by the model over time depend on the modelling technique being utilised: Root Mean Square (RMS) or Electromagnetic transients (EMT). The fundamental difference between EMT and RMS is how the circuit elements are mathematically represented. EMT analysis uses the instantaneous values of the sinusoidal voltages and current. This is done by solving the differential equations of the resistive, inductive and capacitive elements of the network circuits. RMS modelling simplifies these differential equations by representing the circuit elements with algebraic equations. The simplification of the differential equations means that RMS modelling represents the voltages and currents as phasors (i.e. voltage magnitude and phase angle) and are only considered at the fundamental frequency.

As EMT modelling preserves the sinusoidal waveforms and captures harmonics at frequencies other than the fundamental, it has a higher computational burden and slower simulation times compared to RMS. Additionally, EMT models often require more detailed component representations [117]. Achieving a balance between accuracy, data requirements and computational efficiency is crucial to enable simulations of large-scale systems within reasonable timeframes. However, the choice between RMS and EMT simulations also depends on the specific phenomenon being studied. Voltage dips that result from network faults, frequency and rotor angle stability can all be effectively analysed using RMS modelling, which is the method chosen for this work.

RMS tools do not capture some of the very fast transients and control behaviours of IBRs and are more suitable for timesteps down to a few milliseconds [118]. This presents a limitation of the simulation techniques used in this Thesis, where some instabilities that can arise in the fast-acting controllers of IBRs occur with time periods of microseconds. In addition, harmonic frequencies other than fundamental frequency are inherently absent in RMS modelling. As a result, some forms of IBR controller instability cannot be well represented by RMS modelling [47], [117].

All modelling in this Thesis is performed using the 2022 version of DIgSILENT PowerFactory software.

Chapter 3: Impact of Wind Generation on Fault-Induced Frequency Excursions in a Two-Area Test System

Chapters 1 and 2 introduced and discussed some of the challenges that can arise in systems with high a penetration of wind generation and other types of IBRs. Section 2.4 identified that the interactions between network faults and the system frequency could increase. In particular, the concept of fault-induced frequency excursions (FIFE) was introduced and, while it has been studied in some existing power systems, some gaps were highlighted that warrant further investigation.

Understanding the underlying system behaviours that lead to possible instabilities is crucial to operating a secure and reliable power system. This Chapter identifies the fundamental mechanisms by which network faults can result in a short-term deviation in the system frequency during the post-fault period. An essential aspect of the FIFE phenomenon is its relationship with the voltage magnitude during a fault. Hence, voltage and frequency become more interlinked, requiring the analysis of both system properties in study areas that traditionally would have considered them in isolation.

This chapter seeks to build on and consolidate the existing body of work by clearly identifying the main influencing factors of the FIFE problem. To achieve this, a simple test system is developed to reduce the complexity of the studies. First, a clear overview of the fundamental mechanisms that lead to a FIFE and the relationship with voltage dip severity are presented. Then, the impact of a FIFE event causing the unintended disconnection of load through triggering the LFDD protection scheme is assessed, highlighting the risk of quickly transitioning from a low-frequency to a high-frequency event. An analysis of the influence of WT current controls on the extent of possible FIFE events is also performed, including possible amendments to control parameters and strategies to improve the system frequency.

3.1 Test System

In this section a test system is developed to assess the effects of network faults on system frequency and meets the requirements of the model functional specification described in Section 2.6. The test system represents a small and highly simplified network where a large proportion of its generation capacity is distant from the load centre. The system does not intend to represent any real system, but rather emulates a situation where the power transfer from the remote generation source can be interrupted by a fault. The test system consists of two areas interconnected through a 100 km double-circuit AC transmission line with an N-1 transfer capacity of 2,000 MW. The system has a fixed active power demand of 5,000 MW at unity power factor. The test system is shown in Figure 12.

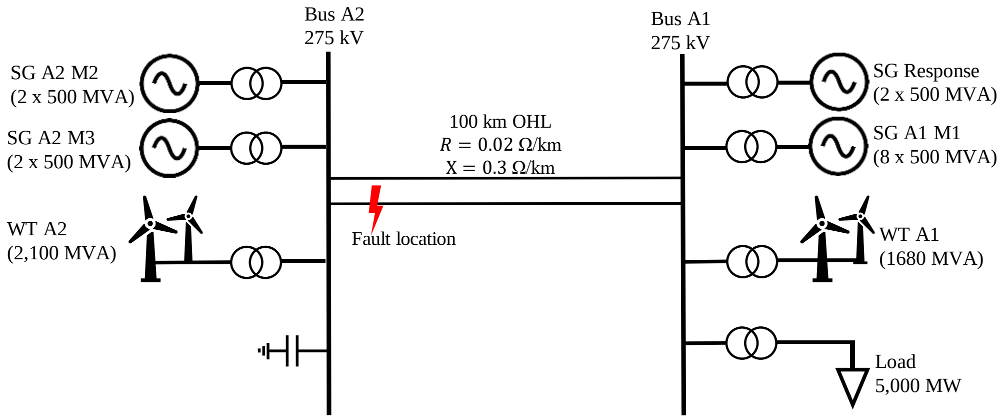

Figure 12: two area test system

The load is supplied by generation connected in both areas and has an initial installed synchronous generation capacity of 7,000 MVA and a wind generation capacity of 3,790 MVA. SGs and WTs exist in both areas of this fictitious power system, allowing an assessment of the effects of changing the type of generation that is exposed to the fault. Details on the characteristics of the generation sources used in the test system are summarised in Table 4.

Table 4: main characteristics of generation types used in the test system

	Synchronous Generation	**Wind Generation**
Total installed capacity (MVA)	7,000	3,790
Total installed capacity (MW)	5,950	3,600
Rated Power Factor	0.85	0.95
H (in MWs/MVA)	5	n/a (grid following)
Unit transformers	X = 0.2 p.u, R = 0.002 p.u	
Dynamic controllers	ESAC1A AVRs (all SGs) IEEE-G1 governor (‘SG response’) [119]	Type 4A, according to IEC 61400-27-1 [120]

The test system uses Type 4A WTs according to the IEC standard 61400-27-1:2020 [120], which specifies standardised dynamic simulation models for wind power plants that can be applied in power system stability studies. The models are suitable for studying positive sequence responses at the fundamental frequency and valid for dynamic voltage phenomena, including faults, where the voltage drops close to zero [120]. Hence, this model is suitable for its intended purpose. However, the standard notes that a typical minimum voltage dip is 0.1 to 0.2 p.u, and notes that during very low voltages the accuracy can be limited in terms of converter control stability. The modular control structure of the type-4A WT model is shown in Figure 13.

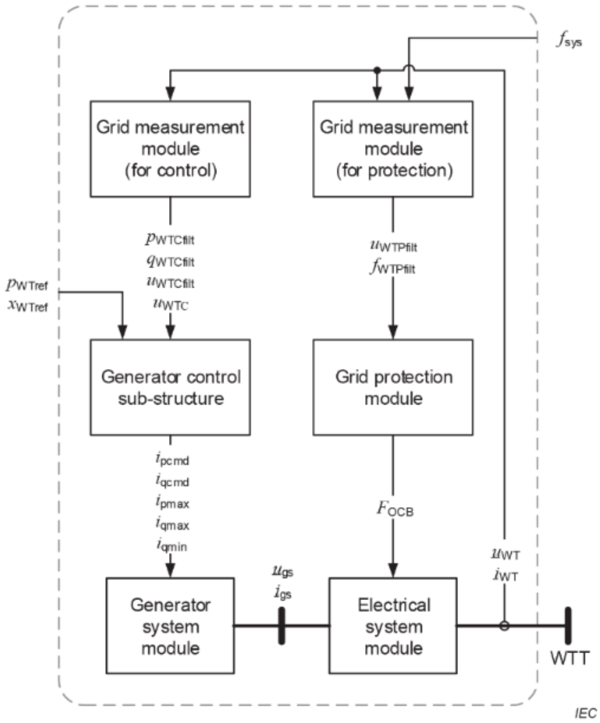

Figure 13: modular structure of type-4A WT according to IEC61400-27-1:2020 [120]

The grid interfacing modules measure the relevant electrical quantities of voltage and power for protection and control purposes. The 'generator control sub-structure' block includes active power control, reactive power control, reactive power limitation, and current limitation functions. These functions dictate the fault ride-through and fault recovery characteristics of the WT. Key adjustable parameters include active and reactive current limits, active and reactive current prioritisation, reactive current gains, FRT control modes, and active power recovery speed. These control parameters influence the active and reactive current commands (i_{pcmd} and i_{qcmd}) and limits (i_{pmax}, i_{qmax} and i_{qmax}) as seen in Figure 13, which are sent to the 'generator system module' block and ultimately define the WT's output. The effects of these parameters are assessed using the test system in this chapter and further evaluated in Chapter 6 with a representative GB test system model that is developed in Chapter 4.

3.2 Generation dispatch scenarios

In these scenarios, the power output from the WTs is increased, thereby reducing the system inertia and fault levels and increasing the amount of NSG affected by the fault. Thus, the influence of high wind penetration on the voltage dip during the fault and the post-fault system frequency is assessed. Furthermore, the mechanisms that lead to a short-term active power deficit, and the consequent frequency drop, are investigated.

The SGs are dispatched according to their merit order ranking; as such, they are displaced by wind generation proportionally to the increase in available wind energy. The SG merit order assignment is denoted M1, M2 and M3, shown in Figure 12, which represents their cost relative to each other in the wholesale market (M3 being the most expensive). First the WTs are disconnected so that the system can't benefit from their potential reactive power contributions. Then, the WTs are increased stepwise from 10% to 100% of their active power ratings. The transfer capacity of the lines from area two (A2) to area one (A1) is respected for N-1 conditions. The SG's output is flexible between its rated active power and its minimum stable export limit (SEL), which is 30 % of its rated active power. Therefore, the wind generation displaces the synchronous generation in order of their merit-order assignment when the demand has been met.

The methodology gives eleven generation dispatch patterns to meet the fixed demand. The reduction in system inertia and the fault levels at each bus occurs in steps as each SG unit is de-committed when it reaches its SEL. The penetration of WTs in the system is represented by the system non-synchronous penetration (SNSP) ratio, which is the proportion of load met by non-synchronous sources, according to [90]. The generation dispatches and SNSP for each scenario are shown in Figure 14. The system inertia and fault levels at bus A1 and A2 for each scenario are shown in Figure 15.

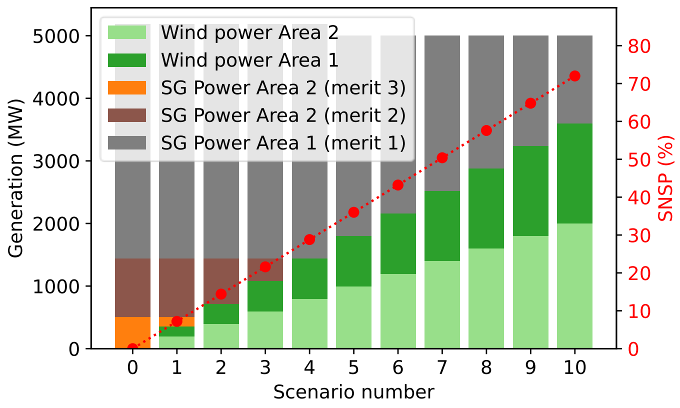

Figure 14: generation dispatch for WTs and SGs in each area and the corresponding SNSP (red line, right axis) for each scenario

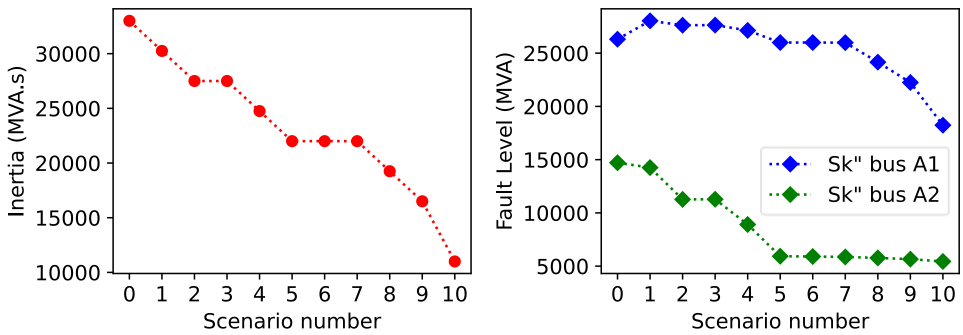

Figure 15: inertia in MVAs (left) and sub-transient fault level in MVA at bus A1 and bus A2 (right) for each scenario

3.3 Effect of wind power penetration on fault-induced voltage dips and post-fault frequency nadir

A 3-phase fault which is self-cleared (i.e. with no circuit breaker actions) of 100ms duration is applied to one of the transmission lines close to area A2 for each scenario. The fault resistance (R_{fault}) and the fault reactance (X_{fault}) are initially zero ohms which are then increased from zero to five ohms in integer steps. These tests demonstrate two primary system dynamic behaviours: (1) the effect of increasing SNSP, and the consequent displacement of SGs, on the severity of the voltage dip during the fault at bus A2 and the post-fault system frequency, and (2) by varying the fault impedance, the influence that the severity of the fault, in terms of voltage depression, has on the post fault system frequency.

Figure 15 shows how the inertia and fault levels reduce as the SNSP increases, which is to be expected. Figure 16 shows the retained voltages at bus A2 close to the fault (calculated as the mean value of the voltage during the fault, in p.u) and Figure 15(b) shows the frequency nadir that occurs in the initial few seconds after the fault (considered as the 'first-dip', ignoring transient spikes, in Hz).

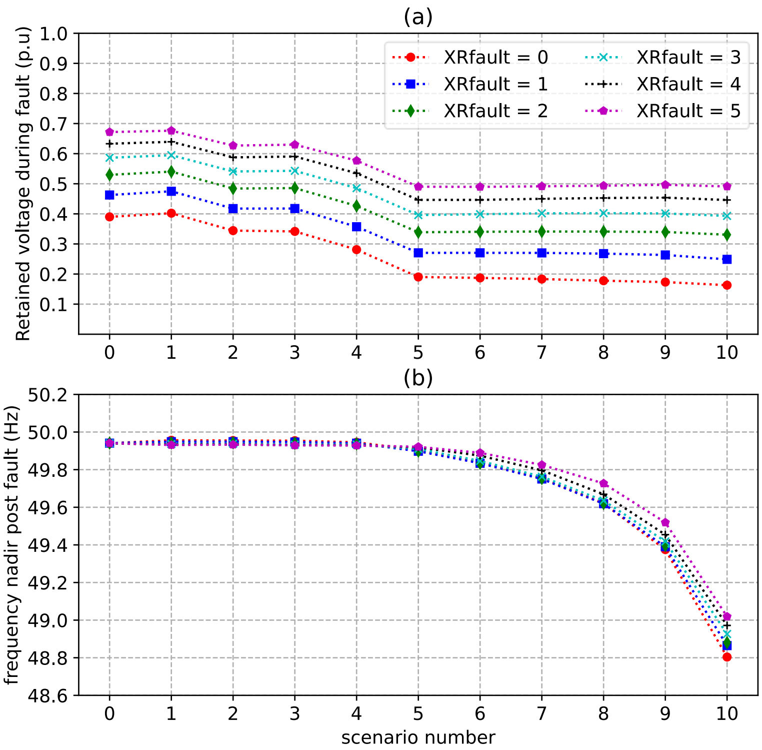

Figure 16: retained voltages during the fault (p.u) at bus A2 (top) and post-fault frequency nadir (Hz) (bottom) for each scenario while varying the fault impedance

In the first five scenarios shown in Figure 16 there are no significant fault-induced frequency dips. During these scenarios, there are low wind outputs (or no wind for scenario zero), very low SNSPs, and SGs are online in area two. The slight deviation from nominal frequency post-fault is caused by typical oscillations in the speed of the SGs due to the effect of the fault. The retained voltages at bus A2 during the fault are also higher and directly correlate with the higher fault levels for scenarios zero to four.

In scenarios five to ten, the wind outputs in area two are enough to displace both SGs in area A2, and post-fault frequency dips begin to be observed. For the same fault impedance, the voltage dip does not change much and is only affected slightly by the changes in power flows (fault levels at bus A2 remain the same). Here, the varying system conditions are the WT loading (from 50 to 100 %) and the power flow across the lines. For higher WT loading, the frequency deviation from nominal increases during the post-fault period and for scenarios nine and ten, the frequency nadir is significantly low.

Increasing the fault impedance improves the voltage depression uniformly across all scenarios and represents fault conditions that are electrically more distant (Figure 16(a)). The effects of the severity of the voltage depression at bus A2 can also be observed in the post-fault frequency, where a higher retained voltage results in a higher frequency nadir (a smaller frequency drop) for the scenarios with a higher SNSP (Figure 16(b)). The mechanisms driving the interaction between the voltage dip and the frequency excursion are discussed in Section 3.4.

3.4 Fundamental mechanisms of the fault-induced frequency excursion

The main interacting factors that are postulated to cause the frequency excursion that follows a fault are:

- The inertial response of connected SGs.
- The depth of the voltage depression.
- The control strategy for the current limitation of WTs during FRT mode.
- The current limits of the WTs.
- The active power recovery profile of the WT post-FRT.

Figure 17a-h shows the responses of the WTs and SGs to two types of faults for scenario 10. From top to bottom: the p.u voltage at bus-A2, the active and reactive currents of WT-A2, the active power of SG-A1-M1, and the rotational speed of SG-A1-M1. The lefthand column, Figure 17a-d, shows the results for fault impedance (Z_f) = 0 Ω. The righthand column, Figure 17e-h, shows the results for Z_f = 7.1 Ω (R_f = X_f = 5 Ω as per Figure 16).

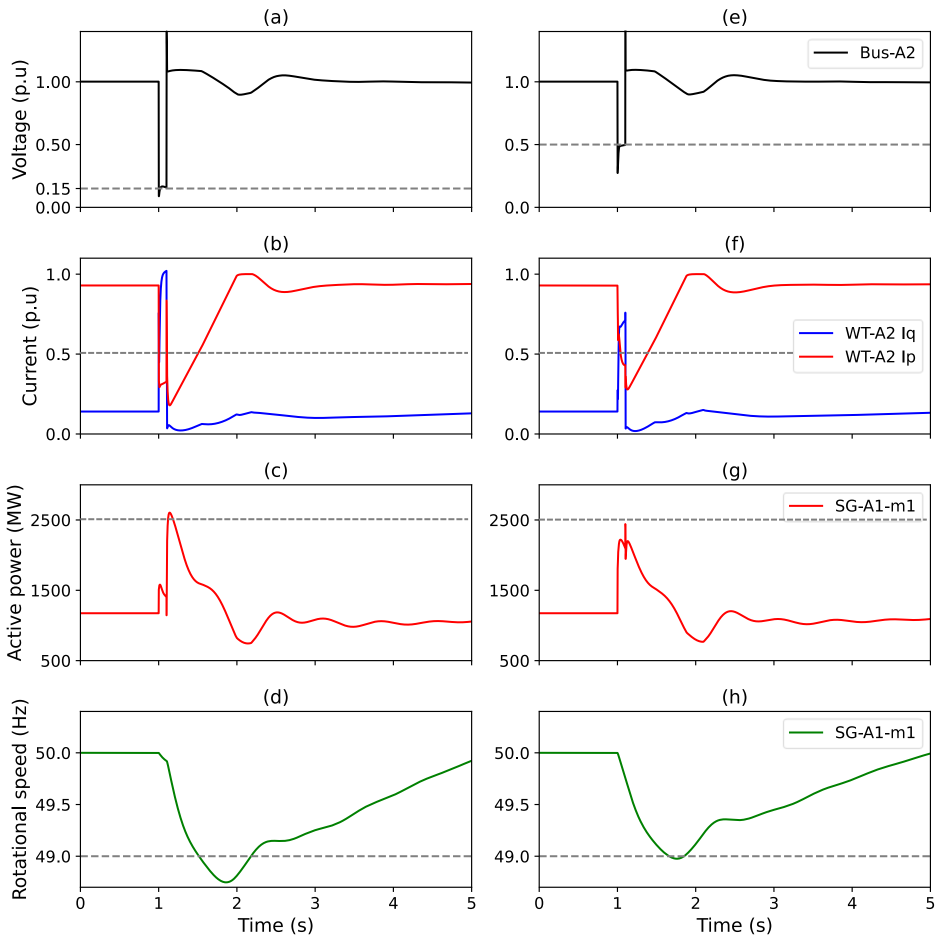

Figure 17: top to bottom: voltage at bus-A2, active and reactive currents of WT-A2, active power and rotational speed of SG-A1-m1. Scenario number = 10. Lefthand column is Rf = Xf = 0 Ω and righthand column Rf = Xf = 5 Ω

3.4.1 Response of type-4A wind generators

The current controls of the WTs provide a standard control strategy during FRT mode. During the fault, the WTs are configured to provide a fast fault current to support system voltage and reactive current is prioritised over the delivery of active current. The influence of the current control strategy and its parameters is assessed further in Section 3.5.

It can be seen from Figure 17b and Figure 17f that, for a more severe voltage depression, the WT feeds in more reactive current and reaches the converter current limit, requiring more active current to be limited. Upon fault clearance and recovery of the system voltage, the converter control mode transitions out of FRT and into normal voltage control mode, which no longer demands a high reactive current. In this case, during non-fault conditions, the WTs provide a droop-based voltage control within a power factor range of ±0.95. As such, the reactive current is quickly reduced post-fault (blue line) as it tracks the voltage. However, the active current (red line) is recovered to its pre-fault value according to a maximum allowable ramp rate constraint, which creates a deficit of active power in the post-fault period.

3.4.2 Response of synchronous generators

The inertial response of the SGs in Area-1 supplies the active power deficit (no SGs are online in Area-2). The deficit is created by the limitation of active current due to the fault, any additional limitation by the converter during the fault and the constrained active power recovery rate of the WT controls. Figure 17c and Figure 17g show that the remaining 'dispatchable' SG online in Area 1 increases its active power to meet the demand immediately after the fault. The required post-fault inertial power response from the SG is higher for a deeper voltage dip as it results in a larger active power limitation from the WTs. The energy delivered through the SG's inertial response is taken from the rotating mass of its rotor and results in a reduction of the rotor speed, as seen in Figure 17d and Figure 17h, resulting in a reduction in the system frequency.

3.4.3 Low-Frequency Demand Disconnection risk

The LFDD scheme, introduced in Section 2.3.4 is an emergency measure to prevent system collapse in the event of a large generation deficit relative to demand. If a fault-induced frequency excursion is severe enough, there is a risk that the LFDD scheme will trigger an unnecessary load disconnection, which should only occur during a longer-term loss of power that is significantly larger than the system's responsive reserves.

Conventional LFDD schemes use frequency relays which measure the frequency locally and automatically compare it with a predetermined threshold. The settings for load shedding and their design philosophy are mainly based on turbine-generator under-frequency limitations and power plant auxiliary performance. The scheme is generally implemented in stages to prevent excessive load shedding and to allow the frequency to recover before the next step. Typical implementations of LFDD thresholds for a 50 Hz system start shedding load between 49.5 and 48.5 Hz and continue to shed load in stages down to 47.5 Hz. The block size, usually specified as a proportion of the total system load, is typically 5 or 10 %. [30], [73], [78].

This simplified test system only intends to demonstrate the possible consequences of a FIFE triggering a demand disconnection. As such, no particular LFDD scheme settings are modelled. The worst-case fault-induced frequency nadir found in this system and for the scenarios studied is 48.79 Hz sustained for >100 ms (scenario 10 for a close-up fault). Reaching this frequency nadir would breach the first LFDD threshold in GB (5% load at 48.8 Hz) [30] and the first two thresholds of the recommended settings for the EU system (5% load at both 49 Hz and 48.8 Hz) [73]. Whether the LFDD relays would trip in practice depends on the locally measured frequency and the frequency measurement times implemented in the scheme, for a more detailed analysis of LFDD frequency measurements specific to the GB scheme, refer to Section 6.3.2.2.

Figure 18(a) shows the system frequency for three cases where 5 %, 10 % and 15 % of the load is tripped (with no time delay) because the frequency reaches a nadir of 48.79 Hz. The load disconnection causes an over-frequency situation as the wind generation returns to its pre-fault value, leaving the system with an excess of generation. Such high-frequency conditions could present a risk of blackout due to the tripping of too much generation based on their over-frequency protection. There will be a reliance on generator control systems to reduce active power outputs and quickly manage the over-frequency situation.

The GB Grid Code allows disconnection of transmission connected generation above 52 Hz (see Figure 9). However, specific protection settings and delays are not publicly known, and discussions with several industry experts suggest that they will vary considerably for different generators depending on age and technology type [72]. The ability to contain the frequency will depend on the Grid Code requirements, the amount of high-frequency response procured by the SO, the controller response times and the droop settings.

In this study, the WTs are not modelled to be frequency responsive. However, some wind farms have demonstrated effective and fast high-frequency responses [107]. In GB, the Grid Code requires generators, including WTs to reduce active power during an over-frequency situation [30]. For generators in an over-frequency responsive control mode, the response should be provided at a droop of 10 % for frequencies above 50.4 Hz, the initial delay should be less than 2 s, and full action should be achieved within 10 s.

For SGs, the minimum stable operation must be respected, and sufficient foot room may not be available if they are dispatched close to their minimum operating point. The effect of insufficient downward reserve that is quickly available during the over-frequency event is observed in Figure 18(b). For illustrative purposes, this frequency-responsive machine is assumed to be able to operate down to zero MW. For the base case, no load is disconnected, so the active power of the SG is recovered to its pre-fault value. For a 5% load disconnection, the SG's governor reduces its active power set-point and can limit the frequency zenith. However, the SG's foot room is depleted for a 10 % or 15 % load disconnection in this system, and a large generation surplus remains.

Observing Figure 18, for the 10 % and 15 % load disconnection cases, as the WT active power recovers, there is a high rate of change of frequency after the load disconnection (with a positive trajectory). In these cases, it is clear that there would be a material risk of reaching generator over-frequency protection settings and initiating a possible system collapse. As these conditions occur during high wind conditions, plenty of foot room should be available for WTs to reduce active power. Regardless, a fast response should be sought to prevent an over-shedding situation leading to a severe over-frequency situation.

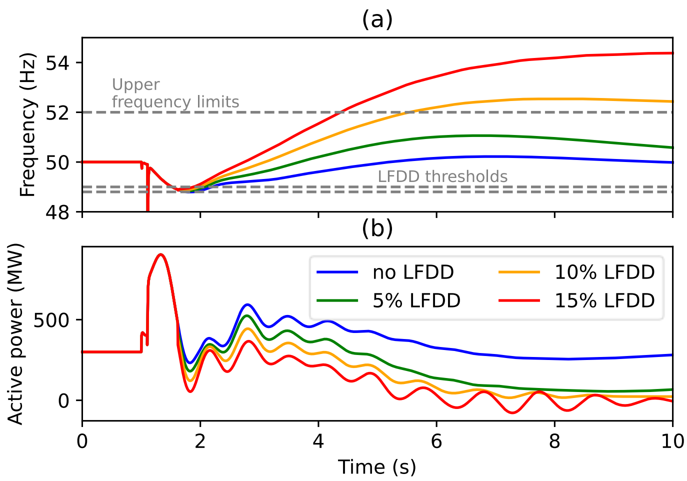

Figure 18: frequency response (a) and active power of frequency responsive SG (b) for scenario 10 with 5 %, 10 %, and 15 % load shedding

3.5 Influence of current control on the fault-induced frequency excursion

As shown in Section 3.4, the fault-induced frequency excursion depends on how the converter delivers its active and reactive current during and immediately after the fault. The response of the WT to a fault is typically dictated by its grid code requirements. The critical control strategies and parameters that will influence the FIFE are the reactive power droop during FRT (K_{FRT}), the prioritisation of reactive or active current and the post-fault active current rate of return (di_p/dt). These factors are assessed in this Section.

3.5.1 Influence of different reactive current/voltage droop

The reactive current support during FRT is based on a steep droop control with a deadband. As illustrated in Figure 19, the deadband (ΔV_{db}) aligns with the lower end of the 'normal' operating voltage range, and the K factor (K_{FRT}) dictates the change in reactive current infeed for a change in system voltage ($\Delta I_q/\Delta V$). Grid codes sometimes specify the minimum K_{FRT}

to ensure that sufficient dynamic reactive power is delivered during fault conditions to support the system voltage.

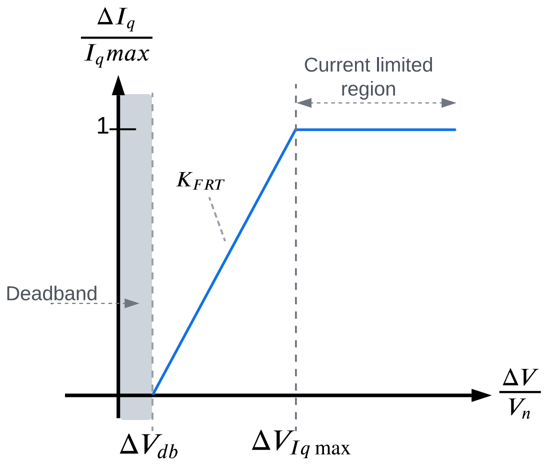

Figure 19: illustration of fault current delivery during FRT mode

Referring to Figure 19, the change in voltage that gives the maximum reactive current ($\Delta V_{Iq\,max}$) is

$$\Delta V_{Iq\,max} = \frac{1}{K_{FRT}} + \Delta V_{db} \tag{10}$$

Therefore, the additional reactive current during FRT mode (ΔI_{qFRT}) is a function of the retained voltage during the fault (ΔV), the threshold when FRT mode is activated (ΔV_{db}), the factor K_{FRT} and the converter current limitation, and can be written as

$$\Delta I_{qFRT} = \begin{cases} I_{qmax} & for \quad \Delta V > \Delta V_{Iq\,max} \\ K_{FRT} \cdot (\Delta V - \Delta V_{db}) \cdot I_{qmax} & for \quad \Delta V_{Iq\,max} > \Delta V > \Delta V_{db} \\ 0 & for \quad \Delta V < \Delta V_{FRT} \end{cases} \tag{11}$$

The converter current magnitude (I_{conv}) is given by

$$I_{conv} = \sqrt{I_p^2 + I_q^2} \tag{12}$$

where I_p is active current and I_q is reactive current.

However, the converter current must be controlled to a value within its rated capacity (I_{max}). Therefore, assuming that reactive power priority is required during FRT mode, then the maximum I_p that can be delivered for a given value of I_q is

$$I_p = \sqrt{I_{max}^2 - I_q^2} \tag{13}$$

The magnitude of I_q required during FRT for different values of K_{FRT} and the corresponding curves for the limited value of I_p are plotted in Figure 20. For a higher value of K_{FRT}, $V_{Iq\ max}$ – the volage at which I_q reaches its maximum possible value – increases and more reactive current is delivered for a smaller change in voltage, resulting in a greater reduction of the active current for the same change in voltage.

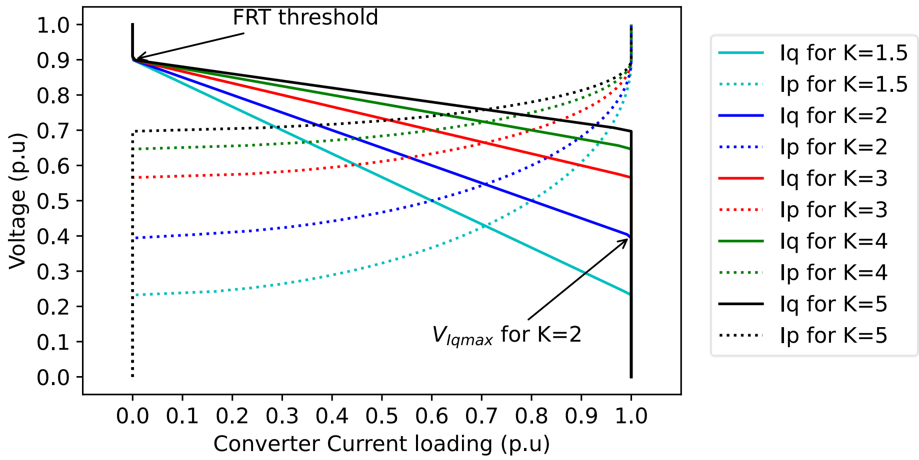

Figure 20: theoretical active and reactive current curves for different values of K during FRT mode: for reactive current priority

The effect of changing the K factor for scenario 10 (Z_f = 7.1 Ω) on the active current of WT-A2, the voltage at bus A2, and the frequency post-fault is shown in Figure 21(a-c). To observe any improvements in the frequency from this effect, V_{PoC} must be greater than $V_{Iq\ max}$ during the fault. For the zero-impedance case, this condition is never met, and maximum reactive current is always required under this control strategy for a more severe fault.

For the higher impedance fault case shown, reducing K_{FRT} to 1.5 improves the frequency profile, see Figure 21(a), as less active current is lost during and immediately after the fault – see Figure 21(b). However, the trade-off is a lower retained voltage during the fault – see Figure 21(c). In this case, with $K_{FRT} = 1.5$, WT-A2 is not providing as much dynamic voltage support during the fault, but the drop in retained voltage for a lower K factor might be acceptable for many locations in the network and, in some circumstances, it might be beneficial to sacrifice local voltage performance over system-wide frequency performance.

For values of K_{FRT} above 2 (the standard parameter value in the reference case), a slight degradation of the frequency profile and a slight improvement in the voltage profile is observed. However, the difference is marginal.

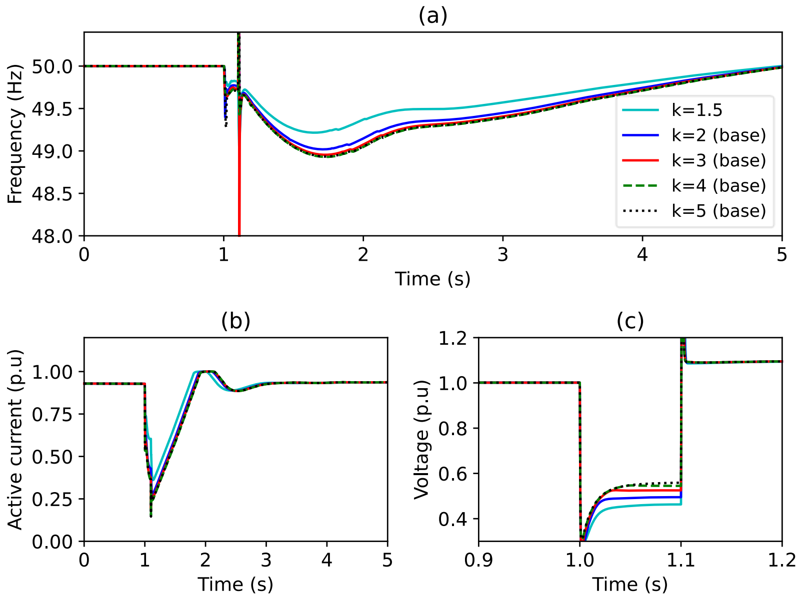

Figure 21: Effect of adjusting K factor during FRT on the system frequency (a), the active current of WT-A2 (b), and the voltage at bus A2 for Scenario 10 and fault impedance = 7.1 Ω

3.5.2 Influence of active or reactive current prioritisation

It is typical for modern grid codes to specify that reactive current is prioritised during a fault, such as in GB [30]. Ireland is an example that specifies active current priority [89]; also see Section 2.4.2. The approach to active current prioritisation is presented below and then assessed for Scenario 10.

The active current priority requires limiting the reactive current when the current reference is above the rating of the converter, for example, as requested by the FRT controller. The concept of either active or reactive current prioritisation is shown in Figure 22(a). The maximum I_q that can be delivered for a given value of I_p for an active current priority scheme is given by

$$I_q = \sqrt{I_{max}^2 - I_p^2} \tag{14}$$

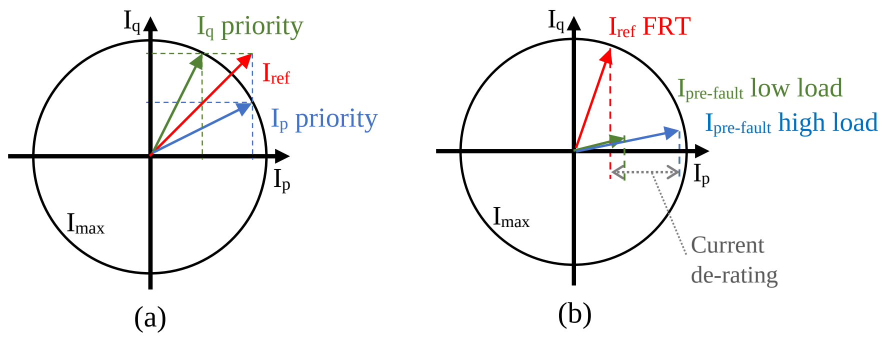

Figure 22: converter current during current-limited FRT mode – (a) concept of active current and reactive current prioritisation technique, and (b) illustration of pre-fault active loading for I_q priority.

Figure 22(b) also demonstrates the effect that pre-fault loading of the WT has on the amount of active power that is at risk from being exposed to the fault. For a higher pre-fault loading of the WT, the greater the reduction of the active current required to achieve high reactive current infeed during FRT (assuming I_q is the priority).

The current limiter of the type-4 WT-A2 is now configured to prioritise the active current over the reactive current. The results for Scenario 10 are shown in Figure 23. An improvement in the active power limitation during the fault is observed, requiring less overall active current recovery, see Figure 23(a). This results in a significantly improved frequency profile, Figure 23(c). As expected, the amount of reactive power delivered during the fault is slightly lower, which is reflected in the voltage depression. However, the reduction in the voltage during active current priority is minimal compared to the improvement in the frequency.

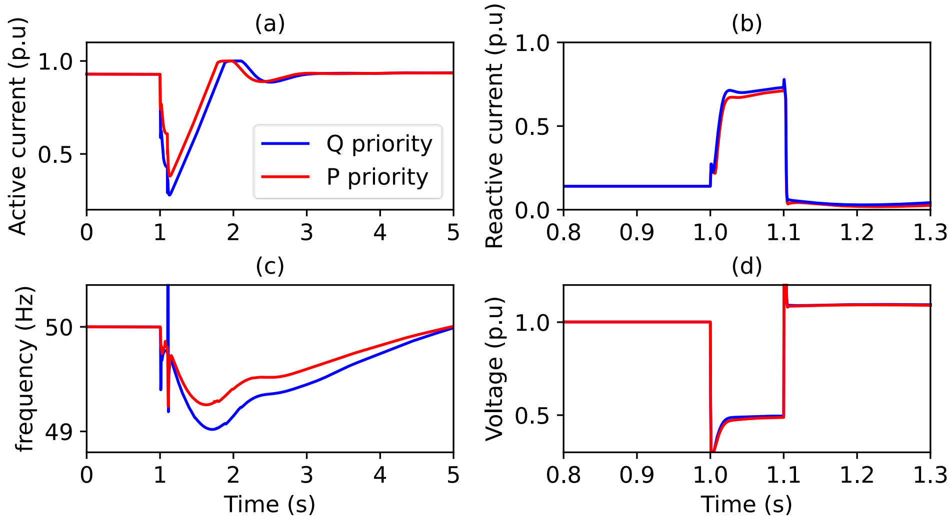

Figure 23: active current of WT-A2 (a), reactive current of WT-A2 (b), frequency (c), and voltage at bus A2 (d) for scenario 10 with reactive power priority (blue line) and active power priority (red line)

3.5.3 Influence of active power ramp rate

Another important aspect is the speed at which the active current can be recovered post-fault (di_p/dt). Some grid codes specify a minimum ramp rate [30], [89]. For example, stating that the pre-fault active power should be recovered within a given time after the system voltage has recovered. Therefore, recovery time also depends on the fast recovery of the voltage waveform.

Figure 24(a) shows the active current recovery, and Figure 24(b) shows the system frequency for varying maximum ramp rates (in $P_{rated}/second$) for scenario 10. For this case, the max. ramp rate has a significant impact on the post-fault system frequency. As the active current takes longer to recover, the larger overall energy deficit must be compensated by the inertial response of the SGs, resulting in a greater reduction in their rotor speeds.

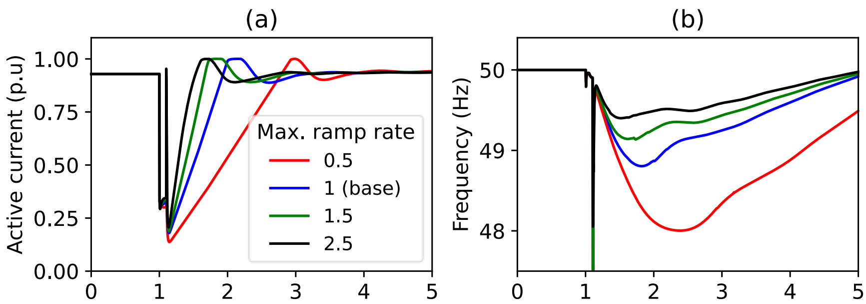

Figure 24:active current (a) and frequency (b) for different active power ramp rate limitations

3.6 Discussion and conclusions

This work has shown that network faults can lead to frequency excursions in the post-fault period when there is a high penetration of GFL IBR. The faults here are self-cleared (i.e. no circuit breaker action occurs), and there is no loss-of-infeed. The frequency dip is temporary, and generators recover any post-fault active power deficit as the voltage recovers after fault clearance. Therefore, any post-fault frequency excursion is a consequence solely of the voltage dip during the fault.

The severity of the voltage dip plays an important role in the size of the post-fault active power deficit, which the inertial response of SGs must balance. The study shows that, assuming the system and its users respond correctly, the system frequency should recover naturally from such events, as the active power is recovered to its pre-fault value. However, in this simple test system, the extent of the frequency dip and its rate of change can be significant enough to exceed the thresholds used in critical system protection schemes such as LFDD. In the event of triggering LFDD, it has been shown that this could lead to an over-frequency situation which must be contained by a fast-acting reduction of active power from wind generation. In such cases, the unnecessary disconnection of load and generation could occur and cascade into a more severe event.

The current control of the WTs in this system can strongly influence the post-fault frequency. Requiring WTs to prioritise supporting the local voltage and feed in fast reactive current during the fault is common. However, in some cases in this study, sacrificing some of the reactive current for some additional active current can bring about notable gains in the frequency performance of the system with only a minimal reduction in voltage performance. The WT's post-fault active power recovery rate is also an important factor in the post-fault frequency. A faster recovery means less overall energy deficit that the SGs must supply, hence less reduction in their rotor speed.

Some grid codes mandate a relatively fast post-fault active power recovery rate. However, as discussed in Section 2.4.2.2, a faster active power recovery rate is not always beneficial from an angular stability perspective and control of the active power recovery can influence the angular stability of SGs [99]–[101]. Therefore, the right strategy and technical requirements for active power recovery might change as systems evolve into very high penetrations of IBR on a local or system-wide level.

The susceptibility of a system to experience adverse frequency conditions is relative to the size of the system, i.e. this issue might be expected to affect smaller island networks first. However, it is also related to the penetration levels of IBR. Therefore, for systems that are approaching very high IBR penetration levels (i.e. > 60 or 70 %), fault-induced frequency instability could start to become an issue in moderately sized island systems, such as that in GB, or even in larger systems, such as when an area becomes split from the wider synchronously interconnected network [121]. In such systems, it is currently not commonplace for a FIFE to be considered a frequency stability risk.

The studies performed in this work are based on a simplified and fictitious system model. This approach helps reduce the complexity of the modelling and has allowed the main effects of the fault-induced frequency problem to be discerned, as well as assessing some of the methods available to avoid potential instabilities. However, while representative of possible system behaviours, the results presented here are not necessarily indicative of what would be seen on real systems that are typically much larger and more complex. This fact motivates the work undertaken and presented in Chapters 4, 5 and 6 of this Thesis: in Chapter 4, a representative power system model is developed to study the system's behaviour in a credible future version of the northern part of the GB power system; in Chapter 5, the fault levels and voltage dips, which influence the possible fault induced frequency excursions, are assessed; and, finally, in chapter 6, frequency stability during network faults is assessed.

Chapter 4: Development of a New Power System Model - the North GB Test System

It is important for test systems that are representative of real systems to be available for use by the wider power system community such that first-level independent evaluations can be performed, and new power system behaviour revealed [22]. The rights of access to the detailed power plant models of equipment installed in the power system are usually reserved by the asset owners and equipment manufacturers to protect their intellectual property. Furthermore, detailed full-scale dynamic models of the transmission and distribution networks are not usually shared or made available for research purposes. For modelling future versions of the system, component models of the assets are not yet available anyway. This is where generic models that are widely accepted to give a reasonable representation of the behaviour of the proposed technology are of high value [122].

As a result of these barriers related to obtaining system data and developing test systems that are representative of real networks, often standardised test systems are used when studying novel phenomena and applying new methods and techniques. This can be a good approach, particularly when proving a specific concept, process or novel methodology. However, the findings that are drawn from studies performed on these test systems are limited in their pertinence to real systems. As an alternative, a simplified representative model can be used that is designed to give a characteristic response of the real system that it intends to represent. However, there will always be some degree of uncertainty regardless of how precisely different phenomena are modelled. Ultimately, for network owners and operators to properly characterise the system's performance and invest in practical solutions, a complete and faithful model of the system should be used.

Chapter 1 highlighted that offshore wind power generation is planned to increase significantly in GB. Much of this new generation capacity will be in Scotland to exploit the high wind resource in the North Sea [123]. Scotland is already a net exporter of power to England and has a high share of the nation's wind power (mostly onshore). The rapid growth in wind generation capacity must be accompanied by an equally fast growth in North to South transmission network transfer capacity [124]. Meanwhile, the fleet of large synchronous generating plant in Scotland is planned to close, resulting in a change of system dynamic properties, and motivating the system operator (NGESO) to seek new types of stability services. These developments make GB, particularly the northern part of the system, a good case study to investigate the evolving system stability challenges.

This chapter describes the research and development of a dynamic power system model that represents a simplified version of the northern part of the GB electricity system. The model, named the 'North-GB-Test-System' or NGBTS, has been constructed, from scratch, based on publicly available network data and uses industry-standard dynamic models. Where possible, the model has been benchmarked against available system performance information, and its response characteristics have been discussed with industry experts[5]. As part of the model development, a comprehensive review of the transmission expansion plans in GB has been performed and implemented in the model, with a 2032 time horizon. As a result, the behaviour of the system considering these changes can be studied. In addition to developing the core power system model, a series of representative generation/demand dispatch patterns are developed which, along with the NGBTS model, are used in subsequent chapters of this Thesis.

4.1 Model requirements and network topology

The power system model developed in this Chapter follows the specifications outlined in Section 2.6, i.e. it shall use RMS time-domain simulations to assess system performance under balanced network fault conditions. Additionally, the power system model must:

- Utilise publicly available data and industry standard component models, applying reasonable and representative assumptions where necessary, to provide a steady-state and dynamic representation of GB power system performance.
- Provide a representation of the full GB power system, with sufficient granularity to accurately assess the impact and propagation of voltage dips in the Scottish transmission area.
- Handle a wide range of GB system operating conditions, including solving AC load flow calculations to determine active/reactive power flows, thereby enabling the calculation of suitable initial conditions for dynamic studies.

[5] I would like to credit Cornel Brozio of Scottish Power Energy Networks for his advice when developing this model and for offering his extensive knowledge of the behaviour and performance of the GB power system.

To maintain model useability, a simplified version of the GB system is created by selecting real system nodes and calculating the impedances between them. The selection of nodes for the bus-branch model follows these general considerations:

- Where possible, select nodes that serve as connecting points for large network elements such that they can be explicitly modelled. For example, HVDC terminals, large offshore wind farms, and the main sources of synchronous generation in Scotland. Otherwise, network elements of similar type are aggregated and modelled at the nearest available busbar.
- Select nodes along main transmission routes that facilitate relatively simple calculation of equivalent resistance, reactance and susceptance of branches. For example, points where the network splits into parallel paths.
- For long transmission routes, implement nodes nearby to reactive power compensation devices such that voltage drops are not unrealistically large.

As the model focusses on Scotland, it is acceptable to aggregate much of the England and Wales transmission network into a single transmission busbar. However, this results in a large amount of lumped generation at one node, giving an unrealistically high fault level, rendering the Scotland/England boundary (B6, see Figure 24) unsuitable as the point of aggregation. Referring to Section 2.1.2, the fault level is a locational metric that is inversely proportional to the equivalent source impedance at the fault location. Hence, to improve the accuracy of analysis in the Scottish area, the point of aggregation is chosen to be further south at approximately the B7a boundary (node number 23 in Figure 25), which is a point where the network becomes highly meshed. All generation south of the B7a boundary is aggregated depending on fuel type and used in determining credible GB-wide dispatches. In addition, node 23 is designated as the slack bus and voltage angle reference (i.e. its angle is zero).

4.2 Model summary

The base power system model is built with data relevant to Q1 of 2022. Figure 25 shows the main transmission substations and power transfer routes. There are three Transmission Owners (TOs) in GB: National Grid Electricity Transmission (NGET) is the TO for the England and Wales system and owns everything south of the B6 boundary, Scottish Power Energy Networks (SPEN) is the TO for central and southern Scotland and owns the network between the B6 and B4 boundaries, and Scottish and Southern Energy Networks (SSEN) is the TO for the north of Scotland region above the B4 boundary.

The model contains 97 nodes (including LV nodes) and 66 lines for the 2022 version and 137 nodes and 86 lines for the 2032 version. The complete network diagrams, as implemented in DIgSILENT, can be found in Appendix A.

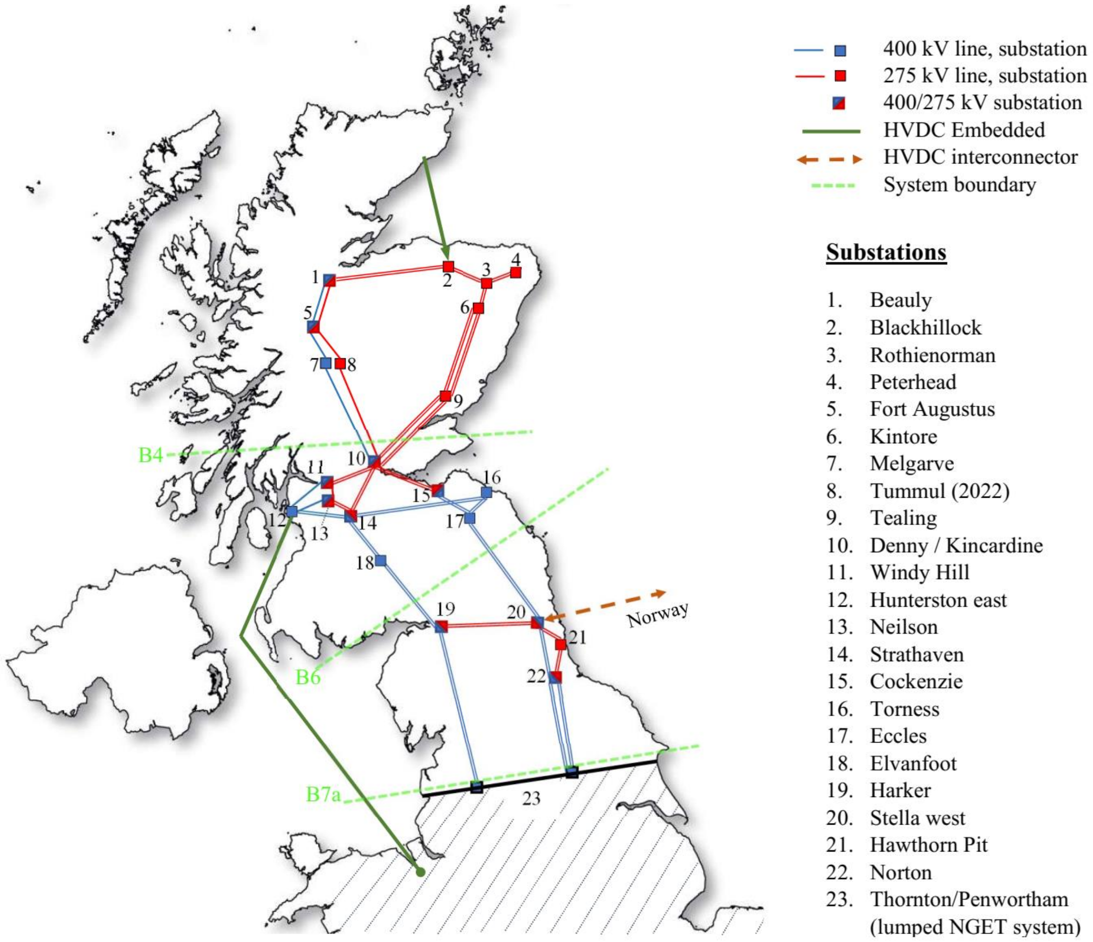

Figure 25:North GB test system - network model for 2022

4.3 Steady-state model configuration

The steady-state power system model construction refers to the data gathering and the technical specifications for the system's components, such that the steady-state behaviour of the system, i.e. assuming all system variables are constant over time, can be analysed. Several data are required for a steady-state model, such as bus and branch connectivity, line and transformer impedances, installed capacities of generation and load at each bus, and voltage control settings. This section describes the process taken to gather network data and make assumptions for parameters not available. Models and parameter assumptions for time domain dynamic system studies are discussed in Section 4.5.

4.3.1 Transmission lines

Each transmission line is modelled in the positive sequence as a three-phase overhead line using the π equivalent model with lumped parameters. Figure 26 shows the equivalent circuit of a three-phase transmission line (with no neutral conductor) selected for use in the model. Referring to Figure 26, $\bar{Z}_s$ and $\bar{Y}_s$ are the self-impedance and self-admittance respectively. These are the input parameters in the form of positive sequence resistance (R in Ω/km), reactance (X in Ω/km), and susceptance (B in μS/km).

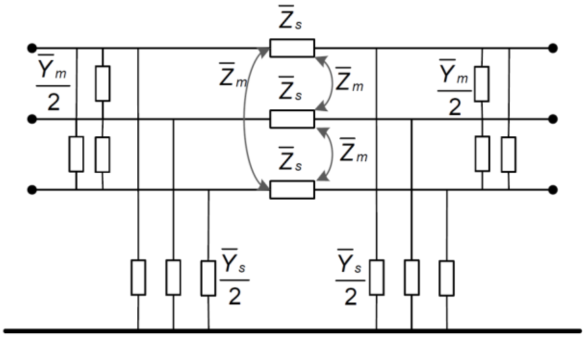

Figure 26: Equivalent circuit of a three-phase line

The lines that are represented in the model have been reduced from the positive sequence line data provided in the NGESO Electricity Ten Year Statement [125]. To make the reduction, all interconnecting lines between the two common nodes that are being represented in the reduced model are assessed using the network diagrams. Then, the equivalent series/parallel impedance can be calculated. An example impedance calculation for a series/parallel combination of lines, and the formula required to convert the ETYS data into power factory inputs, are found in Appendix B. The modelled line parameters are found in Appendix C.

4.3.2 Distribution system demand and distributed generation

There are various data sources for installed quantities of demand and distributed generation in GB, all of which can vary in their level of detail, granularity, and intended use [14]. For the development of the Model, NGESO's Future Energy Scenarios (FES) [126] is used as this provides information at the GSP level and gives projections out to 2050. For demand, three reference points are available for each Grid Supply Point (GSP) location in GB. These being 'winter peak', 'simmer minimum AM', and 'summer minimum PM'. Demand is given as the 'gross' active power (MW), i.e. the figures represent the system demand without the negative contribution from DG. In practice, NGESO as the transmission system operator, observes the 'net' system demand at the interface points to the distribution networks (the GSPs).

Great Britain has reached relatively high penetrations of DG. In 2019, DG made up 35% of total generation capacity, much of it based on variable renewables and is largely unobservable and uncontrollable by the ESO [14]. The FES provides installed capacities for five categories of DG for each GSP: storage, solar, wind, hydro, and 'other'. Energy storage connected to the distribution network, as included in the FES, is not considered in the NGBTS when calculating net demand, as there is too much uncertainty in the operation of these assets. Transmission connected energy storage devices providing frequency response and energy arbitrage are modelled in the 2032 system, see Section 4.4.3. The 'other' DG category is assumed to be made up of CHP plants, which is consistent with the detailed analysis performed on the available DG data sources in GB found in [14].

The spatial distribution of demands and installed capacities of DG in the model are determined by geographically mapping the location coordinates of the GSPs to the nearest modelled transmission busbar. This may result in some error, as it is possible that some GSPs are situated geographically close-by to a transmission substation, but they are fed from a different part of the transmission network. However, this method is considered the most accurate representation given the available data.

Most loads in Scotland are fed from the 275 kV transmission network and are modelled at 11 kV. At each aggregated load point, two identical parallel 275/11 kV transformers, each rated at 120% of the winter peak demand, feed a general load element and a synchronous motor with no active power demand. The latter represents the inertia contribution from the load. Load points are configured as shown in Figure 27. For assumptions on the dynamic response of the loads, see Section 4.5.2.

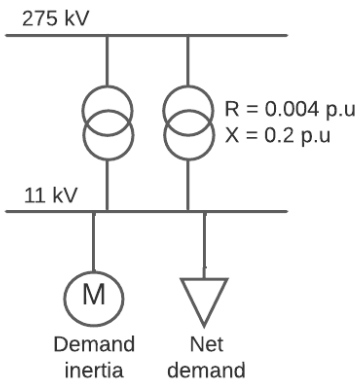

Figure 27: Configuration for modelling load points

The net demand (as seen at the transmission interface points by the ESO) depends on the gross system demand, the installed capacities of DG, and the operating point of that DG at any given time. For the range of assumptions used and the method to calculate the net demand depending on the system conditions, see Section 4.7.3.

4.3.3 Transmission connected generation

Generators are aggregated and lumped into the following categories, which represent the main transmission connected generation types present in the GB system:

- Flexible synchronous generation, e.g. CCGT or large biomass plant
- Non-flexible synchronous generation e.g. Nuclear and some run of river hydro.
- Pumped storage hydro.
- Battery energy storage systems (BESS)
- Onshore wind.
- Offshore wind.

To determine the location and type of generators in the representative model (as of Q2 2022), a combination of data sources has been utilised from Elexon and NGESO, including:

- Balancing Mechanism (BM) Reports ('B1610')
- Balancing Mechanism Unit (BMU) register
- Elexon network mapping statement
- Transmission entry capacity (TEC) register

The main information required for each generator is the rated generation capacity, the network connection point, the reactive power capability and the fuel type. No single source provides all information needed, so some mapping between them is required. However, differences in the labelling of generators between these data sources do not allow fully automated and simple searches to be carried out. Therefore, the fuel type for each generator from the TEC register has been reconciled with the BMU register with a combination of search functions in Excel and manual entry.

For a summary of the installed capacity of generation for the 2022 model version and the 2032 model, see Section 4.4.5.

4.3.4 Static reactive power compensation

Switched capacitor banks and reactors are implemented in the model to provide quasi-steady state voltage control and compensate for the increase or decrease in voltages in the network and support the active power transfer through the system. In general, when a line is heavily loaded, there are higher voltage drops from the sending to receiving end of a transmission line and capacitive reactive power is needed to ensure receiving end voltages remain suitably high. When the system is lightly loaded, voltages can go high due to reactive gain of the transmission lines and inductive reactive power is provided by switching in reactors. The capacitor banks and reactors are modelled according to those stated in the ETYS [125].

4.4 The GB power system in the early 2030s

This section reviews the available information regarding the changing power landscape in GB in terms of the expansion of transmission connected generation and the associated network reinforcements required. Focusing on the north, a 'best guess' picture of what the power system is expected to look like in the early 2030s is applied to the North-GB-Test-System model. It is desirable to extend the model into the mid-2030s and beyond. However, there is not enough information available to make any reasonable judgements, and performing studies that identify new system dynamic behaviour beyond this point might be considered too speculative. Therefore, this model should be periodically updated to include the most up to date view of network development plans. That is not to say that extensions to this model beyond 2035 cannot be made. The model can be a useful first pass to test optioneering of future network upgrade options in the Scottish transmission areas, but that is not the focus of this work.

4.4.1 Transmission network planning

To achieve the offshore renewable energy targets in a timely, cost-efficient, and coordinated manner, the network planning process in GB requires review and reform. Multiple reviews are underway in GB at the time of writing: the ESO's Network Planning Review (NPR), The Department for Business, Energy & Industrial Strategy's Offshore Transmission Network Review (OTNR), and Ofgem's Electricity Transmission Network Planning Review (ETNPR). The general direction of travel is away from generator/developer led projects and towards a more centralised strategic network planning process [127], [128].

One of the main outputs so far of the OTNR is the Holistic Network Design (HND) [124] which, alongside the existing Network Options Assessment (NOA) planning process, includes a high-level design and assessment of the onshore and offshore transmission network infrastructure required to facilitate the connection of offshore wind farms and transfer the power via onshore and offshore transmission infrastructure. Typically, offshore wind connections are via radial connections to shore, often built by the generation developers to reach the nearest suitable onshore connection point. However, with the significant amounts of offshore wind capacity expected, a more careful management of where this power connects is required. Otherwise, significant operational costs will be incurred constraining low carbon generation to manage the AC system within its limited capacity.

Significant onshore and offshore network reinforcements are being proposed. Onshore network reinforcements in GB, such as building new over-head transmission lines, can take many years to develop and the consenting process can be a major source of delay and uncertainty. Hence, where possible, the onshore reinforcement works act on existing power transfer routes, for example, increasing the voltage of existing circuits. However, there are still many new network infrastructure projects required in the AC onshore system, including new circuits and substations. It is acknowledged that, under the current regulatory and consenting environment, many of these projects would not be delivered in time to meet the offshore wind targets, and more generally the energy system decarbonisation targets. Government intervention will be required to expedite the planning process [16], [124], [129].

A lot of the new power transfer capacity is proposed to be added via embedded HVDC links. An embedded link is where two points of the same synchronous AC system are connected in parallel with a DC link system interfaced through inverter/rectifier power electronic converters at each end. The move towards increased HVDC transmission makes sense, not only from a planning and consenting perspective, but also a technical one, as much longer transmission distances can be achieved with HVDC compared to AC systems [35].

Even if HVDC subsea cables are easier to gain consents for as they have a lower visual impact and do not require multiple wayleaves for crossing 3rd party land, there are many other factors that can influence the ability to deliver so many large projects in a relatively short time. Not least of these factors are the availability of equipment being supplied by OEMs, it can take a long time to specify and manufacture the HVDC cable systems and there are only a few specialised suppliers who are in high demand around the world.

The transmission reinforcement projects that currently hold ‘proceed’ or ‘essential’ status that are expected in the north of the GB system and have been applied to the model are detailed in Table 5. They are also shown graphically in Figure 31 of Section 4.4.8. The data and information for each reinforcement project has been gathered and reconciled from [124], [125], [130], [131].

Table 5: network reinforcement and upgrades required over the next 10 years and implemented in the North-GB-Test-System

Category	description
Onshore lines and substations	Beauly to Blackhillock new 400 kV double circuit line.
	Blackhillock to Peterhead new 400 kV double circuit line.
	Upgrade the existing Blackhillock / Rothienorman / Kintore / Alyth / Kincardine east coast 275 kV circuits and substations to 400 kV.
	Upgrade the existing Beauly - Fort Augustus – Tummel/Kinardochy - Bonny Bridge 275 kV circuit to 400kV.
	Denny to Wishaw 400 kV reinforcement - Construct a new 400 kV line to establish a fourth north to south double circuit route.
	Windyhill-Lambhill-Denny North 400 kV reinforcement.
	Kincardine 400 kV reinforcement - Installation of 2 x 400/275kV 1100MVA auto-transformers.
	Denny North add second 400/275 kV supergrid transformer.
	Windyhill - Neilston - Hunterston circuit changes.
	Establish new Cousland 400 kV Substation that combines routes from Torness - Strathaven and Cockenzie - Eccles.
Reactive compensation	New STATCOM rated +- 225MVAr and MSC 100MVAr at newly built 400kV Kinardochy substation.
	New STATCOM rated +- 225MVAr and MSC 100MVAr at newly built 400kV Alyth substation.
	New 200 MVAr Reactor at Hunterston.
	New STATCOM rated +- 150MVAr at Eccles substation.
Offshore reinforcements	Install new 2GW HVDC Link from Spittal 275 kV substation to Peterhead 400 kV substation.
	Install new 2GW east coast HVDC link between Peterhead and Drax (NGET).
	Install new 2GW East Coast HVDC Link Peterhead to the south Humber.
	Install new 2GW Eastern subsea HVDC Link from east Scotland (around Tealing) to south Humber area 2.
	Install new 2GW Eastern subsea HVDC link from Torness to Hawthorn Pit.

4.4.2 Offshore wind generation capacity

For offshore wind developments there are several projects in various stages of development included in the TEC register. All projects with the 'consents approved' status have been assessed individually and all are deemed to be at a late enough stage of development to assume they will be built – see Table 6.

In early 2022 the Crown Estate Scotland7 announced results of the Scotwind leasing round. Scotwind awarded almost 25 GW of new offshore wind leasing options in Scottish waters to 17 individual projects. The winning projects have been offered option agreements which reserve the rights to specific areas of seabed. Developers must then work towards full planning and consenting approval. Projects will only progress to a full seabed lease once all these various planning stages have been completed [132]. The names and locations of all offshore wind projects in Scotland that have been assessed for the model are shown in Figure 28 [133] and their development status, rated capacity, and assumed onshore connection point are detailed in Table 6.

---

[7] The Crown Estate owns the seabed surrounding the GB coastline. They award leases and other types of agreements to organisations who want to build offshore wind and other infrastructure projects, where fees must be paid to the Crown Estate in return for the lease of the seabed.

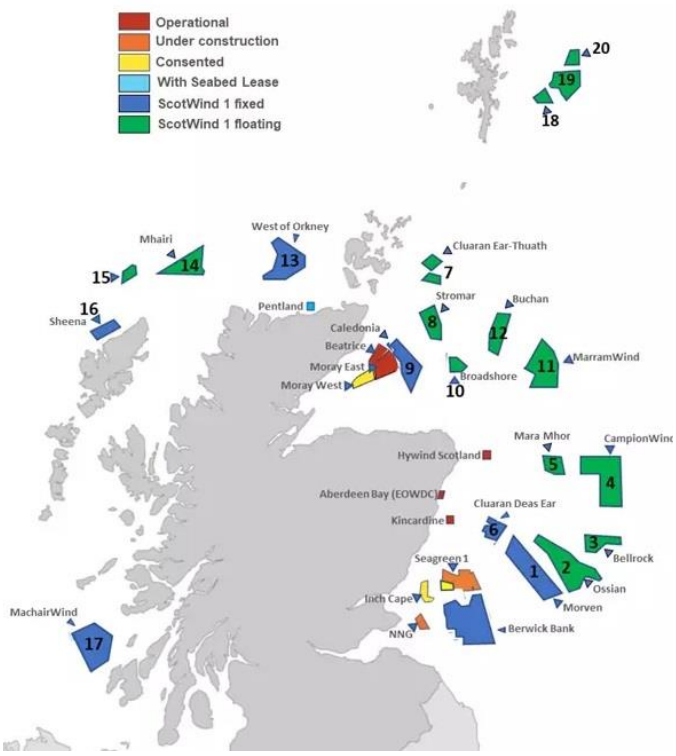

Figure 28: offshore wind developments in Scotland [133]

The 25 GW of potential offshore wind capacity granted in the Scotwind process was more than what many expected. The HND, by NGESO, which a provided a high-level design exercise to coordinate the connection of offshore wind only considered 11 GW of Scotwind offshore projects, as it was published prior to the results of the Scotwind leasing round.

Those that are marked with an asterisk* in Table 6 are considered in the HND by NGESO and their assumed onshore connection point in the model is based on the HND assessment. For the additional sites beyond what was assumed in the HND, the connection design provided in the HND is the starting point, and they are assumed to be ‘piggy backed’ onto the proposed connection infrastructure, which is in turn assumed to be suitably rated. This has resulted in approximately 18.4 GW of Scotwind projects (74% of what was awarded) being assumed to go ahead and included in the model.

No preference is given to any project developer / owner and additional projects are selected for ease of sharing connection infrastructure defined in the HND by NGESO. The final point of onshore connection is subject to further HND and NOA planning reviews and detailed engineering work. The locations of the offshore wind projects, and the network upgrades that are modelled can also be seen in Figure 31.

Table 6: Scottish offshore wind projects assessed for inclusion in the North GB Test System

Site name / map reference (offshore wind developments in Scotland [133]	Development status (As of Q3 2022)	Modelled capacity (MW)	Project built/not built	Modelled onshore PoC [1]
Robin Rigg	Operational	174	Built 2022	NGET4
Aberdeen Bay		95		KINT2
Kincardine		49		KINT2
Moray East		950		PEHE2
Beatrice		588		BLHI2
Seagreen1	Under construction	1,075	Built by 2032	TEAL2
Neart Na Gaoithe		448		TORN4
Seagreen1A	Consents approved	500		COCK4
Inch Cape		1080		COCK4
Moray West		800		BLHI4
Berwick Bank	Awaiting Consents	2,300		STEW4
1*	Scotwind leasing round – option agreements signed	2,907	Built by 2032	ALYT4 / HAWP2
2		2,610	Not built	n/a
3*		1,200	Built by 2032	ALYT4 / HAWP2
4		2,000		
5		798	Not built	n/a
6		1,008		
7		1,008		
8		1,000	Built by 2032	ROTI4
9*		1,000		
10		500	Not built	n/a
11*		3,000	Built by 2032	PEHE4
12		960		
13*		2,000		C/M Link / BEAU2

14		1,500		C/M Link / BEAU4
15		495	Not built	n/a
16*		840	Built by 2032	BEAU4
17*		2,000		HUNE4 / NGET4
Total offshore wind built in Scotland by 2032[2]		**24,446**		
Total offshore wind in GB assumed in 2032[3]		**46,580**		

1. Where two onshore AC connection points are defined, it represents more than one path to shore from the offshore network. The offshore wind capacity is split 50:50 between each connection point.
2. Although built in Scottish waters, some of this capacity is connected to the NGET system in E&W to avoid onshore network constraints.

4.4.3 Onshore generation and energy storage

While much of the new renewable energy capacity is offshore wind, some additional onshore wind is expected in Scotland[8], and a significant amount of new gas CCGT plant, PSH and BESS projects are in various stages of development. A lot of growth in solar PV is also expected. However, new PV is considered as part of the net transmission system load rather than generation supply[9]. (See sections 4.3.2 and 4.7.3).

For all types of onshore generation and energy storage projects, the TEC register is used [134]. Many of the projects that are in the early stages of development might not get built. For onshore wind, BESS and flexible SGs (the latter being made up of gas CCGT, all of which are in E&W), the amount of capacity in development is multiplied by scaling factors depending on their development phase to determine how much to include in the model.

Regarding large nuclear and PSH projects, they are assessed individually. One large nuclear plant, Hinckley Point C, is under construction in the south of England and included in the model. Two PSH projects have had their consents approved and completion dates are expected before 2028, these are assumed to go ahead. In addition to these, seven more PSH projects are listed as ‘scoping’ with a total capacity of 3,274 MW, all located in Scotland. Three of these

[8] There is currently a government ban on building of new onshore wind in England and Wales .

[9] It is difficult to develop large PV generation projects in GB due to limited availability of land (compared to other countries that are seeing PV projects that are a few hundred MW’s or more). Therefore, while the mean project size might still increase, it is still expected that most projects are connected to the distribution networks.

projects, totalling 1,882 MW and with completion dates by 2030, are assumed to go ahead as they are extensions of existing sites so are deemed to be preferable from a consenting perspective. Table 7 shows the capacities of each technology in the planning stages in GB, and the assumptions for how much of it is included in the 2032 model version.

Table 7: Generation capacity of different technologies (excluding offshore wind) at different stages of development and the proportion of each that is assumed to be built by 2032

Technology	Under construction		Consents approved		Awaiting consents		Scoping	
	Capacity (MW)	Built (%)	Capacity (MW)	Built (%)	Capacity (MW)	Built (%)	Capacity (MW)	Built (%)
Onshore wind	298	100	2,624	75	2,061	50%	8,878	25%
BESS	0	100	912	75	1,938	50%	17,813	25%
flexible SG	466	100	10,124	75	4,191	50%	4,344	25%
Nuclear	3,340	100	0	-	0	-	0	-
Pumped Hydro	0	-	822	100	0	-	3,274	57%
Total	**4,104**		**14,482**		**8,190**		**34,309**	

4.4.4 Closure of generating plant

Some generating plant is expected to close between 2022 and 2032. The following assumptions are made for different generating plant closures in GB and considered in the 2032 model version:

- For wind generation, no closures assumed. Most of the capacity has been built after 2010 and should have a design life more than 20 years; sites that would have reached end of life during the 2020's are assumed to be re-powered.
- For pumped storage hydro, no closures assumed. Many PSH projects in GB are quite old (cruachan 1965, foyers 1974, Ffestiniog 1963, Dinnorwig 1984). However, while they are old, it is assumed that the electrical / mechanical systems are restored (which has already occurred at many sites), and the plants are still within the lifespan of the dams and reservoirs.
- For coal plant, all are assumed closed. Coal has been phased out in GB since around 2010.

- For CCGTs, no specific closures are assumed. Most of the CCGT plants were built between 1995 to 2010 [135]. The date on which gas plant might close can depend on many market-driven factors and not simply the end of useful life of the equipment. For fossil-fuel based plant, the most notable of these factors is government policy on the tax for emitting CO2. Unless SGs are paid enough to remain open, for example through a capacity market mechanism, they will cease operations when it becomes uneconomical to continue running. It is noted from Table 7 that there is a lot of large CCGT plant in development, with all of it located in the NGET area. The basic assumption of the model is that flexible SGs are available in the E&W area should they be needed to meet demand and that, if required, they are able to run on zero-emission fuels such as hydrogen or they are using carbon capture and storage such that NGESO is able to operate a zero-carbon electricity system after 2025.
- For nuclear, all anticipated closure dates are publicly available [136] and are considered. Most of the existing nuclear fleet is planned to close before 2032. The three large nuclear plants that are in the northern parts of the system being modelled will all be closed: Hunterston (closed 2022), Torness and Heysham (expecting to close 2028).

4.4.5 Summary of generation capacity 2022 to 2032

Figure 29 shows the generation capacity by technology type determined for the years 2022 and 2032.

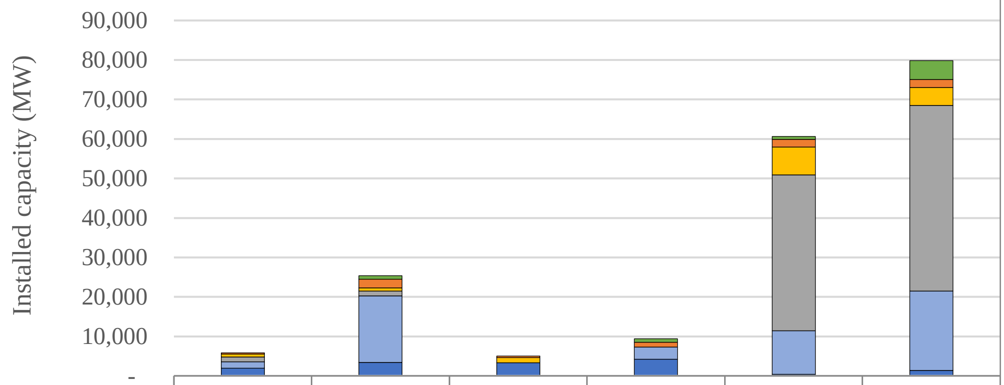

	SSEN 2022	SSEN 2032	SPEN 2022	SPEN 2032	NGET 2022	NGET 2032
BESS	-	956	-	838	723	4,831
PSH	300	2,196	440	1,250	2,004	2,004
SG (non-flexible)	771	771	1,250	-	7,006	4,570
SG (flexible)	1,206	1,206	-	-	39,497	46,978
Offshore wind	1,632	16,861	-	3,028	10,986	20,112
Onshore wind	1,909	3,419	3,339	4,250	443	1,371

Figure 29: summary of generation capacity in 2022 and 2032 assumed in the model

4.4.6 HVDC interconnection

There are several HVDC links in operation in GB and many more planned for the coming decade. ‘HVDC interconnectors’ (HVDC-IC) are those that connect two separate synchronous areas and interconnect two different markets. They are distinct from ‘embedded HVDC’ links. (See Section 4.4.1)

GB currently has interconnection with France, Ireland, Netherlands, Belgium, Denmark, and Norway, and has additional ICs planned to some of these countries as well as to Germany in the coming decade. The NGBTS assumes the same amount of interconnector capacity as scenario 5 of [137] for the 2032 version of the European system, as detailed in Table 8.

Table 8: Planned and operational HVDC interconnectors in GB

Project name	Connecting country	Capacity (MW)	Delivery date / estimated
IFA	France	2000	1986
Moyle	Ireland	500	2002
BritNed	Netherlands	1000	2011
EWIC	Ireland	500	2012
Nemo Link	Belgium	1000	2019
IFA2	France	1000	2021
NSL	Norway	1400	2021
ElecLink	France	1000	2022
Viking Link	Denmark	1400	2023
Greenlink	Ireland	500	2024
NorthConnect	Norway	1400	2025
NeuConnect	Germany	1400	2028
GridLink	France	1400	2030
FAB Link	France	1400	2030
Total		**15,900**	

4.4.7 Electrolytic hydrogen production in Scotland

The use of low carbon hydrogen (H_2) is widely considered as a promising–and sometimes essential–fuel for meeting net zero [138]. Hydrogen is a gas of high calorific value and when burned does not produce carbon dioxide. However, currently, the production of hydrogen is predominantly from fossil-fuel intensive processes, often labelled as "grey hydrogen". Hydrogen being produced for a net zero energy system will have to be either produced by fossil-fuel generation with Carbon Capture, Use and Storage (CCUS), so called "blue hydrogen", or with a low carbon energy source, such as wind power using electrolysers to produce "green hydrogen".

The Scottish Government published the 'draft hydrogen action plan' in 2021 which set an ambition to reach 5 GW of renewable and low-carbon hydrogen capacity by 2030 [139] [140]. In addition, one of the objectives of the Scotwind leasing round (see Section 4.4.2) is to use excess wind generation to create green hydrogen, and many of the Scotwind applicants have outlined their intention to include hydrogen production in their development plans [123]. The main green hydrogen production technologies currently available are alkaline electrolysis (the most mature form of electrolysis) and Proton Exchange Membrane (PEM) methods. Both alkaline and PEM do not require heating so can be quickly dispatched thus can be operated to follow variable wind energy output [141].

Much of the industrial demand for hydrogen in Scotland is situated along the north-east coast, which is also where a significant proportion of the offshore wind will come ashore. The hydrogen generation points in the Model (modelled as demand) are located at near-by electrical nodes to the regional 'hydrogen hubs' proposed in [139] as shown in Figure 30. The four island hubs are not represented in the Model.

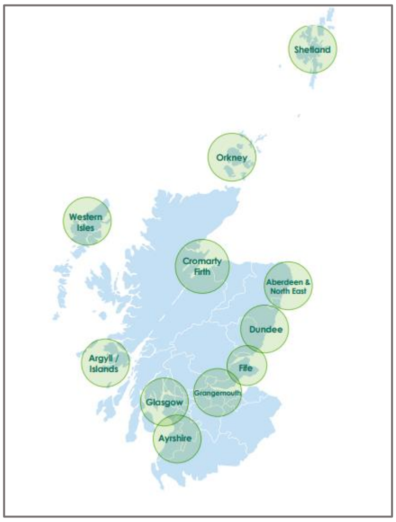

Figure 30: Potential locations of regional hydrogen hubs [139]

The UK central government has also published the 'UK Hydrogen Strategy' [142]. Which was updated in December 2022 with a doubling of the target for low carbon hydrogen production capacity to up to 10 GW by 2030, with at least half of this capacity coming from electrolytic hydrogen [143]. Therefore 5 GW of H_2 is assumed to be connected to the NGET busbar.

There is a lot of uncertainty around the amount of H_2 production capacity and when it will be installed on the system, and the production mix by 2030 will be influenced by a range of factors. These factors include government energy policy, carbon pricing, technology subsidies, technology costs, industry supply chains, and the suitability of gas storage, transmission and distribution infrastructure. Investor confidence and market forces will also dictate the type of projects that will come forward during the 2020s. However, the production and use of H_2 allows higher penetrations of wind, hence it is assumed that the government targets are met.

4.4.8 Summary of network changes: looking to the 2030s and beyond

Figure 31 provides an overview of the locations of the new offshore wind capacity, the new PSH projects, the assumed H_2 electrolyser locations, and the required new and upgraded network reinforcements that are applied to the North-GB-Test-System.

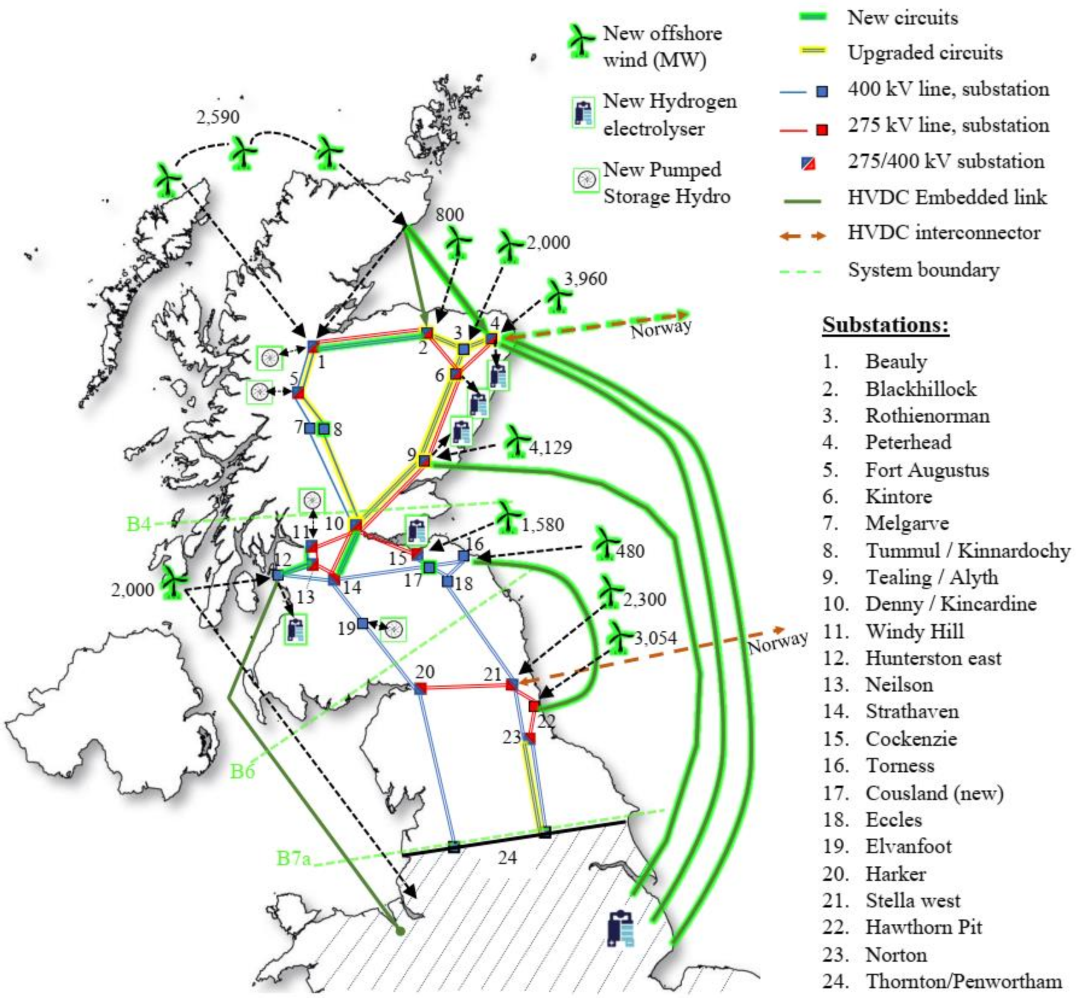

Figure 31: Summary of the network upgrades (yellow highlights) and new network (green highlights) planned for the north of GB transmission system, including new additions of offshore wind, PSH, and hydrogen electrolysers

Chapter 1 introduced the UK Government's ambition to achieve a fully decarbonised electricity system by 2035. The extensive expansion of the electricity network, as described in this section and implemented in the NGBTS model, represents a significant, decade-long investment in laying the foundations for that goal. While the future version of the NGBTS model is based on a 2032 time horizon, it reflects how the system is expected to evolve through the late 2030s and beyond.

4.5 Dynamic modelling and parameterisation of network elements

To study the electro-mechanical transient response of the power system, suitable and representative parameters and dynamic models must be applied to key elements in the system. In the real system, different vendor and control solutions can produce quite different responses. However, in the absence of real data and controller models, typical reference parameters and standardised controller models can be used. In fact, for planning studies where new concepts or phenomena are being studied and detailed vendor models are not yet available, generic models must be used, and these should suffice in providing an initial indication of dynamic behaviour and potential problems.

This section describes the dynamic controllers and parameters used for the key network elements when assessing the stability of the system in response to large signal disturbances and conducted via RMS time domain simulations.

4.5.1 Synchronous generators

Four types of SGs are represented in the Model that represent the dominant generation types in GB: Combined Cycle Gas Turbines (CCGT), Advanced Gas-cooled nuclear Reactors (AGR), Run-of-River, or reservoir fed hydro generators (Hydro), and Pumped Storage Hydro (PSH) with a bi-directional generator/motor arrangement. Fundamentally, each of these types of synchronous machines generate power in much the same way – i.e. they use different prime-movers to spin a rotor via a shaft and drive a generator – but their turbine and generator characteristics can vary, and so do their assumed model parameters. The main SG parameters that influence the dynamic properties of interest in this work are the transient and sub-transient reactance's and the inertia constant of each of the machines.

Gas, nuclear, and other thermal power plant types in the Model are all assumed to utilise a similar type of turbo-generator construction. They are high speed machines with a non-salient pole (cylindrical) rotor and either 2 or 4 poles, which is typical of a generator that raises steam to turn its turbine, such as CCGTs or AGRs. The inertia of a rotating machine is relative to its rotational speed and the mass of its rotating parts. Due to their high rotational speed, these machines can have a high inertia, with inertia constants (H in MWs/MVA) in the rage of 4 to 9 [144].

Hydro generators typically operate at lower rotational speed than steam-driven turbines. Because of this, hydro generators use a 'salient pole' rotor type, which consist of a high number of poles to achieve the required frequency of the synchronous grid (i.e. 50 Hz). Though salient pole rotors are slower than cylindrical rotor types, they typically have very large diameters and large mass contributing towards the machine’s inertia. However, hydro generators still typically have a smaller inertia constant than thermal generators. For hydro generators, H can be in the range of 2 to 4 [144]. For salient pole machines the q-axis reactance’s are much smaller than the d-axis reactance’s (and are ignored by PowerFactory in the salient pole SG model).

The assumptions for transient and sub-transient reactances and inertia constants for SGs in the model have been inferred from a combination of standard assumptions found in the literature from [144] and [24], as well as some projects specific information where available [145] and are summarised in Table 9

Table 9: Synchronous generator parameter assumptions

Synchronous generator type	**Rated unit (MVA)**	R_a **(p.u)**	X''_d **(p.u)**	X''_q **(p.u)**	X'_d **(p.u)**	X_d **(p.u)**	T''_d **(s)**	T'_d **(s)**	**H (MWs/ MVA)**
CCGT (SSEN)	500	0.0021	0.25	0.264	0.34	2.24	0.032	1.01	6.2
Lumped ‘flexible’									5
Nuclear AGR	800	0.0022	0.23	0.242	0.32	2.19	0.051	0.942	5
Hydro-Gen	90	0.0017	0.166	n/a	0.22	1.28	0.031	0.834	3.2
Pumped Storage Hydro	110								4.31
Synchronous compensator	**195**	**0.0016**	**0.153**	**0.153**	**0.2**	**1.73**	**0.031**	**0.908**	**Project specific**

Table Nomenclature: R_a denotes armature resistance. **X** denotes reactance. **T** denotes short-circuit time constant. Subscripts **d**, **q** denote d-axis and q-axis. Super-scripts “, ’ denote sub-transient and transient period. **H** denotes inertia constant.

4.5.1.1 Excitation control of SGs

For all Synchronous generators and Synchronous condensers in the model, a Type AC1A excitation system model, according to IEEE standard 421 [119], is employed to control the terminal voltage of the machine. In this type of Automatic Voltage Regulator (AVR) model the voltage regulator power is taken from a source that is not affected by external transients and is suitable for large power system stability studies [146].

A Power System Stabiliser (PSS) is also used for some generators. The PSSs are used to enhance damping of power system oscillations through excitation control and provides an additional input to the AVR. For simplicity and considering that small signal stability and oscillatory behaviour are not the concern of this work, PSH, hydro generation, and SCs are not fitted with PSSs as they will require different sets of parameters to account for the different operating modes [146]. The standard parameters for both AVR and PSS are maintained.

4.5.1.2 Governor control

A governor model, which is a local controller that acts on the prime mover of the SG, is used to control the speed of the responsive synchronous machine connected to the lumped NGET bus and is set up to provide primary frequency response (PFR). Initially, it is assumed that all the PFR is delivered in the NGET part of the system.

The governor model is a modified version of the IEEEG1 standard speed governor. It has originally been modified and tuned for use in a single bus power system model representing GB and to provide PFR delivery from SGs, such that the full response is delivered ten seconds after a frequency event with an initial delay of two seconds [147], in line with the PFR service in GB. This governor model has been used in multiple frequency response studies in GB [63], [104], and it has been validated against real system events, including the system disturbance in GB on the 9th of august 2019 [66].

4.5.2 Loads

The behaviour of loads in the power system can have a significant influence on its dynamic performance [148]. There is often a lot of uncertainty with load modelling, in both steady-state and dynamic studies, due to the large number of different types of loads that are widely distributed and often have little monitoring and centralised controllability. Different types of loads are found in residential, commercial, and industrial applications. These include small and large motors, lighting, space heating, etc. For example, for resistive loads such as incandescent lamps or electric heaters, the impedance remains constant for changes in voltage and frequency at its connection to the network, while inverter interfaced loads, such as variable speed drives or power supplies will often maintain a constant power during a change in system voltage. It is not always necessary or practical to accurately model all the different types of loads in a power system, and it depends on the nature of the study being performed.

Static load models describe the relationship between the active and reactive power of the load as an algebraic function of voltage and frequency. Although they are static models, the dynamic properties of the load can be approximated through its static model and can therefore be used in dynamic stability analysis. Alternatively, full dynamic load models usually relate the active and reactive power of the loads to the voltage and frequency using differential equations. Static load models are more commonly used [148] [149] and are used in this work.

In practice, aggregated load, as seen at a particular point in the power system, is made up of some mix of constant impedance (Z), constant current (I), and constant power (P) loads. This proportional mix of different types of loads can be represented in dynamic system studies by the polynomial ZIP model and describes the relationship between the change in active and reactive power with a change in system voltage. Here, the relationship with active power is focused on. The active power drawn by the load also has a directly proportional relationship to changes in the network frequency. During a generation deficit leading to a low frequency event, the load also reduces and provides a damping effect by lessening the active power imbalance. The dynamic response of the load, including voltage and frequency dependency, can be described by the following second order polynomial model [7]

$$\mathrm{P} = P_n\left[P_1\left(\frac{U}{U_n}\right)^2 + P_2\left(\frac{U}{U_n}\right) + P_3\right]\left(1 + K_{pf}\Delta f\right) \tag{15}$$

where

P is the power drawn by the load at voltage U and frequency f;

P_n is the nominal power of the load;

P_1, P_2, P_3 are the relative participation factors of the constant Z, I, P parts of the load, respectively;

Δf is the relative change in frequency, equal to $(f - f_n)/f_n$; and

K_{pf} is the change in load demand to change in supply frequency.

Where required in the NGBTS, loads are modelled using the ZIP polynomial model to represent a simplified non-typical load. For example, in the future version of the Model, hydrogen electrolysers (H_2) are modelled as loads with a constant current. Constant current is chosen as they are expected to be interfaced to the grid through converters [150].

In GB, the CLASS Project, ran by Electricity Northwest (a DNO in the UK), performed tests on a wide variety of primary substations (usually 33 to 11 kV) in the distribution network seeking to understand the relationship between voltage and demand for different types of loads. The main intention of the project was to investigate opportunities for voltage management by the DNOs as a demand response service [151]. The CLASS project reported the voltage dependency of the load using an exponential load model, chosen for its simplicity. In this form, voltage dependency of the load to changes in active and reactive power are described by a single exponent and encapsulates the ZIP proportionality of the load response.

Here, the active and reactive powers of the load during voltage and frequency changes are described by

$$P = P_n \left(\frac{U}{U_n}\right)^{K_p} \left(1 + K_{pf} \Delta f\right)$$

$$Q = Q_n \left(\frac{U}{U_n}\right)^{K_q} \left(1 + K_{qf} \Delta f\right)$$

where K_p and K_q are active and reactive power exponents, respectively.

From [151], the values for K_p are in range from 0.67 for domestic loads to 1.97 for mainly non-domestic load types, with the average value of 1.3, and a K_q value of 5.5 assumed for all distribution system demand in the Model.

The loads are modelled with a linear frequency dependency on active and reactive power, with a frequency dependence of 2 % change in power for every 1 Hz change in frequency (or 1 %/%), which is a typical assumption for the GB system [152].

There is also a motor modelled at 11 kV that represents the inertial response of the load, see Figure 27. The motors are set up to have an inertia constant (H) of 2.27 MWs/MW according to [153] and varies with the demand level by scaling the number of motors as demand changes.

4.5.3 Wind turbine generators according to IEC 61400-27-1:2020

For the North-GB-Test-System, all wind generation is assumed to be type-4A 'fully rated' converters according to IEC standard 61400-27-1:2020 [120], refer to Section 3.1 for a description of the IEC WT model control structure.

This model neglects the aerodynamic and mechanical parts and thus does not simulate any injected power oscillations, which is acceptable for frequency stability studies. If the oscillatory behaviour of the system is to be studied, it is recommended to add type 3B and type 4B turbine models that implement the two-mass mechanical model. Currently in the system there is a mix of type-3 and type-4 WTs, but full converter WTs (type-4) seem to be the preferred option for new wind farms, particularly for offshore applications [98].

To avoid instabilities and numerical problems in the simulation, the PLL parameters in the model are configured to freeze the voltage angle measurement during disturbances.

4.5.4 Battery Energy Storage Systems

Battery energy storage systems (BESS) are implemented as static generators with dynamic controllers according to [154]. For some systems studies where a simpler representation is acceptable, a BESS can be modelled as a constant current load. The operating regime of future BESS connecting to the system is relatively uncertain and depends on the available revenue streams from stacking different services, which can depend on the system operating conditions and the network location.

An overview of the control structure implemented for frequency responsive BESS units is shown in Figure 32. The frequency controller allows calculation of the active power dependent on the measured frequency and given droop and dead-band settings, which are set to represent the DC (Dynamic Containment) fast frequency response service in GB. Similar to primary response from governor action, DC provision from BESS is assumed to be delivered from the NGET area. Reactive current support and voltage control is also provided through the P/V control block and specified with droop and deadband settings for controlling the AC voltage.

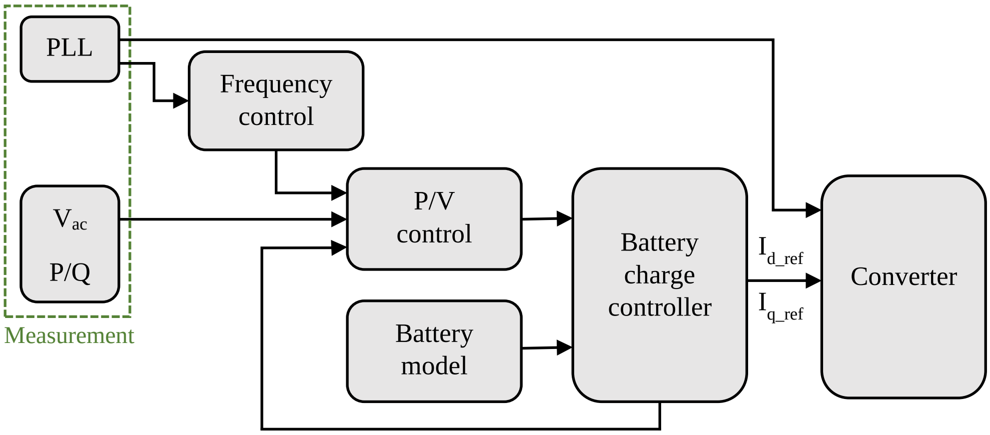

Figure 32: Overview of control structure used for battery energy storage system with frequency control (redrawn and simplified from DIgSILENT model)

The BESS has two constraints: its rated power/current, and the battery energy capacity. The 'battery model' control block allows simple modelling of the DC system, where the energy ratings of the battery can be set by adjusting the number of parallel strings of battery cells to increase the amount of stored energy[10]. For the studies in this work, the energy rating of the battery is set suitably high as full delivery of the service is expected to extend well beyond the timescales of fault recovery.

4.5.5 HVDC converters

[10] It is typical in battery systems (or other systems that use modular DC current sources, such as PV plants), to build up the DC voltage by connecting multiple cells in series (typically called strings) and connect multiple strings in parallel to increase the DC current.

4.5.5.1 Line commutated converters

There is currently one operational embedded HVDC link between Scotland and England. The Western HVDC link is a Line Commutated Converter (LCC) with a transfer capacity of 2.2 GW. LCC schemes have a large inductor on the DC side which maintains the DC current relatively constant. As a result, they draw a very high amount of reactive power from the network, requiring a significant amount of compensation. LCC converters also require a certain level of AC system stiffness at their terminals to ensure proper commutation of their thyristor valves [35]. Commutation failure can occur during faults on the AC system, during which the valves temporarily stop working and the power that was being transferred over the DC link must be temporarily transferred over the AC system. When the AC system voltage recovers, commutation should also be restored.

The dynamic response of an LCC HVDC link is very dependent on the specific control system implementation. For simplicity, and when the specific responses of such a link are not the focus of the study, it is often the case in system studies, such as those in GB, that the LCC HVDC is modelled as a positive or negative demand. In the North-GB-Test-System, a HVDC-LCC steady state and dynamic model is included, which is implemented from the DIgSILENT library. However, depending on the study being performed, the western HVDC link can also be modelled as a two load points. When modelling the link as a load, first a load flow can be calculated with the LCC model in service to determine the reactive power demand at the Hunterston busbar (HUNE4), which can then be applied to the load, if required.

4.5.5.2 Voltage source converters

Voltage Source Converters (or VSCs) use a capacitor on the DC side to maintain a constant DC voltage. The use of IGBTs and advanced switching control allows the VSC to synthesise a voltage waveform of any frequency, phase, or magnitude (within its ratings). This gives VSC converters an inherently flexible capability and they can absorb or generate reactive power at any power factor at either the inverter or rectifier end of the link [35].

As the control of the IGBTs can 'self-commutate', i.e. they are able to switch the valves on and off, they do not necessarily require an AC voltage source at both ends like an LCC does. (For the LCC, the job of switching the valves off is performed by the AC system voltage waveform, hence the need for a stiff AC grid with voltage sources at each end of an LCC link). Hence, they are being increasingly utilised to connect offshore wind farms to shore, and for interconnecting two 'weaker' parts of an AC system. This is not to say that VSC is a 'silver bullet' when it comes to connecting HVDC converters to AC systems when fault levels are low or quasi-steady state voltage sensitivity is high (see discussion on 'System Strength' in Section 2.2), challenging conditions can still arise for stable control of VSCs.

Various available and standardised library models for HVDC systems have been considered for implementation in the NGBTS model[11]. The library model templates chosen are developed by DIgSILENT and gave the most stable performance and flexibility when adjusting parameters. Two types of VSC-HVDC models, that are suitable for balanced RMS simulation, are implemented depending on the type of HVDC link:

- For embedded HVDC links: i.e. connections within GB (see Table 5), the "HVDC MMC 2-Terminal Link (RMS Balanced)" model template is chosen which includes integrated link controls of each terminal and DC cable dynamics. Each side of the 2-terminal link has individual controls, as described below and shown in Figure 33(a), and the cable is modelled as a pi-section as seen in Figure 33(b). Therefore, power losses over the DC cable can be considered.
- For HVDC-ICs: i.e. connections to other synchronous systems (see Table 8), the "HVDC MMC Terminal (RMS Balanced)" model template is chosen which includes a single point terminal and associated controls.

No accompanying documentation is available for this library model. However, through conversation with DIgSILENT staff, it is understood that the model is mainly based on the CIGRE Technical Brochure 604 (Guide for the Development of Models for HVDC Converters in a HVDC Grid) [155], the European grid code requirements, and additional enhancements based on their experience.

Figure 33(a) shows a simplified overview of the control structure (re-drawn from the DIgSILENT model graphic). The slow dynamics of the outer control loops are deployed with AC active power controls (P_{ac}) and reactive power/AC voltage controls (Q/V_{ac}). The FRT controller (the fast dynamics of the outer loop controls), provides fast reactive current infeed and is set up for compliance with GB Grid Code. The inner loop current controls are maintained with the standard parameters, which include a maximum current limit of 1.1 p.u.

---

[11] The availability and implementation of a simple, standardised VSC-HVDC dynamic model has been a critical challenge in developing the NGBTS model. Several standardised models have been reviewed for use, but difficulty can arise when integrating these models and to balance their complexity and useability for bulk system studies. The DIgSILENT model chosen gives the best option for ease of use and stable operation of those considered. However, it is still a complex model and includes many functions and parameters that are not required for the first-level studies that the NGBTS is intended for.

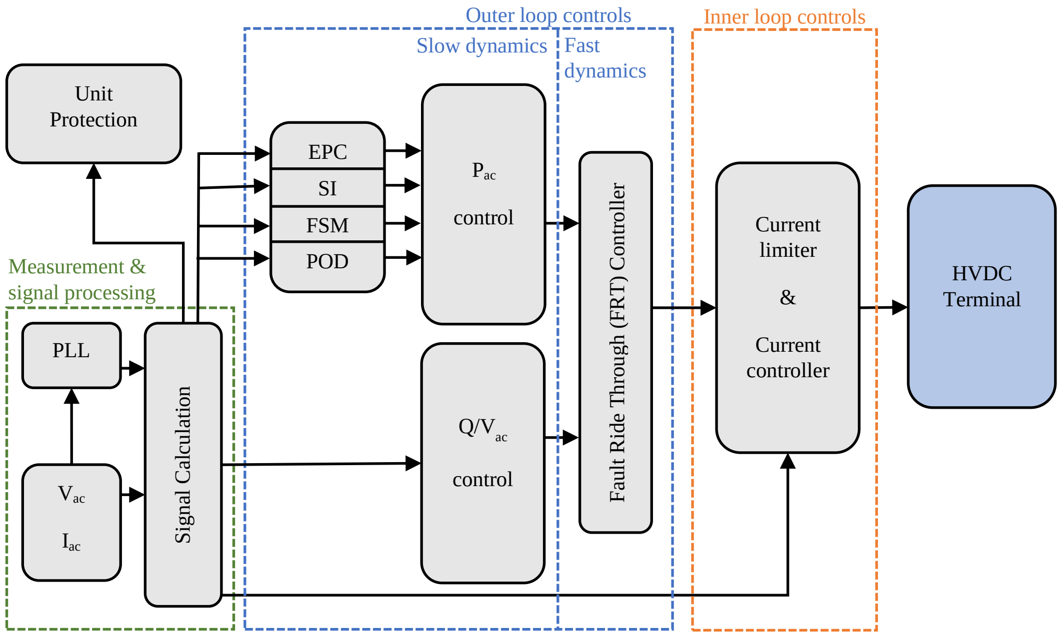

(a) Terminal Control structure

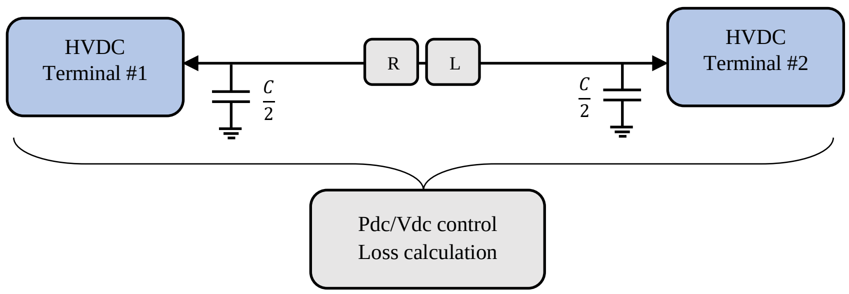

(b) 2 terminal link model structure

Figure 33:Overview of terminal control structure for VSC HVDC interconnectors (a) and two-terminal model structure for embedded links (b) (redrawn and simplified from DIgSILENT library model graphic)

In the quasi-steady state, the VSC HVDC controllers are configured to perform AC voltage control with a droop setting of 5%. Having the HVDC converters (as well as the wind farms) in an AC voltage droop mode allows reactive power sharing of multiple converters that are connected in a close proximity of each other. Ensuring voltage droop control is important for a successful RMS-TDS simulation as, during the fault recovery period when the AC voltage recovers quickly, controllers switch out of FRT mode and the voltage must be controlled back towards its nominal value.

4.5.6 Flexible AC Transmission Systems (FACTS)

Dynamic reactive power compensation devices respond quickly to changing system conditions and regulate their reactive power injection and absorption in close to real-time, to maintain voltage stability and prevent voltage collapse. Sources of dynamic reactive power include SGs, SCs and IBRs (depending on the grid code requirements), and shunt connected flexible AC transmission systems (FACTS) such as the Static Var Compensator (SVC) or the Static Synchronous Compensator (STATCOM) [156].

Where there is a deficit of dynamic reactive power for voltage control, network operators will typically install FACTS. This is often required along long lines with high power transfers which can lead to voltage stability problems in post-fault conditions. In north of GB, the area where this is most prominent and there is a strong need for dynamic reactive power post-fault is close to the B4 boundary between the SSEN and SPEN networks. This is observed in the North-GB-Test-System and has been discussed with network engineers at SSEN and indicated to represent real stability challenges across this boundary.

Both SVC and STATCOM are controlled such that, during steady state, it is operating at a low reactive power load – i.e. close to zero – to ensure that there is sufficient reactive power margin available to quickly respond during unexpected changes/disturbances on the system, for example, during faults.

4.5.6.1 Static Var Compensator

An SVC can have many different configurations but will typically consists of parallel branches of thyristor-controlled reactors and capacitors, fixed reactors, and capacitors, and mechanically switched capacitors and harmonic filters. They can provide continuous regulation of reactive power by changing the firing angle of the thyristors [156]. The SVCs in the NGBTS are implemented with a simple Proportional Integral (PI) based voltage controller with maximum and minimum reactive power limits. In this case, the switching nature of the thyristor-controlled capacitors is not important, and the admittance of the whole SVC is used, where a positive admittance is interpreted as a capacitive reactive power and a negative admittance is a reactive power consumed by the SVC.

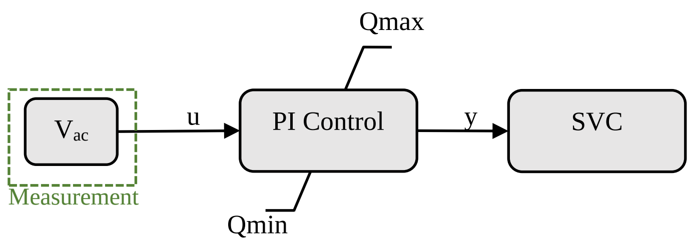

Figure 34: Simplified diagram of control structure for Static VAr Compensator (redrawn and simplified from DIgSILENT model)

4.5.6.2 Static Synchronous Compensator

A Static Synchronous Compensator (STATCOM) is a reactive power regulating FACTS device that is based on VSC technology and connected in shunt with the power system. Unlike the SVC, the STATCOM reactive current is not dependent on the voltage at its connection point, and it can provide its rated reactive current down to very low voltages [156]. In addition, the STATCOM can sometimes operate faster than the SVC. This makes it more useful for boosting low voltages, for example during fault conditions.

The STATCOM model is implemented as a two-level PWM converter with a DC capacitance and a step-up unit transformer. The dynamic controller of the STATCOM takes the network voltage (V_{ac}), the capacitor voltage (V_{dc}), reactive power flow (Q) as measured inputs, and uses a standard PLL block in DIgSILENT. It contains a PI dynamic voltage control block with droop characteristics and current limiting to generate the current reference signals. All STATCOMs are set to 5 % droop and have a 2 p.u current limit according to [157].

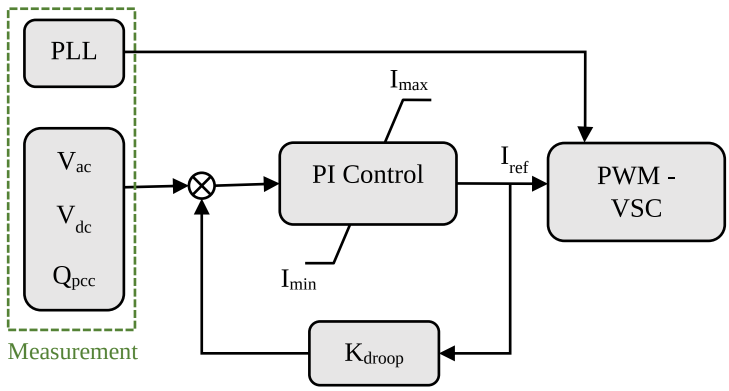

Figure 35:Simplified diagram of control structure for modelled STATCOM (redrawn and simplified from DIgSILENT model)

4.5.7 Model configuration and Parameterisation for dynamic simulations

This section describes some key steps taken to configure the model and tune some control parameters to achieve a representative response when simulating disturbances. The north of GB power system has multiple large-scale IBRs in the planning phase; should all or most of these get built, as is modelled in the NGBTS, design and implementation of the protection and control system for each project will be an extensive task. Furthermore, in practice, these projects will comprise different OEM hardware and software solutions, with different responses and control systems tuned during their design and commissioning.

The parameterisation of the IBR controllers used in standardised models is important when studying representative system behaviours. In this work, configuring the IBR controllers has been crucial for (1) improving the functionality of the model to perform RMS simulation, i.e. its ability to calculate the system's state for subsequent time steps during and after major events, and (2) to give a suitable response that is broadly representative of what is to be expected from certain types of assets on the system. Where possible, the IBR models in the NGBTS are configured to be GB Grid Code compliant. Besides this, the proportional and integral gains for reactive power, active power and current controllers have all been tuned using a simple trial-and-error approach.

In addition to the parameterisation of power system elements, the software configuration should be suitable for the studies being performed. Attention to simulation timestep and model time constants should be made, and to the settings for calculating the initial conditions. When assessing the outputs from a representative RMS model, attention must also be given to interpreting those that signify a characteristic response of the systems being modelled or those that are an artefact of the RMS modelling process and configuration. Throughout the model development, numerous discussions have been held with Dg-PF through their technical support and other expert colleagues to work through modelling and simulation challenges.

Ultimately, the planned network arrangement in the north of GB being modelled here is yet to be extensively studied, and this work contributes towards understanding some of the future requirements.

4.6 Model validation

The purpose of model validation is to assess the ability of the North-GB-Test-System to produce results that are representative of the real system. The process involves comparing its outputs to any available system data that has been produced by the full GB system model. Due to the lack of published data on performance of the system and security margins for the system in the 2032, model validation is only possible for the current 2022 version of the system.

This model validation exercise compares the calculation of steady-state fault levels at the modelled nodes in the test system with the system fault levels published by NGESO each year as part of the ETYS [28]. As the fault levels at different parts of the system are related to the system impedance at the fundamental frequency, comparing them allows an appraisal of how well the system impedances are represented in the model. Then, to give assurance on the dynamic behaviour of the model, the stability-related boundary transfer limits are calculated and compared with those quoted by NGESO. Further to this, the development of the model has been discussed with senior staff at the SSEN and SPEN transmission owner organisations, where the general characteristic dynamic behaviour the model has been said to be representative.

4.6.1 Comparison of system fault levels

In [28], the short circuit currents associated with making and breaking duties of switchgear are published for two special generation/demand dispatch cases: ‘winter peak’ and ‘summer minimum’. These cases are designed to provide existing and potential new users of the system with an initial indication of the potential maximum and minimum short circuit levels across the system. To verify the calculated fault levels, it is necessary to match, as well as possible, these dispatch conditions.

For the winter peak conditions (maximum fault levels), all large power stations are included, whether they contribute active power or not, to simulate the most onerous possible scenario. For this case, all directly-connected generators are modelled. For the calculation of fault levels at the minimum demand, the system demand is set to the minimum annual expectation and only synchronous generator units are switched on to satisfy demand for an intact system (i.e. no component outages). The generation dispatch patterns used when calculating ETYS minimum fault levels are not made publicly available. However, an overview of the system conditions used in the Scottish transmission areas has been obtained through communication with SSEN and SPEN, but the SGs online in England have been estimated.

For each of the winter peak and summer minimum dispatches, the modelled peak instantaneous short circuit current (ip) and the RMS symmetrical short circuit breaking current at 50ms (Ib), are compared, calculated according to the G74 standard [158]

$$i_p = \sqrt{2}\, I_k^{''} + i_{DC} \tag{16}$$

$$I_b = \frac{i_b}{\sqrt{2}} - i_{DC} \tag{17}$$

where $I_k^{"}$ is the initial symmetrical (or "sub-transient") short-circuit current (RMS value) and i_{DC} is the decaying aperiodic component (or DC component) of the short-circuit current, and is equal to

$$i_{DC} = \sqrt{2}\, I_k^{"}\, e^{\left(-2\pi f t_b {}^{R}/_{X}\right)} \tag{18}$$

where t_b is the break time.

For determining breaking currents, a circuit breaker opening time of 50 ms is taken. For determining peak currents, the maximum aperiodic component occurs around 10 ms (or half the period of the first cycle).

Figure 36 and Figure 37 show the modelled i_p and I_b compared to the ETYS published values for winter peak and summer minimum dispatches, respectively, at the key nodes in Scotland for the 2022 model. The error, which is simply the difference between the modelled and the reference value, is plotted as the dark grey and red lines for i_p and I_b respectively.

The ETYS published fault level data have all been generated with a full system model which should produce the best possible representation of the system. In the NGBTS, the network has been simplified by aggregating system elements and making assumptions for data that are not available. This aggregation and use of assumptions allow a reasonable representation to be made of the areas being modelled. However, there will always be differences expected when comparing to a full system model. In general, the following factors contribute towards these differences when calculating fault currents:

- The impedances of network elements in the model, e.g. for transmission lines, have been aggregated based on published technical data.
- The assumptions used for generator and transformer impedances and MVA ratings may differ.
- The assumed X/R ratio; this will affect the aperiodic DC component and consequently the peak instantaneous currents.
- The lumping of generation at transmission nodes rather than discreet representation of multiple generators and their connection infrastructure.
- The assumptions of exactly which generator units are on-line, their ratings, parameters, and their active power output during a load flow calculation.

- The contribution of fault current from DG is not modelled in the NGBTS

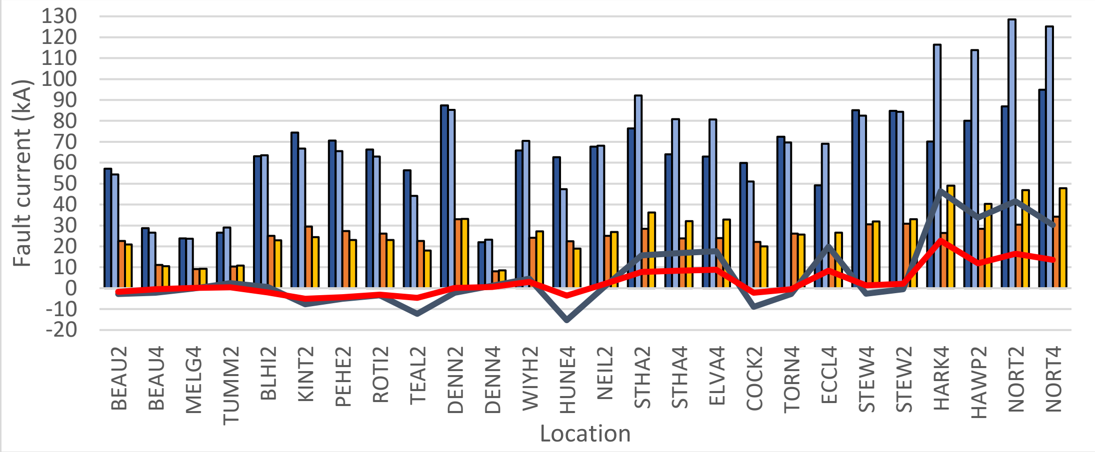

Figure 36: Comparison of initial peak current and RMS break current to published values for winter peak. Legend is shared with Figure 37

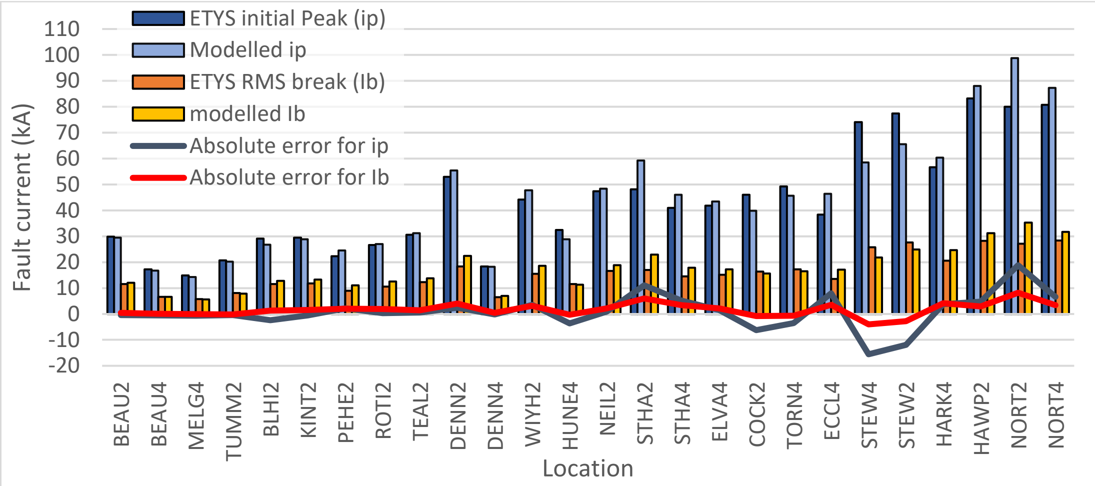

Figure 37:Comparison of initial peak current and RMS break current to published values for summer minimum.

In general, the comparison shows that the model provides a good representation of the fault currents in many locations in the network. There are some locations where the error is relatively high. However, these can be explained and justified. The error in the northern part of the NGET system (right hand side of Figure 36 and Figure 37) is expected to be high and in the positive direction. This is due to aggregating a lot of generation at the 'NGET' bus. Hence, studies concerning locational aspects, such as fault analysis, performed on the NGBTS should focus on the Scottish part of the network.

The Strathaven (STHA) and Eccles (ECCL) nodes in the southern Scottish region both exhibit an overestimation of fault levels when compared to the ETYS data. Through communication with SPEN it is understood that when calculating the ETYS fault levels, these substations are run in a 'split' arrangement as there is concern that fault levels are too high in this area. In practice these substations are a double busbar configuration with a bus-coupling circuit breaker. In a split arrangement, the bus-coupler is open, splitting the busbars, and resulting in lower fault levels due to an increase in the effective impedance. Conversely, the bus-coupler is closed for a 'solid' running arrangement. Network substations in the Nort-GB-Test-System are represented by single busbars, with no bus couplers, i.e. a 'solid' arrangement, and therefore are expected to produce higher fault levels.

4.6.2 Voltage and transient stability performance

To give assurance on the dynamic performance of the NGBTS model, a wide range of double circuit faults are applied for the summer minimum and winter peak scenarios. The faults are applied to all double circuits (or single circuits where only one line exists) at 2%, 50% and 98% along the distance of each line, and on all the critical transmission routes.

4.6.2.1 Testing critical boundary transfer conditions

The winter peak demand condition that is used to calculate the fault levels does not yield the highest possible boundary transfer conditions. Therefore, the power supply in each area north of the boundary is increased stepwise to increase the boundary transfers and critical faults are applied across each respective boundary to determine the stability-related boundary transfer limits. To compensate for the increase in generation, demand is reduced in England. In addition, the SGs are set close to their peak active power loading to give a 'worst case' condition, as they will be more prone to pole slipping at high load.

An example of the process to determine the stability limits is given in Figure 38 for a double circuit fault applied on the eastern B6 transmission route. For Figure 38 (a), the B6 boundary flow is just below the stability limit, and the system voltages (top) and SG rotor angles (bottom) both recover from the disturbance. For Figure 38 (b), the B6 boundary flow is just above the stability limit (approximately 3,880 MW in Table 10). In this case, the rotor angles of the SGs in the Scottish region (north of the fault) diverge from the rest of the system until separation occurs, and the system voltages collapse.

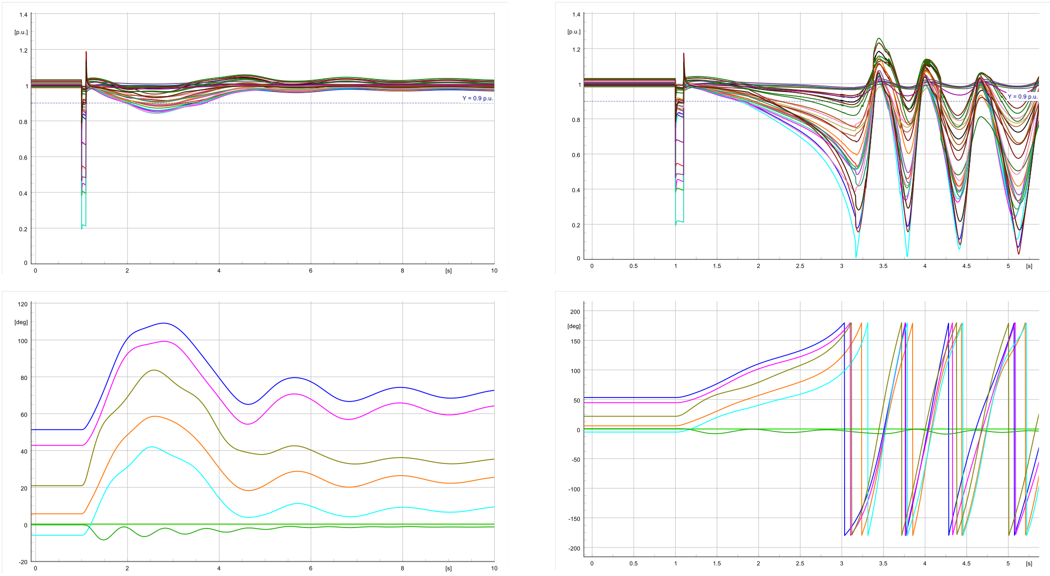

(a) (b)

Figure 38: example of stable and unstable B6 boundary transfers for a double circuit fault. (a) shows system voltages (top) and SG rotor angles (bottom) for just stable power flows, and (b) shows unstable power flows

In practice, the voltage and angular stability limits across the B4 and B6 boundaries will be dependent on many factors, and, in fact, the limiting factor can change with the prevailing system conditions. Furthermore, it is possible that higher peak boundary transfers can be achieved in the NGBTS, for example, by adjusting the generation dispatch or tuning of controller parameters.

The boundary transfer limits stated in the ETYS are driven by thermal constraints (limits of some individual super-grid transformers), and not stability limits [127]. It is not possible to verify conditions leading to these thermal limits in the NGBTS due to aggregation of network elements. Through discussion with industry experts, it is understood that: firstly, the boundary limits stated in the ETYS might only include steady state analysis, and secondly, the stability limits can often be very close to the thermal limits, and that, in practice, during certain onerous conditions, the stability limits can be below those stated in the ETYS. As shown in Table 10, the system in 2022 as represented in the Model nevertheless exhibits similar secure boundary transfer limits to those reported in the ETYS. The same process is performed to determine boundary transfer limits in the 2032 version of the system. These cannot be validated but are included in Table 10.

Table 10: Comparison of modelled and published boundary transfer limits in 2022 for validation, and new boundary transfers calculated for 2032 (not validated)

Year	Boundary name	Modelled boundary transfer limit (AC) in MW	Total modelled boundary transfer limit (including embedded DC link transfers) in MW[1]	ETYS stated transfer limits
2022	B4	3,325	3,325	3,200
	B6	3,880	6,080	6,100
2032	B4	5,200	11,200	n/a
	B6	4,000	8,200	n/a

1. In 2022, only the western HVDC embedded link is in service. In 2032, all additional HVDC embedded links are service as detailed in Table 5. The AC transfer limit does not include the DC link capacity.

4.7 Methodology for dispatching the North-GB-Test-System

To dispatch the model some simplified logic is applied that represents the wholesale market arrangements in GB. This section describes the general principles and assumptions made. The outcome of implementing this methodology allows the creation of a wide set of representative generation dispatch scenarios that can be applied to the current 2022, and future 2032 version of the system.

4.7.1 Overview of dispatch methodology

An overview of the process followed to dispatch the power system model is shown in Figure 39. The figure shows some of the main inputs and outputs at each stage of the process, as well as the constraint and balancing actions taken to determine the suitability of each case study. First, the following variables are selected to define the scenario inputs: the time of day, the season, the gross system demand, the wind conditions, and outputs of DG. Then, the net transmission system demand is calculated, and the available low-cost generation is dispatched. At this point the residual demand is calculated and used to provide a price signal to the flexible 'price-responsive-assets' (HVDC-IC, BESS, PSH). A check is then performed on the initial balance between generation and demand: if there is a generation excess, H_2 electrolyser load is added to the system. An AC load flow is then calculated, and balancing is performed by the slack generator. If a generation surplus remains, the system is re-dispatched by curtailing wind. The security of the system is now checked: firstly via a steady-state contingency analysis to confirm that voltage and thermal limits of network elements are respected, and secondly by applying faults to the critical system boundaries (B4 and B6) to confirm stable power transfer with RMS time domain simulations. If voltage, thermal or stability limits are found to be exceeded, then the system is re-dispatched by curtailing wind or bringing on any remaining capacity of H_2 load in the Scottish transmission regions. The assumptions and approach taken are described in detail in the following subsections.

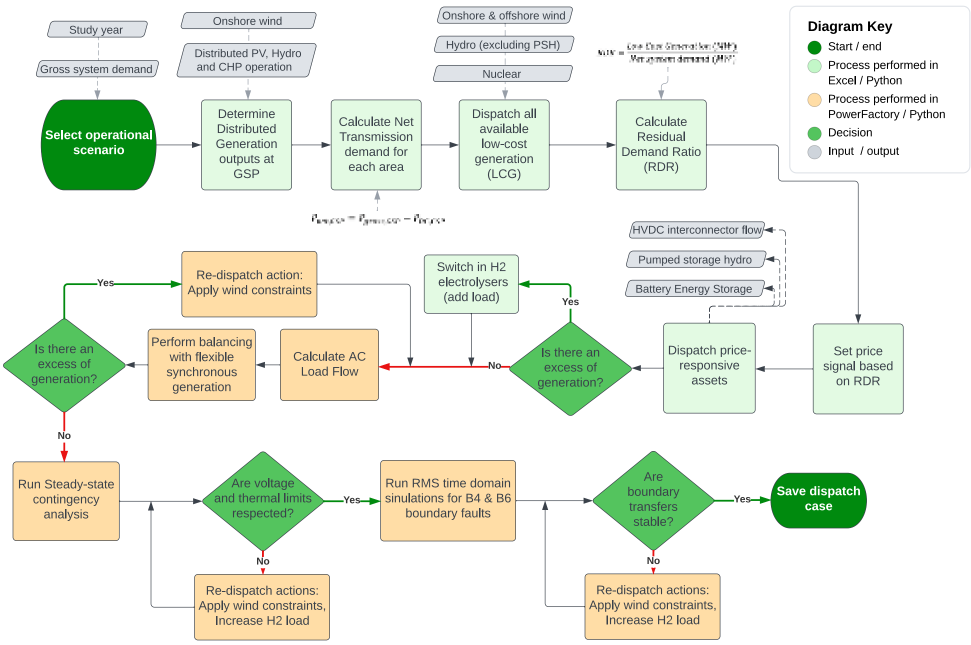

Figure 39: Process flow diagram of dispatch methodology

4.7.2 Merit order of Generators

Generation participating in the GB wholesale market is scheduled by its owners in merit order. Electricity generation is, for the most part, dispatched to meet the system demand. That is, it follows a 'load-following' arrangement. In the wholesale market, generators bid in their price to produce the required amount of power and contribute to meeting the system demand. Each generator is ranked in order of increasing price (in £/MWh), which is known as the merit order. The marginal cost to produce the final MW required to meet the system demand sets the price paid to all other generators below them in the merit order stack. The price at which generators bid into the day-ahead and real-time markets is dictated by their upfront costs to generate electricity (or their 'short-run' marginal cost) which is typically driven by the cost of fuel. In general, thermal power plants have the highest marginal cost and become the 'price setters', in GB, this is often CCGT plants running on natural gas.

Generation types that bid in with a low marginal cost include nuclear power plants, and renewables such as wind, solar and hydro. Baseload nuclear power plants typically have a low marginal cost due to high start-up costs and are committed for longer time periods. They are also very expensive to constrain-off and the ESO is expected to constrain-off wind power first. The output of a nuclear plant in GB is primarily dictated by its technical availability and is largely decoupled from the system demand level: hence the term ‘baseload’ power. When maintenance is required on a nuclear plant that requires de-energisation from the grid, the outages can be lengthy. However, when operational, they are typically run at full load. An availability of 75% for the combined nuclear fleet in GB is assumed, based on historic observed performance [159].

Renewables have very low operational costs, and their output is mainly dependent on the availability of the natural resource. Dispatch of wind is discussed in Section 4.7.4. The run-of-river hydro units will also have very low short-run costs and will generate based on the available flow of water and technical availability.

In principle, with higher penetrations of renewables on the system, a lowering of the wholesale electricity price will be observed as the more expensive – often fossil fuel based – generation is pushed out of merit. This is termed the ‘merit order effect’ and has been observed in many electricity markets around the world [160]. Figure 40 shows an example of a merit order stack in the wholesale market with the dominant types of generation in GB. When dispatching the power system model, wind, solar, hydro, and nuclear are all classed as low-cost generation and are dispatched first. The remaining system demand (including demand from PSH, BESS and HVDC-ICs – see Section 4.7.5) is met with ‘next-in-merit’ generation which, in GB, is mostly made up of flexible gas with some large-scale bio-mass plant.

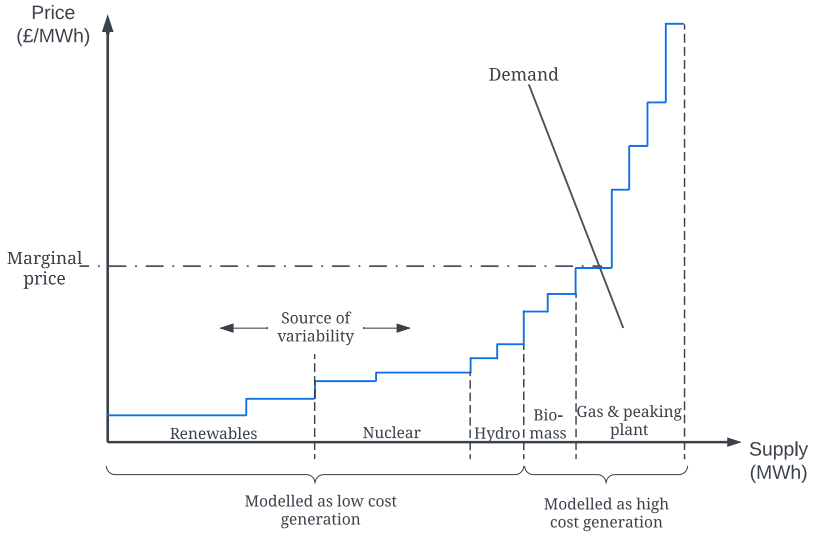

Figure 40: example of the merit order of generators in the wholesale electricity market including low-cost and high-cost generator types in the model, adapted from [138]

4.7.3 System demand and distributed generation

DG capacity tends not to be dispatched by the short-term wholesale market. For DGs that are variable renewables, they operate based on their available resource. For other more controllable DG types, such as CHP units, their output will be based on the operating regime of the user, which in turn may be driven by external factors such as temperature control. Regardless of the type of DG, high penetrations lead to an increasingly localised supply resulting in a less schedulable generation portfolio for the Transmission System Operator (TSO) [14].

The installed capacities of DG at each load point in the model is determined according to Section 4.3.2. The wholesale market generation dispatch and system operational actions by the ESO are performed at the transmission level, i.e. centralised generation is dispatched to meet the demand that is 'net' of DG. The net transmission system demand at each GSP ($P_{net,GSP}$) is calculated according (19) from the gross GSP demand ($P_{gross,GSP}$), the DG installed capacities ($P_{ratedDG,GSP}$) and the assumed DG capacity factor ($CF_{DG,GSP}$) determined based on the demand scenario detailed in Table 11.

$$P_{net,GSP} = P_{gross,GSP} - \left(\sum_{i} P_{ratedDG,GSP,i} * CF_{DG,GSP,i} \right) \tag{19}$$

where i is the DG type of either wind, PV, hydro, or CHP.

For the system to accommodate very high aggregated outputs from the amounts of wind power planned to be on the system, demand will also need to be high, noting that demand can also come from exporting ICs, PSH and BESS. Therefore, it is of interest to study both high and low demand scenarios. Five gross system demand set-points are considered that cover a range of snapshots from the minimum to maximum demand. Some general assumptions are then applied to determine the DG outputs based on diurnal and seasonal behaviour to determine the net transmission system demand for each scenario. These are detailed in Table 11.

Table 11: Gross demand, net demand, and distributed generation capacity factors for each demand case study

Name	**Time of day & time of year**	**Gross system demand (MW)**		**DG capacity factor (%)**			
		2022	2032	PV[2,3]	Hydro[4]	CHP[5]	Wind[6]
D1	Summer min., night-time[1]	20,858	19,921	0	20	20	Changes within demand scenario
D2	Summer min., Afternoon[1,2]	29,400	29,807	60	20	20	
D3	Demand mid-point, daytime[3]	37,816	40,707	30	39	55	
D4	High demand, evening	45,000	51,101	0	60	70	
D5	Winter peak, evening[1]	54,773	61,494	0	60	70	

1. Gross demand and installed capacities of DG at GSP level are taken from the System Transformation scenario of [126].
2. Peak solar PV outputs coincide with summer minimum afternoon demand, capacity factor has been estimated from [161].
3. Average capacity factors for hydro and CHP are applied to the ‘demand mid-point’ case according to [14], and a moderate daytime solar capacity factor is assumed to be half of the peak.
4. In general, the availability of Hydro generation is higher during the winter, due to higher rainfall [162].
5. Distributed CHP outputs are assumed to be high during the winter evening cases, and low during summer.
6. The output of wind DG takes the onshore wind capacity factor for the area in which it is located. See Section 4.7.4 for how the wind capacity factors are determined.

According to the FES, the gross peak load is expected to grow in the period to 2031/32, but the minimum demands are not predicted to change by very much. In the case of the summer night-time minimum, demand could decrease slightly. Meanwhile, the capacity of DG is expected to increase, where most of this is expected to be solar PV in the NGET area. This means that the net transmission demand is set to notably decrease in the coming decade for the low demand scenarios. However, it might be the case that after the mid 2030s (beyond the modelling done in this work), the uptake of electrified heating technologies and EVs could be enough to offset this decrease in net demand.

When considering the case in Scotland, its proportion of the national demand is very low compared to the proportion of the installed generation capacity, which is high. In some of the cases studied here, Scottish GSPs become net exporters of energy as the DG outputs exceed the local demand. Among other challenges, this can have significant impacts for the operation of the LFDD scheme, jeopardising its operation should it be required to shed load in a major system event [72].

4.7.4 Dispatch of wind generation

The influence of increasing wind penetration on system stability is the primary focus of this work. Therefore, incorporating a realistic profile of wind power outputs into the modelling is important to achieve results that are representative of actual system conditions. For example, it is important to understand what the realistic peak output of all wind farms can be during very windy conditions, and what is the likelihood that all wind farms in Scotland are simultaneously producing their rated power output.

As part of the work undertaken in [163] at the University of Strathclyde, a tool has been developed to help inform transmission network investment that provides an extended dataset of wind farm capacity factors for all wind farms in Scotland and some offshore wind farms in England. The dataset uses 40-plus years of simulated wind power outputs for all existing and planned transmission connected wind farms in Scotland as of 2019. The capacity factor data from that work has been utilised as an input to the scenarios developed in this work, allowing the spatial correlations between different areas of the system to be respected. The dataset also allows a realistic representation of the difference between onshore and offshore wind farm outputs. Offshore wind farms can achieve higher annual average capacity factors due to larger turbine size and higher wind speeds.

First, the data is sorted by the Scotland-wide capacity factor (CF). The Scotland-wide CF is a function of the CFs of each category of resource - onshore or offshore, located in the SPEN or

SSEN area - weighted by the total capacity of wind farms in each category. Six different snapshots are then selected from the time-series data that represent a range of wind power outputs in Scotland. Each of these snapshots are selected as the average hourly capacity factors that are closest to the 20%, 40%, 60%, 80%, 90% and 99% quantiles. Each quantile represents the amount of time that is spent below this capacity factor value on an aggregated Scotland-wide basis. Note that more snapshots are taken towards higher aggregated wind power outputs, i.e. the 90^{th} and 99^{th} percentiles are take in addition to the 80^{th}. From each representative hourly wind profile, the capacity factors are calculated for onshore and offshore installations for each transmission area, i.e. SSEN, SPEN, and NGET. As a result, for each scenario, a spatially correlated onshore and offshore average capacity factor is applied. Figure 41 shows the quantile plot for the 40-year time series data, with the six selected representative hours used in the Scenarios.

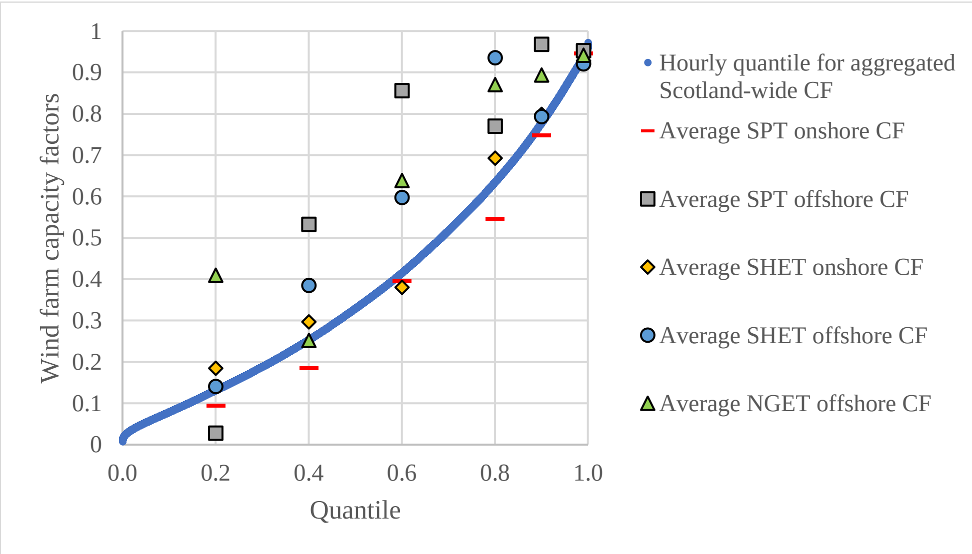

Figure 41: quantile plot for Scotland wide capacity factors and the area capacity factors for each selected scenario

Figure 41 shows that wind farms in Scotland can often reach high aggregate wind power outputs. The 50^{th} percentile (often termed the P50 value), relates to an approximately 33% Scotland-wide capacity factor. However, for approximately 10% of the year, the Scotland-wide capacity factor can be expected to be at least 80%, yielding very high instantaneous wind power outputs. As expected, the offshore wind capacity factors are consistently higher than the Scotland wide average. This selection of six sets of capacity factors is applied to each scenario being assessed.

Onshore wind farms can achieve a high annual availability in the region 95 – 99% [164], [165]. However, offshore wind farms can require increased maintenance effort and longer mean-time-to-repair due to their location far offshore making access and maintenance more challenging [165]. Long term availability data is not publicly available for offshore wind, and the industry is evolving. It is expected that, over time, maintenance practices will become increasingly efficient, alongside improving component reliability and average availability factors would increase. A technical availability of 95% of all offshore wind turbines, and 98% of all onshore wind turbines is assumed.

4.7.5 Residual demand and price responsive assets

Flexible price responsive assets, such as pumped storage hydro (PSH), HVDC interconnectors (IC), and, to an increasing extent, Battery Energy Storage Systems (BESS) also play a big role in meeting demand (or creating a demand for excess generation). These systems will typically operate based on the wholesale price of electricity, acting as a sink of power (or a load) when the price of electricity is low, and a source of power when prices are high. The dispatch of price responsive assets is controlled by the amount of residual demand in any given scenario. Price responsive assets are all modelled as transmission connected.

4.7.5.1 Calculation of residual demand

Based on the power available from low-cost generation and the level of net transmission system demand, the residual electricity demand is calculated. Here, the residual demand is defined as the net transmission system demand (considering only the distribution system, or 'GSP' demand), that cannot be met by low marginal cost generation, including nuclear. The general principle of the approach is that the lower the residual demand the cheaper the wholesale electricity price is, and vice-versa, which in turn creates trading opportunities for 'price responsive assets' on the system. The 'Residual Demand Ratio' is the ratio of low-cost generation to total GSP demand and is calculated as:

$$RDR = \frac{\sum low\ cost\ generation}{\sum P_{net,GSP}}$$

Based on the RDR, five price setpoints are determined, which are used to dispatch the price responsive assets, i.e. PSHs, BESS' and HVDC-ICs. The RDR prince settings are shown in Table 12.

Table 12: Residual demand ratio values and associated price signals for dispatching the power system model

Price setting	RDR (%)
Low	RDR > 100%
Medium Low	75% < RDR < 100%
Medium	50% < RDR < 75%
Medium high	25% < RDR < 50%
High	RDR < 25%

4.7.5.2 Pumped storage and BESS

Pumped storage and BESS plants are assumed to operate an energy arbitrage regime, i.e. they will be pumping to fill the reservoir or charging their batteries when electricity is cheap, and they will be generating or discharging to the grid when energy is more expensive. Pumped hydro and BESS will also play a key role in closer to real-time operation by correcting imbalances in the spot market.

When developing the scenarios to be studied, PSH and BESS are assumed to have sufficient reserve capacity to operate at their instantaneous power rating. In practice, for example during long lasting windy conditions, it is possible that water reservoirs become full, or a battery's state of charge is at its maximum, resulting in conditions that do not allow continued pumping or charging respectively.

4.7.5.3 HVDC interconnection

HVDC-ICs operate based on a price differential between the two electricity markets that they connect. GB currently has 8.4 GW of HVDC interconnection that is planned to almost double to 15.9 GW by the early 2030s (see Section 4.4.6). The net interconnector flow in GB is a complex picture that, during any given market settlement period, depends on the conditions present in multiple different power markets and can follow a more stochastic profile. The price differential between interconnecting markets and the consequent IC power flows will depend on many inter-related factors, such as: the generation background in each system, government policy, carbon pricing mechanisms, fuel prices, land constraints, availability of natural resources.

This work draws on publicly available market data downloaded from [166] for HVDC dispatches in 2022, and the analysis undertaken, and conclusions presented in [167] for the early 2030s system. The study in [167] modelled the European electricity market using the ANTARES modelling framework to assess the value of interconnection in a changing EU electricity system. Currently, on average, GB is one of the more expensive electricity markets compared to its neighbours with which is shares interconnection, resulting in GB being a net importer of power. However, in part due to the planned expansion of wind power, it is expected that GB will transition to a lower cost market and become a net exporting nation as a result.

To represent a range of HVDC-IC power flows, the maximum net import, maximum net export, average annual transfers and mid-points in between are calculated for 2022 and 2032 for the North-Sea Link (NSL), North-Connect (NC) (both connected in the north of GB) and the net flow of all the other HVDC-ICs in the NGET region. Figure 42 (a) and Figure 42 (b) show the HVDC-IC flows with varying RDR.

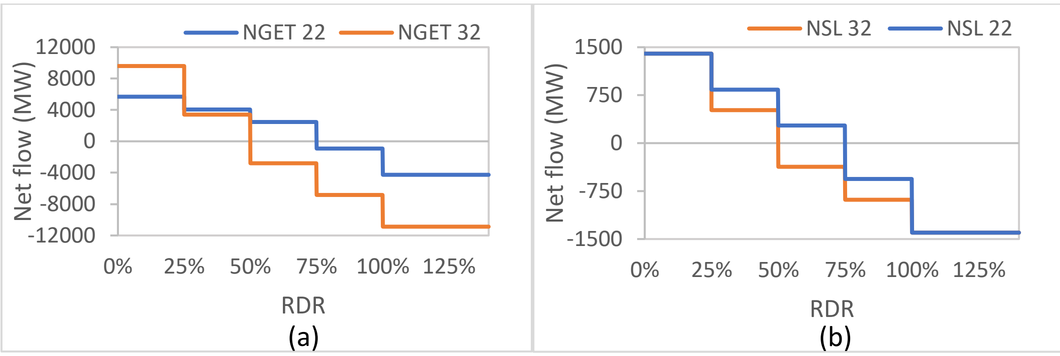

Figure 42: HVDC interconnector power flows for 2022 and 2032 based on the residual demand ratio (RDR) for (a) net flow in NGET area, and (b) the North-Sea Link. The North Connect link takes the same as NSL 32

4.8 Case studies

Using the assumptions and rules in Section 4.7, a series of generation/demand dispatch scenarios are developed that represent a range of system conditions. These scenarios are designed to exhibit variation in the demand on the system and in the types of generation dispatched to meet it. The scenarios consist of six different cases for wind outputs which are overlaid onto five net system demand snapshots. In total, before discarding any uncredible dispatches or adding in any sensitivities, this results in 60 demand/generation dispatch scenarios. The scenario names contain the demand case, the wind case, and the study year in the format: 'D(x)' for gross demand case from Table 11, 'W0.(x)' for the Scotland wind capacity factor from Figure 41, and 'Y(x)' for the study year.

4.8.1 Operational constraints

The self-dispatching of generators, storage assets, and interconnectors by their owners through the wholesale market does not always provide a feasible secure generation dispatch. The ESO must operate the system in compliance with the SQSS [8]. For each of the demand/generation dispatch scenarios, some constraints are applied to respect the following criteria:

1. System-wide balance of demand and generation.
2. Steady-state thermal and voltage limits.
3. System voltage and angular stability for critical boundary faults.

Refer to Figure 39 in Section 4.7.1 for the process of applying the constraints and balancing actions to each scenario. The constraints above are written in the order in which they are checked and applied. Should the generation dispatch be infeasible, the system is re-dispatched by either curtailing wind power or by bringing on additional demand via H_2 electrolysis.

4.8.1.1 System balancing

The system-wide demand, including losses, must be balanced with generation. In an unconstrained dispatch, either an excess of demand, or an excess of generation can occur. During periods of low demand and high renewable generation outputs, there can be an excess of generation on the system and there is no remaining capacity on the flexible price responsive assets or H_2 production to consume the additional power. In these cases, all the generation on the system has a low marginal cost. From the perspective of the current market and operational arrangements, it is unclear how these resources would be dispatched, and which resources would be most economically curtailed.

The first operational action to address a generation excess is to increase demand from H_2 production in all areas. For the purposes of assessing high levels of generation outputs in Scotland, any remaining imbalance between generation and demand is corrected by curtailment of wind in England and Wales. Generation in Scotland is curtailed where exports from Scotland exceed the network's security criteria (see Section 4.8.1.2), which also contributes towards correcting a generation surplus. In practice, generation in England and Wales might also be curtailed for other reasons, e.g. constraints on local parts of the network not included in the Model. Figure 43 in Section 4.8.2 shows the cases that require adjustments to be made to the unconstrained market dispatch.

In some cases, when low-cost generation outputs are higher than national distribution system demand, signals are provided to the flexible price responsive assets to 'take-off' a high amount of power. However, if the ICs, PSHs, and BESS all export, pump, or charge close to their rated capacity, it can lead to a significant amount of additional demand being added to the system which is no longer met by low-cost generation. This needs to be met by higher-cost fossil-fuel based synchronous plant. However, from an environmental perspective, it is not logical to be burning high amounts of gas only to export this power over an interconnector. To limit this, the IC exports are reduced in some cases.

4.8.1.2 Steady-state contingency analysis

To check the state of the system during abnormal conditions, i.e. during the outage of system elements, the 'contingency analysis' module is used in PowerFactory. The contingency analysis first performs an AC load flow calculation for the intact system, then a subsequent AC load flow for each contingency case. The contingencies defined include an outage of all single circuit and double circuit transmission lines, and a selection of network transformers and generators.

For the 2032 cases, there are four new embedded HVDC transmission circuits off the east coast of GB adding to the north-south power transfer capacity. Each link is expected to be rated at 2 GW and, in the HND design by NGESO, is assumed to be a bi-pole configuration with metallic return and sufficient pole separation such that each pole can be considered as a separate transmission circuit [124]. Therefore, for the embedded HVDC links, the contingency is assumed to be a loss of 50 % of the embedded link's capacity. For the HVDC ICs, namely the North-Connect and the North-Sea interconnectors, these are both rated at 1400 MW and assumed to be a monopole configuration, i.e. a contingency is included considering the loss of 100 % of the link's capacity.

The contingency analysis checks that the post-outage network voltages and thermal loads are maintained within their operating limits. For voltages, all transmission busbars are maintained within ±5 % of nominal voltage levels. For thermal ratings, all transmission lines are maintained within 120 % of their continuous thermal rating for the immediate post-fault condition to allow for short-term ratings to be utilised. In practice in GB, a ratings schedule is applied and the 20-minutes, 10-minutes, 5-minutes and 3-minutes ratings can be used to manage thermal loading of transmission assets in operational timescales [168]. The 20- and 10-minutes ratings allow for operational actions to be performed post-outage by the control room, and the 5- and 3-minutes ratings can be used in coordination with an automatic generator inter-tripping scheme. The short-term ratings of lines are not publicly available. The 120 % allowable post-fault short-term loading assumed here is representative of a 10-minute rating [168], [169], and in such cases, the ESO would re-dispatch generation post-fault to bring the line loading down.

Several cases are found to breach the post-fault thermal and voltage limits. For cases that are not secure: first, any remaining H_2 demand is utilised (which may have already been switched in for system balancing purposes), and then any additional generation in the constrained area is curtailed until the security limits are respected. Curtailments are applied to the wind generators on an equal basis in each area, depending on the location of the constraint.

4.8.1.3 Stable boundary transfers

As discussed in Section 4.6.2, the stability limits can often be very close to the thermal limits, and, in practice, during certain conditions, the stability limits might become the limiting factor. Whether the limiting factor is thermal, voltage or stability related depends on the prevailing system conditions. However, stability-enhancing assets in the network, for example, dynamic voltage support or series compensation, can increase the stability boundary.

The final step to ensure the case is feasible is to check for stable boundary transfers across the B4 and B6 boundaries. An RMS simulation is run while applying a double-circuit fault on each transmission route crossing the boundaries. The faults are cleared by opening the circuit breakers of both lines and checking that bus voltages and generator rotor angles recover after the fault has been cleared. For the cases studied, no constraints are applied due to unstable boundary transfers. Therefore, the limiting factors are always thermal or voltage related.

4.8.2 Applied operational constraints

Of the sixty cases, twenty-five require some adjustment due to operation constraints; for details on how these are applied. Of these, three cases are discarded, seven cases can be corrected by adding demand from H_2 to absorb excess wind generation, and fifteen cases require additional generation curtailment to reach a system balance or respect security criteria. For the discarded cases, the amount of wind curtailed results in a final balanced dispatch similar to a case already existing in the dataset. As such, they are discarded from the set studied further in this work. Figure 43 shows, for the cases that require them, the adjustments made to the unconstrained market dispatch.

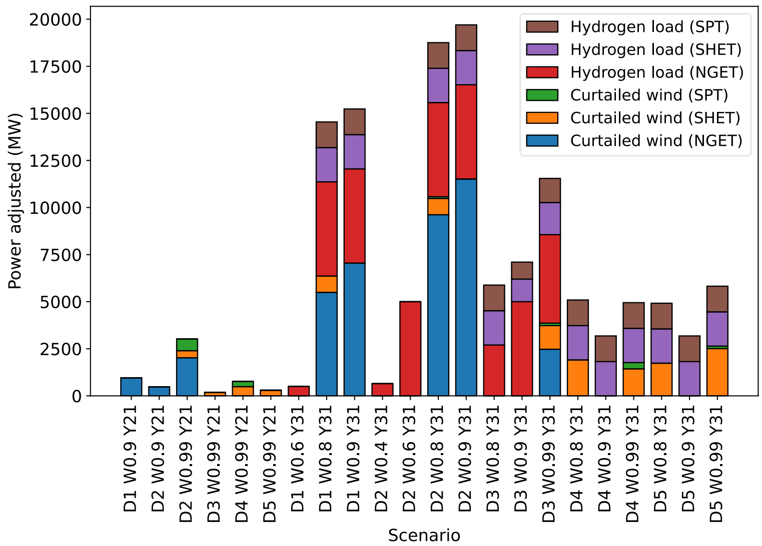

Figure 43: power adjustments in MWs required from operational actions (system balancing and contingency analysis) - wind generator curtailment and added hydrogen demand in each area

During low demand and high wind conditions, an excess of generation is common, and – sometimes extensive – adjustments are required to correct it. These are shown as balancing actions in the NGET area. For some 2032 cases, up to 20 GW of excess power must be removed from the system via generator reductions or load increases. For higher demand cases, fewer actions are required for system balancing, but regional constraints are still required in the Scottish transmission areas to respect thermal and voltage limits. In all 2032 cases, adding demand from H_2 electrolysers significantly reduces the wind curtailments required in each area and, in some cases, completely offsets the need to curtail generation. For the same wind speed assumptions, the amount of power curtailment required in the 2032 system is much higher than in 2022.

A generation surplus is easily reached for demand case D2 (summer daytime low demand with high distributed PV output). In general, in GB, more frequent and higher peak wind speeds occur during winter compared with summer [162]. However, low wind speeds can be experienced throughout the year. It is not simply the case that GB gets low winds in summer and high winds in winter; instead, winters have more variable winds and include higher winds that are absent in the summer [170].

Wind speeds and solar irradiance – and their respective aggregate power outputs – have, in general, a negative correlation. Studies in [170], [171] show that in GB, there is a clear shift in the distribution of wind speeds towards higher winds during cloudy conditions, particularly in winter. Therefore, high wind and solar outputs typically do not occur simultaneously. However, this is not to say that high wind and solar outputs cannot coincide, but their absolute peaks are unlikely to occur. In GB, coincident high wind, high solar and low demand can occur during late spring, e.g. during a bank holiday or weekend [172]. Under these conditions, the ESO would need to carry out significant curtailment.

Figure 43 highlights that more generation curtailments are required in the SSEN region (northern Scotland) compared with the SPEN region (central/southern Scotland). This curtailment is partly because of the very high installed capacity of wind being planned in SSEN, but also that all excess generation from the SSEN area transmitted through the AC system must go through the SPEN system. As such, an increase in demand or decrease in generation in SSEN reduces the flow into and out of the SPEN area, reducing the overall power excess. Therefore, H_2 (or other forms of demand response) might be of higher value in the SSEN area for the studied system.

4.8.3 Selected case studies

The final generation dispatches for each case study (post-operational actions) are shown in Figure 44. These selected case studies exhibit a broad range of credible operating system conditions and, after applying network constraints, represent conditions close to the system's limits for the modelled network. The scenarios show the importance of assets that add demand to the system, e.g., HVDC-ICs, BESS, PSH, and H2, which are needed in future cases to absorb excess wind outputs.

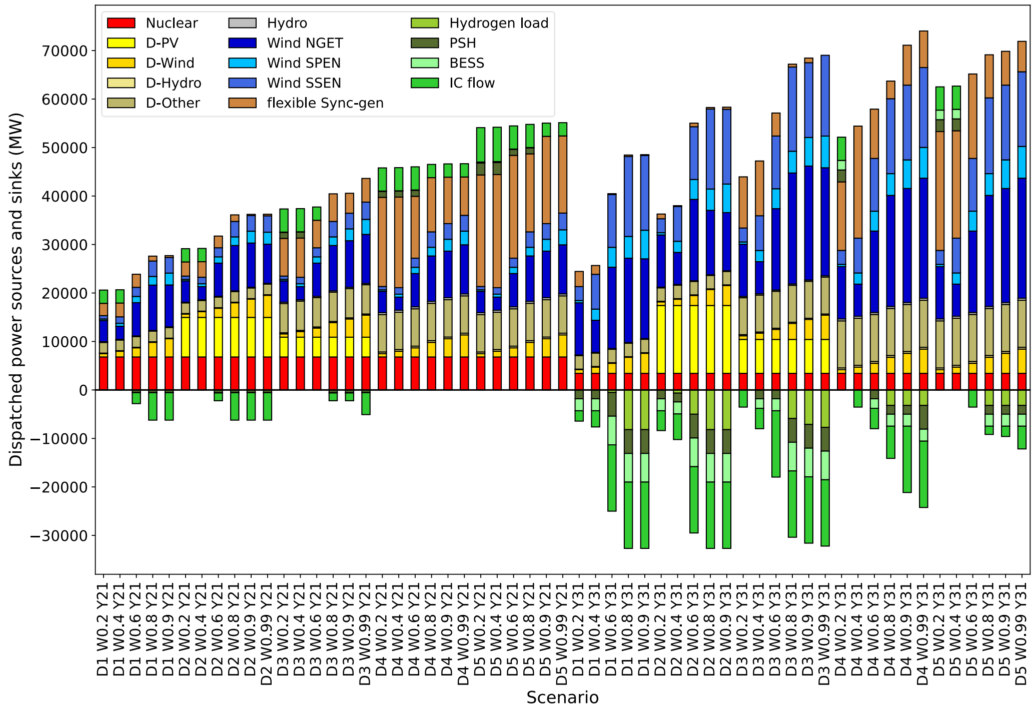

Figure 44: Generation and demand dispatches for all selected scenarios

Chapter 5: A Decade of Electricity System Transition in GB - Effects on System Dynamic Properties

Chapter 1 introduced the significant changes expected in the GB system, especially in the Scottish regions, which have been implemented in the NGBTS described in Chapter 4. Chapters 1 and 2 also introduced and described how the network's inertia and fault levels are two fundamental indicators of the system's ability to maintain a balanced and synchronised state following disturbances. Furthermore, IBRs are widely understood to reduce system inertia and fault levels in transmission systems.

The impacts of reducing fault levels (and sometimes inertia) are often described interchangeably as lowering the "system strength" at a particular point in the network [173]. In recent years, the understanding of system strength has been evolving, and the term has been used to describe a broad set of operational challenges [41], [50]. These include, for example, the correct operation of protection systems or sub-synchronous control interactions of IBRs. However, as the penetration of IBRs becomes more dominant in the system and new challenges emerge, using the fault level metric, while it remains related, can become less effective in assessing some of the issues often classified under the term system strength.

To address some of these challenges, National Grid ESO (NGESO) in GB has gone some way towards defining minimum inertia and fault level requirements [16], [21]. Via the Stability Pathfinder (SPf) tender exercises, NGESO seeks to procure inertia and fault levels in the GB transmission network. NGESO is also reforming GB's frequency response and reserve services (See Section 2.3.2). However, it is important to understand the nature of the changes to these dynamic properties to assess the system's future needs and determine the types, locations, and volumes of solutions.

The work in this chapter reviews the meaning of system strength in the context of reducing fault levels in the system. Then, using the NGBTS developed in Chapter 4, a quantitative assessment of the changes in the inertia and fault levels in the GB system is provided. As the NGBTS has been extended to include a credible version of the future Scottish transmission network in 2032, the cumulative changes to these critical dynamic system properties can be assessed at the system and regional levels. The review highlights some challenges when using the fault level metric as a system stability indicator. To the author's knowledge, no published works quantify the cumulative influence these generation and network expansion plans have on the range of fault levels expected in Scotland. In addition, the voltage dips resulting from a wide-range of faults are assessed, highlighting the changing nature of power system dynamics where IBRs are the dominant source.

The case studies used in this Chapter are those developed in Chapter 4, Section 4.8.

5.1 Stability pathfinder program

In GB, NG ESO launched the Stability Pathfinder (SPf) programme, with a competitive tendering process for procuring new stability services. Unlike typical voltage or frequency management services, the SPf does not seek to dispatch active or reactive power. Instead, the SPf seeks to add inherent SG characteristics in the form of inertia and short circuit level to aid frequency management and provide immediate post-fault response to limit voltage drop and contain voltage angle change.

SPf is an availability-based service where providers should offer the following properties above the current Grid Code technical requirements: short circuit level of >1.5 p.u. of rated capacity, inertial response, and transient voltage stabilisation. The essence of the SPf is to act as a voltage source behind an impedance and analogous to a synchronous machine. Therefore, it cannot be met by the current implementation of grid following IBRs.

The SPf program is being managed in three phases:

- Phase 1 concluded in 2020 and focused on procuring inertia at any location in GB; phase 1 assets are included in the 2022 version of the NGBTS model.
- Phase 2 concluded in 2022 and is focused on increasing the short circuit levels in Scotland. It was also open for non-synchronous technologies, such as grid-forming converters, and awarded projects are currently under development and construction. The effect that SPf phase 2 is expected to have on fault levels across the Scottish network is modelled in Section 5.3.2.
- Phase 3 contracts were awarded in late 2022 and focused on procuring both short circuit level and inertia in England and Wales. Phase 3 projects are aggregated at the NGET4 busbar in the NGBTS and included in the 2032 modelling.

Most of the capacity procured was awarded to synchronous compensators (SCs) [145]. SCs are a type of DC excited synchronous motor that is unloaded, i.e. its shaft is free spinning. The purpose of an SC is to regulate conditions on the system rather than convert from mechanical to electrical energy, and it does not act as a source or sink of active power. SCs are a relatively old technology that were used as sources of reactive power for voltage regulation before the development of static compensators, which replaced SCs due to their enhanced flexibility and reduced maintenance costs. SCs are now experiencing a revival as they can be used to increase both system inertia and fault levels [109], [174]. SCs are currently being deployed by several TSOs internationally; for example, Energinet in Denmark [175], ERCOT in Texas, AEMO in Australia [50] and NGESO in GB [145].

5.2 Changes to inertia

Low inertia conditions typically occur during low demand and high wind generation. The system inertia, net transmission system demand and wind generation for each case are shown in Figure 45. The range of system inertia values is similar across the two study years. In 2032, as expected, there is a reduction in thermal generation compared with 2022. However, the reduction in inertia is offset, to some extent, by the SPf program and additional PSH projects, which are online and pumping during high wind conditions. During high demand and low wind conditions in future 2032 cases, there is still a need for dispatchable generation, which is assumed to come from SGs, resulting in high inertia cases.

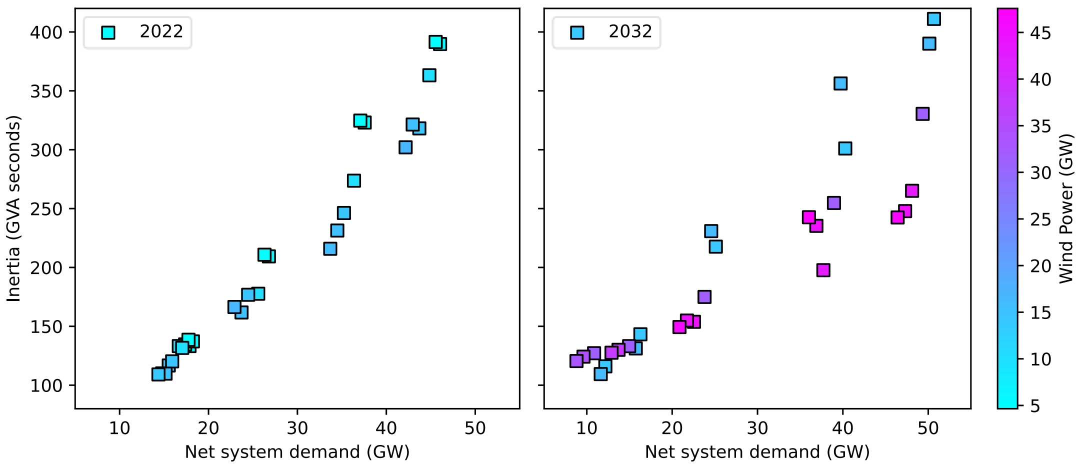

Figure 45: inertia, demand and wind power for the range of case studies for 2022 (left) and 2032 (right)

Figure 46 compares the system generation and demand conditions (left plot) and the inertia contribution from different sources (right plot) for each study year for case D2 W0.8. Over the ten years to 2032, only a slight increase in the summer afternoon minimum demand is expected (see Section 4.7.3. However, over 13 GW of DG, mostly PV, is added to the system. For the same summer minimum demand case and solar PV capacity factor assumptions, the minimum net transmission system demand is reduced from 15.2 GW in 2022 to 8.8 GW in 2032. Meanwhile, increases in the transmission connected wind can mean that generation from DG and wind can reach almost double the national demand. In the case studies here, the excess power after operational constraints is absorbed by PSH and BESS or exported over HVDC-ICs. Very low net demand can present several challenges to the system operator. High volumes of DG, which are neither observable nor controllable, can add significant uncertainty to operational procedures, impact system stability and reduce the effectiveness of automatic defence mechanisms such as under-frequency load shedding [14], [72].

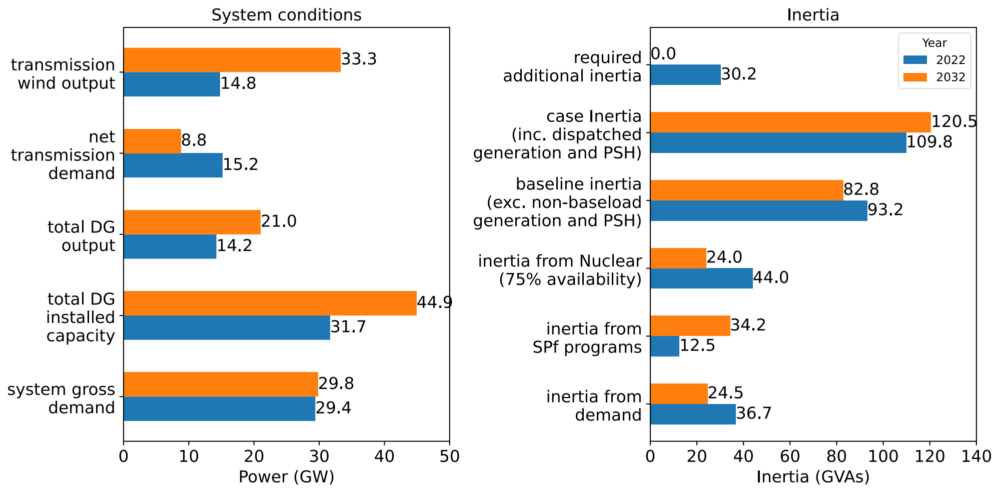

Figure 46: System conditions for case D2 W0.8 for each study year

The right-hand plot of Figure 46 shows the sources of inertia between the two years. The inertia from demand has been calculated according to the methodology published by NGESO in [176]

$$H_{demand} = max\,(2.27 \cdot Demand_{net}\,, 2.1 \cdot Demand_{gross} + DG_{wind} + DG_{PV}) \tag{20}$$

where H_{demand} is the demand inertia, *net* and *gross* denote transmission system and national demand, respectively, and DG_{wind} DG_{PV} are the distributed generation outputs.

Inertia from demand decreases even though the national demand is similar. In practice, there is much uncertainty regarding the inertia embedded in the distribution system. NGESO's calculation uses historic interconnector tripping events to determine the total inertia and then relates this to the generation inertia, of which they have more visibility [176]. Demand inertia is typically calculated from transmission system demand, but as demand grows in the future, inertia from demand may not continue to scale up proportionally as most of this growth is expected to come from EVs and heat pumps, which are non-synchronous resources [126].

For these comparative case studies, the baseline inertia, i.e. the minimum inertia on the system that should usually be available, is only reduced by approximately 11%, even though there has been a significant increase in IBR installed capacity (including DG). The reduction in inertia from the closure of large nuclear generators is mainly offset by the build-out of SCs, with some GFM BESS procured under the SPf programs (see Section 5.1). The final inertia for these cases is higher for 2032 due to the additional PSH capacity on the system. The ESO currently operates a minimum inertia level of 140 GVAs, which is expected to be lowered to 102 GVAs in the mid-2020s [16]. As such, for the 2022 case and using the ESO's minimum inertia level of 140 GVAs, an additional 30.2 GVAs would be required to maintain frequency stability within the SQSS limits should a loss of the largest infeed occur.

The analysis here indicates that without imposing any minimum inertia limits and assuming the SPf assets get built, the baseline inertia does not significantly drop by the early 2030s. Moreover, new synchronous plants are expected to come online, replacing much of the lost inertia from the closure of the existing fleet of traditional thermal generation.

5.2.1 Regional inertia

The reduction of system inertia impacts frequency stability, which is often considered at the system level. However, Section 2.5.1 highlighted that inertia distribution affects the dynamics within and between different areas of a synchronous system.

The distribution of inertia for each GB transmission zone is shown in Figure 47. The box plots show the spread of inertia values in each area for all the case studies[12]. The NGET area holds most of the demand and generation, and the range of inertia values in this area remains similar under the modelled assumptions. The NGBTS only explicitly models the northern part of the NGET system, and the remaining network generation and demand are lumped. The SPEN area (central Scotland) shows a decline in inertia mainly attributed to the loss of the Torness nuclear plant, which is only partially replaced by new SPF and PSH projects. The SSEN area (northern Scotland) sees an increase in local inertia as most of the large new PSH projects are planned for this area. The SSEN area also has the highest increase in IBRs added to the system between 2022 and 2032. Adding the PSH projects in this region might bring additional system stability benefits by adding inertia and fault level. The effect of the PSH projects' status on fault-

[12] It should be noted that the case studies represent a wide range of operating conditions, close to their expected minimums and maximums. However, they do not consider the duration over which these conditions occur and, therefore, do not show a distribution of regional inertia throughout the year.

induced frequency instability in the northeastern part of the system is studied further in Section 6.4.1.

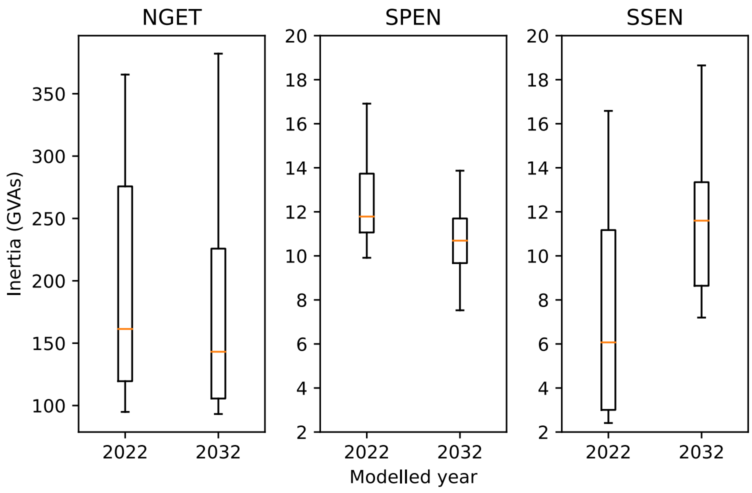

Figure 47: Distribution of inertia for each transmission area in GB (north of Scotland, Central Scotland and England and Wales) for all case studies.

5.3 Changes to fault levels

This Section assesses current and future fault levels in the Scottish regions of the GB transmission network. The fault level is dependent on the status of both SGs and IBRs. Also, the fault level at any point in the network is a function of the electrical proximity (i.e. the impedance) to the sources of fault current. Thus, the fault level depends on the system's configuration and the generation dispatch pattern at any given time.

Having network elements out of service, such as transmission circuits due to forced outages or planned maintenance, will change the network impedance and can reduce the fault levels in the locality of the outage. Planned maintenance is also typically scheduled during times of low demand. Network outages have not been assessed in this work. However, in [26], the authors find that equipment outages in some areas of Scotland can reduce the fault levels more than a change to the status of the available SG units. Therefore, determining the minimum fault levels at a particular location should include a credible outage schedule.

The fault level studies in this work are performed using the case studies developed in Section 4.8 with the following assumptions and methodology:

- Series capacitors at Eccles 400 kV and Elvanfoot 400 kV are bypassed, according to [177].
- Three-phase short circuits with zero fault impedance are simulated at each 275 kV and 400 kV busbar.

- The ‘complete’ method is used according to G74 [158], which is initialised from a preceding load flow calculation.
- Demand points have a fixed sub-transient fault level contribution of 1.1 MVA per MVA of aggregate peak demand, according to G74 [158].
- Converter fault infeed contributions are 1.1 p.u in the sub-transient period.
- For 2022, no SPF2 is considered as these have not yet been commissioned for the modelled year. They are included in the 2032 results.

5.3.1 Change in fault levels from 2022 to 2032

Figure 48 shows the calculated three-phase sub-transient fault levels $(S_k^{''})$ for the main transmission busbars in Scotland. For each scenario, no decrease in the fault levels is observed at any of the modelled locations. In fact, it is found that a significant increase in the three-phase fault level is expected. The following reasons can account for the increase:

- **Network reinforcement works:** significant upgrades are planned to increase the north-south transfer capacity. Additional parallel AC lines and higher-rated voltages reduce the impedance between network locations.
- **Substantial increases in generation capacity:** although these are primarily from IBRs with a lower fault infeed (assumed to be 1.1 p.u in this case), the aggregated rated capacity is very high compared to the existing capacity.
- **Large new PSH projects:** these projects add significant fault level (and inertia) and are likely to be online during high wind conditions.

The finding that fault levels are increasing in Scotland contradicts the common expectation that fault levels decrease as IBRs become more prevalent. Section 2.2 noted that declining fault levels are often attributed to emerging system stability challenges in power systems with IBRs. However, this finding reinforces the point that future system operability risks may not always be tied to low fault levels. On the contrary, the rise in fault levels presents significant implications for power system infrastructure and protection. High fault currents can surpass the design ratings of equipment such as transformers, circuit breakers, and busbars, leading to overheating and potential failure. Additionally, protection systems, calibrated for specific fault current limits, may need to be adjusted or upgraded to maintain operational reliability.

Another risk posed by increasing fault levels is the challenge they present to quickly and cost-effectively achieving a decarbonised electricity system. As network assets approach their fault level ratings, new connections will trigger network reinforcements due to their contribution towards the fault level rise, driving up grid connection costs and extending project timelines.

This can become a significant barrier for renewable energy developers, with some projects potentially becoming financially unviable due to the increased cost burden and connection delays.

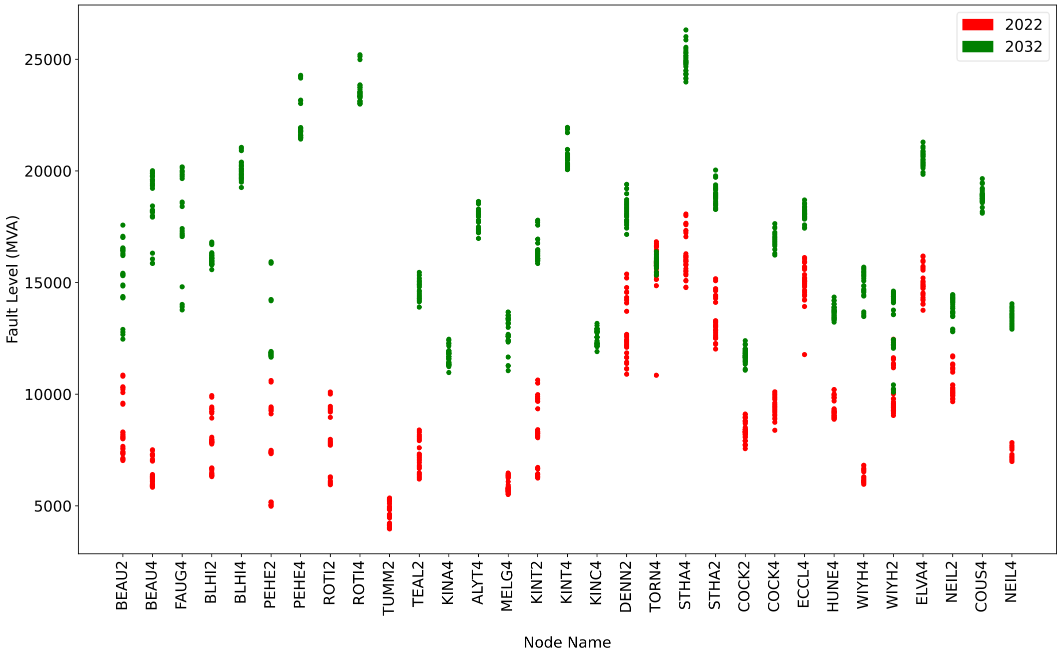

Figure 48: range of three-phase fault levels for 2022 and 2032 at transmission busbars in Scotland – all busbars left of KINT4 (inclusive) cover northern Scotland, right of KINT4 (exclusive) cover central Scotland.

Locations with SGs or PSHs, e.g. at BEAU2 or PEHE2, are observed to have a more variable range in fault level due to these sources' contributions being dispatched depending on the wind power outputs. The fault infeed contributions from IBRs are more constant than SMs; this is discussed further in Section 5.4.1.

5.3.2 Effects of Stability Pathfinder Phase 2

As mentioned in Section 5.1, phase 2 of the SPf (SPf2) program focused on procuring fault levels in Scotland. The winning projects of the SPf2 tender have been modelled at the closest available locations based on the published tender results [145].

Figure 49 shows the case 'D2 W0.8' for 2022 with and without the contribution from SPf2. This dispatch case study is one of the lower fault level cases. Low demand and high wind cases generally have lower fault levels for the range of dispatch conditions modelled. However, the fault level at different locations varies with the status of the SGs and PSHs. The SPf2 program has more impact around the Beauly (BEAU) and Blackhillock (BLHI) areas (left-hand side of the plot), which are in the north of Scotland, compared to the central Scotland locations. The total fault level from awarded projects in this area considerably exceeded the fault level requirement identified at the tender launch: at Blackhillock, 1,300 MVA was tendered for, and 3,157 MVA was procured [145].

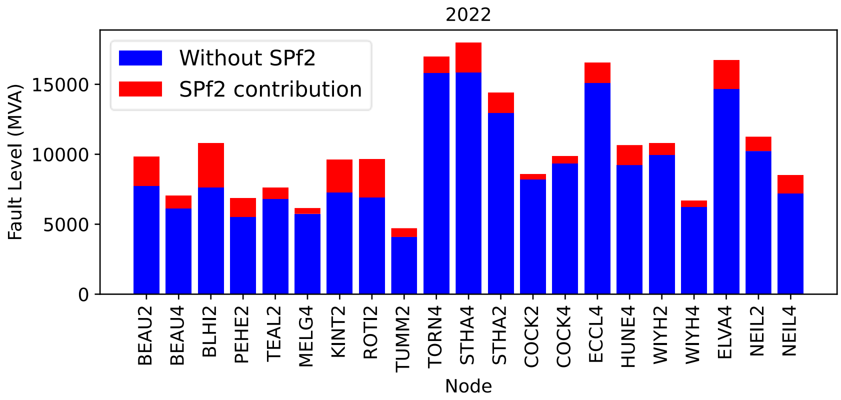

Figure 49: fault levels for case study D2 W0.8 in 2022: with and without the contributions from the stability pathfinder phase 2 projects

5.3.3 Fault level provision from converter interfaced resources

Section 5.3.1 showed that the three-phase fault levels in Scotland are expected to increase following the planned network upgrades and new generator connections. Much of this fault level will come from IBRs in the future. Some calculations of minimum fault level (e.g. for use in an SCR calculation) do not consider contributions from grid-following IBRs. For example, NGESO only considers the contribution from online SGs when calculating their 'summer minimum' fault levels [28], and the same is true when calculating the AFL metric by CIGRE and its use by AEMO [37], [173]. Excluding the fault level contribution from IBRs indicates that it is not believed to contribute towards system stability in the same way as fault level provision from SMs. The value of fault level contributions from synchronous and non-synchronous sources is still an open question, and, as discussed in Section 2.2, it depends on how the fault level metric is being used.

Figure 50 shows the contribution of fault level from synchronous and non-synchronous sources for the D2 W0.8 case comparing 2022 and 2032. The synchronous fault level contribution is calculated with the same dispatch, but the sub-transient fault level for all IBRs is set to zero $\left(S_k^{"} = 0\right)$. Where common nodes exist between the two years, they are plotted side-by-side. Otherwise, a single bar is displayed. The D2 W0.8 case for each year has similar gross demand and the same assumptions for wind farm capacity factors. However, as shown in Figure 46, the installed capacity of DG and transmission-connected wind is much higher in 2032.

Figure 50 shows the overall increase in fault level to 2032 at every location modelled for the D2 W0.8 cases. To varying extents, the increase in fault levels is provided by both synchronous and non-synchronous sources. At many locations, the synchronous fault level has increased significantly, by more than that provided by the SPf2 program (see Figure 49). The increase in non-synchronous fault level is also significant and, at some locations, contributes a large proportion of the overall fault level in 2032. The only location where the total fault level does not increase is Torness (TORN4). At TORN4, a large nuclear plant has retired, so the synchronous fault level has dropped but is replaced by a non-synchronous fault level after the connection of new wind farms and HVDC.

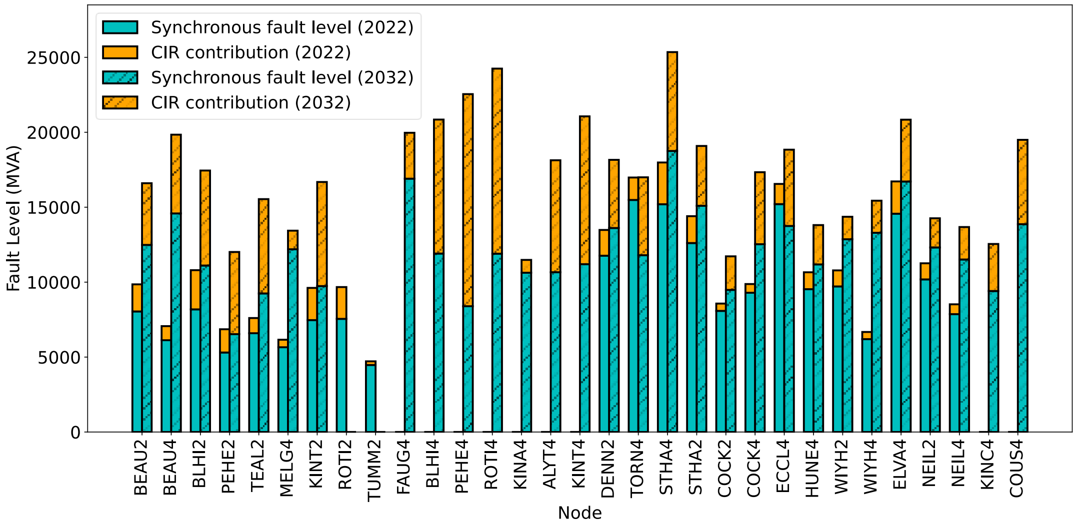

Figure 50: fault levels for case study D2 W0.8 in 2022 and 2032: contributions from synchronous and non-synchronous sources

5.4 Fault-induced voltage dips

During network faults, the voltage drops due to the low impedance to ground, causing a near collapse of the voltage at the fault location. The severity of this voltage depression depends on the fault level and the system topology. The lower the fault level, the lower and more widespread the voltage dip and the lower the system's resilience to faults.

A series of faults across the system have been simulated to assess voltage dips in Scotland today and in the future. For each generation dispatch pattern developed in Section 4.8, faults are applied to each single circuit transmission line at 2 %, 50 % and 98 % along its length, giving a total of 5,376 fault cases. The magnitude of the voltage at each location during the fault is calculated using steady-state simulation techniques with the G74 method. Similar to the fault level assessment, the line faults in this assessment are zero impedance balanced three-phase faults.

Figure 51 shows Kernal Density Estimate (KDE) plots for twelve selected busbars, showing the distribution of voltage dips across the range of faults and system conditions. The KDE visualises the probability density. Therefore, assuming that the occurrence of each simulated line fault is equally likely to happen, it shows the likelihood that a fault in the system will result in a given voltage dip. The plots show some locations where the voltage is less than zero, this is a consequence of the graphical representation, and voltages cannot go below 0 p.u.

The top six plots of Figure 51 show locations in northern Scotland. There is generally a much higher density at higher per-unit voltages in 2032 at these locations. These results suggest that the voltages at northern locations are more resistant to change during network faults in 2032, which aligns with the increased fault levels at these locations. The bottom six plots are in central Scotland. Here, the distribution of voltage dips remains quite similar, suggesting that the system's performance concerning fault severity is neither materially improved nor degraded.

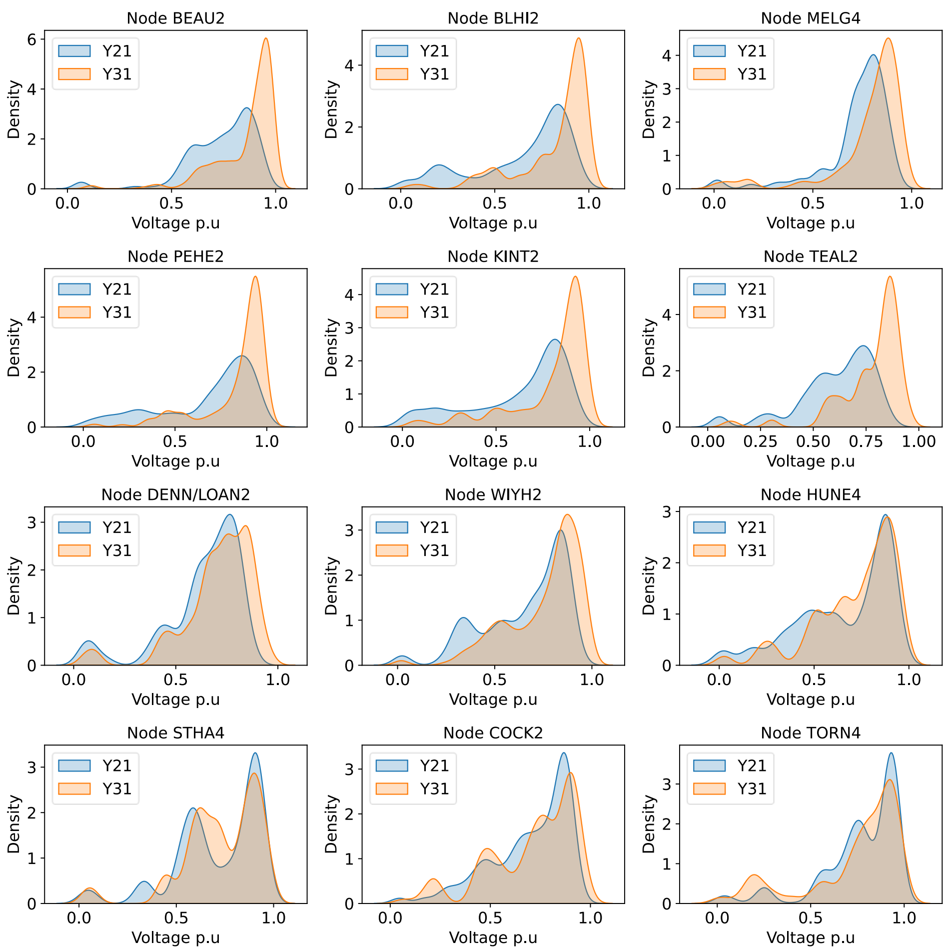

Figure 51: kernel density plots for 12 different transmission busbars showing the distribution of voltage dips across the range of fault cases.

The steady-state calculation method uses simplifications to calculate the fault level and voltages. The standards defining the implementation of these calculation techniques are designed for estimating network fault levels and are widely accepted [25], [158]. However, it is not standard practice to study voltage dips using these methods. To confirm the suitability of these voltage dip calculations, RMS TDS simulations for a sample of the same faults have been performed to compare to the G74 method. The RMS TDS simulations have a significantly higher computational burden than steady-state methods. As such, a sample of fault cases has been considered. The sample includes a high wind and low wind case for each demand scenario, and it is ensured that a fault close to each busbar in the system has been simulated for each scenario. RMS studies are considered more accurate and account for the impacts of different dynamic controllers and their settings. The voltage dip reported for the RMS study is calculated as the average voltage during the fault period.

Figure 52 compares the voltage dips calculated by steady-state and RMS dynamic simulation for each study year. Generally, there is a very good fit between the two with R^2 values of 0.98, showing that the G74 method gives a good representation of the retained voltage during a fault. The largest error for some faults is approximately 15 %, which tends to occur close to busbars with high IBR penetration. The voltage magnitude calculated via RMS simulation is higher than the G74 estimate for these errors. Therefore, the G74 results shown in Figure 51 are pessimistic.

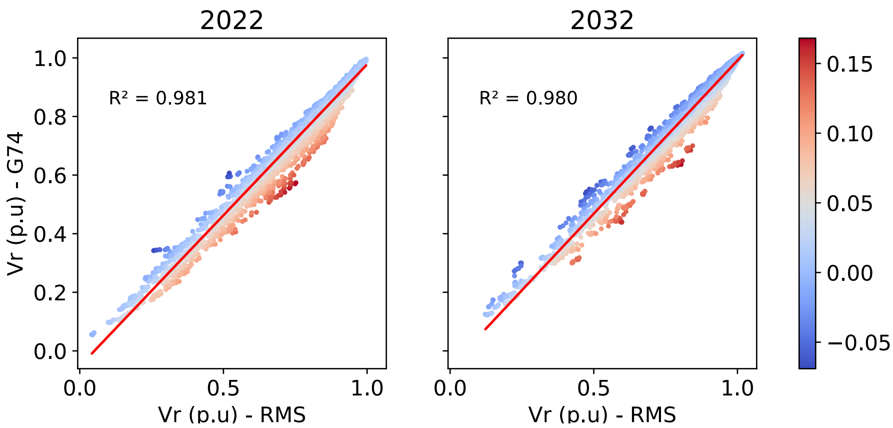

Figure 52: comparison of steady-state and RMS dynamic simulation techniques for calculating voltage dips

5.4.1 Dynamic voltage support during different system operating conditions

SGs and IBRs are essential sources of dynamic voltage control to maintain and stabilise voltages during faults. Most modern IBRs are required to provide steady-state and dynamic voltage control. In GB, the fault infeed from IBRs comes in the form of a controlled dynamic reactive current support delivered proportionally to the voltage dip, according to the Grid Code [30].

For conventional SGs, the provision of reactive power during steady-state or transient conditions requires them to be connected to the grid and spinning at synchronous speed. If an SG has not self-dispatched and is out-of-merit, it will typically disconnect from the grid. Therefore, an SG will not be synchronised or provide fault infeed if not dispatched.

Intermittent renewable sources, such as wind, will typically be scheduled before any conventional thermal generation due to their low short-run marginal costs. Most IBRs can utilise their full capacity for active or reactive power generation and can quickly deliver this active and reactive power independently of each other (within the current-limited capability) [35]. In addition, modern WTs can generate reactive power even when the wind turbine is stopped [178]. PV systems can also generate reactive power without sunlight [179]. However, these features may not be enabled as standard [180]. WFs may sometimes disconnect from the grid, e.g. for planned or unplanned maintenance, or during sustained periods of zero wind speeds where the WF has lost its auxiliary power supplies. Otherwise, a wind farm will typically remain connected to the grid even during low or zero wind speeds. Therefore, compared to SGs, the provision of dynamic voltage control from IBRs is much less dependent on the energy market.

Dynamic voltage support mechanisms often must respond rapidly to voltage disturbances. For example, modern FACTS and their control systems can adjust reactive power levels in milliseconds, providing fast voltage control [156]. Modern IBRs also provide fast reactive power response akin to a STATCOM [35]. From a system perspective, the widespread deployment of IBRs provides distributed fast dynamic voltage control at many parts of the system. These effects can be seen in Sections 5.3.1 and 5.4 as increasing fault current infeed and improvements of voltage dips during faults.

5.5 Discussion and conclusions

This work has provided an in-depth review of the critical system dynamic properties that influence system stability: the inertia and fault levels. For the last decade, increasing renewable energy penetration has been synonymous with reduced inertia, fault levels and system stability margins. To date, in GB, the expansion of IBRs has been in parallel with the retirement of SGs and, particularly in the north, IBRs have become the dominant power source. Hence, the displacement of SGs by IBRs has been closer to a like-for-like capacity replacement, reducing inertia and fault levels.

Analysis of the changes expected over the next decade does not show the same trend. If reasonable assumptions are made regarding the status of planned projects over the coming ten years, this work shows that inertia and fault levels are expected to be at least similar or higher than those of 2022. This finding is not to say that there are no emerging system stability challenges; instead, it highlights the changing nature of power system dynamics where IBRs are the dominant source. In the Scottish region, the system has already reached one that can be characterised by low inertia and fault level.

This work has shown that expanding IBR capacity in the northern part of GB, alongside the network reinforcements, can significantly bolster the three-phase fault levels in this part of the network. The increased fault level also improves the voltage magnitude during fault conditions. Furthermore, compared to SGs, the dynamic reactive power support provided by IBRs is less dependent on the energy market, as IBR technologies tend to remain connected to the grid over a wider range of operating conditions and provide their designed response across most or all of their rated capacity.

On the other hand, the increase in fault levels can lead to the exceedance of network asset ratings and incorrect protection settings during fault conditions, which has important implications for reliable system operation. In addition, where fault levels increase throughout the network, this can jeopardise the timely and cost-effective connection of new renewable generation projects. This work demonstrates that more attention should be paid to the implications of rising fault levels and finding solutions, ahead of time, to manage the associated risks.

On the other hand, the expansion of IBR capacity is expected to bring new challenges. Not least are the possible new oscillation modes and interactions between different controllers. Indications of these types of events are already being observed in the Scottish system; on the 24th of August 2021, at around 04:50, a sub-synchronous oscillation (SSO) event occurred where voltages on the 400 kV network oscillated between approximately 355 kV and 435 kV at a frequency of 8 Hz [181]. During this event, two similar oscillations occurred 30 minutes apart, each lasting for around 20-25 seconds, during which some users tripped off the system. The SO has not published any detailed analysis of the event at the time of writing. In [26], an analysis of the system conditions during the event showed that the fault levels at the time were not unusually low, indicating that the event might not be prevented by maintaining minimum fault levels. For some of these problems, e.g. controller interactions, SSO, or protection system issues (see Section 2.2), the fault level contribution from grid-following IBRs might not be beneficial and may even exacerbate the issue.

Defining a minimum threshold for fault level at any given location is challenging, partly because it depends on how the low fault level manifests itself into operational issues. Defining a minimum fault level requirement may not always provide a solution to the problem at hand and could lead to the commissioning of new synchronous assets such as SCs, where the most cost-effective solution to the problem might have been better tuning of the controls of IBRs or existing synchronous machines (refer to Section 2.2). Moreover, where SCs are installed to improve the fault level, "system strength" or system inertia, further stability challenges can arise, such as introducing new oscillatory modes between the slower SC controls and fast IBR controllers [18]. These issues were observed in the ERCOT grid following the installation of two SCs in the Panhandle area. Dynamic studies identified active power oscillations between the SCs and the SGs in the rest of the ERCOT grid, and further inter-area and intra-area oscillation modes were found following some contingencies.

The work in this chapter and the review of fault level as a metric for system strength in Section 2.2 has highlighted several open questions, particularly regarding the use of fault level, the contributions from grid-following IBRs, and how to measure system strength in a IBR-dominated system. It is, therefore, essential to understand the system's needs clearly (for example, in defining voltage regulation and small signal stability requirements) to ensure the security of supply can be achieved most cost-effectively.

Chapter 6: Fault-Induced Frequency Excursions in the Future GB Power System

Chapter 2 highlighted that the interactions between network faults and system frequency could increase with high penetrations of IBR. In Chapter 3, simulations performed on a simple two-area system investigated the underlying system behaviours that lead to post-fault active power deficits and consequent fault-induced frequency dips. Chapter 3 showed that the severity of the voltage dip and the FRT requirements imposed on IBRs play an important role in the size of the post-fault active power deficit.

So far, these challenges have been more of an issue for smaller isolated systems, e.g. in the Irish transmission grid (see Chapter 2), and the two-area test system of Chapter 3. However, the FIFE problem is also related to the penetration levels of IBR and may become a concern for the reliable operation of moderately sized island systems, such as that in GB. Another factor reinforcing this concern is the massive transformation of the power system as it transitions towards low-carbon operation. In the north of GB, numerous large IBRs are planned alongside several new HVDC transmission systems, increasing the density of IBRs in some areas. As IBRs are current-limited devices, and the existing approach is to maximise reactive current support during faults, a disturbance that occurs in areas with a high density of IBRs can potentially interrupt a large proportion of the system's active power generation.

Using the NGBTS, this Chapter assesses the possibility of fault-induced frequency excursions in the Scottish transmission grid. First, a method is developed to screen for the worst-case conditions from a FIFE perspective. The potential for FIFEs is then examined using time domain simulations. The worst-case fault conditions are then analysed in detail, and an extensive set of sensitivities are simulated to judge how severe these situations can get in this area of the system. Analysis of both secure and non-secure fault types has been provided for the highly constrained and IBR-dense northeastern part of the system in 2032. Finally, various possible solutions are assessed, including procuring inertia, procuring fast-frequency response, and implementing changes to wind farm requirements. Ultimately, the planned network arrangement in the north of GB being modelled in this Chapter is yet to be extensively studied, and this work contributes towards understanding some of the future system behaviours and requirements.

6.1 Screening for worst-case conditions

It has been identified through the review of literature in Chapter 2 and the simulations performed in Chapter 3 that the main influencing factors for a FIFE are the following:

- The fault ride-through requirements of IBRs: the converter is required to supply fast fault current to support the system voltage.
- The severity of the voltage dip: fast fault current provision is proportional to the retained voltage and, vice-versa, the retained voltage is proportional to the magnitude of the fast fault current provision.
- Pre-fault loading of wind generators: the higher the pre-fault active current, the more active current must be limited to deliver the reactive current required during FRT.
- The active power recovery time: a longer recovery time requires more inertial energy to supply the load in the post-fault period.
- The system inertia: higher inertia resists the change in frequency.

Considering these factors, assessing possible FIFE issues requires studying a wide range of network faults and system conditions. Typically, the SO or TO is aware of the worst-case contingencies that might trigger instabilities. These faults are often double circuit faults across the main transmission corridors that, if they were to happen, would lead to high power flows over a high-impedance path. However, the specific network faults that induce the largest temporary active power deficits – and lead to fault-induced frequency excursions – might not be the same as the typical worst-case contingencies studied to confirm voltage and angular stability limits.

Existing screening metrics, such as the SNSP (formula (12) in Section 2.4.2.1), or the various formulations of SCR (e.g. formulas (5), (6) and (7) in Section 2.2.1), do not capture many of these influencing factors. The SNSP is a system-wide metric that provides an instantaneous measure of the penetration of IBRs. While a high SNSP might suggest that faults could result in FIFE issues, it does not indicate where the worst-case faults might occur. SCR metrics give a regional measure expressed by the ratio of network fault level to the nominal power of an infeed. However, SCR does not account for the operating point of IBRs or their FRT requirements, which are critical factors in the FIFE issue. Additionally, as demonstrated in Chapter 5, fault levels in IBR-dense areas of the GB system can increase significantly, rendering SCR ineffective for this purpose.

This section develops a novel metric and methodology to screen for the worst-case faults from a FIFE perspective. To save computational time, the method uses steady-state studies – load flow and short circuit calculations – to obtain the pre-fault loading of generators and estimate the voltage dips during a wide selection of generation dispatch scenarios and fault cases[13]. Using the pre-fault machine loadings and calculated voltage dip magnitude, a simplified FRT and current limiting strategy (based on the GB Grid Code) is applied and the aggregated amount of active current that has to be limited by WTs to meet their reactive current infeed requirements during the voltage dip is calculated. The new metric, called the 'Current-at-Risk' or CaR, is quantified by comparing the active current that has been limited during the fault with the pre-fault active current.

The influence of different reactive current droop settings was described in Chapter 3, section 3.5.1. The GB Grid Code requires IBR to provide fast fault-current provision such that, for a voltage of less than 0.9 p.u, reactive current shall be injected above the black line shown in Figure 53 [30]. According to this requirement, to be GB grid code compliant, the K factor must be a minimum of K=3.28, and at least 1 p.u of the converter's maximum reactive current must be delivered for a retained voltage of 0.5 p.u. These parameters are considered the base case for calculating the Current-at-Risk metric.

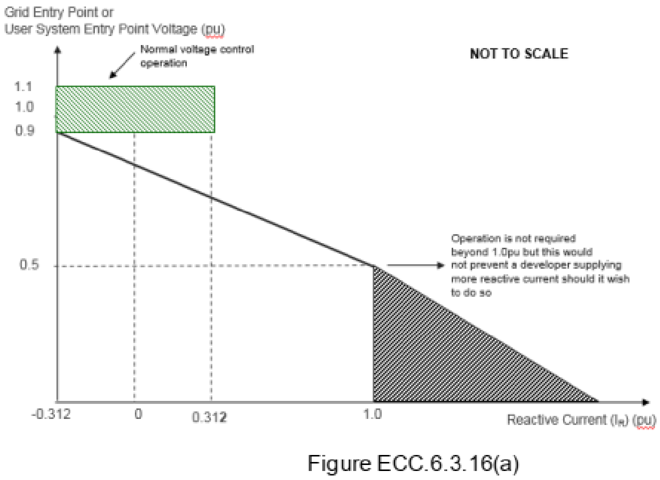

Figure 53: GB grid code requirements for fast fault current injection [30]

[13] The accuracy of steady-state short circuit analysis in calculating the voltage depression compared to RMS simulations is presented in Section 5.4.

The procedure for calculating the CaR metric, which is implemented via an automated python based script, is described in the flow chart shown in Figure 54. The dispatch scenarios are those developed in Section 4.8, and the fault cases are those considered in Chapter 5. To remind the reader, 30 generation dispatch cases are considered for each study year, 2022 and 2032 and, for each dispatch scenario, faults are applied at 2 %, 50 % and 98 % along the length of each single circuit line, giving a total of 5,376 fault-cases.

First, pre-fault data is collected from the load flow calculation for the intact system. Then, after applying a fault using the G74 short circuit calculation method [158], the retained voltage at each transmission busbar is collected. The voltage-dependent reactive current is then calculated using the retained voltage and the grid code requirements for FRT. Considering the converter limits, the maximum active current can then be determined (using equations (11) and (12) for ΔI_q and I_{pmax} respectively, from Chapter 3. For each IBR, if the active current available before the fault is greater than the maximum active current allowed during the fault, then the converter active current is limited at I_{pmax} . The 'Current at Risk' metric, which relates to each fault case, is the weighted average of the total active current that has been limited during the fault and is defined as

$$CaR\ (p.u) = \frac{\sum_i^n \left| I_{p,postfault,i} - I_{p,prefault,i} \right|}{\sum_i^n I_{p,prefault,i}} \tag{21}$$

where I_p is active current of the ith generator.

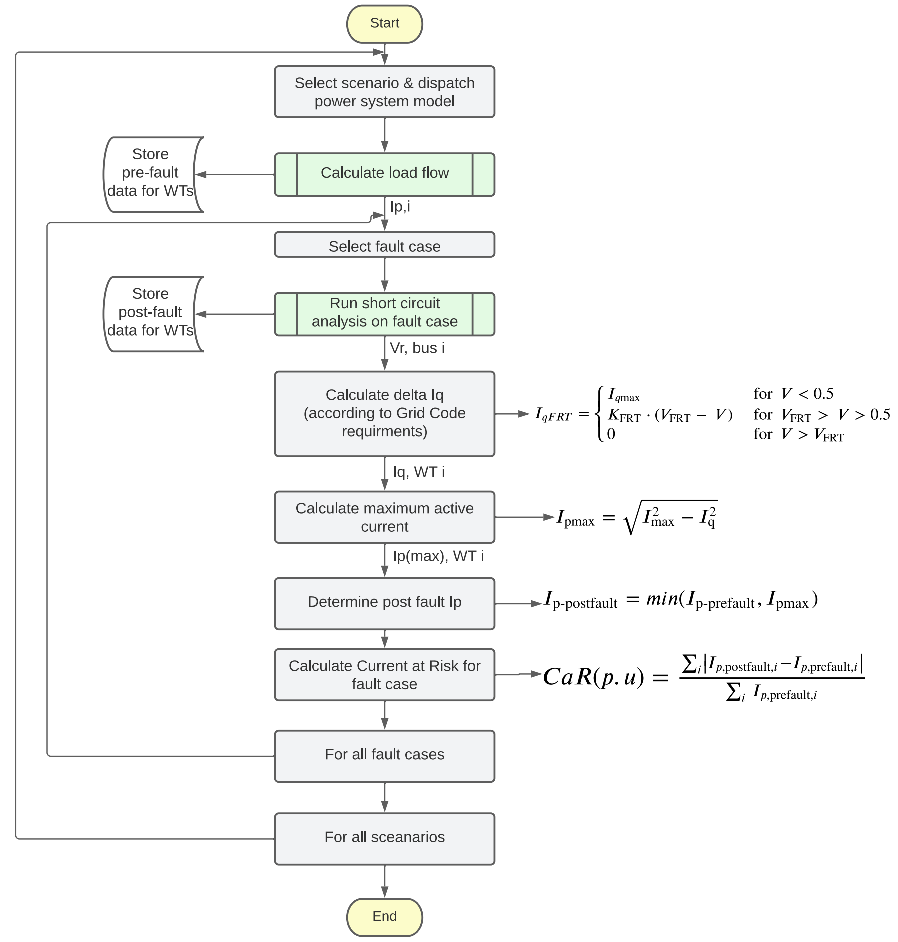

Figure 54: 'Current-at-Risk' calculation methodology

The CaR indicates which faults will most strongly impact generation from IBRs. The intention of calculating the CaR is to reduce the number of faults required to be studied in detail using RMS time domain simulations. However, system inertia is also an important factor when assessing frequency stability. Therefore, to improve the suitability of the CaR metric as an indicator of worst-case faults from a fault-induced frequency stability perspective, cases that exhibit both a high CaR and a low inertia are selected for time domain simulations. Figure 55 shows the spread of calculated CaRs plotted against the total system inertia for each fault case. To capture the expected worst cases conditions, all scenarios with a CaR greater than 0.075 and inertia less than 275 MVAs are carried forward. In addition, a representative sample of 200 additional fault cases from outside these boundaries is included to ensure a complete range of system conditions are considered to assess the accuracy of the CaR metric. In total, 231 cases for 2022 and 275 cases for 2032 are carried forward.

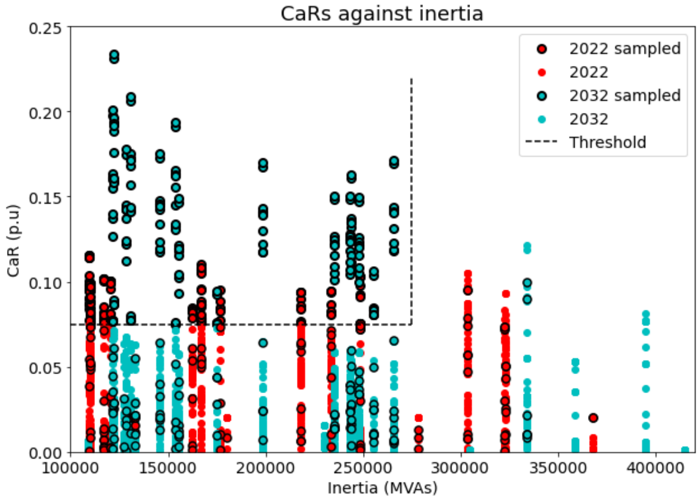

Figure 55: CaR against inertia for each fault case, highlighting (with a black outline) the cases considered for time domain simulations.

For each of the 506 cases, the frequency nadir at the modelled system's Centre of Inertia (COI) is found through time domain simulation (See Section 6.2). The correlation of the CaR metric and the COI frequency is shown in Figure 56. In general, larger frequency deviations are found for higher values of CaR. For the 2032 cases, due to the higher penetration of IBRs, higher CaR values are observed which correlate with larger COI frequency deviations.

Some divergence between the CaR and COI frequency nadir can be observed in Figure 56, which is due to assumptions made during steady-state fault level and voltage dip calculations in DIgSILENT (version 2022). Section 2.1.1.2 highlighted that the short-circuit contribution of IBRs should be modelled by a non-linear current vs. voltage relationship that respects the converter current limits. Traditional static fault level calculations treat converters as voltage sources during the sub-transient period, with fault current contributions based on equivalent fault impedance but capped at the converter's rating (1.05 p.u in this case). For close-up faults, the converter enters a current-limited mode, providing maximum current, as expected. However, for more distant faults, the fault current contribution decreases based on the impedance seen by the converter. This effect is also seen in Section 5.4 Figure 52, shows that steady-state calculations techniques can underestimate the voltage for some cases by up to 15%. This is a known issue, and later versions of DIgSILENT software have implemented an iterative calculation approach which should increase the accuracy and reduced the divergence seen in Figure 56. Regardless of these inaccuracies, the CaR metric is shown to be a good indicator to identify a range of faults that can lead to a low frequency nadir in the post-fault period.

This metric is just for screening for faults to be studied using time domain simulations that will allow analysis of the frequency profile, including its RoCoF, and consider the dynamics of converter current and voltage controllers. Furthermore, the active power recovery rates cannot be captured in the CaR calculation process. This process allows the engineer to select the specific faults and system conditions of interest, reducing the time to run multiple dynamic simulations.

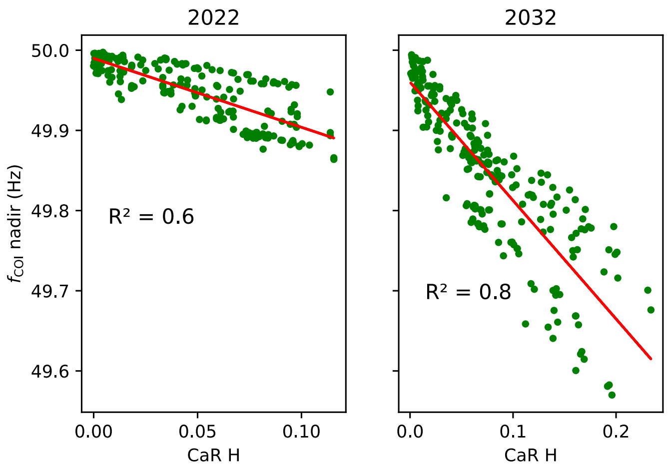

Figure 56: correlation of CaR to centre of inertia frequency nadir

The application of CaR is straightforward and could be used in planning studies to screen for fault-induced frequency stability risks. It could also be integrated into system operational tools to identify high-risk conditions and, if needed, take actions to secure the system against specific faults.

6.2 Modelling of fault-induced frequency excursions in the current and future Scottish Power system

This section outlines the model set up related to frequency responsive reserves, the system-level frequency stability metrics used and, finally, the results for the selected case studies from Section 6.1 are presented.

6.2.1 Procurement of frequency response

NGESO must procure sufficient volumes of frequency response and reserves to maintain the system's frequency within the limits defined in the SQSS. For background on frequency response services and SG governor and BESS control models, see sections 2.3.2, 4.5.1 and 4.5.4, respectively. Primary frequency response (PFR) and Dynamic Containment (DC) are the main post-fault frequency response services at the time of writing. In the model, PFR is delivered from a governor-controlled SG and DC from a frequency-controlled BESS. Slower acting services, such as secondary frequency response and reserve or longer duration balancing through the BM, are not modelled as they are considered to respond outside the timescales of interest for temporary active power deficits.

Currently, the HVDC-ICs are the largest single infeed to the system, with the largest being the NSL at 1400 MW. Although the NSL is explicitly modelled in the NGBTS, in all the high wind dispatch cases considered, the NSL is exporting power and does not represent the largest infeed. With a view of the demand, generation and network flows, the expected inertia level is known. The current policy, according to an NGESO webinar [182], is to secure a 1260 MW loss to 49.2 Hz using everything apart from DC (i.e. this is mostly primary, secondary and EFR (220MW)). Then, for a loss infeed risk of greater than 1260 MW, DC is procured. For the frequency stability studies here, the frequency response volumes are fixed for each dispatch scenario being modelled, based on a consistent loss of infeed assumption of 1260 MW for both the 2022 and 2032 system variants.

For the 2022 system, the amount of PFR is adjusted to secure the loss risk, while the BESS response is maintained at 220 MW, which is the volume of the EFR service today. In 2032, more of the DC service is expected to be procured and EFR has been phased out [182]. In practice, the amounts of each post-fault service that would be procured will depend on the bids made by different technology providers in the frequency response ancillary services market. Determination of the optimal amount of post-fault response is not the focus here, but the sensitivity of the FIFE to the amount of DC service procured from BESS is tested in Section 6.5.2.

6.2.2 System frequency metrics

The Centre of Inertia (COI) frequency is used to assess a fault's effect on system frequency. The COI frequency is a useful and widely accepted metric to describe the overall system frequency of a synchronous area [183], [184]. The COI frequency is the sum of all synchronous machine speeds weighted by the machine inertias and is calculated by

$$\omega_{COI} = \frac{\sum_i^N \omega_i \cdot H_i}{\sum_i^N H_i} \tag{22}$$

$$f_{COI} = \omega_{COI} \cdot f_{nom} \tag{23}$$

where ω_i is the p.u rotational speed and H_i is the inertia in MVAs of the i^{th} synchronous machine and f_{nom} is the system's nominal frequency.

The system RoCoF can also be determined from the COI frequency. In this Section, a simple RoCoF calculation metric is used that represents the average change in frequency over a given time. Typically, RoCoF is measured by protection systems over a specified time window to avoid nuisance tripping, i.e. such that any action triggered by RoCoF measuring devices is based on a reliable measurement of the frequency trajectory at the measured location. The GB requirements for RoCoF-based LoM protection are discussed in Section 6.3.1. The method used by NERC to calculate RoCoF determines the average change in frequency in the initial 500 ms after a frequency disturbance [185], according to

$$RoCoF\ (Hz/s) = \frac{(f_{nom} - f_{0.5})}{0.5} \tag{24}$$

In practice, when the system moves away from its steady-state condition, the frequency varies across the different locations of the system, and there is no single system frequency or RoCoF. The regional variations in system frequency are discussed and analysed in Section 6.3.2.

6.2.3 Fault-induced frequency excursions in the current and future GB power system

Figure 57 shows the COI frequency nadir and corresponding RoCoF for each fault-case[14]. For the 2022 cases, the frequency does not fall outside the normal operating range of ±0.2 Hz. However, for some faults in 2032, the post-fault frequency nadir can be much lower, showing that the system-wide frequency can move relatively far from nominal and outside the normal operational range following a fault.

The frequency can fall quickly in the immediate post-fault period, leading to high post-fault RoCoFs. According to NGESO's Operability Strategy Report [16], beyond 2025, the operational policy will be to secure a loss of infeed of up to 1800 MW while operating with minimum inertia of 102 GVAs and keeping the RoCoF within 0.5 Hz/s. However, the studies here show that the average RoCoF in the 500 ms after a fault can easily exceed this limit for some post-fault conditions without any permanent infeed loss.

[14] Of the 506 cases selected cases, 49 fail to converge or give reliable outputs during RMS simulation. However, similar cases remain in the dataset, and a suitable range of operating conditions have been represented.

The average RoCoF values shown in Figure 57 (calculated according to formula (24)), represent the average change in frequency in a 0.5 s time period, which is a commonly used window to measure RoCoF [29], [185], [186]. However, the RoCoF will typically be highest immediately after the event and will decay or even tend towards zero or positive values within this time. The RoCoF signal and the practical RoCoF limits are discussed further in Section 6.3.1.

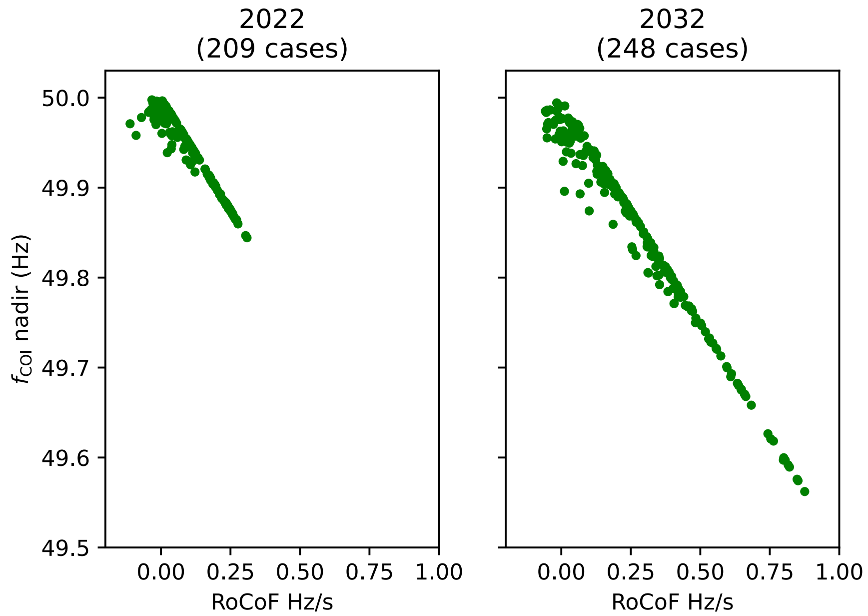

Figure 57: COI frequency nadir and RoCoF for each fault-case for 2022 (left) and 2032 (right)

6.3 Analysis of worst-case faults

The fault conditions with the worst-case frequency nadirs (and RoCoFs, as they are the same) are shown in Table 13. The lowest COI frequency nadir is 49.56 Hz with an average RoCoF of 0.88 Hz/s. For all these cases, as might be expected, they occur during the low-demand scenarios with high wind outputs. For details on the dispatch conditions for each case, refer to Section 4.7. The case 'D2 W0.8' has low daytime summer demand, high distributed PV outputs, and high offshore wind speeds in northern Scotland. The fault locations for all faults shown in Table 13 are on lines connecting to the Rothienorman (ROTI4) busbar, which is found to be the critical fault location.

Table 13: ten cases for 2032 with the lowest fault-induced frequency nadir

Dispatch case	**Faulted line**	**Fault position (%)**	**f_{COI} nadir**	**Ave RoCoF**
D2 W0.8	ROTI4_KINT4	2	49.56	0.88
D2 W0.8	ROTI4_PEHE4	2	49.57	0.85
D2 W0.8	BLHI4_ROTI4	98	49.58	0.85
D2 W0.8	ROTI4_KINT4	2	49.59	0.82
D3 W0.99	ROTI4_KINT4	2	49.59	0.82
D1 W0.8	ROTI4_PEHE4	2	49.60	0.81
D2 W0.8	ROTI4_PEHE4	98	49.60	0.80
D1 W0.8	BLHI4_ROTI4	98	49.60	0.80
D3 W0.8	BLHI4_ROTI4	98	49.62	0.76
D1 W0.8	ROTI4_PEHE4	98	49.62	0.75

Figure 58 shows a zoomed image of the northeastern part of the NGBTS network model, with the worst-case fault location at ROTI4 marked with the red lightning bolt. ROTI4 is a new substation currently under construction and will be up-rated to 400 kV as part of the network reinforcement works before 2032. The planned developments in the northeast area are significant, and a large proportion of the system's generation and network transfer capacity will be concentrated in this area. The critical nodes Blackhillock (BLHI), ROTI, and Peterhead (PEHE) will all play a major role in transferring power generated from onshore and offshore wind in the north of Scotland towards the major load centres in England.

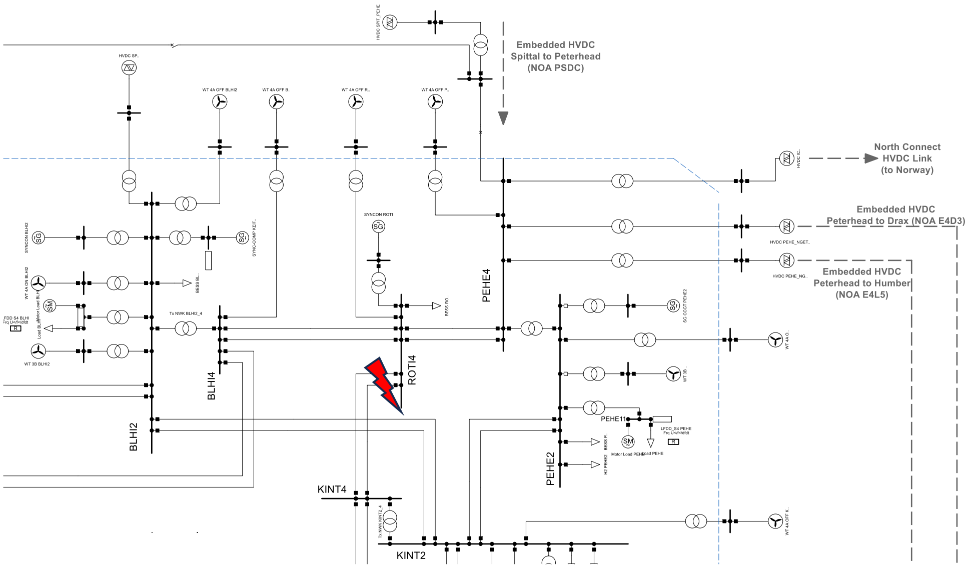

Figure 58: zoomed area of the North-East part of the network in 2032 with fault location marked in red

Figure 59 shows a voltage-dip heat map for the worst-case fault close to ROTI4, demonstrating the severity of the fault in the system. The colours represent the voltage magnitude, calculated via time domain simulation at 50 ms after fault inception and accounts for FRT controls and rise time of reactive power support. The voltage at ROTI4 dips close to zero, and all surrounding busbar locations are exposed to voltages of less than 0.5 p.u (shown by varying shades of red). The reach of the fault extends west to Beauly (BEAU), south to the Alyth/Kintore (ALYT/KINT) busbars and just beyond the B4 boundary, where voltages are between 0.5 and 0.9 p.u (shown by blue shades). IBRs connected to any non-green busbars will be in FRT control mode and are at risk of contributing towards a post-fault short-term active power deficit.

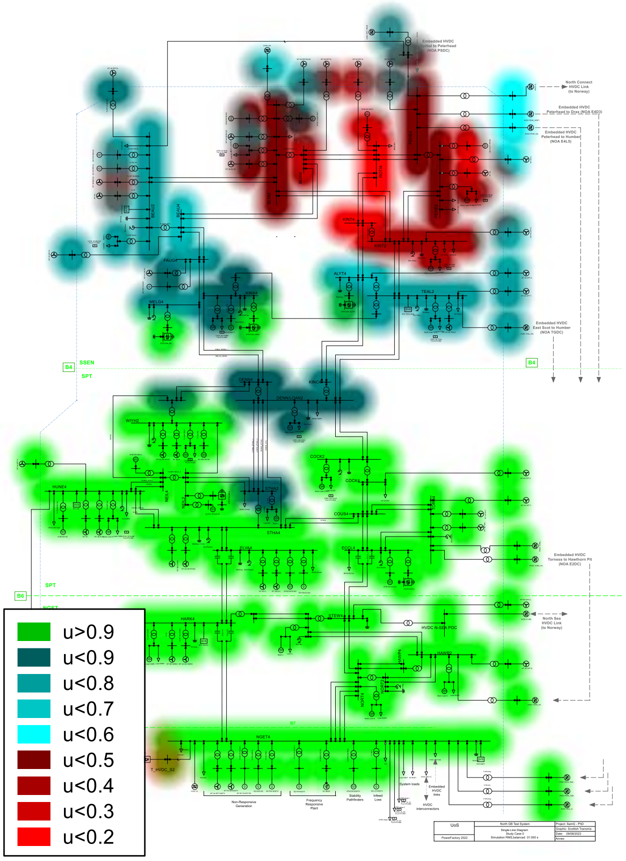

Figure 59: voltage heat map for faulted line ROTI4_KINT4 (2 % from ROTI4) with D2 W0.8 generation dispatch case (2032 network)

Figure 60 shows the system's dynamic response to the fault. Figure 60(a) and (b) show the voltage magnitudes and voltage angles of nearby locations. During steady-state conditions, the PLL of grid-following IBRs precisely tracks the voltage angle of its PoC. During the voltage dip, a rapid phase angle jump can occur, as shown in the simulation, which, in some cases, has been known to lead to loss of synchronism of IBRs as it loses its angle reference [34], [187]. The main influencing factors of the phase jump are the grid impedance, the export level of the IBR, the voltage dip severity, and the PLL parameters [34], [187]–[189]. Looking at the PEHE4 busbar, the voltage phase angle initially jumps by approximately 20 degrees to a peak of 58.8 on fault inception. It then declines during the fault, followed by a sharp drop to -33 degrees on fault clearance before oscillating back to its pre-fault value. It is outside the scope of this work to assess PLL loss of synchronism due to fault-induced voltage dips and phase angle jumps. The system impacts of faults that lead to tripping of local IBR are assessed in Section 6.4.3.

Figure 60(c) shows the sum of active powers for all IBRs (WTs and HVDCs) in the system. In the 200 ms after fault clearance, there is a significant short-term drop in active power being supplied to the system. The primary contributors to the active power deficit are the post-fault active power recovery of the wind farms. During this time, the shortfall in supplying the load is served by the inertial response of the available SGs and SCs. The net sum of the SG active powers is negative in this dispatch case due to all PSHs being in pumping mode, and the pumping capacity exceeds the generation from SGs.

Figure 60(d) shows the COI frequency, which reaches its nadir within 500 ms of the fault occurring, resulting in a high transient RoCoF, as shown in Figure 60(e). The results for Section 6.2.3 showed the average rate of change over the initial 500 ms following fault inception to be -0.88 Hz/s for this fault. However, during this period, the RoCoF peaks at -2.17 Hz/s and returns close to zero within the 500 ms window. RoCoF limits are discussed further in Section 6.3.1.

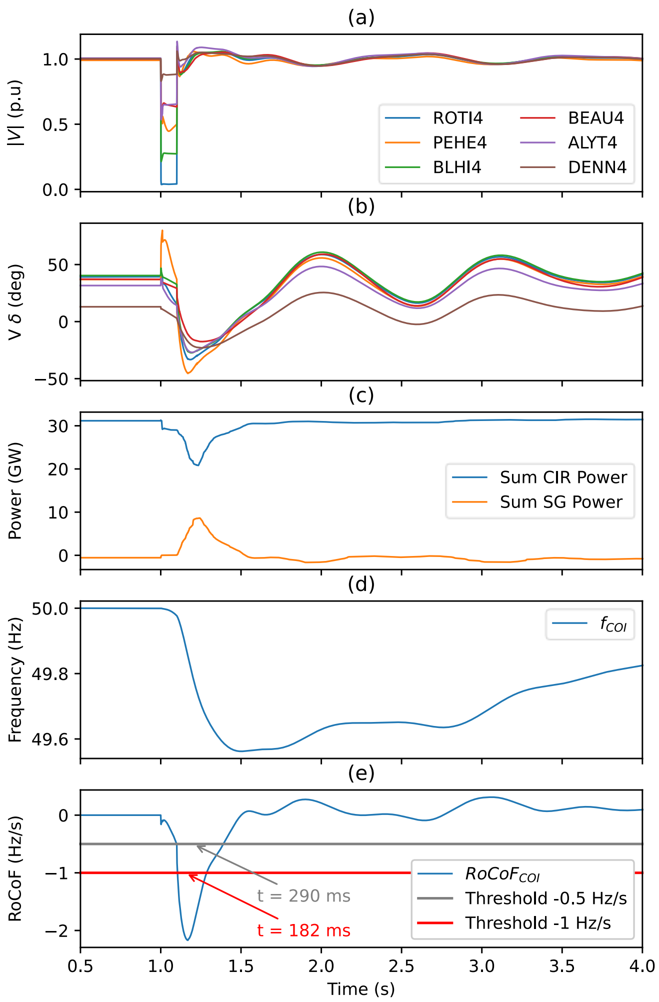

Figure 60: system dynamic response to the worst-case fault. From top to bottom: (a) voltage magnitudes of nearby busbars, (b) voltage angles of the same busbars, (c) sum of all IBR and SM power outputs, (d) COI frequency and (e) COI RoCoF with the time periods for which thresholds are exceeded

6.3.1 RoCoF limits

The practical RoCoF limit on the GB system is driven by two main factors: the first, which is the most well-known issue, is maintaining the RoCoF below the thresholds set for LoM protection systems that are required to be implemented on DG (see Section 0 for background), and the second is the RoCoF withstand capability of SMs. There is a third factor relating to the successful operation of the LFDD scheme: should the RoCoF be high, the system frequency can quickly exceed multiple LFDD frequency thresholds and not allow sufficient time for the stages of the scheme to operate [72]. However, the LFDD risks with high RoCoF are related to a permanent loss of infeed, i.e. a genuine need to shed load, rather than short-term transients.

The G99 connection standard requires DG to have a RoCoF protection threshold of 1 Hz/s with a time delay of 0.5 s [29]. The time delay requirement is not a measurement window; it is defined that the protection shall operate if the measured RoCoF exceeds the specified threshold for at least 500 ms. Figure 60(e) shows that the system RoCoF for this fault exceeds the 0.5 Hz/s operational threshold for 290 ms and the LoM protection threshold for 182 ms. Therefore, tripping of DG would not be expected. Even so, reaching such high RoCoF values that exceed the DG LoM protection settings across a wide area is not desirable. For this future case study, which considers a summer daytime with high distributed PV outputs, DG offsets much of the national demand. The national demand, DG generation outputs and resulting net-transmission demand are shown in Table 14. PV capacity grew considerably through the 2020s (see Section 4.3.2 and 4.7.3) and constitutes a high proportion of the system's overall generation for this case. On that account, the impact of exceeding LoM protection settings is very high.

Table 14: National demand and distributed generation outputs for case 'D2 W0.8'

National demand and DG	**Power (MW)**
National demand (gross)	- 29,807.0
PV output	13,991.6
Hydro output	123.4
'Other' (thermal) output	2,772.8
Wind output	3,308.9
Total DG generation	**20,196.8**
Transmission system demand (net)	**- 9,610.2**

High and more frequent RoCoFs in the system also have implications for SMs due to the mechanical limitations of individual machines. High RoCoF events can cause additional stresses on the generator, and SGs can experience torque swings, pole slipping and momentary reverse power [190]–[192]. Consequently, SG plant owners and system operators are concerned that high RoCoF events can cause short-term damage, generator disconnections and excessive long-term wear and tear. References [190]–[193] all study RoCoF withstand capability in the context of a loss of infeed or system split; they do not discuss fault-induced frequency transients. In addition, they focus on SGs and do not tend to study the impact on SCs.

RoCoF withstand capability requirements do exist in some grid codes. However, requirements can vary, and no consensus exists on RoCoF measurement techniques or how capability should be defined [192]. In GB, there is no clear Grid Code requirement in this regard, so it cannot be assessed in the context of these fault cases. However, from the modelling results shown here and in Section 6.3.2 on regional RoCoF values, the time for which the RoCoF must be withstood is crucial. Given that fault events in the future can lead to increased frequency deviations, as shown here, resulting in high RoCoFs, it should be ensured that new and existing generators are robust, over the long term, to the expected RoCoFs on the system.

6.3.2 Regional effects of the fault

Large disturbances, such as a three-phase fault and its clearance, cause transients in the power system during which the synchronous machine rotor speeds oscillate. The COI frequency defined in (22) and used in 6.2.3 is a useful method to represent the frequency of the entire system. However, in practice, and especially during transients, there is no such thing as a single system frequency, and the COI does not capture the local frequencies made up of the voltage sources in the system at different locations. In addition to the short-term active power deficits leading to the slowing of rotor speeds (i.e. the primary mechanism for the FIFE phenomenon), the fault also induces regional frequency variations.

The main frequency stability concerns in GB regarding short-term low-frequency dips are the risk of unintentional load shedding by LFDD relays and generation tripping by RoCoF or under-frequency relays. LFDD relays and DG are both widely distributed throughout the distribution networks. Hence, these risks may transpire at a local level.

6.3.2.1 Assessment of modelling regional frequencies

The method used by Dg-PF, (and some other common RMS simulation tools [194]) to calculate frequency at electrical nodes is to use the derivative of the voltage phase angles [195].

During a simulation, voltage angles are determined relative to the reference machine. The frequency at each node (f_i) is found by adding the frequency deviation to the frequency of the reference machine (f_{ref}, which remains unchanged), according to

$$f_i = f_{ref} + \Delta f = f_{ref} + \frac{d\theta}{dt} \tag{25}$$

From a modelling perspective, assessing the local frequencies and their rates of change in a spatially disaggregated RMS model is a challenge. Using only the voltage angle derivative, a sharp voltage angle change (e.g. due to a three-phase fault) will cause an observed local jump in frequency due to the transient $d\theta$/dt. As such, for busbars remote from the reference bus or the 'centre frequency', the frequency changes during transients can be excessively large and include numerical issues and signal noise [194], [196]. When monitoring the frequency variable of nodes, these issues are observed in the NGBTS, particularly for locations close to the fault and with a high concentration of IBRs. Methods to improve the estimation of the frequency at different electrical nodes are proposed in [194], [196], [197]. In general, including both the SG machine speeds and the voltage phase angle is considered and found to improve the accuracy.

Measuring frequencies throughout the system can be done by monitoring these busbar frequencies or monitoring the rotor speed of local SMs, which determines the frequency of the generated electrical output. Here, a comparison is made between these different modelled variables. Based on the model development assumptions described in Section 4.4 several synchronous machines still exist to obtain a rotor speed measurement in the northern part of the GB system. In fact, due to the development of large-scale PSH and the Stability Pathfinder programmes (see Section 5.1), there is an increase in the presence of synchronous voltage sources in both Scottish transmission regions in this 2032 case. For this comparison, the large CCGT at Peterhead (node PEHE2) is switched on and run as an SC (i.e. not changing the dispatch) such that the SM synchronous speed and the nearby frequency measurement devices can be compared close to the fault location. Normally, the PEHE2 CCGT is out of merit and switched off for this dispatch case. The fault is the same as described in Section 6.3, except it is applied to both circuits (double circuit fault).

Figure 61 shows frequencies at three locations close to the fault: Beauly 275 kV (BEAU2), Peterhead 275 kV (PEHE2) and Rothienorman 400 kV (ROTI4). Each bus has at least one SM and WT connected, and for BEAU2 and PEHE2, there are also GSPs with LFDD relays at the load points. Figure 61 shows the differences in the SM synchronous speed and the frequency measurement taken by the WT controllers and the LFDD relays.

For the WT controllers, a voltage measurement device provides the bus voltage and frequency to the dynamic controller model. The protection system module filters the frequency signal measured at the bus through a 1st order lag with a default but adjustable time constant of 5 ms. For the LFDD relay, the voltage measurement device is implemented with a 'frequency measuring time' with a default value of 10 ms; this time step can be considered as the precision of the measurement. These controller and relay parameters significantly influence the measured frequency at their location. Each column of plots in Figure 61 represents each location, and each row of Figure 61 shows the variation in filter and measurement time constants for the WFs and relays according to Table 15.

Table 15: time constants used to compare frequency measurements of WTs and LFDD relays

Parameter	**Default**	**Default x5**	**Default x10**
WT time constant for frequency measurement filter (ms)	5	25	50
LFDD relay frequency measurement window (ms)	10	50	100

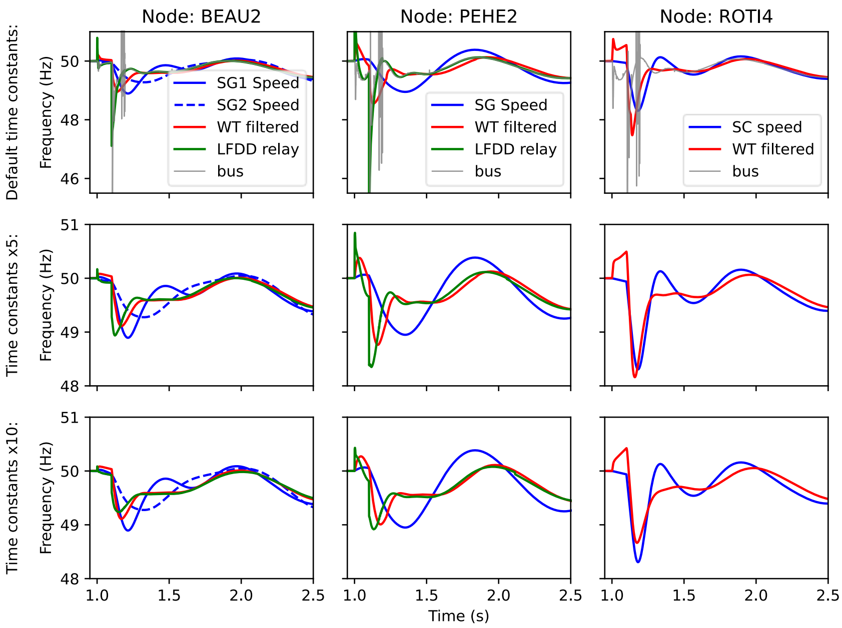

Figure 61: Synchronous machine speeds and frequency measurements at Beauly 275 kV (BEAU2), Peterhead 275 kV (PEHE2) and Rothienorman 400 kV (ROTI4). Each column is a node. Each row shows different values for the controller time constant and frequency measurement window. The SG, SC, WT and LFDD measurements shown are all local to the node, for example. SG1 and SG2 speed in the left-hand column are SGs connected at BEAU2, and 'WT filtered' in the right hand column is the frequency measurement by the WT at ROTI4.

Considering the default parameters and the unfiltered busbar frequencies, Figure 61 shows that the frequency calculated at the busbars exhibits large spikes and a lot of noise (light grey, top row). Furthermore, with the default (lower) time constant parameters, these excessive spikes can be passed through to the frequency measurements of the relays and the WT controllers with almost instantaneous spikes in frequency as the voltage phase angle jumps on fault inception (at t = 1 s) and, to a larger extent, on fault clearance (opening of the double circuit after 100 ms).

The default time constants lead to inconsistent frequency nadirs and rates of change between the measurement devices and the synchronous speed of local SMs. Increasing the time constants by five times (middle row) attenuates the fast changes in frequency, which is observed further with an increase to ten times the default values (bottom row). The additional filtering reduces the inconsistencies. However, setting the time constants too high risks masking low-frequency nadirs. For all locations, the differences in the frequency transients between the measurements and the SM rotor speeds align after one or two seconds following the fault.

Figure 61 also shows that frequency measurements from the relays and the WT controllers can have a higher rate of change immediately after the fault. The rotor position of the SMs cannot change instantly to adjust to the phase angle change, and the SM rotor speed rate of change depends on the machine inertia. However, the rate of change also depends on the proximity to the fault. For example, for the SC at ROTI4, the rate of change of its rotor speed (right-hand plots, blue line) is high due to it being close to the fault (it is also a low inertia machine); this has the effect of aligning the SC speed and the WT measurement.

A practical frequency measurement device (e.g. a PLL, PMU or frequency relay) must also adjust its position to track the transient frequency profile. Real frequency measurement devices can also perceive phase angle changes as large frequency deviations, threatening any relay or control system that makes a decision based on frequency or RoCoF [198]. However, the response will depend heavily on the algorithm used to perform the measurement and any filtering implemented to account for noise [199].

6.3.2.2 Regional frequencies of the study case

This section assesses the regional frequencies for the worst-case fault described in Section 6.3 (Peterhead CCGT is switched off again). Relays and WT controllers have the ‘time constants x5’ settings (see Table 15). Figure 62 shows the regional frequencies and RoCoFs measured at the LFDD relays (top left and top right, respectively), the frequencies at local WFs (bottom left) and the speed of local SMs (bottom right).

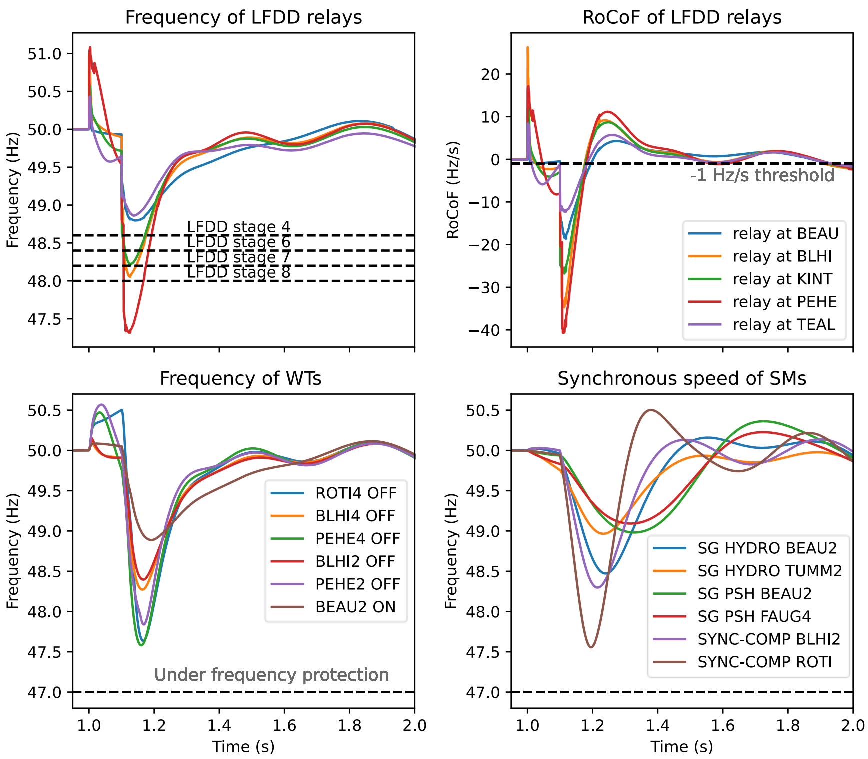

Figure 62: frequency at LFDD relays (top left), RoCoF at LFDD relays (top right), frequency at local wind farms (bottom left) and frequency of local synchronous machines (bottom right)

For some relay, WF and SM locations close to the fault, the frequency transients can reach very low values. Frequency nadirs of approximately 47.5 Hz are observed at the WF and SC at Rothienorman and the WF at Peterhead. The GB Grid Code allows generator disconnections at 47 Hz with no specified delay time. For Grid Code requirements relating to frequency, see Figure 9 of Section 2.3.4.

For the LFDD relays to trip, the frequency signal must remain below the threshold for the duration of the measurement window. The GB Grid Code allows a maximum operating time for low-frequency relays of 150 ms, and the total operating time of the scheme, including circuit breaker operating time, should be less than 200 ms [9]. The requirements for the scheme operating time apply equally to each LFDD stage, as seen in Section 2.3.4. A review of typical manufacturer data sheets shows that modern 11 kV and 33 kV circuit breaker operating times range from 55-60 ms [200]. However, circuit breakers in the distribution networks are of varied ages, and some may have longer opening times. Therefore, assuming a circuit breaker opening time (including any communication delay) of between 60 to 100 ms, to be compliant with the Grid Code the frequency measurement window of the LFDD relays should be between 100 to 140 ms.

In the SSEN area, only four of the nine LFDD stages are implemented; these are stages four (48.6 Hz), six (48.4 Hz), seven (48.2 Hz) and eight (48 Hz). In this case, the frequency measured by the LFDD relays at Peterhead exceeds all four stages but recovers within the frequency measurement time. However, the frequency is below the LFDD stage four threshold for approximately 87 ms, so it is not far from unintentional load shedding. LFDD thresholds are also exceeded at Blackhillock and Kintore. All these locations are one bus away from the fault location. Compared to local SM speeds (where available), the frequency transients measured by the LFDD relays are of similar magnitude and duration. Considering the modelling and measurement challenges outlined in Section 6.3.2.1, there is uncertainty whether, in practice, an LFDD relay at this location would (1) truly experience such a frequency transient and (2), if it did, there are likely to be differences in the way that the relay calculates and filters the measured frequency. Regardless, this analysis does expose a significant risk, with some concerning regional low-frequency transients in the immediate post-fault period. For faults in this area in the future GB power system, there may be an increased risk of unintentional load shedding.

The analysis in section 6.3.2.1 showed that, due to the voltage phase-angle jump on fault clearance, the initial rate of change in the frequency measured by WTs or LFDD relays can be higher than the derivative of the SM rotor speeds. Therefore, the peaks of the RoCoF signals in the top-right-hand plot of Figure 62 might be higher than expected. Having said that, regardless of which frequency signal is monitored in this simulation, the rate of change of frequency at some nodes can easily be in the region of 2 Hz within 100 ms (or 20 Hz/s), meaning that peak regional RoCoF values are very high. For this fault, the initial peak RoCoF measured at any LFDD location recovers within approximately 120 ms, well below the 500 ms time delay of RoCof LoM protective relays and slightly faster than the COI RoCoF shown in Section 6.3.

6.4 Case study sensitivities

Based on the reference case study detailed in Section 6.3, this section investigates possible sensitivities to the assumptions made. The primary areas of investigation are the system planning assumptions in the locality of the fault and the fault type.

6.4.1 Pumped storage hydro and HVDC interconnector projects

Large-scale energy infrastructure projects are always uncertain and have many barriers throughout their development. The NGBTS model makes various assumptions regarding the successful completion of PSH and HVDC projects, as detailed in Chapter 4. PSH and HVDC will influence the local dynamic properties of the system, e.g. fault levels and inertia, and the power flows, as they are both flexible assets with the ability to absorb excess generation within – and transfer generation out of – the area. Therefore, if some of these planned projects do not connect to the grid, they may impact the FIFE.

At the time of writing, some of the new large-scale PSH projects assumed to connect to the northern part of the system are yet to receive planning consent, which is a significant development milestone. The reference case study is adjusted for the Beinn Bhuidhe (600 MVA, connected at BEAU2)[15] and Coire Glas (1,470 MVA connected at Fort Augustus (FAUG4)) projects not being built. For the HVDC projects in the pipeline, the NorthConnect link is a proposed HVDC-IC (1,400 MW connected at PEHE4) between northeast Scotland and Norway. The project has experienced significant delays and recently had its license rejected by the Norwegian government [201], [202]. The case study is also adjusted for the NorthConnect project not being built.

The reference case study has high wind outputs, PSHs are pumping, the NorthConnect HVDC is exporting, and the AC and embedded DC transmission systems are close to their maximum transfer capacity. Reducing pumping and export capacity north of the B4 boundary increases the north-south power flow and requires generation curtailment to respect the N-1 security criteria (see Section 4.8.1.2). Chapter 3 showed that the higher the WT loading, the more active current limitation is required during a voltage dip, contributing to a more severe FIFE. Therefore, the method of curtailing wind generation, i.e. either reducing capacity or reducing active power output, and the proximity of the curtailed WTs to the fault location will also influence the post-fault frequency.

Four different scenarios are considered to apply constraints to the case study. Two scenarios consider that operational actions are performed by adjusting the active power set-point of WTs, one where all WTs north of the constraint are curtailed equally, the other where curtailment is applied remotely from the fault. The other two scenarios consider the case where less wind capacity is online, i.e. they are either not built or simply unavailable, both local to the fault and remote from the fault. Reducing wind capacity addresses the constraint while ensuring that the remaining WTs are at the same loading as the reference case. For 'remote from fault' curtailment, it must still be done north of the B4 boundary to achieve a lower boundary transfer; WTs in the northwest, at nodes BEAU2 and BEAU4 are curtailed, which are still

[15] The MVA capacities and locations stated here are those assumed in the NGBTS model.

affected by the voltage depression. Table 16 details the case studies considered for each PSH and HVDC project outcome and the method of re-dispatch.

Table 16: case studies considered for PSH and HVDC planning outcomes

Case Name	PSH projects built?	North Connect HVDC built?	Method of re-dispatch
Reference	Yes	Yes	None
PSH 1	No	Yes	Curtail all wind north of B4 equally
PSH 2	No	Yes	WF curtailment remote from fault
PSH 3	No	Yes	WF reduced capacity remote from fault
PSH 4	No	Yes	WF reduced capacity local to fault
HVDC 1	Yes	No	Curtail all wind north of B4 equally
HVDC 2	Yes	No	WF curtailment remote from fault
HVDC 3	Yes	No	WF reduced capacity remote from fault
HVDC 4	Yes	No	WF reduced capacity local to fault

Figure 63 shows the frequency response to the reference fault for each case study in Table 16. The left-hand plots are for PSH not built cases, and the right-hand plots are for HVDC, while the top plots show the effect on the COI frequency, and the bottom plots show the frequency close to the fault, measured by the synchronous speed of the SC at ROTI4. If these assets are not built, it can impact the COI frequency. However, the impact is relatively small and depends on the curtailment method.

Curtailing all wind farms north of the B4 boundary equally improves the COI frequency (cases PSH1 and HVDC1). This method of curtailment reduces the active power loading of all WTs affected by the voltage depression resulting in less active current limitation required during FRT mode. For the PSH1 case, it appears to offset any reduction in COI frequency caused by the loss of inertia. The worst effect on the frequency comes from reducing WF capacity at Beauly (PSH3 and HVDC3, representing a case where less capacity is built off the northwest coast). This curtailment method leaves all WFs at the same high loading of the reference case. In practice, it may not be practical or cost-effective to curtail generation based on the risk of a three-phase fault occurring in a particular location. The curtailment will depend on the bids and offers provided by generators to the ESO in the BM. It should be noted that each case study has slightly different power flows; therefore, some minor differences are expected.

When the PSH capacity in the area is not built, the synchronous speed of the SC at ROTI4 (close to the fault) deviates further from 50 Hz in the post-fault period. The post-fault dynamics of any contingency are not only dependent on the total system inertia but also the spatial distribution of inertia in the grid. Due to the lower regional inertia, the SC's transient reduction in rotor speed at ROTI4 is higher, suggesting that frequencies local to the fault might be degraded.

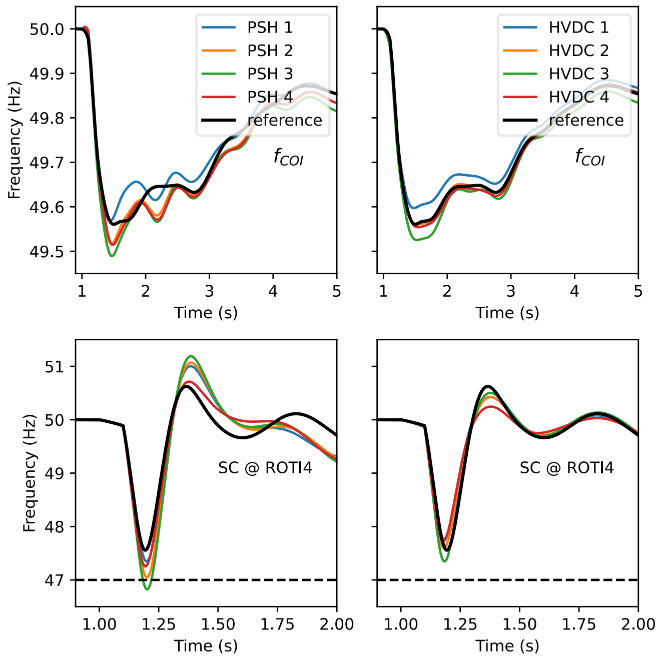

Figure 63: COI frequency (top row) and frequency of SC at ROTI4 for each planning sensitivity. The left column shows PSH cases, and the right shows NorthConnect HVDC cases.

The main risks with low local frequency nadirs in the post-fault period are that the thresholds of the LFDD scheme are reached or, in the more extreme case, the low-frequency protection of generators is reached. As discussed in Section 6.3.2.2, the risk of load shedding depends on the time spent below the threshold and the measurement window. Figure 64 evaluates the regional risk of unintentional load shedding for the PSH3 case study. The locations that exceed each LFDD frequency threshold and the duration that each threshold is exceeded are shown.

Three locations with distribution GSPs, BLHI2, PEHE2 and KINT2, all exceed the LFDD stage four threshold of 48.6 Hz for over 100 ms. The expected frequency measurement windows of LFDD relays are uncertain but should be in the region of 100 to 140 ms to be grid code compliant, see Section 6.3.2.2. At KINT2, stage six is exceeded for over 100 ms, and the other locations are close to the tripping region. These results show that the regional risk of unintentional load shedding has increased when the PSH projects are not built.

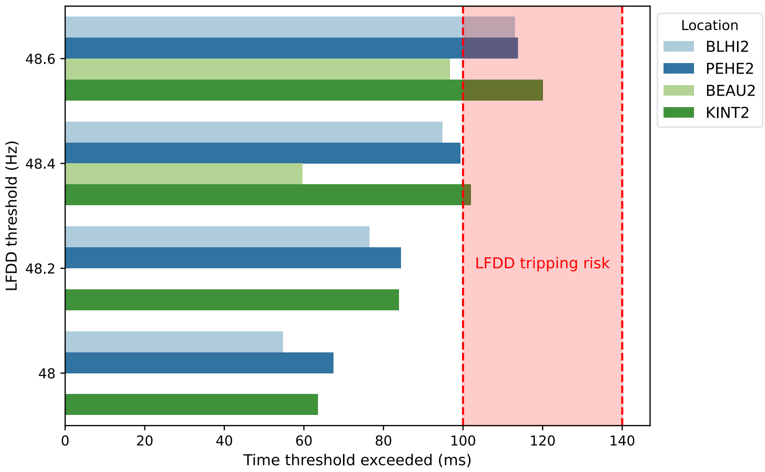

Figure 64: regional risk of load shedding for the PSH3 case study for each location: areas that exceed LFDD thresholds and the time for which those thresholds are exceeded.

6.4.2 Fault severity and performance of protection systems

The duration of the fault and the depressed voltages in its vicinity are dictated by the operating times of local protection systems and circuit breakers, i.e. the fault clearance time. The fault affects the amount of active power transferred to the AC transmission system in two ways: (1) the depressed voltage reduces active power transfer, and (2) the FRT controllers of IBRs are forced to limit active power to support the system with fast reactive current injection. Therefore, the fault duration may influence the FIFE.

6.4.2.1 Fault case studies

The GB Grid Code stipulates different fault-ride-through performance requirements depending on the fault clearance time. The main protection systems in GB are designed to clear a fault within a maximum time of 140 ms. In practice, in GB at transmission grid voltages, i.e. 275 and 400 kV, they are expected to operate within 100 ms [203], [204]. Different FRT performance requirements for generators exist for faults lasting less than or greater than 140 ms. For this analysis, faults cleared within 140 ms are considered 'secure', and the protection system has performed within acceptable bounds. Conversely, 'non-secure' faults last for more than 140 ms, and the performance of the protection system has been compromised in some way.

Various types of secure and non-secure faults are investigated and shown in Table 17. The impact of fault clearance time, the clearance method, and the effect of single or double-circuit faults are considered for secure faults. It was discussed in Section 2.2.2 that recent works have identified an increasing risk to the efficient operation of some types of protection schemes as the penetration of IBRs becomes dominant. For non-secure faults, two cases are considered that will lead to longer clearance times: delays in fault detection, i.e. the time taken for the relay to detect a fault successfully, and delays in fault isolation, i.e. the circuit breaker failing to open the circuit.

The grid code stipulates that for faults lasting less than 140 ms, a generator's active power shall recover to at least 90 % of its pre-fault value within 0.5 seconds of the voltage recovery. However, for faults that last more than 140 ms, this is relaxed to 1 second. The non-secure fault cases are run with both recovery times to assess the impact.

Table 17: Description of different fault types considered for their sensitivity to frequency variations

Fault case	**Fault Reference**	**Wind power recovery rate**	**Total fault duration (ms)**	**Description** **SC = single circuit** **DC = double circuit**
Secure (Type-A)	reference	0.5 s	100	SC self-cleared fault
	OL	0.5 s	100	SC with line isolated
	SC FFC	0.5 s	50	SC with fast fault clearance
	SC SFC	0.5 s	140	SC with slow fault clearance
	DC SFC	0.5 s	140	DC with slow fault clearance
Non-secure (Type-B)	SC DFC FR	0.5 s	200	SC with delayed fault detection
	DC LBF FR	0.5 s	200	DC with local breaker failure
	DC RBF FR	0.5 s	300	DC with remote breaker failure
	SC DFC SR	1 s	200	As above but with extended active power recovery times, as allowed by Grid Code for non-secure faults
	DC LBF SR	1 s	200	
	DC RBF SR	1 s	300	

Figure 65 and Figure 66 illustrate the concept of a possible local and remote breaker fail situation in GB [204]. In both cases, the bus-coupling circuit breakers are opened instead of the line circuit breaker to isolate the fault. The total fault clearance time and system voltage profiles depend on whether the local or remote end circuit breakers fail to open. In the NGBTS model, all substations are modelled as single busbars. As such, the breaker-fail protection is emulated by operating the line breaker but with an extended opening time, which gives a similar effect.

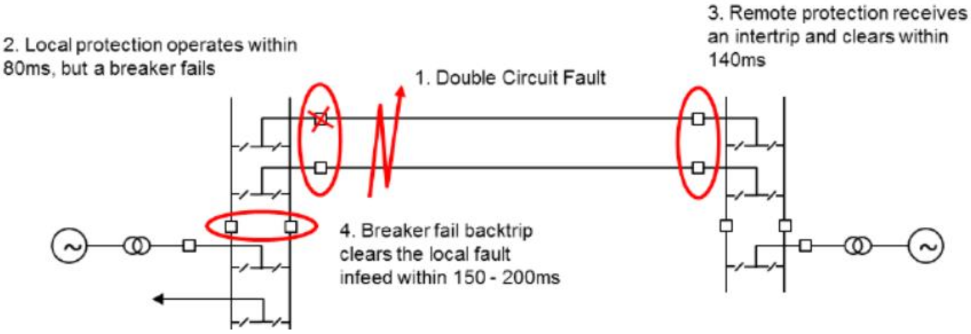

Figure 65: double circuit fault with the failure of a local circuit breaker [204]

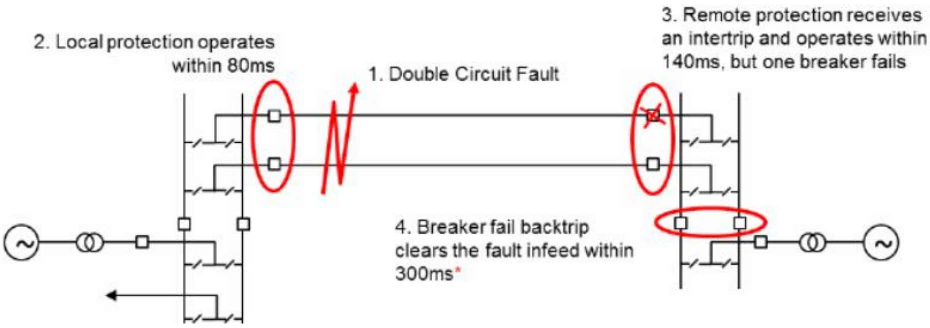

Figure 66: double circuit fault with the failure of a remote circuit breaker [204]

6.4.2.2 Simulation results

The CoI frequency trace for each fault case in Table 17 is shown in Figure 67, with the secure faults in the left-hand plot and non-secure faults in the right-hand plot. The reference case is shown with a thick dashed black line. Only minor variations are observed in the system CoI frequency for all secure fault types and non-secure faults when the same active power recovery rates are assumed. Some minor improvements can be seen for fast fault clearance or for a remote breaker fail case. Nevertheless, the variations from the reference case are small, showing that the fault duration does not significantly impact the severity of the fault-induced frequency excursion.

This finding is somewhat counterintuitive, as a longer fault duration would be expected to result in more extended periods of active power deficit. However, as seen in the demonstration of the case study in Section 6.3, the main loss of active power and required delivery of the inertial response occurs in the first few hundred milliseconds following the fault clearance rather than during the fault itself.

For the non-secure, longer-duration faults, accounting for the allowance for generators to recover their active power more slowly does have a more substantial impact on the system frequency. The reason behind this relaxation of the active power recovery rate for longer fault clearance times is not stated in the grid code or any known publicly available documentation.

The non-secure faults with slower power recovery bring the frequency close to the operational limits in GB as defined in the SQSS, allowing the frequency to reach 49.2 Hz if it returns within 60 s [8].

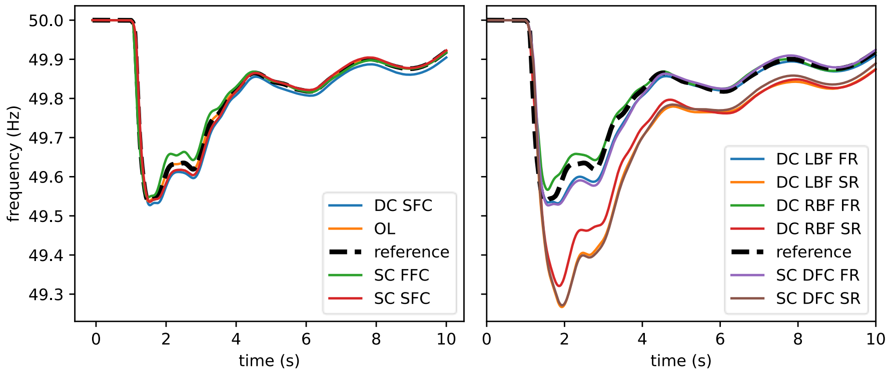

Figure 67: COI frequency for various types of faults. Faults are defined in Table 17

The voltage profiles for the three types of non-secure faults are shown in Figure 68. The fault is applied on the line(s) connecting the 'ROTI4' and 'KINT4' busbars, close to 'ROTI4', which goes close to zero volts on fault inception. The other busbars shown are all one bus away. The thick dashed black line is the FRT voltage against time curve for IBRs, and the dashed blue line is the FRT requirement for SGs, i.e. if the voltage at a generator connection point is below the dashed lines, tripping is allowed.

For the breaker-fail cases, the voltages at the busbars surrounding the fault depend on the location of the failed breaker. For the local breaker fail (that is local to the fault, at the ROTI4 end, shown in the left-hand plot), the ROTI4 voltage exceeds the FRT requirement, and local generation would trip. However, for a remote breaker fail (middle plot), the voltage recovery at the KINT4 end of the line takes longer. Due to the impedance of the line, the voltage remains above the FRT requirement, and no generation loss at ROTI4 would be allowed. For the delayed fault clearance case (longer detection time, shown in the right-hand plot), IBRs and SGs would be expected to trip at ROTI4, KINT4 and, for SGs, BLHI4.

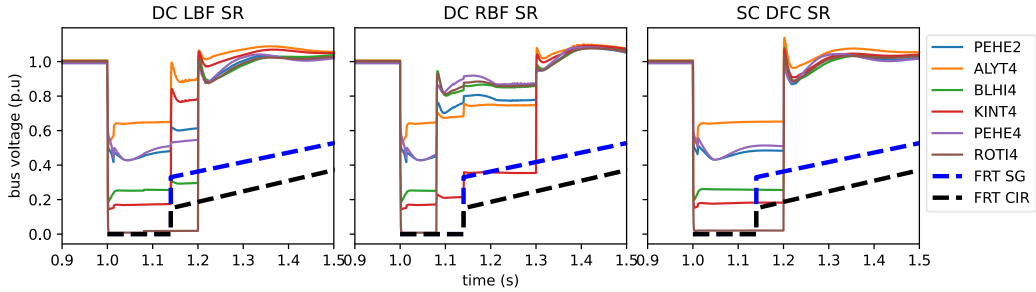

Figure 68: voltage profiles for buses close to the fault and their FRT voltage against time curves. Faults are defined in Table 17

It would be expected that, upon the loss of generation due to not riding through the fault, whether tripping is allowed by the grid code or not, this would contribute towards further degradation of the system frequency. Faults that lead to a loss of infeed are the topic of the next section 6.4.3.

6.4.3 Faults with a loss of generation

In theory, the loss of generation from a 'secure' fault that is not on the connection circuit should not happen, as generators (and other apparatus) are required to ride through, support and recover from most types of faults. Nevertheless, these types of events do happen, and Section 2.4.1 identified several international examples of normally-secure network faults leading to the unexpected disconnection of generation. In addition, Section 6.4.2 presented some examples of non-secure faults that result in conditions where generation would be allowed to disconnect (e.g. due to delayed circuit breaker action). This section studies the impact of disconnections as a result of faults to assess the cumulative effects of the temporary and permanent power deficits. The following fault conditions are assessed:

- The reference fault with loss of generation: this case considers that the normally-secure reference fault leads to the loss of the local wind farm at ROTI4, e.g. due to the fault inducing a control interaction within the wind farm.
- Fault 'DC LBF SR' at ROTI4 with loss of generation: as studied in Section 6.4.2, the double circuit fault with a local breaker failure would cause the WF and the SC at ROTI4 to exceed the FRT voltage-time curve (Figure 68), and tripping would be expected. Slow recovery of the remaining WFs is allowed.
- Fault DC LBF SR at PEHE4: here, the double circuit fault with local breaker failure is applied on the lines from ROTI4 to PEHE4, close to PEHE4. The interest in this fault location is the high wind and HVDC capacity at this busbar in the future power system.

6.4.3.1 Reference fault with loss of ROTI4 Offshore wind farm

For the analysis of this fault, the WF at ROTI4 is assumed to be the largest single infeed to the system at 1,688.1 MW. Accordingly, the amount of DC frequency response procured is increased from 480 MW to 840 MW to ensure this loss can be contained within the frequency limits associated with an infrequency loss risk of 49.2 Hz (see Section 2.3.2). The hypothesis is that due to the fault-induced short-term active power deficit, if the system experiences a network fault that leads to a permanent loss of infeed, the system frequency would be degraded compared to if the loss of infeed were to occur without the network fault.

Figure 69 compares the system frequency response to the reference fault (black lines), the reference fault with the WF at ROTI4 tripping 100 ms after fault clearance (blue lines), and just the WF tripping without any fault (orange lines). The initial decline in frequency is the same for the fault only and the fault + trip cases, proving that the effects of the fault itself govern the shape of the early part of the frequency profile. The combination of the fault and the generation loss leads to a faster and deeper frequency decline than the generation loss alone. However, for both cases, the frequency stabilises at 49.2 Hz , and the frequency profiles converge after approximately 13 seconds as the main effects of the fault have passed.

Observing the delivery of PFR and DC in Figure 69, with the fault-only case, the frequency responsive SG delivers an inertial response, followed by a delay (implemented in the governor model), and the responsive BESS quickly delivers active power proportional to the frequency. Both responses for the fault-only case are not sustained. However, faster delivery of PFR and DC occurs for the fault + trip case compared to the trip only. The reason for the faster frequency decline is seen in the penultimate plot of Figure 69, showing the sum of power outputs from all SMs. The inertial response required by the system to balance the fault-induced active power deficit is substantial. The summed SM inertial response is proportional to the COI RoCoF; as seen in the bottom plot, the RoCoF for the fault or the fault + trip cases are similar, as described in Section 6.3. The RoCoF for the trip-only case is within the operational RoCoF limit of 0.5 Hz/s to which NGESO intends to operate the system [16].

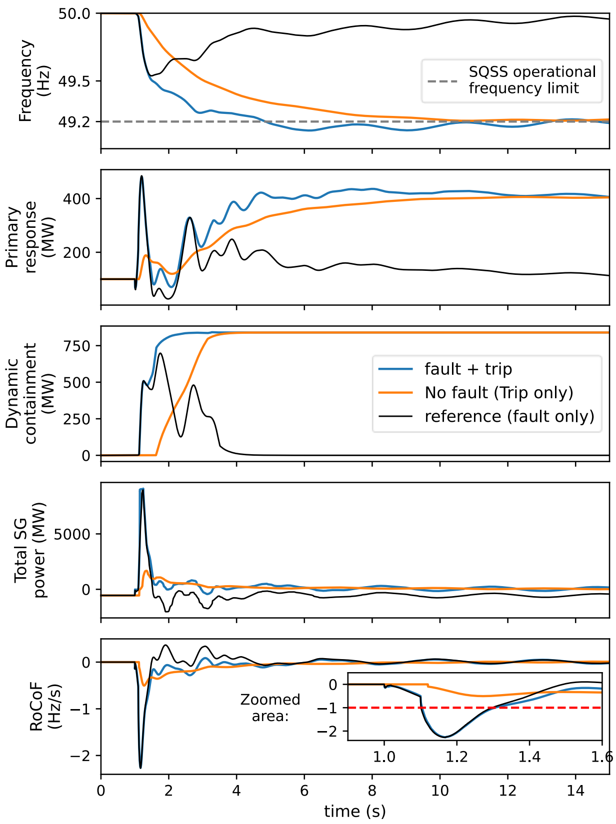

Figure 69: loss of infeed event compared to a fault + loss of infeed event.

This analysis shows that when considering the effects of a fault, the frequency nadir can be lower and RoCoF can be higher. Therefore, if system frequency, RoCoF and frequency response volumes are calculated based solely on the loss of infeed – as is typical operational practice – then operational security criteria can be exceeded if that same infeed loss occurs due to a fault event. However, in this case, the COI frequency nadir does not reach critical protection thresholds. Therefore, it could be argued that securing the fault and the loss of infeed could result in additional and unnecessary costs to the consumer.

6.4.3.2 Double circuit fault with local breaker failure at ROTI4

The voltage profile for a double circuit fault with local breaker failure (DC LBF) at ROTI4 is shown in Figure 68. If this fault were to occur, tripping the WF and the SC at ROTI4 would be allowed as the voltage exceeds their FRT voltage/time curve requirements. Figure 70 shows the COI frequency for this case, compared with the secure fault + trip from Section 6.4.3.1, which resulted in a loss of the same WF (left plot). The frequency nadir reached for the breaker fail case is approximately 0.2 Hz lower, even though the infeed loss is the same. Furthermore, the high RoCoF in the immediate post-fault period is more sustained. The degraded system frequency is due, in part, to the loss of the SC at ROTI4, but predominantly it is due to the slower recovery of some of the local wind farms that are exposed to a fault that lasts in excess of 140 ms, as shown in Figure 67.

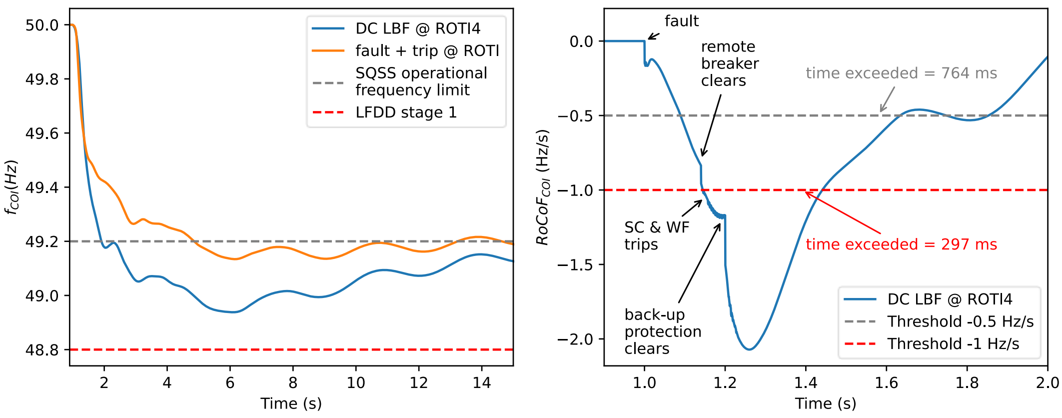

Figure 70: COI frequency for DC LBF compared to the fault + trip (left) and COI RoCoF for DC LBF case (right)

The right-hand plot of Figure 70 shows the COI RoCoF for the breaker-fail case. The RoCoF continues to decline quickly during the fault period, which, in total, lasts for 200 ms until the backup protection clears the line with the failed breaker. In this case, the higher and more sustained RoCoF exceeds the operational limit of 0.5 Hz/s for 764 ms, well above the 500 ms typical measurement window. The 1 Hz/s DG protection settings threshold is exceeded for longer than the previous cases, at 297 ms, but remains within the window.

NGESO do not justify the 0.5 Hz/s operational RoCoF limit in [16]. It has been suggested anecdotally that thermal generation assets in the distribution networks are likely to trip when RoCoF exceeds this threshold for a period assumed to be 500 ms. Therefore, there is a high likelihood that this situation would lead to further tripping of these assets.

If generator controls are programmed to exercise their right to come back slowly during these types of faults, there is an increased risk of very high RoCOF and possible generation loss, worsening the event. Considering the influence that longer active power recovery times can have on the system frequency and RoCoF during a fault-induced frequency event, the need for this grid code requirement should be reviewed. If modern WT technology can return within the standard 0.5 s for any fault type, it has been shown here to improve the FIFE.

6.4.3.3 Double circuit fault with local breaker failure at PEHE4

In this case, the double-circuit fault with local breaker failure is applied on the lines between ROTI4 and PEHE4, close to the PEHE4 busbar, as seen in Figure 71. This area's IBR capacity is very high, particularly at PEHE4, which has multiple large offshore wind connections, three large embedded HVDCs and an HVDC IC. The sub-sea embedded HVDC links transfer much of the wind generation in the north of Scotland south to England. The rated MW capacity of each connection is shown in Figure 71, with '+' indicating a generator or 'inflow' and '–' indicating a HVDC 'outflow' from PEHE4. Figure 72 shows the voltages at nearby busbars for the fault and the FRT voltage/time curves. During this fault, everything at PEHE4 and any synchronous plant at PEHE2 is at risk of disconnection. The CCGT at PEHE2 is not in merit for this case; if it were, there would be additional generation curtailment required to respect network export limits.

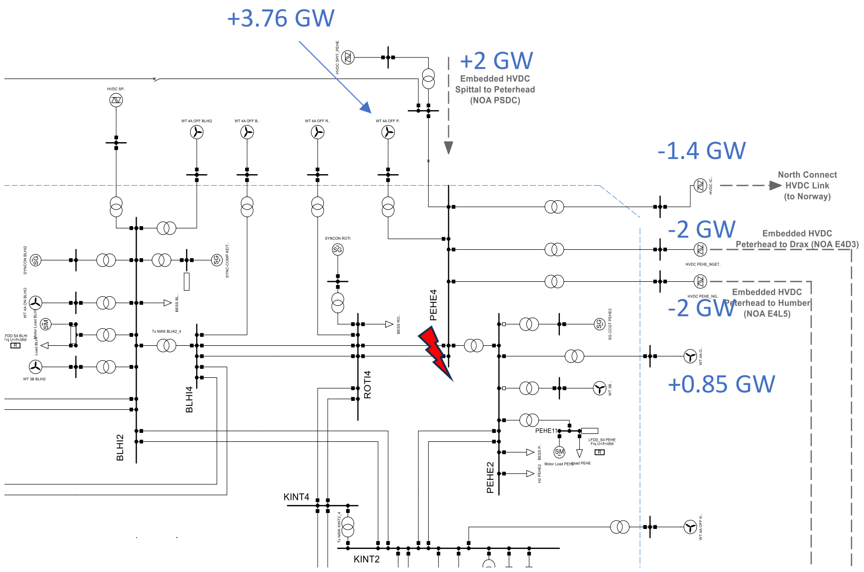

Figure 71: northeastern part of the network model with double circuit fault applied at PEHE4 with rated capacity of connected IBRs.

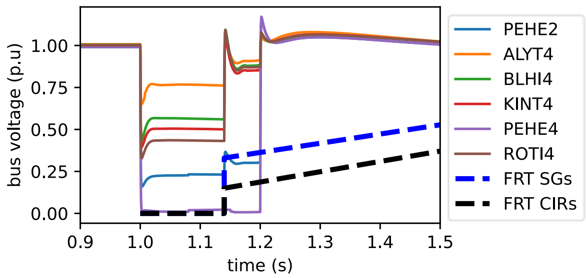

Figure 72: voltage profiles at local busbars for DC LBF fault at PEHE4 and FRT voltage/time curves

The FRT voltage/time curves stipulated by the grid code are a minimum performance requirement. There is a notable difference in asset type in terms of ownership at the PEHE4 location. The three 2 GW embedded links will all be owned and specified by the TO, SSEN, and the WF connection by the developer. Both parties have different incentives when developing this infrastructure which will, in reality, all be developed, specified and procured at different times over the next decade or more. The WF owners are motivated by minimisation of their own costs and, therefore, could be expected to meet the minimum performance requirements but not exceed them.

On the other hand, a TO is also incentivised to keep costs low but might also direct more concern towards reliability and system impacts of disturbances. For example, through discussions with industry representatives, it is understood that the existing embedded HVDC link at BLHI2 can withstand low voltages for longer than the Grid Code FRT requirements. Of course, improving the reliability of transmission infrastructure is good engineering practice. This point motivates two case studies for this fault: the first is that the fault only trips the WF connections at PEHE4, and the embedded HVDCs can ride through. The second is that everything connected to PEHE4, including the embedded HVDC links, precisely meets the minimum requirements in the Grid Code and trips during the fault.

Figure 73 shows the post-fault conditions for the DC LBF fault on lines ROTI4_PEHE4 for the case where only the wind farm trips during the fault. The under-voltage protection of the WF at PEHE4 operates 150 ms after fault inception, and the backup protection of the faulted line (breaker fail) operates after 200 ms. The top two plots of Figure 74 show nearby busbars' voltage magnitudes and voltage phase angles. After fault clearance, because the WF at PEHE4 has tripped, continued operation of the HVDC links result in a large net import into PEHE4, quickly overloading the remaining healthy lines into PEHE2, as shown in Figure 73. The increase in power flows over these lines into Peterhead causes the voltage angle difference between PEHE2 and PEHE4 and the rest of the system to increase beyond 180 degrees and lose synchronism, as seen in Figure 74. This is a dangerous condition, potentially leading to cascade tripping of lines and generators and possible blackout of at least part of the system.

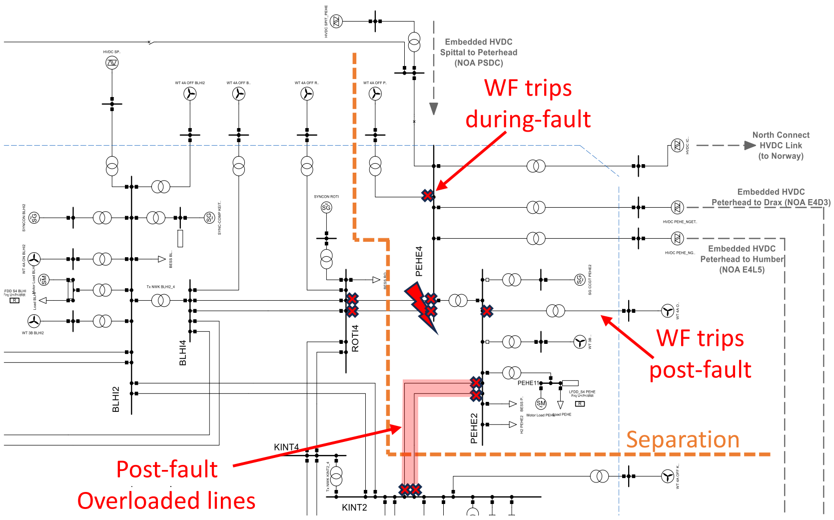

Figure 73: Post-fault conditions when wind trips at PEHE4 - showing overloaded lines and post-fault breaker status.

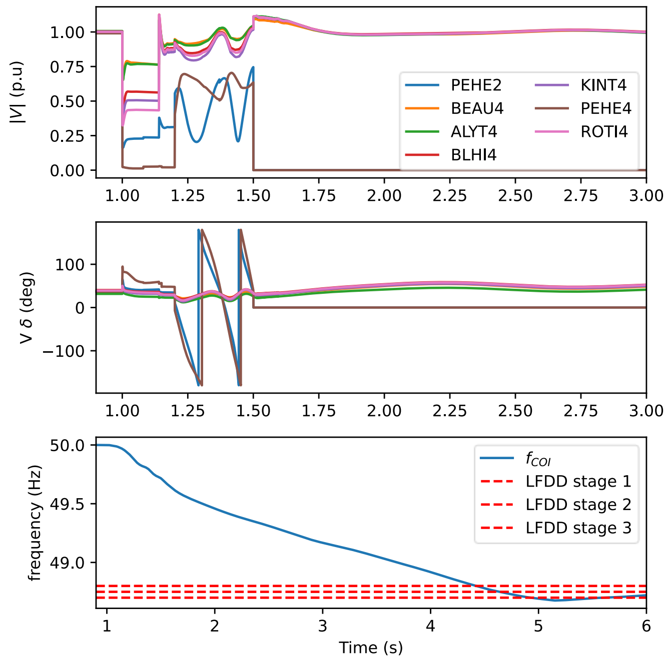

Figure 74: voltage magnitude and voltage angle for nearby busbars and COI frequency for DC LBF fault at PEHE4 (wind only trips)

For this case, it is assumed that the overloaded PEHE2_KINT2 275 kV double circuit lines trip at 1.5 s, as seen in Figure 74, where the voltages at PEHE2/4 go to zero. At this point, uncontrolled islanding has occurred, separating the Peterhead area from the rest of the AC system, seen by the dashed orange line in Figure 73, causing further infeed loss from the WF at PEHE2. Demand is also lost in the Peterhead area, offsetting the system's net generation loss. After the islanding has occurred and the Peterhead area is isolated from the rest of the system, the voltages at the remaining busbars recover. It is noted that the PEHE4 busbar remains non-synchronously connected to the AC system through multiple parallel DC links. What would happen in this situation is unclear, but they are expected to lose their reference and trip.

The overall net generation loss leads to a decline in system frequency, as seen in the bottom plot of Figure 74. At approximately 4.4 s, the first load-shedding stage is reached in the NGET system and stages two and three operate soon after (LFDD stages one, two and three are only applied in E&W). The frequency then begins to recover after the load shedding. If the LFDD scheme does its job correctly (as is modelled here), the successful operation of stages 1-3 should result in shedding no more than 20 % of the system's load. However, the success of the LFDD scheme can depend on the amount of DG located downstream of the LFDD relays within the distribution network. In this case, distributed PV outputs are high in GB (see Table 14), and much of this DG capacity is located behind LFDD relays. As the LFDD scheme disconnects generation and demand, each load-shedding stage has a lower net effect at the transmission system interface [14], [72]. Therefore, as shown in [72], it is likely that more than three stages of load shedding would be required to arrest the decline in frequency and, hence, more than 20 % of load would be disconnected. Possible solutions to this LFDD challenge are also discussed in [72].

Figure 75 shows the post-fault conditions when the HVDCs at PEHE4 also trip due to the fault (or due to controlled inter-tripping or fast de-loading triggered by the WF disconnections). In this case, HVDCs are tripped 50 ms after the WF trips. In the model, the embedded HVDC link from Spittal in the north is represented by a single 'incoming' HVDC terminal, but in reality, this link is in parallel with the AC system. If this link were to trip or be de-loaded, the power would be pushed onto the AC system: this is modelled by switching-in an alternative route to BEAU4 to the west. Therefore, this case study assumes that the northernmost part of the AC system from Beauly to Spittal, which is due to be reinforced but not modelled in the NGBTS, can safely transfer the extra power.

When the HVDCs are tripped, no line overloading or angular separation occurs, and the voltages recover after the backup protection operates, as seen in Figure 76. This fault event still seriously impacts the system, causing a sizeable initial phase angle jump at PEHE4, large post-fault phase angle swings, and a low frequency that cannot be contained within SQSS limits (Figure 76). However, there is no load shedding required. While the resulting network power flows around PEHE4 are within limits, the main transfer routes south over the B4 boundary become marginally overloaded (the transformers at KINC4 are at 117 % loading).

However, this is within typical short-term ratings, and the control room could take post-fault re-dispatch action.

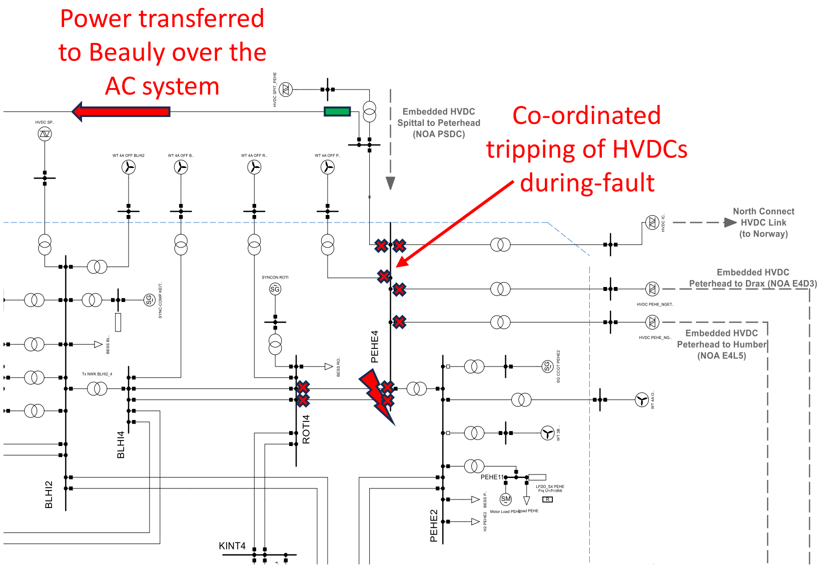

Figure 75: post fault system conditions with controlled tripping of HVDCs

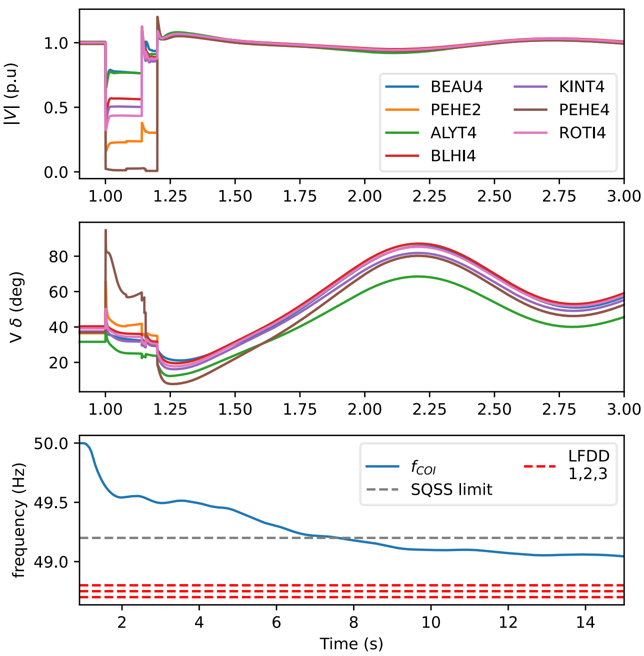

Figure 76: voltage magnitude and voltage angle for nearby busbars and COI frequency for DC LBF fault at PEHE4 (wind trips with HVDC inter-tripping)

It is acknowledged that the worst-case faults here are not secured events. Being non-secure implies that the balance between impact and likelihood of them occurring has historically been deemed low enough that it does not make economic sense to secure against them. It might be accepted that some local generator disconnections occur because of the severity of some faults, and those generator disconnections exceed the reserve volumes by a sufficient amount to initiate load shedding [204]. Be that as it may, as the system changes, it is also essential to analyse possible system events to identify high-impact contingencies and implement special protection and control schemes where necessary.

6.5 Methods to improve fault-induced frequency excursions

Sections 6.2.3 assessed multiple faults across a range of future generation dispatch conditions, and the worst of these is examined in detail, considering several sensitivities, in Sections 6.3 and 6.4. The results show that undesirable frequency conditions, at both a local and system-wide level, can occur due to faults, even when there is no infeed loss. Accordingly, it is necessary to investigate possible solutions to improve the fault-induced frequency excursions in the future.

Typical methods to manage system frequency within the security criteria in GB include:

- maintaining a minimum amount of system inertia;
- procuring more frequency response, including increasing the speed of some response services to manage declining system inertia; and
- raising the DG RoCoF protection thresholds.

All the methods listed above concern the system-wide frequency decline following a loss of infeed without considering the dynamics of a network fault. As shown in Chapter 3 adjusting the grid code requirements for grid-following converters can improve the system frequency response to faults. Furthermore, changing the fault responses of converters within their already-designed capability might yield cost-effective improvements.

This section assesses these various available methods to improve the FIFE issue. It extends on the methods considered in Chapter 3 and in the published literature by giving more focus to converter current ratings, current limits, FRT requirements and by applying the findings of the highly simplified network model to the more detailed representative NGBTS model. Furthermore, consideration is given to the benefit of procuring DC and inertia to address the FIFE.

6.5.1 Procurement of inertia

It is well known that increasing the mechanical inertia in the system increases the resistance to changes in frequency. In recent years, it has been common for NGESO to dispatch out-of-merit synchronous plants to boost the system inertia so that, in the event of losing the largest loss of infeed, the frequency can be contained within the SQSS limits. One of the main limitations has been the risk of losing DG on legacy RoCoF LoM protection settings. (See Section 0). In the future, much of this risk will be removed (by paying generators to update protection systems and updating the codes), and, along with faster acting response services, it contributes towards NGESO reducing the minimum inertia limit on the system from 140 GVAs to a minimum of 102 GVAs [16]. Alternatively, inertia can be procured by adding SCs or IBRs utilising grid forming control with an energy store.

It was seen in Section 6.4.1 that if the PSH projects in Scotland do not get built, the reduction in regional inertia degrades the regional frequencies after the fault. It was found that the local frequency nadirs can be lower, increasing the regional risk of load shedding. Inherently, this also means that regional RoCoFs can be higher. Higher regional RoCoFs in low inertia areas of GB are also indicated by other published works, such as [110]. Thus, these tests consider adding inertia in the northeastern part of the system, close to the fault, and adding inertia in the south, far from the fault.

The method of adding inertia to the south (NGET) area is through increasing the MVA rating of the SC; this SC represents the lumped inertia procured over all phases of the stability pathfinder program in E&W. The method of adding inertia to the northeast (SSEN) is by increasing the inertia constant of the SC at ROTI and by switching on the CCGT at PEHE2. The SC at ROTI4 is a low inertia machine [145], typical of an SC that does not utilise additional mass, such as a flywheel [144]. For the ‘SSEN + 2 GVAs’ case, it is assumed that this machine incorporates additional mass to increase its inertia constant. Then, in addition, for the other SSEN cases, all units of the CCGT at PEHE2 are switched on and dispatched at 0 MW such that the power flows and WF outputs are not affected, i.e. assuming that the CCGT can be run as an SC.

Table 18: machine adjustments and total inertia added to the system for each case study

Case Name	Machine(s) adjusted	Machine rating (MVA)	Machine inertia constant (s)	Additional inertia for case (GVAs)
Reference	SC @ NGET4	1250	20	0
	SC @ ROTI4	315	1.49	
	CCGT @ PEHE2 (off)	1530	6.2	
NGET + 10 GVAs	SC @ NGET	1750	20	10
NGET + 20 GVAs	SC @ NGET	2250	20	20
NGET + 30 GVAs	SC @ NGET	2750	20	30
SSEN + 2 GVAs	SC @ ROTI4	315	8	2.05
SSEN + 10 GVAs	SC @ ROTI4	315	3.1	10
	CCGT @ PEHE2 (on)	1530	6.2	
SSEN + 13.6 GVAs	SC @ ROTI4	315x2	8	13.58
	CCGT @ PEHE2 (on)	1530	6.2	

Figure 77 shows the COI frequency and RoCoF for each case detailed in Table 18. Adding inertia to the NGET system has less influence on the COI frequency and RoCoF than might be expected although a slight improvement is observed in the initial post-fault frequency. When adding inertia local to the fault in the SSEN area (at ROTI4 and PEHE2), the RoCoF is noticeably improved. However, the difference is only appreciable for the higher inertia cases. Comparing the ‘NGET + 10 GVAs’ and the ‘SSEN + 10 GVAs’ cases, the benefits of inertia local to the fault can be seen. For the cases where the CCGT at PEHE2 is on, the improvements cannot only be attributed to the additional regional inertia. The CCGT also increases fault levels and retained voltages during the fault, which can reduce the active current limitation of the local WFs.

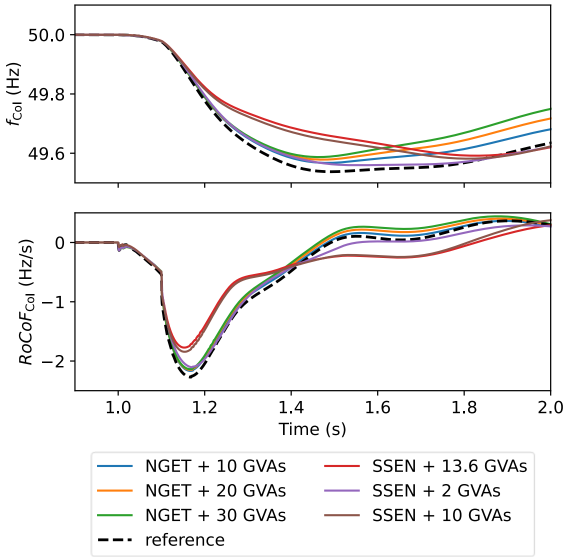

Figure 77: COI frequency and RoCoF for variations in inertia

Figure 78 shows the regional frequencies at the nearby locations close to the GSPs (supply points to the distribution network), close to the assumed location of LFDD relays. The frequencies reported here are measured by the dynamic model of the local WF and filtered as discussed in Section 6.3.2.1. These locations are at the highest risk of localised load shedding for the reference case. When the large unit at PEHE2 is online, the local LFDD risk has been removed altogether, and none of the frequencies at these locations reach the LFDD thresholds. Making the SC at ROTI4 a high-inertia machine does little to improve local frequencies.

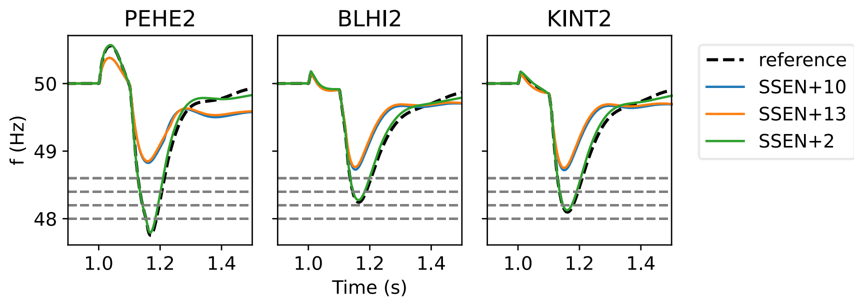

Figure 78: regional frequencies for cases that add local inertia and LFDD thresholds applicable to the SSEN area

In summary, when adding inertia to the system to address FIFE, it is most beneficial when located in the region of concern. However, for the case shown here, the amount of inertia required to make an appreciable improvement is relatively high. Adding inertia-carrying machines with voltage source behaviour, whether SMs or grid-forming IBRs with an energy store, to a region might bring several other benefits, e.g. improving voltage sensitivity, CCTs or power transfer capability (see Section 2.5.2). In the future, improving fault-induced frequency challenges will also be a factor to consider when siting such assets.

6.5.2 Procurement of Dynamic Containment (DC)

The DC service provides fast active power delivery proportional to system frequency and must initiate a response within 0.5 s and deliver its full response within 1 s. Therefore, the response is close to the timescales of the post-fault active power deficit and can potentially improve the FIFE. Table 19 details the case studies assessed for varying the amount of DC.

Table 19: cases considered for increasing the provision of dynamic containment

Case Name	Rating of responsive SG (MVA)	No. of BESS units	BESS unit rating (MW)	DC procured (rated) (MW)
reference	775	7	120	480
4 units	0	4	120	480
7 units	0	7	120	840
10 units	0	10	120	1,200
13 units	0	13	120	1,560
16 units	0	16	120	1,920

Figure 79 shows how increasing the provision of DC influences the post-fault COI frequency and RoCoF compared to the reference case study. The active power output of the BESS units (bottom plot) that provide DC is proportional to the frequency measured at the NGET bus in the south where the BESS is connected. The NGET bus is close to the COI, as this location has some larger lumped SGs and SCs but is still a distinct location with its own regional frequency profile. Hence, the BESS response does not precisely follow the COI frequency shown in the plots.

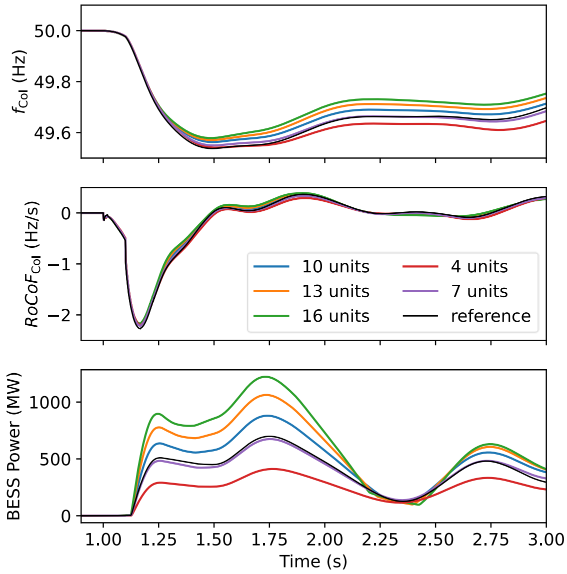

Figure 79: provisions of DC and their influence on the fault-induced frequency excursion

Adding more DC in England is not an effective way of mitigating the frequency dip for this case, with only minor improvements to the COI nadir and no real improvement to the RoCoF. These results suggest that procuring fast frequency response from BESS or other providers to mitigate FIFE in GB might not be cost-effective.

The location of BESS providing fast frequency control could influence its effectiveness in mitigating the FIFE. The analysis of the FIFE event in Section 6.3 showed that the frequency dip is caused by a sizeable and short-term active power deficit from IBRs (mostly WTs) which occurs within the first 0.5 seconds following fault clearance. The region of the GB power system being studied already has a very high installed capacity of IBRs. Increasing this capacity by adding large BESS introduces significant modelling challenges related to interactions between IBRs and the numerical stability of the model. Hence, the assessment of regional frequency response requirements from BESS is outside the scope of this study and is highlighted as further work.

6.5.3 Adjustments to wind farm requirements

In Chapter 3 it was shown that, on a simple two-area test system, the current control of the WTs can strongly influence the post-fault frequency. Through adjusting the voltage dependent reactive power support during FRT, notable gains in the frequency performance of the system can be achieved with minimal sacrifice of the reactive current and voltage performance. In addition, it was shown that the WF's post-fault active power recovery rate is also an important factor in the post-fault frequency. These control parameters – which are categorised as FRT parameters – are retested here to determine their impact on the NGBTS, from a base of their minimum requirements defined in the GB grid code [30].

In addition to the common FRT parameters, alternative methods are considered that can improve the active power delivery from WTs. These are grouped into two further categories. The first relates to the current limitation control and focuses on the concept of applying an individual limit to the reactive current and prioritising the active current, effectively adjusting the ratio between the delivered d-axis and q-axis output currents. Second is testing the influence of an increased short-term rating in the capacity of the converters, which could be achieved by mandating a minimum short-term rating in the grid code.

Each of these proposals has cost implications; most adjustments to FRT and current-limiting control parameters can likely be implemented via software updates to converter control systems. Increasing short-term ratings, however, will result in additional hardware and associated costs. Besides, altering the dynamic response of generators to faults could also result in adverse technical consequences, e.g. in pursuit of improving frequency stability, voltage or angular stability might be degraded. The analysis in this section provides a holistic technical assessment of these methods, judging the benefits by studying their effect on the reference case.

6.5.3.1 Effects of control strategies and current ratings on the FIFE

Table 20 shows the settings used for each of the three categories under test. For the current-limiting strategy, both Q priority and P priority techniques are utilised. For Q priority, which is the standard approach in GB, the maximum Iq is limited between 0.6 and 1.05 per unit with the intended effect of reducing the amount of Ip that must be curtailed by converters in FRT mode. The default assumption for Imax is 1.1 p.u, which is increased in steps to 1.5 p.u, while keeping the default maximum Iq limit at 1.05. The K factor, which represents the voltage-dependent reactive current during FRT, is reduced from its minimum grid code requirement (see Figure 53), and the maximum allowable active power ramp rate (in p.u/s) is increased.

Table 20: adjusted parameters for different converter control strategies and current ratings

Strategy	Name	Default value for reference case	New parameters considered
Current limiting control strategies	Q priority / Iqmax	On / 1.05	0.9, 0.8, 0.7, 0.6
	P priority / Iqmax	Off / 1.05	On / 1.05
Increasing short-term current ratings	Imax (during Voltage dip)	1.1	1.2, 1.3, 1.4, 1.5
FRT parameters	K factor	3.28	2.5, 1.8
	dPmax (max. power ramp rate)	1.5	2, 3, 4, 5

Figure 80 compares each control strategy and parameter's influence on some of the key system performance indices. The categories are shown in each column (with their own legends), and each row represents the following: the top row is the COI frequency nadir, the second row is the total energy lost from IBRs in the one-second period following fault inception, the third row is the retained voltages at nearby busbars and the bottom row is the maximum deviation of local synchronous machine speeds.

Each proposed change across all categories appreciably improves the COI frequency. At the system level, all changes lead to a lower energy loss from IBRs in the transient period of the fault (fault inception + 1 s), which directly affects the COI frequency. For the current limiting strategies, P priority gives the best performance in terms of COI frequency. However, the retained voltages at local busbars (calculated as the average voltage during the fault-on period) are lower for the P priority strategy and the more aggressive limits on Iq. When the short-term current limits of the converter are increased, the most significant improvements are observed. The total energy lost is much less for Imax values of 1.3 or above, reducing from 2,664 MWs to 1,103 MWs for the Imax=1.5 case, and the COI frequency is close to normal operating limits. In addition, the retained voltage around PEHE4 is improved.

An interesting outcome is that the total 'first-swing' speed deviation of the local SMs is also reduced, suggesting an improvement in their transient stability. The reduction in speed deviation might be counter-intuitive as, typically, reducing P while increasing Q from IBRs, i.e. the opposite intention of the changes made here, is known to improve the transient stability of SGs (see Section 2.4.2.2 for discussion and references). The rotor angle response of SMs and the technical trade-offs of each category are assessed further in the next section.

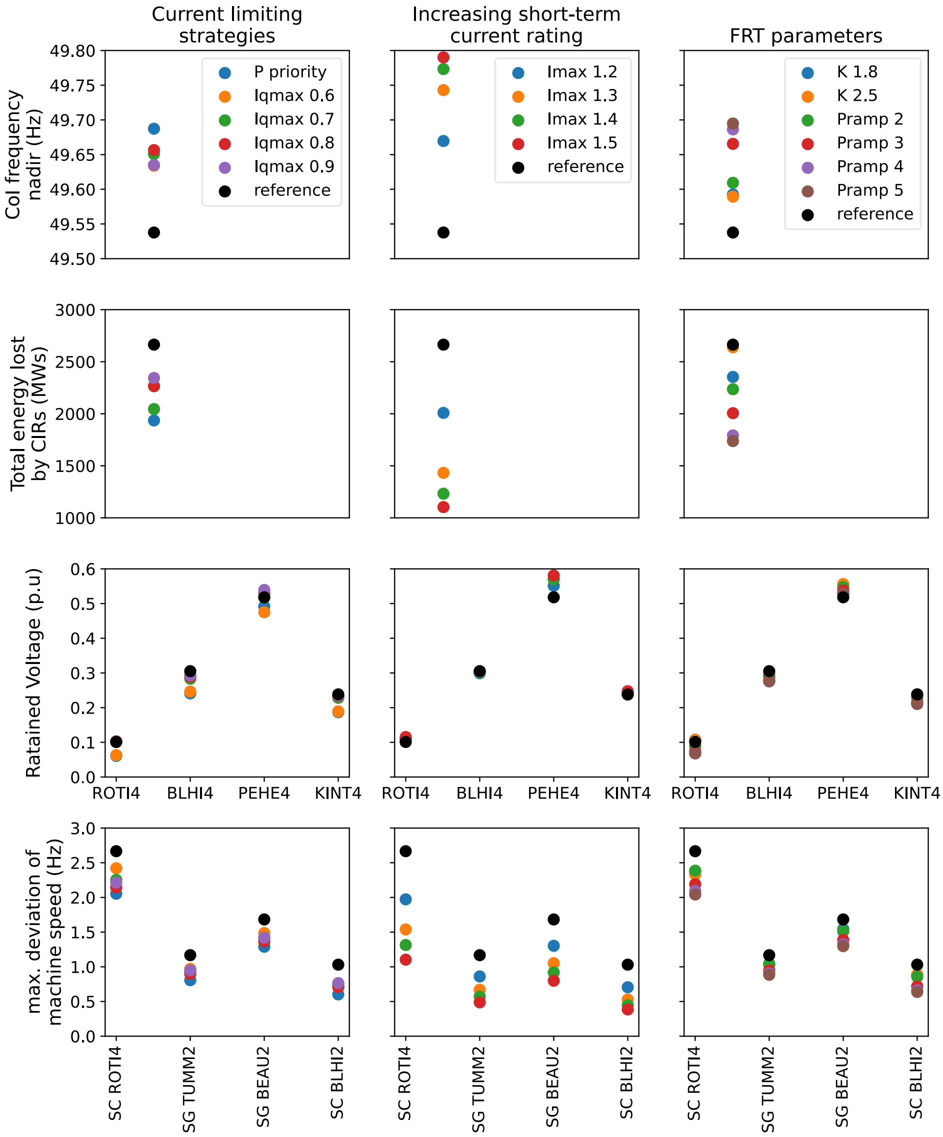

Figure 80: comparison of the relative influence that each control strategy (columns) has on the COI frequency nadir (top row), the energy lost from IBRs (2nd row), retained voltages (3rd row) and maximum deviation of local machine speeds (bottom row).

6.5.3.2 Inter-related stability factors when adjusting wind farm requirements

Referring to Section 2.1.5, which introduces the basic principles of rotor angle stability of SGs, and the swing equation in formula (4), the rate of change of angular deviation of an SG is higher for a greater imbalance between mechanical and electrical power. As such, during a fault, any means of increasing the exported power of an SG could reduce the imbalance of torque and reduce the rotor acceleration. The review in Section 2.4.2.2 cited several studies that find reducing the active power provision of IBRs during the fault, and recovering more slowly after the fault, can improve the rotor angle stability of nearby SGs.

However, the published works reviewed in Section 2.4.2.2, for example [99]–[102], either use highly simplified test systems or do not consider high penetrations of IBRs in the fault vicinity. They focus on reducing the IBRs active power injection to improve the first swing of the rotor angle by increasing the electrical output power of adjacent accelerating SGs. The setup used in these referenced studies does not allow for the effects of a fault propagating in a meshed network and causing a fault-induced active power deficit from multiple IBRs.

In the future GB system reference case studied here, the rotor angle acceleration during the fault-on period is not the primary concern. This work has identified that, for regions of a system with a high penetration of IBRs – particularly grid following WTs – that are at high output, the post-fault active power deficit can be extremely high, which dominates the transient behaviour of the SGs in the system as it applies a high decelerating power on the rotors (similar to a loss of infeed event).

Figure 27 shows one case study from each category. The top row of plots is the system response, and the middle and bottom rows are at the BEAU2 and ROTI4 locations, respectively. BEAU2 has a hydro generator (110 MVA, loaded to 86.2 %), and ROTI4 has an SC (315 MVA), and these rows of plots show bus voltages, machine rotor angles and active power output. At the system level, the following all reduce the COI frequency nadir, RoCoF and system inertial response required, listed in order from most to least benefit: increasing the short-term current ratings to 1.3 p.u; utilising a P-priority current limiting strategy; and reducing the Kfactor to 1.8.

At BEAU2, the retained voltage during the fault is degraded from the reference for each case. The most significant degradation is for the P-priority control strategy, which causes the voltage to decline during the fault by almost 0.2 p.u, signifying a lack of dynamic reactive power support. The effect of the lower voltage can be seen in the lower active power of the SG during the fault and the slight increase in rotor angle coming out of the fault. However, due to the large active power deficit in the immediate post-fault period, a sizeable inertial response is required from the SG to serve the load as the voltage recovers. The SG's active power output quickly increases, P_e becomes much greater than P_m and causes a high decelerating force on the rotor.

At ROTI4, the voltage goes to zero as it is very close to the fault. As the fault is close to the SC at ROTI4, it might be expected that the rotor angle would increase during the fault; however, there is little impact during and just after the fault-on period. Compared to an SG, there are some differences in the response as the machine is an SC. Most prior work on the stability of SMs focuses on SGs. A critical feature of the transient stability of an SG is its pre-disturbance loading, where highly loaded machines tend to operate closer to their stability limits and can more easily lose synchronism following a disturbance [7]. SCs do not have a dedicated mechanical load; thus, during normal operation, the mechanical and electrical output power of an SC is close to zero. Therefore, improving the active power export during the fault does not apply, and there is less concern (in the traditional sense) regarding the stability of SCs than SGs.

Some exceptions are emerging in the published literature where the angular stability of SCs is more of a concern. In [205], it is shown that the rotor angle of an SC co-located with a IBR can be more critical as the generator side voltages are improved and, for a fault at the common PoC, the SC must absorb the additional IBR power that cannot be exported to the network. Another example is in the Panhandle area of the ERCOT grid in Texas, where two SCs were installed to improve SCRs and provide voltage support. However, it was later found that new inter-area and intra-area oscillation modes arose that were insufficiently damped [50], [206]. However, these cases are outside the scope of this work.

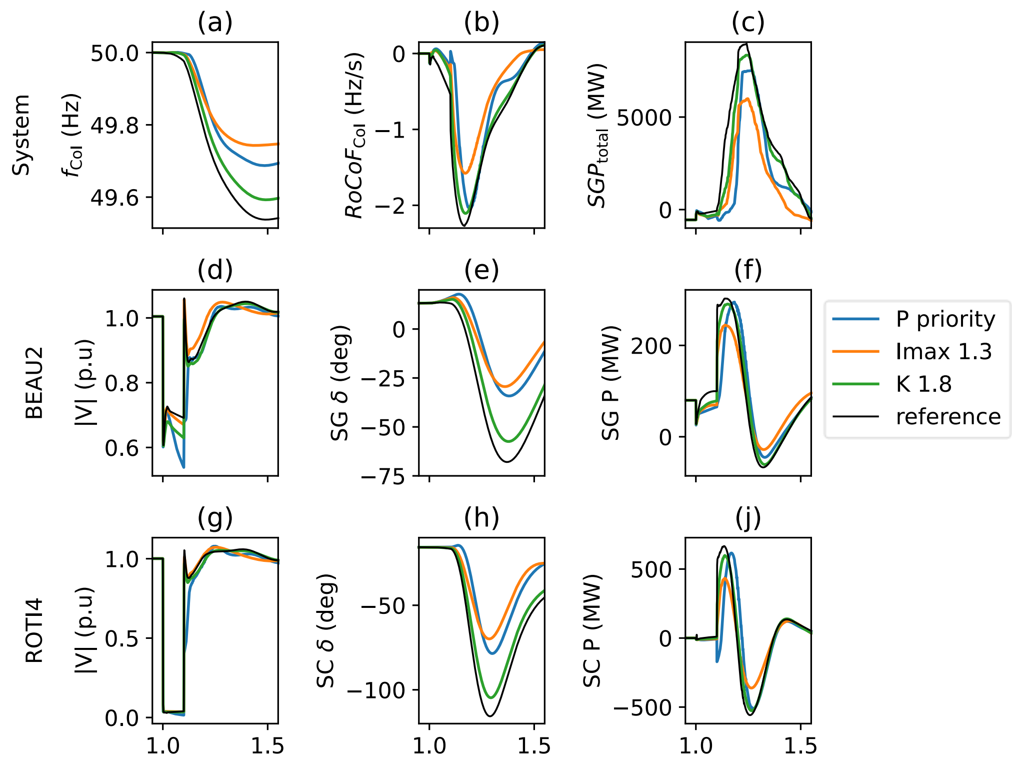

Figure 81: system performance for a selection of converter control and capacity changes – showing the impact on synchronous machine rotor angle performance.

At ROTI4, reducing the post-fault active power deficit of IBRs reduces the inertial response delivered by the SC and results in less decelerating power on its rotor, thereby improving both angular stability and frequency stability. However, there are some tradeoffs regarding the voltage performance, and a P-priority current limiting strategy might require additional voltage support.

6.5.3.3 Cumulative gains from control changes

The most effective method for improving the FIFE is increasing the short-term capacity of the converters. However, this comes with additional hardware costs. There may be cumulative gains from a combination of changes to the requirements for IBRs. The combination of changes assessed here is shown in Table 21.

Table 21: combination of control parameters considered

Strategy	Name	reference case value	New value
Current limiting control strategies	Q priority / Iqmax	On / 1.05	On / 0.9
short-term current ratings	Imax (during Voltage dip)	1.1	1.2
FRT parameters	K factor	3.28	2.5
	dPmax (max. power ramp rate)	1.5	3

The top row of Figure 82 shows, from left to right, the system frequency response, RoCoF and system inertial response. By reducing the overall inertial energy required post-fault, the combination of updates significantly improves the COI frequency and RoCoF. The frequency nadir is close to the operational limits of ±0.2 Hz, and the RoCoF, while still relatively high, has been improved and the time spent above the thresholds is reduced. The local voltages at PEHE4, BLHI4 and ROTI4, shown in the middle row, are not meaningfully degraded. The improvements in active power delivery by the WFs is shown on the bottom row; for locations with non-zero voltages, the fault-on active power is improved, and for all these locations, the post-fault recovery of active power is improved.

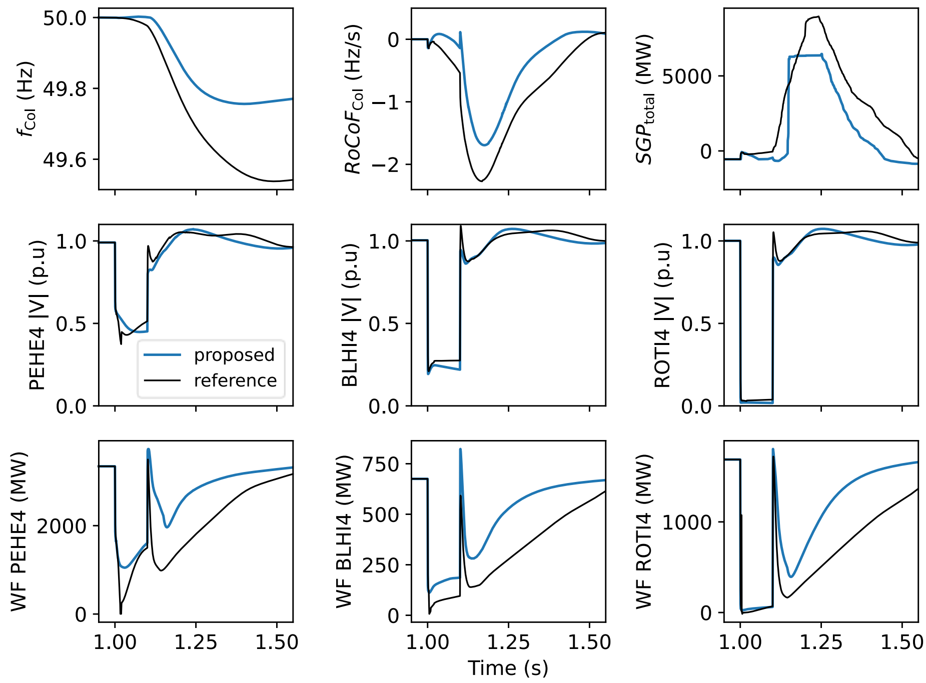

Figure 82: system-wide frequency and inertial response (top row) and local voltages and wind farm active power responses (middle and bottom rows, respectively)

It was found in Section 6.5.1 that procuring inertia in the fault region can improve the regional frequencies. This is to be expected from adding an inertia carrying voltage source. In that case, the regional risk of breaching LFDD thresholds was removed altogether. However, the improvements to the system frequency via the IBR control system changes can also be seen at the regional level. Figure 83 shows the LFDD risk for the reference case and the proposed combination of control and current rating parameters. The updates result in lowering the local frequency sensitivity in the fault region, and the risk of localised load shedding has been reduced.

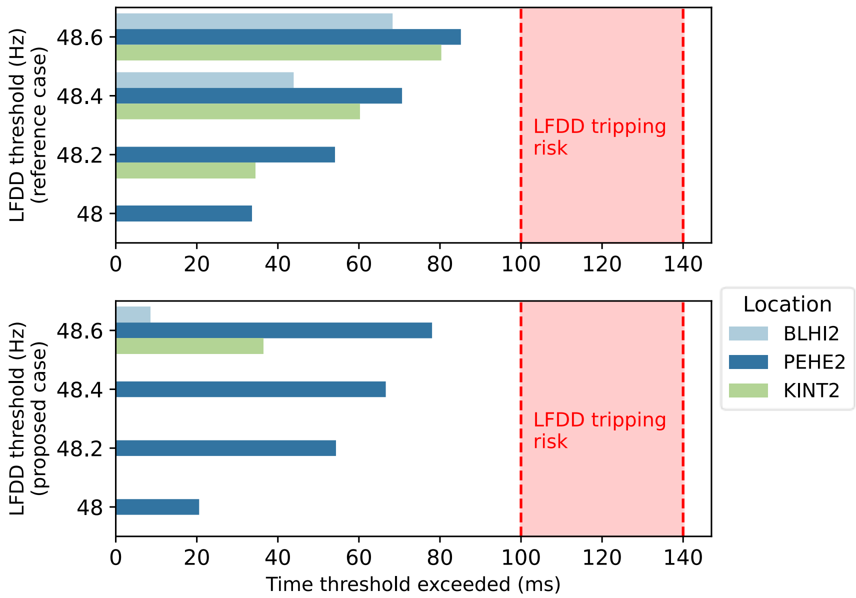

Figure 83: LFDD risk for reference case (top) and proposed combination of control updates (bottom)

6.6 Chapter discussion and conclusions

This chapter has comprehensively assessed fault-induced frequency stability in the future GB power system. The work has identified that voltage disturbances in the IBR-dense locations of the network can lead to significant system-wide frequency dips, high system RoCoFs, and additional regional frequency risks that could lead to local unintentional load shedding. It is shown that these types of disturbances in the future GB system could increase the risk of network frequencies deviating outside of acceptable bounds and; therefore, jeopardise meeting the fundamental functional criteria of the power system identified in Section 1.1.

Various GB-specific assessment criteria have been applied to assess deviations from the nominal frequency and its rate of change at a system-wide and regional level. The level of impact and risks are summarised in Table 22.

Table 22: Assessment criteria and associated level of risk for frequency and RoCoF limits

Assessment criteria	Max. duration of exceedance	Associated risk
$49.8\ Hz < f < 50.2\ Hz$	Any	Operating frequency range by NGESO.
$49.5\ Hz < f < 50.5\ Hz$	Any	Statutory frequency limits as defined in the SQSS and Grid Code.
$49.2\ \text{Hz} < f < 49.5\ Hz$	60 s	Infrequent occurrences are allowed according to the SQSS and Grid Code.
$48.8\ \text{Hz} < f < 49.2\ Hz$	-	Frequency is outside the allowable range. No load or generation tripping is allowed.
$47\ \text{Hz} < f < 48.8\ Hz$	100 – 140 ms	Load shedding occurs in stages. Risk of unnecessary loss of load.
$f < 47\ Hz$	none	Generation disconnection is allowed on under-frequency. High risk of blackout.
$-0.5\ Hz/s < \frac{df}{dt} < 0\ Hz/s$	Any	Within intended operational limits by NGESO.
$-1\ Hz/s < \frac{df}{dt} < -0.5\ Hz/s$	500 ms	RoCoF is outside of the intended operation range – possible risk of loss of DG and cascading events.
$\frac{df}{dt} < -1\ Hz/s$	500 ms	RoCoF exceeds DG LoM protection settings. High risk of loss of DG and cascading events.

6.6.1 Problems found

In the 2032 network, when there is a high wind output, faults in the northeastern part of the system are the worst cases from a FIFE perspective. System-wide COI frequency nadirs can be as low as 49.54 Hz (for the base case assumptions), which exceeds the normal operating frequency range and is close to statutory frequency limit of 49.5 Hz. These faults initiate a response from DC service providers, although the transient frequency deviations tend to recover within the normal operating range of ± 0.2 Hz within a few seconds. The results suggest that deviations from normal might become more frequent.

Although the magnitude of the frequency deviation does not exceed statutory limits, it has a high rate of change. The total active power deficit might only last a few hundred milliseconds after the fault; however, it can be significantly large as a proportion of the total generation, leading to a relatively rapid change in the system frequency in the immediate post-fault period. The average RoCoFs of the COI frequency in the 500 ms from fault inception can reach -0.88 Hz/s, and the peak COI RoCoF can reach -2.17 Hz/s. However, the RoCoF does recover within the protection system time delay defined in the DG connection codes. Nonetheless, these RoCoFs are regarded as high for the GB system, particularly as they are felt throughout the system, far from the fault location.

Assessment of regional frequencies for the reference case fault showed that the deviations in local frequencies are much higher than the COI frequency (noting the challenges of modelling frequency across the system). It is found that frequencies in the fault vicinity can easily breach the thresholds of the LFDD scheme, highlighting a risk of localised load shedding. In addition, frequencies measured by WF generation can be close to their under-frequency protection thresholds.

UK electricity industry system development plans include constructing large-scale pumped storage hydro plants local to the worst-case fault location. It has been found that should these not get built, only relatively minor impacts are observed in the system COI frequency. However, the regional frequencies are degraded due to reduced local inertia, which increases the risk of localised load shedding. This finding was corroborated when assessing the influence of procuring additional inertia in the fault region. Simulations show that if inertia is procured locally to the fault location, regional frequencies can be significantly improved, and these risks reduced.

A selection of secure and non-secure faults was assessed to investigate the impact of fault severity and fault duration of the FIFE. In general, it was found that for different types of three-phase faults, even if they are not cleared within normal protection clearance times, the type of fault alone does not significantly impact the COI frequency nadir of the FIFE. However, for longer duration faults, accounting for the allowance in the Grid Code for generators to recover their active power more slowly, substantially impacts the system frequency, highlighting the importance of ensuring minimum active power recovery rates from IBR. The reason behind this relaxation of the active power recovery rate for longer fault clearance times is unknown. If modern IBR can recover faster from any possible fault event, an update to the grid code should be investigated to offset this risk.

It has been found that if an infeed loss occurs due to a network fault the frequency nadir can be lower and RoCoF can be higher compared to considering the same loss of infeed without a network fault. If the effects of the fault are not considered in system security assessments, these types of events can become technically non-compliant with the security criteria. For cases studied in this work, the COI frequency nadir when the fault is accounted for does not reach critical protection thresholds. Therefore, it could be argued that securing the fault and the loss of infeed could result in additional and unnecessary costs to the consumer. However, for a fault and loss of infeed, the system RoCoF is considerably higher than the loss of infeed alone.

The severe non-secure faults studied with longer clearance times result in local generation exceeding their FRT voltage-time curves and would be allowed to trip. Being non-secured events implies that the balance between impact and likelihood of them occurring has historically been deemed low enough that it does not make economic sense to secure against them. In these cases, it might be accepted that some local generator disconnections and load shedding occur. However, the extent of such events must still be limited, and the expected consequences should be known as best possible. For a fault in the northeast close to Peterhead, the studies identified a possible partial system split in this area from the rest of the AC system, and uncontrolled islanding of generators and loads could lead to cascading outages. To manage this risk, the potential value of a coordinated protection and control scheme between the wind generators and the HVDC links is highlighted.

6.6.2 Solutions studied

A range of methods to improve the possible FIFEs has been investigated. These methods include procuring more inertia and volumes of fast frequency response services and enforcing wind farm performance changes by mandating different grid code requirements of IBRs.

It is found that changes to IBR requirements are significantly more beneficial than procuring inertia or DC when trying to improve the FIFE. Inertia procurement can be costly, and it is found here that a large amount of local inertia is required to make an appreciable difference. Traditional means of procuring inertia are building SCs or instructing SGs to be online that were out-of-merit. SCs have a high capital cost, and bringing on SGs can have a high operational cost as they must respect their minimum stable generation level, possibly leading to constraints on low carbon generation. Another option is the use of grid forming converters, which is discussed at the end of this section.

Controlling the severity of the FIFE is best done by limiting the active power deficit during the fault and recovering quickly post-fault. Due to the current-limited nature of the IBRs, this is at the expense of reactive power support. In some of the FRT and current limiting control settings tested, the reduced dynamic reactive power from IBRs appreciably degrades the retained voltages during the fault. The more aggressive reactive current limiting strategies, such as low maximum limits for Iq or prioritising Ip, might lead to unacceptable voltage conditions. Therefore, due to the potential implications for voltage stability, it would be wise to exercise caution if implementing a P-priority current limiting strategy similar to that mandated by the Irish grid code.

Reduced retained voltage and increased active power delivery from IBRs can also degrade the rotor angle stability of local SGs. However, in the cases studied here, it is found that the dominating factor of the first-swing rotor angle is governed by a decelerating force applied in the post-fault period due to the active power deficit. Therefore, reducing this active power deficit by any means improves the rotor angle stability of the local SGs and SCs.

It has been shown that several marginal changes to grid-following IBR requirements can bring cumulative benefits. The combination of changes tested here are:

- reducing the voltage-dependent reactive current during FRT;
- requiring IBRs to have a short-term rating of 1.2 p.u,;
- limiting the maximum reactive current to 0.9 p.u during FRT; and
- increasing the active power recovery ramp rate by a factor of 2.

With these changes, the FIFE can be improved for the worst-case scenario, and the COI frequency is close to the operating range of ± 0.2 Hz.

6.6.2.1 What about adding grid forming converters?

An alternative source of inertia and fault level to the solutions assessed here is the use of converters that implement grid-forming (GFM) control. Unlike traditional grid-following (GFL) converters, which synchronise with the local grid voltage and inject current, behaving as current source, GFM converters are controlled to behave like voltage sources. This allows them to emulate SGs by actively regulating voltage and frequency. A GFM converter that provides an inertial response delivers active and reactive power in proportion to frequency and phase changes at the grid interface, contributing positively to the system's frequency stability [19], [57], [58].

However, like GFL converters, GFM converters remain current-limited devices. They are borne of similar hardware, and therefore, during disturbances, their maximum current output is constrained by similar design parameters. GFMs are still required to prioritise active or reactive current during current saturated operation. In addition, GFM units do not have the inherent energy storage required for sustained response unless they are paired with technologies such as batteries, supercapacitors, or flywheels.

Currently, it remains unclear whether the large WTs or HVDC projects considered in this study will be required to implement GFM control strategies. Therefore, the focus of this work has been on exploring solutions that address the limitations of GFL converters to evaluate the extent to which GFM control would be necessary in a real-world system.

Despite their potential, the characteristics of GFM converters suggest that during faults, their ability to mitigate fault-induced frequency dips, as studied in this chapter, would still be constrained by current-limiting behaviour. Additional converter capacity or integrated energy reserves may be required to effectively handle large disturbances. In high-penetration GFL environments, adding GFM units would likely provide benefits similar to those of SGs or SCs studied here. As such, the findings here suggest that modifying grid code requirements for GFL converters remains a technically advantageous and cost-effective solution to address fault induced frequency stability issues.

Chapter 7: Conclusions, Recommendations and Further Work

Chapter 1 outlined the changes expected in GB in the coming few decades. These changes can be broadly summarised into (1) a very high increase in the installed capacity of wind, particularly in Scotland, (2) an unprecedented increase in DC transfer capacity from Scotland to England and (3) significant AC reinforcement works. The dynamic behaviour of power systems changes as they transition from synchronous machines to non-synchronous converter-interfaced resources. These changes are typically characterised by a change in the inertia and fault levels on the system, which, in turn, alter the sensitivity of the system's frequency and voltages. This research has assessed how the power system's dynamic properties might change and what effect they can have on the future system in GB, as it moves towards fully decarbonised operation.

Chapter 1 also introduced the differences between SMs and IBRs, highlighting the non-synchronous current-limited nature of IBRs. These differences were elaborated in Chapter 2, which outlined the fundamental principles and background regarding the system's stability, limits and operational requirements in the context of increasing IBR penetration. The challenge of managing system frequency and keeping voltages within limits during operational timescales falls on the TSO. Hence, many TSOs, including NGESO in GB, have already begun to take measures to counter the loss of services provided by power stations with SGs. These changes also bring about new mechanisms and system behaviours that have not been previously planned for and require novel investigations and solutions. This research has investigated a possible new frequency stability mechanism in GB, which is interrelated with network voltage disturbances rather than loss of infeed events.

The literature review in Chapter 2 identified that the interactions between network faults and system frequency could increase with high penetrations of IBR. Gaps in the literature were identified regarding the study of the FIFE phenomenon, which could benefit from further analysis regarding the following aspects:

(1) how voltage and frequency interact relating to FRT requirements for IBRs;
(2) what are the technical trade-offs concerning the system's performance for different FRT requirements;

(3) how does this challenge apply to larger island systems such as GB; and
(4) what measures can be taken to mitigate the detrimental effects of fault-induced active power deficits through existing IBR control measures.

The concept of FIFE was then studied in Chapter 3 using a simple two-area test system to describe some of these interactions. The simulations explained the underlying system behaviours that lead to post-fault active power deficits and consequent fault-induced frequency dips. The extent of the frequency dips observed in the two-area system during transient fault conditions was sufficiently large and fast to cause concern for secure system operation, potentially breaching typical operating limits and risking the disconnection of generation and load under RoCoF or LFDD protection schemes. This study in Chapter 3, reinforced by the existing studies in the literature reviewed in Chapter 2, shows that the extent to which these power deficits impact the frequency stability is primarily related to the severity of the fault, the penetration and loading of IBRs, the proximity of the fault to highly loaded IBRs and the active and reactive power control requirements of IBRs. These findings warrant further study on how a FIFE might propagate in the GB system, considering the expected increase in IBRs, which has yet to be studied.

A new power system model has been developed as part of this work to allow the study of the effects of generation and transmission capacity expansion plans on the GB system's dynamic behaviour. The model provides a higher degree of fidelity in the northern part of the GB network, compared to existing GB models in the public domain. In addition, the model integrates a credible version of the future GB power system that is required to achieve zero-carbon operation beyond 2035.

Compared to the 'generic' test systems already available in the literature, the model developed in this work represents a real and up-to-date network with known parameters that constrain its operation in credible ways. This model, as well as a series of generation dispatch scenarios that represent the GB electricity market arrangements, has been used in Chapter 4 to study changes to the GB system's dynamic properties and in Chapter 5 to study fault-induced frequency excursions.

Chapter 2 provided a qualitative review of the meaning of system strength and its relationship to fault level. Chapter 5 provided a quantitative review of the cumulative effects of system changes on the magnitudes of fault levels in the Scottish network from 2022 to 2032. This independent fault level assessment improves the understanding of the nature of the fault level challenge in Scotland. It has been found that fault levels in 2032 significantly increase throughout the Scottish transmission system, going against the familiar narrative of reducing fault levels. Much of this growth in fault level is supplied by IBRs, and it is shown that the voltage depressions during faults can become less resistant to change due to the overall increase in fault level and dynamic reactive power support that IBRs provide.

Much attention in the industry has been given to the effects of reducing fault levels. However, substantially increasing fault levels leads to the exceedance of network asset ratings and incorrect protection settings during fault conditions, which has important implications for reliable system operation. In addition, where fault levels increase throughout the network, this can jeopardise the timely and cost-effective connection of new renewable generation projects. This work demonstrates that more attention should be paid to the implications of rising fault levels and finding solutions, ahead of time, to manage the associated risks.

Chapter 5 has also highlighted that, although fault level and system strength are related, a low fault level at a given location does not necessarily mean that the quasi-steady state voltage sensitivity is high. Furthermore, established metrics for system strength are based on the fault level and an equivalent Thevenin impedance, meaning that they may not properly represent the system's behaviour in the context of high converter penetration. Hence, it is argued that there is a need to make a clearer distinction between low fault level issues and high voltage sensitivity. Making this distinction can be useful because, in general, there can be different solutions which satisfy one or the other. For example, some challenges, such as converter control interactions, could be resolved via solutions that do not provide additional fault level. However, the fault level remains closely related to the magnitude of the voltage depression during faults.

Chapter 6 studied the possible impacts of FIFEs on the Scottish transmission grid, addressing the main research question. The work has identified that, in the future system, disturbances in the IBR-dense locations of the network can lead to significant system-wide frequency dips, high system RoCoFs, and additional regional frequency stability risks. The worst-case faults have been identified as those in the northeastern part of the system, which has been studied in detail. At the system level, as represented by frequency at the system's centre of inertia, the frequency deviations due to faults alone can reach values close to the statutory limits in GB of 49.5 Hz. Although this would be considered a significant system event, it does not reach critical protection thresholds such as generator under-frequency or LFDD and should recover without dispatching additional reserves. However, the frequency excursion occurs quickly, and the RoCoF transients at the system level are very high and are found to breach RoCoF LoM protection thresholds in the fault recovery period, but tend to recover within the 500 ms delay window used for RoCoF protection devices. Nonetheless, the system-wide RoCoF transients for these types of faults are considerably higher than a loss of infeed event, which may cause concern for the system operator.

At the regional level, i.e. close to the fault, frequency deviations can be much higher than at the centre of inertia. It is found that frequencies in the fault vicinity can breach the thresholds of the LFDD scheme, highlighting a risk of localised load shedding. In addition, frequencies can reach values close to the generator's under-frequency protection thresholds. Unintentional load or generator disconnections can potentially escalate an event that should have been secure into a cascading loss of generation and load. The frequency event on August 9th 2019 in GB showed that triggering the LFDD scheme can have significant consequences, with some uncertainty regarding the risk of disconnecting supplies to critical infrastructure.

Several possible solutions have been investigated to offset the risk of FIFE in GB. The solutions in this work have focused on possible changes to grid code requirements for IBRs. One of the primary factors at the root of this challenge is how grid-following IBRs control their active power profile when subjected to voltage disturbances. This characteristic is determined by the grid code requirements for IBRs, their rating and their current limitation control. In GB, FRT requirements have prioritised reactive current over active current to support the network voltage. In addition, a relatively fast recovery rate for active power of a maximum of 0.5 seconds already exists. However, it is found that increasing the ratio of active to reactive current delivery during the fault and further increasing the speed of its recovery can significantly benefit the FIFE, reducing the system-wide and regional effects. These changes to IBR requirements are also observed to be more beneficial than alternative solutions, such as procuring fast frequency response or additional system inertia, which are the most common solutions for managing frequency stability.

Adjusting how IBRs respond to faults will have knock-on effects on other aspects of the system's dynamic performance. It was found in the literature review in Chapter 2 that a shortfall of some of the available studies is that they did not assess some of these trade-offs. Increasing the active-to-reactive current ratio will reduce dynamic voltage support and affect voltage performance (unless current ratings are increased to achieve the increase in active current). In most cases, small increases in active power delivery can improve the frequency without any voltage degradation. However, at some nodes assessed, there are limits to this, and in some cases, severely limiting reactive current might lead to a lack of voltage support. It was also considered that increasing the delivery of active power and the speed of active power recovery of IBRs can degrade the angle stability of local SGs by limiting their active power export during the fault and recovery period. However, the opposite is found to be true for these types of faults in GB. This analysis has found that the mechanisms driving the FIFE also dominate the SGs rotor angle change, which is governed by a decelerating force applied in the post-fault period due to the active power deficit. Therefore, during some types of faults and counter to traditional transient stability assumptions, improving active power delivery from IBRs can also improve the rotor angle stability of the local SMs.

The long-term electricity system infrastructure plans incorporated into the NGBTS model form the foundation of the network requirements needed to operate a zero-carbon system by 2035 and beyond. This model has enabled the study of the system's needs, and how they change, in the coming decades. The findings presented in this thesis lead to several recommendations for identifying and addressing the technical requirements critical to the proposed transformation of the electricity system.

7.1 Key recommendations

Some key recommendations for the attention of NGESO, the TO's and system operators, network owners and regulatory bodies can be drawn from this work, as follows:

- New methods need to be developed for defining the system's requirement's that are currently expressed by a deficiency in fault level. Defining a minimum fault level requirement does not always solve the problem and fails to capture the true behaviour of IBRs. A clear distinction between low fault level issues and high voltage sensitivity should be made.
- More attention should be given to the implications of rising fault levels in the network to manage the risk of exceeding network asset ratings and protection system requirements. If not managed in advance, fault level constraints will lead to higher costs and delays in connecting renewable generation projects, impacting the system's pace of decarbonisation.
- To manage frequency stability in the future, the impact of networks faults on the system-wide and regional frequencies should be considered by the system operator. Mitigating actions should be implemented in advance to manage the associated risks to system security.
- To mitigate the risk of large active power deficits immediately following network faults, it is recommended to amend the Grid Code to increase the ratio of active to reactive current delivery during faults and accelerate active power recovery after fault clearance. These changes are expected to be within the capabilities of modern IBR technologies, pending consultation with converter OEMs.

- The grid code requirement allowing a longer active power recovery time (1 second instead of 0.5 seconds) for faults lasting more than 140 ms should be reviewed and shortened if possible. It has been found that when these conditions occur, they can lead to very large frequency deviations, increasing the risk of operational issues and potential cascading outages.

7.2 Further work

This Thesis has succeeded in answering the research questions and has made several contributions to the body of research regarding frequency stability and its relationship with network disturbance events. However, additional tasks that are outside the scope of this research could be undertaken to extend the work presented here.

As discussed in Chapter 6, Section 6.6.2.1, an alternative to the solutions assessed here might also be investigating how the system would respond if converters had grid-forming control. It has been noted that the benefits could still be limited as GFM converters are still current-limited devices and do not have any significant inherent energy storage. Furthermore, GFMs may still be required to prioritise active or reactive current during current saturated operation. Therefore, further work could determine to what extent these challenges would apply to GFM converters.

Another potential method of improving FIFEs could be regional delivery of fast frequency response. As noted in Section 6.5.2, provisions of DC from BESS located in England (far from the fault) is not found to give much improvement to the frequency nadir of the event. However, some regional benefits might be observed when the DC service is delivered in the fault vicinity. Further work in this regard would include determining the extent of possible improvements to regional frequency nadirs and RoCoFs during a FIFE event from placing DC in Scotland. Similar findings (at best) are expected to those observed when adding inertia. Hence, it is still expected that the most effective solution is to reduce the power deficit at its source, i.e. by changing WT control parameters, as discussed in this Thesis. Some additional model development may be required to increase the penetration of IBRs in the northeastern area of the model to undertake this work.

An assessment of the practical limitations of active power recovery rates of different IBRs would be beneficial to inform grid code requirements. It is understood from the literature review that the constraints for wind turbines exist due to electro-mechanical stresses induced by ramping power. In addition, the ramp rate might also depend on the pitch control during high wind speeds [88]. However, little information exists in the available literature. The limitations will likely be different for different OEMs. Therefore, industry consultation would be required to implement any changes to the grid code in this regard.

Further work could be done on testing metrics that can be used in system operational timescales to assess the risk of FIFEs. In Ireland, the SNSP is used. However, this metric has limitations for detecting conditions that lead to FIFEs as it does not consider the location of faults or loading of individual WTs. This work has presented a simple new metric: the current-at-risk, which does consider these factors. If FIFE was confirmed as a regional system security risk, applying this metric could be further developed and tested to determine operational limits.

The NGBTS model developed in this work has progressed to a point suitable for the work at hand. Considering the massive expansion plans in GB in the modelled network area, it will be necessary and beneficial to continue to update the model. This further model development could include future planned projects as they are confirmed and improve its capability by adding further functionality. For example, more detailed protection systems could be implemented, zero-sequence data could be obtained to analyse unbalanced faults, or an investigation could be made into converting the model to perform EMT studies.

The simulations of different options for the configuration of FRT requirements described in this thesis are necessary and practical starting points to inform possible future system behaviour and revision of grid code requirements, but they are not complete. The studies presented here utilise standardised models of generators and their controls in a representative system model. It would be necessary to perform these analyses on the full network model for GB with, as far as possible, models of actual converter controls to validate the types of responses observed in these studies. When conducting these studies, many of the learnings presented in this work can be carried forward, for example, the screening method for determining likely worst-case fault conditions and knowledge of the main effects. In practice, generator controls for different assets might be controlled to behave differently from those assumed in this study.

References

[1] R. Neukom, N. Steiger, J. J. Gómez-Navarro, J. Wang, and J. P. Werner, “No evidence for globally coherent warm and cold periods over the preindustrial Common Era,” *Nature*, vol. 571, no. 7766, pp. 550–554, 2019, doi: 10.1038/s41586-019-1401-2.

[2] R. Neukom *et al.*, “Consistent multidecadal variability in global temperature reconstructions and simulations over the Common Era,” *Nature Geosci.*, vol. 12, no. 8, pp. 643–649, 2019, doi: 10.1038/s41561-019-0400-0.

[3] Intergovernmental Panel on Climate Change, “Climate Change 2023: Synthesis Report. Summary for Policymakers.” pp. 1–34, 2023.

[4] Intergovernmental Panel on Climate Change, “Overarching Frequently Asked Questions and Answers,” no. June. pp. 1–2, 2023.

[5] United Nations, “Paris Agreement Paris,” *United Nations Treaty Collect.* , vol. 7, no. 7, pp. 1–16, 2019.

[6] UK Government, “uk-becomes-first-major-economy-to-pass-net-zero-emissions-law,” *Climate change and energy - news story*, 2019. https://www.gov.uk/government/news/uk-becomes-first-major-economy-to-pass-net-zero-emissions-law.

[7] P. Kundur, *Power System Stability and Control*, 1st ed. McGraw-Hill, Inc., 1994.

[8] National Grid, *National Electricity Transmission System Security and Quality of Supply Standard - Version 2.5*, no. April. 2021, pp. 1–94.

[9] National Grid Electricity System Operator Limited, “The Grid Code,” 2021.

[10] National Grid ESO, “System Operability Framework - Whole system SCL,” 2018. [Online]. Available: https://www.nationalgrideso.com/research-and-publications/system-operability-framework-sof.

[11] Climate Change Committee, “Delivering a reliable decarbonised power system.” p. 130, 2023.

[12] UK Government, “Offshore Wind Net Zero Investment Roadmap.” 2023.

[13] National Grid ESO, “Future Energy Scenarios 2023.” 2023.

[14] S. Gordon, C. McGarry, and K. Bell, “The growth of distributed generation and associated challenges: A Great Britain case study,” *IET Renew. Power Gener.*, pp. 1–14, 2022, doi: 10.1049/rpg2.12416.

[15] National Grid ESO, “National Trends and Insights.” 2021, [Online]. Available: https://www.nationalgrideso.com/research-publications/system-operability-framework-sof.

[16] National Grid ESO, “Operability Strategy Report 2023.” [Online]. Available: https://www.nationalgrideso.com/research-and-publications/system-operability-framework-sof.

[17] National Grid ESO, “Operating a Low Inertia System,” 2020. [Online]. Available: https://www.nationalgrideso.com/research-and-publications/system-operability-framework-sof.

[18] IEEE Power System Dynamic Performance Committee, “Stability definitions and characterization of dynamic behavior in systems with high penetration of power electronic interfaced technologies,” *IEEE Syst. J.*, vol. 11, no. April, pp. 2108–2117, 2020.

[19] B. Shakerighadi *et al.*, “An overview of stability challenges for power-electronic-dominated power systems: The grid-forming approach,” 2022, doi: 10.1049/gtd2.12430.

[20] Y. Gu and T. C. Green, “Power System Stability With a High Penetration of Inverter-Based Resources,” 2022, doi: 10.1109/JPROC.2022.3179826.

[21] National Grid ESO, “NOA Stability Pathfinder Phase 2 - Invitation for Expressions of Interest,” 2020.

[22] K. Bell and A. Tleis, “Test system requirements for modelling future power systems,” 2010, doi: 10.1109/PES.2010.5589807.

[23] IEEE/CIGRE Committee on Power System Dynamic Performance, “Definition and classification of power system stability,” *IEEE Trans. Power Syst.*, vol. 19, no. 3, pp. 1387–1401, 2004, doi: 10.1109/TPWRS.2004.825981.

[24] Nasser Tleis, *Power Systems Modelling and Fault Analysis - Theory and Practice*, Second Edi. Elsevier Ltd, Academic Press, 2019.

[25] British Standards Institution, “BS EN 60909-0:2016 Short-circuit currents in three-phase a.c. systems, Part 0: Calculation of currents,” 2016.

[26] S. Gordon, Q. Hong, and K. Bell, “Implications of Reduced Fault Level and its Relationship to System Strength: A Scotland Case Study,” *CIGRE Paris Sessions - C4*. 2022.

[27] P. M. Anderson, C. Henville, R. Rifaat, B. Johnson, and S. Meliopoulos, *Power system protection*, Second ed. IEEE Press, 2022.

[28] National Grid ESO, “Electricity Ten Year Statement - Appendix D: Fault levels,” 2020.

[29] Energy Networks Association, “G99 Engineering Recommendation: Requirements for the connection of generation equipment in parallel with public distribution networks on or after 27 April 2019,” 2020.

[30] National Grid Electricity System Operator, *The Grid Code*, no. Issue 6 Revision 11. 2022, p. 606.

[31] N. Hatziargyriou, J. Milanovic, C. Rahmann, C. Canizares, D. Hill, and I. Hiskens, “Definition and Classification of Power System Stability - Revisited & Extended,” *IEEE Trans. POWER Syst.*, vol. 36, no. 4, 2021, doi: 10.1109/TPWRS.2020.3041774.

[32] A. Dixon, *Modern Aspects of Power System Frequency Stability and Control*. Academic Press, 2019.

[33] Electric Power Research Institute, “Power System Dynamics Tutorial,” 2009. [Online]. Available: www.epri.com.

[34] Ö. Göksu, R. Teodorescu, C. L. Bak, F. Iov, and P. C. Kjær, “Instability of wind turbine

converters during current injection to low voltage grid faults and PLL frequency based stability solution," *IEEE Trans. Power Syst.*, vol. 29, no. 4, pp. 1683–1691, 2014, doi: 10.1109/TPWRS.2013.2295261.

[35] A. Monti, F. Milano, E. Bompard, and X. Guillaud, *Converter-based dynamics and control of modern power systems*. Academic Press, 2020.

[36] S. K. Ma, H. Geng, L. Liu, G. Yang, and B. C. Pal, "Grid-synchronization stability improvement of large scale wind farm during severe grid fault," *IEEE Trans. Power Syst.*, vol. 33, no. 1, pp. 216–226, Jan. 2018, doi: 10.1109/TPWRS.2017.2700050.

[37] CIGRE Working Group B4.62, *Connection of Wind Farms to Weak AC Networks*, no. December. 2016.

[38] North American Electric Reliability Council (NERC), "Integrating Inverter-Based Resources into Low Short Circuit Strength Systems," no. December, p. 47, 2017.

[39] National Grid ESO, "System Operability Framework - Impact of declining short circuit levels," 2018.

[40] Australian Energy Market Operator (AEMO), "System strength in the NEM explained," 2020.

[41] ENTSO-E, "High Penetration of Power Electronic Interfaced Power Sources and the Potential Contribution of Grid Forming Converters," p. 32, 2019.

[42] IEEE and ANSI, "IEEE Guide for Planning DC Links Terminating at AC Locations Having Low Short-Circuit Capacities," 1997.

[43] ERCOT, "2019 Panhandle Regional Stability Study," 2019.

[44] D. Kim, H. Cho, B. Park, and B. Lee, "Evaluating influence of inverter-based resources on system strength considering inverter interaction level," *Sustain.*, vol. 12, no. 8, pp. 1–18, 2020, doi: 10.3390/SU12083469.

[45] H. Xiao, Y. Zhang, X. Duan, and Y. Li, "Evaluating Strength of Hybrid Multi-Infeed HVDC Systems for Planning Studies Using Hybrid Multi-Infeed Interactive Effective Short-Circuit Ratio," *IEEE Trans. Power Deliv.*, vol. 8977, no. c, pp. 1–1, 2020, doi: 10.1109/tpwrd.2020.3020957.

[46] Powerlink Queensland and GHD Advisory, "Managing system strength during the transition to renewables," 2020. [Online]. Available: https://arena.gov.au/assets/2020/05/managing-system-strength-during-the-transition-to-renewables.pdf.

[47] X. Wang, L. Harnefors, and F. Blaabjerg, "Unified Impedance Model of Grid-Connected Voltage-Source Converters," *IEEE Trans. POWER Electron.*, vol. 33, no. 2, 2018, doi: 10.1109/TPEL.2017.2684906.

[48] C. Henderson, L. Xu, and A. Egea-Alvarez, "PN admittance characterisation of grid supporting VSC controllers with negative sequence regulation and inertia emulation," *23rd European Conference on Power Electronics and Applications (EPE'21 ECCE Europe)*. Sep. 06, 2021.

[49] O. Gomis-Bellmunt, J. Song, M. Cheah-Mane, and E. Prieto-Araujo, "Steady-state impedance mapping in grids with power electronics: What is grid strength in modern power systems?," *Int. J. Electr. Power Energy Syst.*, vol. 136, no. October 2021, p. 107635, 2022, doi: 10.1016/j.ijepes.2021.107635.

[50] B. Badrzadeh *et al.*, “System Strength,” *CIGRE Sci. Eng. Power Syst.*, vol. 20, pp. 5–26, 2021.

[51] D. Wilson, V. Terzija, J. Yu, A. Nechifor, and M. Eves, “MIGRATE Project: Deliverable 2.1 requirements for monitoring & forecasting PE-based KPIs,” 2018.

[52] X. Wang and F. Blaabjerg, “Harmonic Stability in Power Electronic-Based Power Systems: Concept, Modeling, and Analysis,” *IEEE Trans. Smart Grid*, vol. 10, no. 3, pp. 2858–2870, 2019, doi: 10.1109/TSG.2018.2812712.

[53] G. D. Irwin, A. K. Jindal, and A. L. Isaacs, “Sub-synchronous control interactions between type 3 wind turbines and series compensated AC transmission systems,” *IEEE Power Energy Soc. Gen. Meet.*, 2011, doi: 10.1109/PES.2011.6039426.

[54] T. Shi, D. Nayanasiri, and Y. R. Li, “Sub-synchronous oscillations in wind farms an overview study of mechanisms and damping methods,” *IET Renew. Power Gener.*, vol. 14, no. 19, pp. 3974–3988, 2020, doi: 10.1049/iet-rpg.2020.0479.

[55] C. Hardt, D. Premm, P. Mayer, F. Mosallat, and S. Goyal, “Practical experience with mitigation of sub-synchronous control interaction in power systems with low system strength,” *CIGRE Sci. Eng.*, vol. 21.

[56] D. Liu, Q. Hong, A. Dyśko, D. Tzelepis, G. Yang, and C. Booth, “Evaluation of HVDC System’s Impact and Quantification of Synchronous Compensation for Distance Protection,” *IET Renew. Power Gener.*, pp. 1–12, 2022.

[57] Sandia National Laboratories, “Impact of Inverter-Based Resource Negative-Sequence Current Injection on Transmission System Protection,” 2020.

[58] A. Banaiemoqadam, A. Hooshyar, and M. A. Azzouz, “A Control-Based Solution for Distance Protection of Lines Connected to Converter-Interfaced Sources during Asymmetrical Faults,” *IEEE Trans. Power Deliv.*, vol. 35, no. 3, pp. 1455–1466, 2020, doi: 10.1109/TPWRD.2019.2946757.

[59] S. Kumar Mutha, A. Shrestha, V. Cecchi, and M. Manjrekar, “Analysis of Negative-Sequence Directional Element for Type-IV Wind Power Plants under Various Control Methodologies,” doi: 10.1109/NAPS50074.2021.9449692.

[60] L. Huang *et al.*, “Grid-Synchronization Stability Analysis and Loop Shaping for PLL-Based Power Converters with Different Reactive Power Control,” *IEEE Trans. Smart Grid*, vol. 11, no. 1, pp. 501–516, 2020, doi: 10.1109/TSG.2019.2924295.

[61] M. Paolone *et al.*, “Fundamentals of power systems modelling in the presence of converter-interfaced generation,” *Electr. Power Syst. Res.*, vol. 189, 2020, doi: 10.1016/j.epsr.2020.106811.

[62] J. Chen, F. Prystupczuk, and T. O’Donnell, “Use of voltage limits for current limitations in grid-forming converters,” *CSEE J. Power Energy Syst.*, vol. 6, no. 2, pp. 259–269, 2020, doi: 10.17775/CSEEJPES.2019.02660.

[63] M. Nedd, J. Browell, K. Bell, and C. Booth, “Containing a Credible Loss to within Frequency Stability Limits in a Low-Inertia GB Power System,” *IEEE Trans. Ind. Appl.*, vol. 56, no. 2, pp. 1031–1039, Mar. 2020, doi: 10.1109/TIA.2019.2959996.

[64] L. Meng *et al.*, “Fast Frequency Response From Energy Storage Systems-A Review of Grid Standards, Projects and Technical Issues,” *IEEE Trans. Smart Grid*, vol. 11, no. 2, 2020, doi: 10.1109/TSG.2019.2940173.

[65] National Grid ESO, “Frequncy Response Services.” https://www.nationalgrideso.com/industry-information/balancing-services/frequency-response-services#:~:text=We have a licence obligation,might result in frequency variations. (accessed Aug. 18, 2024).

[66] C. MacIver, K. Bell, and M. Nedd, “An analysis of the August 9th 2019 GB transmission system frequency incident,” *Electr. Power Syst. Res.*, vol. 199, pp. 378–7796, 2021, doi: 10.1016/j.epsr.2021.107444.

[67] National Grid ESO, “Operability Strategy Report 2021,” 2021.

[68] Ofgem, “Investigation into the power outage that occurred on 9 August,” 2020.

[69] National Grid ESO, “Frequency Risk and Control Report,” 2022. [Online]. Available: https://www.ofgem.gov.uk/publications/investigation-9-august-2019-power-outage.

[70] CIGRE Task Force C2.02.24, “Defense plan against extreme contingencies,” 2007.

[71] K. Bell *et al.*, “Planning to Manage Power Interruption Events,” *CIGRE Technical Brochure 433, WG C1.17, ELECTRA 69*, no. 252, 2010.

[72] S. Gordon, C. McGarry, J. Tait, and K. Bell, “Impact of Low Inertia and High Distributed Generation on the Effectiveness of Under Frequency Load Shedding Schemes,” *IEEE Trans. Power Deliv.*, vol. 37, no. 5, pp. 3752–3761, 2022, doi: 10.1109/TPWRD.2021.3137079.

[73] H. Haes Alhelou, M. E. Hamedani Golshan, T. C. Njenda, and N. D. Hatziargyriou, “An Overview of UFLS in Conventional, Modern, and Future Smart Power Systems: Challenges and Opportunities,” *Electr. Power Syst. Res.*, vol. 179, no. February 2019, p. 106054, 2020, doi: 10.1016/j.epsr.2019.106054.

[74] A. Derviškadić, Y. Zuo, G. Frigo, and M. Paolone, “Under frequency load shedding based on PMU estimates of frequency and ROCOF,” *arXiv*, pp. 1–6, 2018.

[75] H. Haes Alhelou, M. E. Hamedani Golshan, T. C. Njenda, and N. D. Hatziargyriou, “An Overview of UFLS in Conventional, Modern, and Future Smart Power Systems: Challenges and Opportunities,” *Electr. Power Syst. Res.*, vol. 179, Feb. 2020, doi: 10.1016/J.EPSR.2019.106054.

[76] U. Rudež, T. Škrjanc, and R. Mihalič, *Chapter 12: Emergency active-power balancing scheme for load frequency control*. 2023.

[77] Ofgem, “9th August 2019 power outage report,” 2020.

[78] ENTSO-E, “Technical background for the Low Frequency Demand Disconnection requirements,” 2014. Accessed: Feb. 20, 2023. [Online]. Available: https://eepublicdownloads.entsoe.eu/clean-documents/Network codes documents/NC ER/141215_Technical_background_for_LFDD.pdf.

[79] European Commission, *Commission Regulation (EU) 2017/2196. Establishing a network code on electricity emergency and restoration, Article 15 Automatic under-frequency control scheme*. 2017.

[80] National Grid ESO, “Low Frequency Demand Disconnection,” 2017.

[81] National Grid ESO, “Appendices to the Technical Report on the events of 9 August 2019,” 2019.

[82] National Grid ESO, “ESO Operational Transparency Forum 14th April 2021 - webinar

recording - published presentation slides," no. April. 2021.

[83] North American Electric Reliability Corporation, "San Fernando Disturbance - Southern California Event: July 7, 2020," 2020.

[84] North American Electric Reliability Corporation, "Odessa Disturbance - Texas Events: May 9, 2021 and June 26, 2021," 2021.

[85] North American Electric Reliability Corporation, "2022 Odessa Disturbance - Texas Event: June 4, 2022," 2022.

[86] Joint NERC and Texas RE Staff Report, "Panhandle Wind Disturbance," 2022.

[87] Australian Energy Market Operator (AEMO), "Trip of Mortlake Power Station – Blue Gum substation 500 kV line and operation of circuit breaker fail protection on 9 July 2023," 2023.

[88] Z. H. Rather and D. Flynn, "Impact of voltage dip induced delayed active power recovery on wind integrated power systems," *Control Eng. Pract.*, vol. 61, pp. 124–133, 2017, doi: 10.1016/j.conengprac.2017.01.003.

[89] EirGrid, "EirGrid Grid Code Version 12," 2023.

[90] J. O'Sullivan, A. Rogers, D. Flynn, P. Smith, A. Mullane, and M. O'Malley, "Studying the maximum instantaneous non-synchronous generation in an Island system-frequency stability challenges in Ireland," *IEEE Trans. Power Syst.*, vol. 29, no. 6, pp. 2943–2951, 2014, doi: 10.1109/TPWRS.2014.2316974.

[91] H. W. Qazi, P. Wall, M. Val Escudero, C. Carville, N. Cunniffe, and J. O' Sullivan, "Impacts of Fault Ride Through Behavior of Wind Farms on a Low Inertia System," *IEEE Trans. Power Syst.*, pp. 1–9, Jun. 2020, doi: 10.1109/TPWRS.2020.3003470.

[92] EIRGRID and SONI, "The DS3 Programme: Delivering a Secure, Sustainable Electricity System (brochure)." Accessed: Jan. 08, 2024. [Online]. Available: http://eur-lex.europa.eu/LexUriServ/LexUriServ.do?uri=Oj:L:2009:140:0016:0062:en:PDF.

[93] S. Nolan, N. Delaney, H. Gerard, and et al, "EU-SysFlex Project - Deliverable D3.1: Product definition for innovative system services," 2019. [Online]. Available: https://eu-sysflex.com/.

[94] E. Vittal, M. O'malley, and A. Keane, "Rotor Angle Stability With High Penetrations of Wind Generation," *IEEE Trans. POWER Syst.*, vol. 27, no. 1, p. 353, 2012, doi: 10.1109/TPWRS.2011.2161097.

[95] R. M. Tumilty, C. G. Bright, G. M. Burt, O. Anaya-Lara, and J. R. Mcdonald, "Applying series braking resistors to improve the transient stability of low inertia synchronous distributed generators," 2007.

[96] R. I. Hamilton, "Uncovering the predominant factors influencing the transient stability margin in power systems with increasing renewable generation using interpretable machine learning," PhD Thesis. The University of Strathclyde, 2022.

[97] T. Ackermann, *Wind power in power systems*. Wiley-Blackwell, 2012.

[98] A. A. Van Der Meer, M. Ndreko, M. Gibescu, and M. A. M. M. Van Der Meijden, "The effect of FRT behavior of VSC-HVDC-connected offshore wind power plants on AC/DC system dynamics," *IEEE Trans. Power Deliv.*, vol. 31, no. 2, pp. 878–887,

Apr. 2016, doi: 10.1109/TPWRD.2015.2442512.

[99] A. Mitra and D. Chatterjee, "Active Power Control of DFIG-Based Wind Farm for Improvement of Transient Stability of Power Systems; Active Power Control of DFIG-Based Wind Farm for Improvement of Transient Stability of Power Systems," *IEEE Trans. Power Syst.*, vol. 31, no. 1, 2016, doi: 10.1109/TPWRS.2015.2397974.

[100] Y. Zhang, M. Ding, P. Han, H. Sun, W. Yang, and Z. Chen, "Analysis of the Interactive Influence of the Active Power Recovery Rates of DFIG and UHVDC on the Rotor Angle Stability of the Sending-End System," *IEEE Access*, vol. 7, pp. 79944–79958, 2019, doi: 10.1109/ACCESS.2019.2923341.

[101] S. Konstantinopoulos and J. H. Chow, "Dynamic Active Power Control in Type-3 Wind Turbines for Transient Stability Enhancement; Dynamic Active Power Control in Type-3 Wind Turbines for Transient Stability Enhancement," 2021, doi: 10.1109/PESGM46819.2021.9638092.

[102] K. Johnstone, "Mitigating the erosion of transient stability margins in Great Britain through novel wind farm control techniques," University of Strathclyde, 2019.

[103] Q. Hong *et al.*, "Fast frequency response for effective frequency control in power systems with low inertia," *J. Eng.*, vol. 16, 2019, doi: 10.1049/joe.2018.8599.

[104] M. Nedd, W. Bukhsh, C. MacIver, and K. Bell, "Metrics for determining the frequency stability limits of a power system: A GB case study," *Electr. Power Syst. Res.*, vol. 190, p. 106553, 2021, doi: 10.1016/j.epsr.2020.106553.

[105] National Grid, "Frequency Response Technical Sub Group Report," 2011. Accessed: Feb. 20, 2023. [Online]. Available: https://www.nationalgrid.com/sites/default/files/documents/28745-Final Technical Sub Group Report.pdf.

[106] L. Badesa, F. Teng, and G. Strbac, "Conditions for Regional Frequency Stability in Power System Scheduling - Part II: Application to Unit Commitment," *IEEE Trans. Power Syst.*, vol. 36, no. 6, pp. 5567–5577, Nov. 2021, doi: 10.1109/TPWRS.2021.3073077.

[107] Orsted, "Enhanced Frequency Control Capability (EFCC) Wind Package Report: Frequency Support Outlook," 2018.

[108] National Grid ESO, "GB 36 Bus Electricity Transmission Network Model," *NGESO website*, 2023. https://www.nationalgrideso.com/research-and-publications/gb-36-bus-electricity-transmission-network-model.

[109] D. Tzelepis, Q. Hong, C. Booth, P. N. Papadopoulos, J. Ramachandran, and G. Yang, "Enhancing Short-Circuit Level and Dynamic Reactive Power Exchange in Gb Transmission Networks under Low Inertia Scenarios," *SEST 2019 - 2nd Int. Conf. Smart Energy Syst. Technol.*, 2019, doi: 10.1109/SEST.2019.8849020.

[110] B. A. Osbouei, G. A. Taylor, O. Bronckart, J. Maricq, and M. Bradley, "Impact of inertia distribution on power system stability and operation," in *2019 IEEE Milan PowerTech, PowerTech 2019*, 2019, pp. 1–6, doi: 10.1109/PTC.2019.8810689.

[111] H. Urdal, R. Ierna, J. Zhu, C. Ivanov, A. Dahresobh, and D. Rostom, "System strength considerations in a converter dominated power system," *IET Renew. Power Gener.*, vol. 9, no. 1, pp. 10–17, 2015, doi: 10.1049/iet-rpg.2014.0199.

[112] M. Yu, R. Ierna, H. Urdal, and J. Zhu, "Effects of swing equation-based inertial

response (SEBIR) control on penetration limits of non-synchronous generation in the GB power system," 2015.

[113] J. Boyle, T. Littler, and A. Foley, "Review of frequency stability services for grid balancing with wind generation," *J. Eng.*, vol. 15, pp. 1061–1065, 2018, doi: 10.1049/joe.2018.0276.

[114] M. Kang, E. Muljadi, and Y. Cheol Kang, "Stable Adaptive Inertial Control of a Doubly-Fed Induction Generator," *IEEE Trans. Smart Grid*, vol. 7, no. 6, 2016, doi: 10.1109/TSG.2016.2559506.

[115] R. Ierna *et al.*, "Effects of VSM convertor control on penetration limits of non-synchronous generation in the GB power system," *15th Wind Integration Workshop*. 2016.

[116] M. Ndreko, S. Rüberg, and W. Winter, "Grid forming control scheme for power systems with up to 100% power electronic interfaced generation: a case study on Great Britain test system," *IET Renew. Power Gener.*, vol. 14, no. 8, pp. 1268–1281, 2020, doi: 10.1049/iet-rpg.2019.0700.

[117] CIGRE Working Group C4.56, *CIGRE Technical Brochure 881: Electromagnetic transient simulation models for large-scale system impact studies in power systems having a high penetration of inverter-connected generation*. 2022.

[118] J. Daniel Lara *et al.*, "Revisiting Power Systems Time-domain Simulation Methods and Models," *IEEE Trans. Power Syst.*, 2023, doi: 10.1109/TPWRS.2023.3303291.

[119] IEEE Power and Energy Society, "IEEE Standard 421.1-2021: Definitions for Excitation Systems for Synchronous Machines," 2021.

[120] International Electrotechnical Commission, *IEC 61400-27-1:2020 Wind energy generation systems: Electrical simulation models - Generic models*. 2020.

[121] F. Reyer *et al.*, "ENTSO-E Continental Europe Synchronous Area Separation on 08 January 2021," 2021.

[122] P. Pourbeik *et al.*, "Generic Dynamic Models for Modeling Wind Power Plants and Other Renewable Technologies in Large-Scale Power System Studies," *IEEE Trans. Energy Convers.*, vol. 32, no. 3, pp. 1108–1116, Sep. 2017, doi: 10.1109/TEC.2016.2639050.

[123] Scottish Government, "ScotWind Offshore Wind Leasing Round: statement by the Net Zero Secretary - 18 January 2022," Jan. 18, 2022. https://www.gov.scot/publications/scotwind-offshore-wind-leasing-round-statement-net-zero-secretary-18-january-2022/ (accessed Dec. 13, 2022).

[124] National Grid ESO, "Pathway to 2030 - Holistic Network Design," 2022. Accessed: Oct. 10, 2022. [Online]. Available: https://www.nationalgrideso.com/document/262681/download.

[125] National Grid ESO, "Electricity Ten Year Statement: Appendix B - System technical data," 2021.

[126] National Grid ESO, "Future Energy Scenarios 2022 - Regional breakdown of FES data (workbook)," 2022.

[127] National Grid ESO, "Electricity Ten Year Statement - Main Report," 2022.

[128] Ofgem, “Consultation on the initial findings of our Electricity Transmission Network Planning Review,” 2021. [Online]. Available: www.ofgem.gov.uk.

[129] National Grid Energy System Operator, “Network Options Assessment 2021/22 Refresh,” 2022.

[130] Scottish Power Transmission, “Transmission Owner Reinforcement Instruction (TORI) Quarterly Update Report,” 2022. Accessed: Oct. 06, 2022. [Online]. Available: http://www.spenergynetworks.co.uk/pages/beauly_denny_overhead_line_up.

[131] Scottish and Southern Energy Networks - Transmission, “Scottish Hydro Electric Transmission plc Transmission Owner Reinforcement Instruction (TORI) Quarterly Update Report Q3,” 2022, Accessed: Oct. 06, 2022. [Online]. Available: www.ssen-transmission.co.uk.

[132] Crown Estate Scotland, “Our role in offshore wind.” https://www.crownestatescotland.com/scotlands-property/offshore-wind/our-role-in-offshore-wind (accessed Feb. 05, 2023).

[133] Offshore Wind Scotland, “The offshore wind market in scotland.” https://www.offshorewindscotland.org.uk/the-offshore-wind-market-in-scotland/ (accessed Feb. 05, 2023).

[134] National Grid ESO, “Transmission Entry Capacity Register,” 2022.

[135] Department for Business Energy & Industrial Strategy, “Digest of UK Energy Statistics (DUKES): Power stations in the UK (DUKES 5.11),” 2022.

[136] EDF Energy, “Nuclear power stations in the UK.” https://www.edfenergy.com/about/nuclear/power-stations. (accessed Apr. 14, 2022).

[137] C. MacIver, W. Bukhsh, and K. R. W. Bell, “The impact of interconnectors on the GB electricity sector and European carbon emissions,” *Energy Policy*, vol. 151, p. 112170, Apr. 2021, doi: 10.1016/J.ENPOL.2021.112170.

[138] Climate Change Committee, “The Sixth Carbon Budget: The UK’s path to Net Zero,” 2020. [Online]. Available: https://www.theccc.org.uk/wp-content/uploads/2020/12/The-Sixth-Carbon-Budget-The-UKs-path-to-Net-Zero.pdf.

[139] Scottish Government, “Draft Hydrogen Action Plan,” 2021.

[140] Scottish Government, “Scottish Offshore Wind to Green Hydrogen Opportunity Assessment,” 2020.

[141] Department for Business Energy & Industrial Strategy, “Analytical annex to the Hydrogen Strategy, Net Zero Hydrogen Fund Consultation, Low Carbon Hydrogen Business Model consultation, and Low Carbon Hydrogen Standards consultation,” 2021.

[142] Department for Business Energy & Industrial Strategy, “UK hydrogen strategy,” 2021. doi: 10.1002/cind.859_6.x.

[143] Depertment for Buisiness Energy and Inductrial Strategy, “Hydrogen Strategy update to the market: December 2022,” 2022.

[144] CIGRE Working Group A1/C4.66, “Guide on the Assessment, Specification and Design of Synchronous Condenser for Power System with Predominance of Low or Zero Inertia Generators,” 2022. doi: 10.1002/bapi.201390039.

[145] National Grid ESO, "Stability Pathfinder Phase 2 Tender Results," 2022. Accessed: Feb. 20, 2023. [Online]. Available: https://www.nationalgrideso.com/future-energy/projects/pathfinders/stability/Phase-2.

[146] IEEE Power and Energy Society, *IEEE Standard 421.5-2016: Recommended Practice for Excitation System Models for Power System Stability Studies*. 2016.

[147] M. Nedd, "Changes to System Inertia and the impact on frequency response requirements (PhD Thesis)," University of Strathclyde, 2020.

[148] CIGRE Working Group C4.605, "Modelling and Aggregation of Loads in Flexible Power Networks," 2014.

[149] A. Arif, Z. Wang, J. Wang, B. Mather, H. Bashualdo, and D. Zhao, "Load Modeling—A Review," *IEEE Trans. Smart Grid*, vol. 9, no. 6, pp. 5986–5999, 2018, doi: 10.1109/TSG.2017.2700436.

[150] C. Pascalau, T. B. Soeiro, N. H. Van Der Blij, and P. Bauer, "Electrical Energy Conversion for Low Temperature Electrolysis - Challenges and Future Trends," 2021, doi: 10.1109/PEMC48073.2021.9432571.

[151] Electricity North West, "Customer Load Active System Services (CLASS) Second Tier LCN Fund Project Closedown Report," 2015.

[152] A. Dixon, "Chapter 5 - Techniques available for calculating frequency response requirements," in *Modern Aspects of Power System Frequency Stability and Control*, A. Dixon, Ed. Academic Press, 2019, pp. 55–86.

[153] National Grid ESO, "ESO Operational Transparancy Forum (3rd November 2021)."

[154] DIgSILENT, "PowerFactory Technical Reference - Battery Energy Storage System Template," 2022.

[155] CIGRE Working Group B4.57, *Guide for the development of models for HVDC converters in a HVDC grid (Technical Brochure 604)*. CIGRÉ, 2014.

[156] CIGRE Study Committee B4: DC Systems and Power Electronics, "Flexible AC Transmission Systems (FACTS) - CIGRE Green Book," 2020. [Online]. Available: http://www.springer.com/series/15209.

[157] ABB, "PCS100 STATCOM Dynamic Reactive Power Compensation - Technical Catalogue," Accessed: Oct. 15, 2022. [Online]. Available: www.abb.com/pcs100-power-converters.

[158] Energy Networks Association, "Engineering Recommendation G74 Issue 2 2020: Procedure to meet the requirements on IEC 60909 for the calculation of short-circuit currents in three- phase AC power systems - Effective from 1 st July 2021," 2021.

[159] UK Department for Business Energy and Industrial Strategy, "Plant loads, demand and efficiency (DUKES 5.10)," 2022.

[160] W. Antweiler and F. Muesgens, "On the long-term merit order effect of renewable energies," *Energy Econ.*, vol. 99, p. 105275, Jul. 2021, doi: 10.1016/J.ENECO.2021.105275.

[161] The University of Sheffield, "PV Live." https://www.solar.sheffield.ac.uk/pvlive/ (accessed Feb. 22, 2023).

[162] C. Gavin, "Seasonal variations in electricity demand," 2014. [Online]. Available:

www.bmreports.com/bsp/bsp_home.htm%0Awww.bmreports.com/bsp/bsp_home.htm%0Ahttps://assets.publishing.service.gov.uk/government/uploads/system/uploads/attachment_data/file/295225/Seasonal_variations_in_electricity_demand.pdf%0Ahttps://www.gov.uk/government/.

[163] R. Graham, J. Browell, and K. Bell, "Simulated 40-year time-series of wind power output in Scotland: Interim dataset specification and evaluation," *(confidential Report)*, no. March, 2021.

[164] J. K. Kaldellis and D. Zafirakis, "The influence of technical availability on the energy performance of wind farms: Overview of critical factors and development of a proxy prediction model," *J. Wind Eng. Ind. Aerodyn.*, vol. 115, pp. 65–81, Apr. 2013, doi: 10.1016/J.JWEIA.2012.12.016.

[165] D. Cevasco, S. Koukoura, and A. J. Kolios, "Reliability, availability, maintainability data review for the identification of trends in offshore wind energy applications," *Renew. Sustain. Energy Rev.*, vol. 136, Feb. 2021, doi: 10.1016/J.RSER.2020.110414.

[166] ELEXON, "BM Reports - Generation by Fuel Type." https://www.bmreports.com/bmrs/?q=generation/fueltype (accessed Jun. 23, 2022).

[167] C. MacIver, W. Bukhsh, and K. R. W. Bell, "The impact of interconnectors on the GB electricity sector and European carbon emissions," *Energy Policy*, vol. 151, Apr. 2021, doi: 10.1016/J.ENPOL.2021.112170.

[168] National Grid ESO, "Future of the Electricity National Control Centre-Thermal Constraint."

[169] C. M. Lai and J. Teh, "Comprehensive review of the dynamic thermal rating system for sustainable electrical power systems," *Energy Reports*, vol. 8, pp. 3263–3288, Nov. 2022, doi: 10.1016/J.EGYR.2022.02.085.

[170] P. E. Bett and H. E. Thornton, "The climatological relationships between wind and solar energy supply in Britain," *Renew. Energy*, vol. 87, pp. 96–110, Mar. 2016, doi: 10.1016/J.RENENE.2015.10.006.

[171] Y. He, A. H. Monahan, and N. A. McFarlane, "Diurnal variations of land surface wind speed probability distributions under clear-sky and low-cloud conditions," *Geophys. Res. Lett.*, vol. 40, no. 12, pp. 3308–3314, 2013, doi: 10.1002/grl.50575.

[172] National Grid ESO, "Summer Outlook." 2022.

[173] Australian Energy Market Operator (AEMO), "System Strength Requirements Methodology: System Strength Requirements & Fault Level Shortfalls," no. June, pp. 1–63, 2018.

[174] M. Nedd, K. Bell, and C. Booth, "Containing Loss Risk in a Low Inertia Gb Power System," *Proc. - 2018 IEEE Int. Conf. Environ. Electr. Eng. 2018 IEEE Ind. Commer. Power Syst. Eur. EEEIC/I CPS Eur. 2018*, 2018, doi: 10.1109/EEEIC.2018.8494455.

[175] H. Abildgaard and N. Qin, "Synchronous Condensers for reliable HVDC operation and bulk power transfer and a hydro-dominated power systems," 2015.

[176] National Grid ESO, "ESO Operational Transparency Forum (14th July 2021)."

[177] NGET, SSENT, and SPEN, "2020 ETYS and NOA Study guidelines final," *(unpublished document)*. 2020.

[178] J. MacDowell, S. Dutta, M. Richwine, S. Achilles, and N. Miller, "Serving the Future: Advanced Wind Generation Technology Supports Ancillary Services," *IEEE Power Energy Mag.*, vol. 13, no. 6, pp. 22–30, Nov. 2015, doi: 10.1109/MPE.2015.2461331.

[179] SMA AG, "Technical Information Sheet: Q at Night - Reactive power outside feed-in operation with SUNNY CENTRAL series."

[180] Power System Consultants UK Ltd (PSC), "Q-Flex Project Reactive Power Technology Catalogue." 2022, [Online]. Available: https://www.pscconsulting.com.

[181] National Grid ESO, "Operational transparency forum (3rd November 2021)," *(online presentation)*. .

[182] National Grid ESO, "Response requirements webinar," 2021. https://players.brightcove.net/867903724001/default_default/index.html?videoId=6279191756001 (accessed Feb. 17, 2023).

[183] F. Milano, *Power System Modelling and Scripting*. Springer, 2010.

[184] S. You *et al.*, "Calculate Center-of-Inertia Frequency and System RoCoF Using PMU Data," 2021, doi: 10.1109/PESGM46819.2021.9638108.

[185] NERC (North American Electric Reliability Corp.), "Essential Reliability Services Task Force Measures Framework Report," 2015.

[186] ENTSO-E, "Frequency Stability Evaluation Criteria for the Synchronous Zone of Continental Europe," 2016.

[187] J. Chen, M. Liu, H. Geng, T. O'donnell, and F. Milano, "Impact of PLL Frequency Limiter on Synchronization Stability of Grid Feeding Converter," *IEEE Trans. POWER Syst.*, vol. 37, no. 3, 2022, doi: 10.1109/TPWRS.2022.3145636.

[188] L. Fan, Z. Miao, D. Ramasubramanian, and H. Ding, "Operational Challenges of Solar PV Plus Storage Power Plants and Modeling Recommendations," *IEEE Open Access J. Power Energy*, 2023, doi: 10.1109/OAJPE.2023.3284375.

[189] L. Fan, Z. Wang, and Z. Miao, "Large Angle Deviation in Grid-Following IBRs Upon Grid Voltage Dip," 2023, doi: 10.1109/TEC.2023.3302812.

[190] DNV KEMA, "An independent analysis on the ability of Generators to ride through Rate of Change of Frequency values up to 2Hz/s," 2013.

[191] L. Saarinen, P. Norrlund, W. Yang, and U. Lundin, "Linear synthetic inertia for improved frequency quality and reduced hydropower wear and tear," *Int. J. Electr. Power Energy Syst.*, vol. 98, pp. 488–495, Jun. 2018, doi: 10.1016/j.ijepes.2017.12.007.

[192] K. Chan, J. Oesterheld, S. Temtem, and J. Haldemann, "Investigations on ROCOF withstand capability on large synchronous generators," *CIGRE Sci. Eng.*, vol. 13, 2019, [Online]. Available: http://www.cigre.org/Menu-links/.

[193] ENTSO-E, "Rate of Change of Frequency (RoCoF) withstand capability: ENTSO-E guidance document for national implementation for network codes on grid connection," 2018. [Online]. Available: https://energy-charts.de/power_de.htm.

[194] F. Milano and A. Ortega, "Frequency Divider," *IEEE Trans. POWER Syst.*, vol. 32, no. 2, p. 1493, 2017, doi: 10.1109/TPWRS.2016.2569563.

[195] DIgSILENT Power Factory, "Technical Reference for Voltage Measurement," 2022.

[196] J. Nutaro and V. Protopopescu, “Calculating Frequency at Loads in Simulations of Electro-Mechanical Transients,” *IEEE Trans. Smart Grid*, vol. 3, no. 1, p. 233, 2012, doi: 10.1109/TSG.2011.2173359.

[197] C. S. Hsu, M. S. Chen, and W. J. Lee, “Approach for bus frequency estimating in power system simulations,” *IEE Proc. - Gener. Transm. Distrib.*, vol. 145, no. 4, 1998.

[198] A. J. Roscoe, A. Dyko, strathacuk Ben Marshall, M. Lee, H. Kirkham, and G. Rietveld, “The Case for Redefinition of Frequency and ROCOF to Account for AC Power System Phase Steps.”

[199] M. Paolone *et al.*, “Fundamentals of Power Systems Modelling in the Presence of Converter-Interfaced Generation.”

[200] ABB, “ABB HD4 gas insulated MV circuit breakers,” 2018. Accessed: Aug. 04, 2023. [Online]. Available: https://tinyurl.com/e8wkf3kc.

[201] N. Skopljak, “Norway-UK interconnector hits a snag with license application refusal,” *Offshore Energy News*, Mar. 16, 2023. .

[202] Office of Gas and Electricity Markets (OFGEM), “NorthConnect-regime withdrawal letter,” Dec. 2022.

[203] National Grid, “Electricity Ten Year Statement,” 2019.

[204] National Grid, “Workgroup Report GC0062 - Fault Ride Through,” 2015.

[205] X. Liu *et al.*, “Transient Stability of Synchronous Condenser Co-located with Renewable Power Plants,” 2023, doi: 10.1109/TPWRS.2023.3271025.

[206] E. Rehman, M. G. Miller, J. Schmall, S. H. Huang, and J. Billo, “Stability Assessment of High Penetration of Inverter-Based Generation in the ERCOT Grid,” *IEEE Power Energy Soc. Gen. Meet.*, vol. 2019-Augus, pp. 4–8, 2019, doi: 10.1109/PESGM40551.2019.8973727.

Appendix A: Network Diagrams

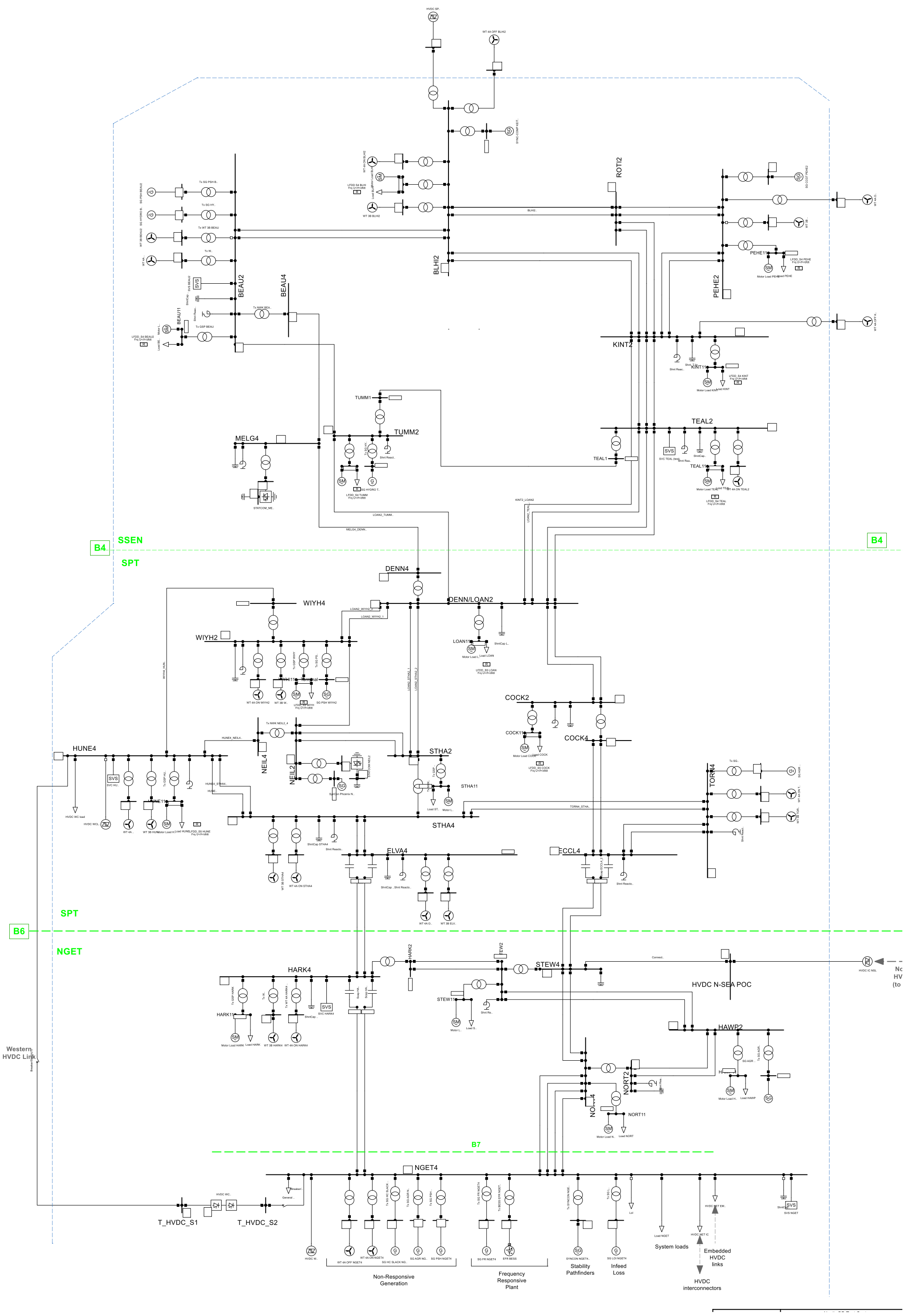

Figure A1: NGBTS network diagram – 2022 model

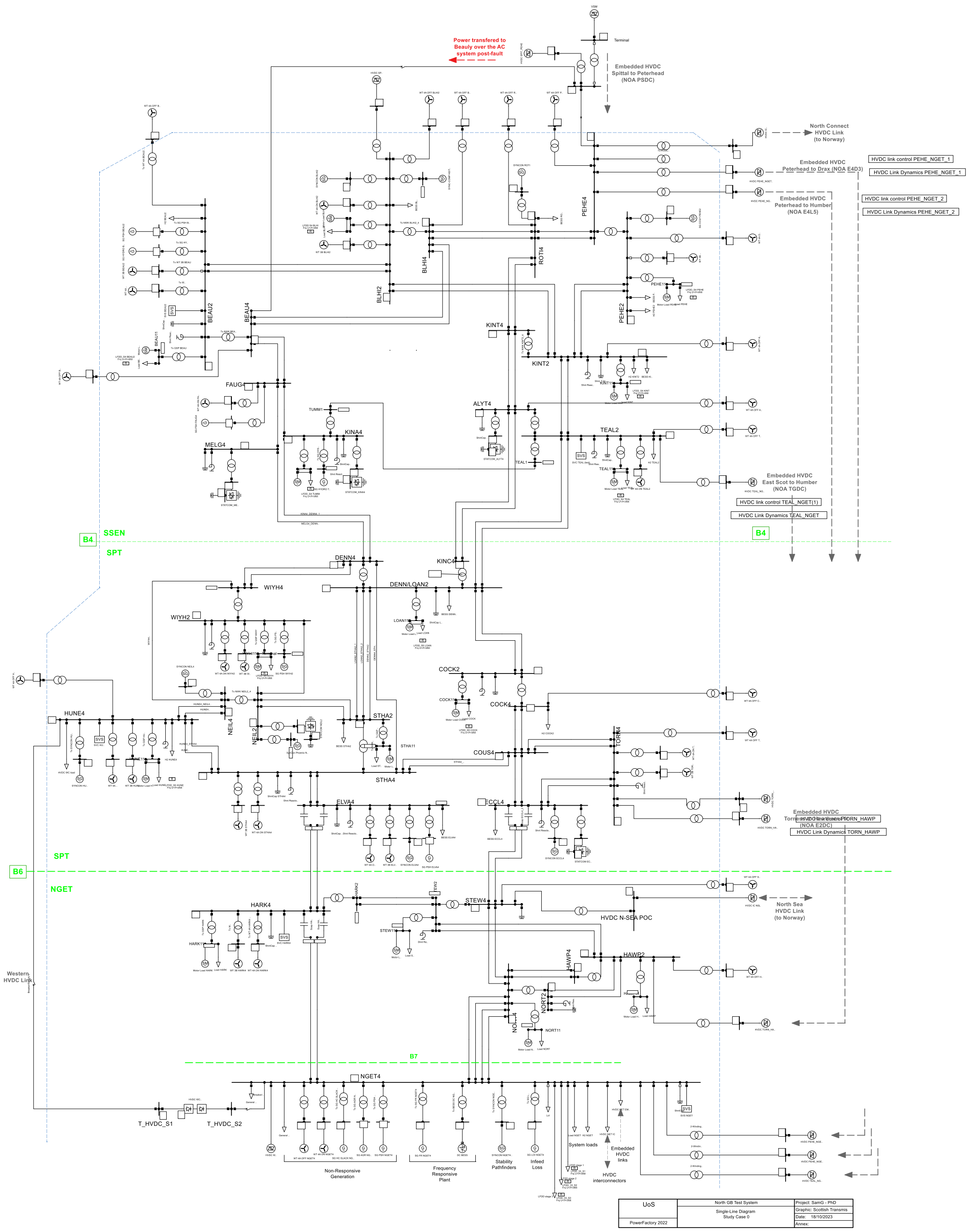

Figure A2: NGBTS network diagram – 2032 model

Appendix B: Transmission Line Data Calculation Methodology

Table B1 - Formulas used for line data calculations

Per unit impedance (Z):	$$Z_{pu} = \frac{Z_{\Omega}}{Z_{base}}$$
Base impedance:	$$Z_{base} = \frac{kV_{base}^2}{MVA_{base}}$$
Per unit susceptance (B):	$$B_{p.u} = \frac{2\pi f C}{Y_{base}}$$ where f is frequency and C is shunt capacitance of the line.
Base admittance (Y):	$$Y_{base} = \frac{1}{Z_{base}}$$
Series/parallel combinations of n number of connected lines for Resistance (R), Reactance (X) and Capacitance (C):	$$R_{eq.parallel} = \left(\sum_{i}^{n} R_i^{-1}\right)^{-1}$$ $$X_{eq.parallel} = \left(\sum_{i}^{n} X_i^{-1}\right)^{-1}$$ $$C_{eq.parallel} = \sum_{i}^{n} C_i$$ $$R_{eq.series} = \sum_{i}^{n} R_i$$ $$X_{eq.series} = \sum_{i}^{n} X_i$$

An example line impedance calculation along the transmission path between Harker and Penwortham in Northern England is provided below in Figure B1.

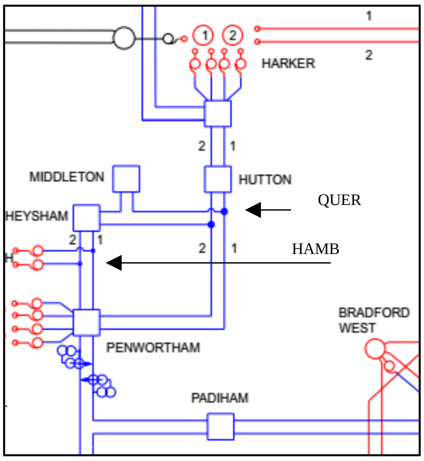

Figure B1: snapshot of ETYS network diagram, northern England [125]

The equivalent impedance between Harker and Penwortham ($Z_{eqHARK-PENW}$) is equal to:

$$Z_{eqHARK-PENW} = Z_{HARK-HUTT} + Z_{HUTT-QUER} +$$

$$\left(Z_{QUER-PENW} \mid\mid \left(Z_{QUER-HEYS} + Z_{HEYS-HAMB} + Z_{HAMB-PENW}\right)\right)$$

Appendix C: Transmission Line Data

Table C1 and C2 display the calculated transmission line type data for the model years 2022 and 2032, respectively. All line types in table C1 are valid for the 2022 model. All line types in table C2 are valid for the 2032 model and are new lines (N in the 'status' column) or have been upgraded from the 2022 version (U in the 'status' column).

Table C1 – Transmission line data for 2022 model

line name	Voltage (kV)	Length (km)	R (Ω/km)	X (Ω/km)	B (uS/km)	Rating (kA)
BEAU2_TUMM2	275	127.9	0.021	0.307	3.779	4.01
TUMM2_LOAN2	275	114.4	0.020	0.297	3.870	4.01
BEAU4_MELG4	400	72.6	0.020	0.306	3.780	4.01
MELG4_DENN4	400	146.0	0.021	0.305	3.790	4.01
BEAU2_BLHI2	275	110.0	0.043	0.311	3.616	1.96
BLHI2_ROTI2	275	35.4	0.038	0.333	3.491	2.29
ROTI2_PEHE2	275	47.4	0.038	0.333	3.491	2.29
ROTI2_KINT2	275	23.2	0.030	0.333	3.491	2.90
BLHI2_KINT2	275	50.9	0.045	0.309	3.677	1.96
PEHE2_KINT2	275	70.5	0.039	0.329	3.466	2.29
KINT2_TEAL2 R1	275	100.6	0.046	0.403	2.910	1.46
TEAL2_LOAN2 R1	275	90.6	0.035	0.319	3.741	2.00
KINT2_TEAL2 R2	275	115.7	0.038	0.330	3.479	2.00
TEAL2_LOAN2 R2	275	101.3	0.037	0.325	3.767	2.00
KINT2_TEAL2	275	184.6	0.037	0.324	3.596	2.00
TUMM1_TEAL1	132	75.0	0.101	0.388	4.853	1.31
LOAN2_STHA2 R1	275	65.8	0.017	0.242	4.119	3.15
LOAN2_WIYH2	275	49.9	0.033	0.308	3.673	2.20
LOAN2_COCK2	275	89.1	0.032	0.313	3.657	2.90
WIYH2_NEIL2	275	25.5	0.033	0.323	3.586	2.01
NEIL2_STHA2	275	35.4	0.032	0.309	3.676	2.35
WIYH4_HUNE4	400	79.5	0.028	0.310	3.999	2.01
HUNE4_STHA4	400	94.3	0.027	0.310	3.798	4.00
HUNE4_NEIL4	400	35.8	0.032	0.329	4.098	1.91
TORN4_STRA4	400	129.7	0.028	0.301	5.563	3.57
HARK4_ELVA4	400	77.1	0.028	0.305	3.731	3.19

ELVA4_STHA4	400	48.6	0.028	0.303	3.742	3.19
TORN4_ECCLE4	400	36.3	0.020	0.283	11.689	3.36
ECCLE4_COCK4	400	65.9	0.035	0.343	3.362	1.62
ECCLE4_STEW4	400	102.2	0.014	0.274	4.210	4.80
HARK2_STEW2	275	83.8	0.045	0.320	3.743	1.62
HARK4_PEWO4	400	171.8	0.019	0.115	4.303	4.80
STEW2_HAWP2	275	72.8	0.036	0.346	3.378	2.86
HAWP2_NORT2	275	51.4	0.007	0.101	3.667	2.90
STEW4_NORT4	400	60.9	0.020	0.300	3.605	3.67
NORT4_THTO4 R1	400	100.6	0.021	0.300	3.858	4.01
NORT4_THTO4 R2	400	97.8	0.017	0.271	16.939	3.49

Table C2 – New and upgraded transmission line data for 2032 model (in addition to lines still in service from table C1)

line name	Voltage (kV)	Length (km)	R (Ω/km)	X (Ω/km)	B (uS/km)	Rating (kA)	status
BEAU4 _FAUG4_1	400	50.7	0.018	0.291	3.91	4.013	N
BEAU4 _FAUG4_2	400	48.6	0.020	0.306	3.78	4.013	N
FAUG4 _KINA4	400	80.2	0.018	0.290	3.91	4.013	N
KINA4 _DENN4	400	89.8	0.019	0.291	3.90	4.013	N
FAUG4 _MELG4	400	24.0	0.020	0.307	3.78	4.013	U
BEAU4_BLHI4	400	110.0	0.018	0.291	3.91	4.013	N
BLHI4_ROTI4	400	35.4	0.032	0.309	3.68	2.887	N
ROTI4_PEHE4	400	47.4	0.032	0.309	3.68	2.887	N
ROTI4_KINT4	400	23.2	0.032	0.309	3.68	2.887	N
KINT4 - ALYT4	400	99.5	0.032	0.309	3.68	2.887	N
ALYT4 - KINC4	400	80.5	0.032	0.313	3.65	2.887	N
LOAN2 - STHA2 R1	275	65.8	0.020	0.274	4.12	3.149	U
DENN2 - STHA2 R2	275	37.0	0.032	0.343	5.15	2.880	N
DENN4 - STHA4	400	44.4	0.032	0.342	5.66	2.880	N
DENN4_WIYH4	275	49.9	0.032	0.309	3.68	2.897	N
LOAN2 - COCK2	275	84.8	0.032	0.313	3.66	2.897	U
NEIL2_STHA2	275	35.4	0.032	0.309	3.68	2.351	N
NEIL4 - HUNE4	400	35.0	0.032	0.323	3.58	2.006	N
STHA4 - COUS4	400	80.8	0.033	0.324	3.57	3.811	N
COUS4 - BRNX4	400	51.4	0.021	0.309	3.74	3.569	N
BRNX4 - ECCL4	400	34.2	0.021	0.300	3.83	3.640	N

COUS4 - ECCLE4	400	55.3	0.033	0.345	3.36	2.887	N
COCK4 - COUS4	400	10.6	0.033	0.345	3.36	1.617	N
HAWP2_NORT2	275	51.4	0.022	0.544	3.67	2.901	U
HAWP4_NORT4	400	60.3	0.017	0.278	4.12	4.013	N
NORT4_THTO4 R1	400	94.4	0.020	0.298	3.87	4.011	U